Year : 2021

STRESS-DRIVEN SYNAPTIC PLASTICITY WITHIN THE LATERAL HABENULA INSTRUCTS ADAPTIVE BEHAVIORS

Nuño Pérez Álvaro

UNIL | Université de Lausanne
Faculté de biologie et de médecine

Département des Neurosciences Fondamentales

STRESS-DRIVEN SYNAPTIC PLASTICITY WITHIN THE LATERAL HABENULA INSTRUCTS ADAPTIVE BEHAVIORS

Thèse de doctorat en Neurosciences

présentée à la

Faculté de Biologie et de Médecine
de l'Université de Lausanne

par

Álvaro Nuño Pérez

Master in molecular neurosciences, University of Amsterdam, NL

Jury

Prof. Dr. Nicolas Toni, Président
Prof. Dr. Manuel Mameli, Directeur
Prof. Dr. Camilla Bellone, Experte
Prof. M.D. Dr. Robert C. Malenka, Expert

Thèse n° 292

Lausanne, January 2021

Programme doctoral interuniversitaire en Neurosciences des Universités de Lausanne et Genève

LEMANIC NEURO SCIENCE DOCTORAL SCHOOL

UNIL | Université de Lausanne

UNIVERSITÉ DE GENÈVE

UNIL | Université de Lausanne

UNIVERSITÉ DE GENÈVE

Programme doctoral interuniversitaire en Neurosciences des Universités de Lausanne et Genève

Imprimatur

Vu le rapport présenté par le jury d'examen, composé de

Président·e	Monsieur	Prof.	Nicolas	**Toni**
Directeur·trice de thèse	Monsieur	Prof.	Manuel	**Mameli**
Expert·e·s	Madame	Prof.	Camilla	**Bellone**
	Monsieur	Prof.	Robert	**Malenka**

le Conseil de Faculté autorise l'impression de la thèse de

Monsieur Alvaro Nuno Perez

Master in molecular neurosciences, University of Amsterdam, NL

intitulée

STRESS-DRIVEN SYNAPTIC PLASTICITY WITHIN THE LATERAL HABENULA INSTRUCTS ADAPTIVE BEHAVIORS

Date de l'examen: 29 janvier 2021
Date d'émission de l'Imprimatur: Lausanne, le 11 février 2021

pour Le Doyen
de la Faculté de Biologie et de Médecine

Prof. Niko GELDNER
Directeur de l'Ecole Doctorale

Acknowledgements

What a journey! It feels like it was yesterday when I was leaving the Netherlands to start my PhD thesis. I joined the group of Manuel Mameli three years ago, still unable to control my tremors whenever my supervisor would stare at me while performing an experiment. Throughout my thesis, I managed to overcome this issue, for which I am grateful. But, more importantly, I earnt scientific maturity and critical thinking along with it. None of this could have happened without the invaluable mentorship and support received from several different people.

Manuel belongs to the uncommon group of individuals who are able to pass on knowledge without you realizing it. One day I would find myself disagreeing with a particular thing he supported, and sometime after I would propose an idea that very much resembled his way of thinking. Express your ideas concisely (do not beat around the bush), be open about your experimental results with the people around you, and be proactive when facing unexpected troubles down the road. These are the professional improvements that I absorbed from Manuel, which I will carry with me henceforth. In the personal front, Manuel also made a prominent contribution. Indeed, the complementarity between science and pleasure, in the context of social gatherings with your colleagues and collaborators (pre-Covid-19), is something that I now consider to be essential for ensuring a healthy and productive working environment. Moreover, Manuel would always support me whenever I was tempted to undertake personal projects beyond the research life. For all these things, I thank you, Manuel.

The remaining members of Manuel's group have not only been peers, but also family. Throughout all these years, I could count on them for literally anything, always coming up with fresh ideas and solutions to my endless problems. I owe to **Massimo** the possibility that my project acquired a decent behavioral twist, since his mentorship in handling mice was impeccable. **Salvatore** was always there to encourage me during periods of low mood, and he trained me in calcium imaging approaches. **Arnaud** taught me to anticipate the potential flaws of a given experimental approach. **Anna Tchenio** always awoke in me a great deal of optimism. I am grateful to **Kristina** for visiting the laboratory where I was conducting my Master's thesis, thanks to which I discovered the Mameli group. And **Mauro** and **Joseph**, well... I thank them for being the way they are, a constant source of jokes and good times.

I would also like to thank the **Department of Fundamental Neuroscience** as a whole for hosting my work, the directress **Claudia Bagni** for supporting the entire PhD community, **Leonardo** for helping me to troubleshoot in the behavioral facility, and **Kim** for starting as a colleague and gradually turning into my life companion. From my Master's period in the Netherlands, I would like to thank **Paloma** for teaching me how to open cells during patch-clamp experiments.

Last but not least, I would like to express eternal gratitude to my beloved **family**. They have always been supportive and caring, despite the physical separation between us. Believe it or not, you too made this possible!

Abstract

It is routine to feel the pressure during intense academic periods, or to suffer from an injury. Indeed, we are exposed to stressful events throughout the extent of our lives. Some of these situations occur unexpectedly, thus denying the possibility to develop contingency plans, in which case we refer to uncontrollable or inescapable stressors. Other instances, hereby defined as controllable or escapable forms of stress, allow us to learn associations between sensory cues and noxious stimuli in order to make predictions. These predictions guide future actions with the aim of avoiding sources of stress. Importantly, whether a stressor is escapable or inescapable has greatly contrasting repercussions on behavior. The former often leads to adaptive or coping behaviors, while the latter instead drives pathological adaptations such as behavioral despair, anhedonia and cognitive deficits. However, the neural underpinnings of such divergence are far from being understood. This is the subject I want to address with my PhD thesis.

Stress modifies the function and synaptic properties of different brain regions. My focus is on the epithalamic lateral habenula (LHb), whose neurons are widely activated by predictable and unpredictable stressful events. The habenular complex influences diverse behaviors, including reward seeking and escape from threats, through the control of the dopamine and serotonin signaling in the ventral tegmental area and raphe nuclei, respectively. Notably, stressful experiences evoke synaptic adaptations in the LHb, and these changes have a prominent impact on behavior. Considering the stress susceptibility and behavioral control of habenular neurons, we hypothesized that escapable and inescapable forms of stress might exert dissimilar effects on behavior, through the induction of divergent forms of synaptic plasticity in LHb neurons.

To test this hypothesis, we employed specific behavioral paradigms in order to model escapable and inescapable stress, together with fiber photometry to measure neuronal calcium dynamics, and whole-cell patch-clamp electrophysiology to assess synaptic function. The main conclusion of my doctoral work is that escapable stress promotes coping escape behaviors through the potentiation of AMPA transmission in LHb neurons, whereas inescapable stress drives cognitive impairments by the weakening of habenular glutamatergic synapses. By providing specific synaptic mechanisms within discrete neuronal circuits, my PhD thesis demonstrates that stressful experience differentially modulates behavior by guiding the direction of synaptic plasticity. Altogether, these results broaden our understanding on the biological basis of coping and pathological behaviors, and might prove useful to assign an etiology to stress-driven adaptations that are so frequently observed in the clinic.

Résumé

Chacun de nous a souffert un jour d'une blessure, ou a été confronté à des moments de stress notamment lors de périodes d'examens intenses. En effet, nous sommes exposés à des événements stressants tout au long de notre vie. Certaines de ces situations surviennent de façon inattendue sans offrir la possibilité de développer des plans d'urgence, auquel cas on parle de facteurs de stress incontrôlables ou inévitables. Au contraire, lorsque nous pouvons prendre le contrôle de ces situations désagréables, définies ici comme stress contrôlable ou évitable, elles peuvent augmenter nos capacités d'apprentissage. Plus particulièrement, le stress évitable induit des associations entre des signaux sensoriels et des stimuli nocifs dans une perspective d'adaptation, par la prédiction et l'anticipation. En effet, ces prédictions guident les actions futures, propices à éviter les sources de stress. En outre, le fait qu'un facteur de stress soit évitable ou inévitable a des répercussions très contrastées sur le comportement. Le premier cas engendre fréquemment des comportements adaptatifs, tandis que le second entraîne plutôt des adaptations pathologiques telles que la résignation, l'anhédonie et les déficits cognitifs. Cependant, les fondements neuronaux d'une telle divergence sont loin d'être compris. C'est la question que je souhaite aborder avec ma thèse de doctorat.

Le stress modifie la fonction et les propriétés synaptiques de différentes régions du cerveau. Je me concentre sur l'habénula latérale épithalamique (HbL), dont les neurones sont largement activés par des événements stressants prévisibles et imprévisibles. L'HbL influence divers comportements, y compris la recherche de récompenses et l'évitement des menaces, à travers le contrôle de la signalisation de la dopamine et de la sérotonine dans la zone tegmentale ventrale et les noyaux du raphé, respectivement. Les expériences stressantes notamment évoquent des adaptations synaptiques dans les neurones de l'HbL, et ces changements ont des répercussions sur le comportement. Compte tenu de la sensibilité au stress et du contrôle comportemental des neurones habénulaires, nous avons émis l'hypothèse que les facteurs de stress évitables et inévitables induisent des formes divergentes de plasticité synaptique dans les neurones de l'HbL, donnant lieu à des adaptations comportementales distinctes.

Pour tester cette hypothèse, nous avons utilisé différents paradigmes comportementaux afin de modéliser le stress évitable et inévitable, l'imagerie par photométrie en fibre pour mesurer la dynamique neuronale du calcium, ainsi que l'électrophysiologie patch-clamp pour évaluer la fonction synaptique. La principale conclusion de mon travail de doctorat est que le stress évitable favorise les comportements d'évasion grâce au renforcement de la transmission du récepteurs AMPA dans les neurones de l'HbL, alors que le stress inévitable entraîne des troubles cognitifs en affaiblissant les synapses glutamatergiques. En fournissant des mécanismes synaptiques spécifiques dans des circuits neuronaux distincts, ma thèse de doctorat démontre que l'expérience stressante, selon son caractère évitable ou non, a un impact bidirectionnel sur la plasticité synaptique orientant ainsi le comportement. Ces résultats élargissent notre compréhension de la base biologique des comportements d'adaptations et pathologiques, et pourraient s'avérer utiles pour attribuer une étiologie aux adaptations au stress si fréquemment observées en clinique.

List of abbreviations

AAV	Adeno-associated virus
ACTH	Adrenocorticotropic hormone
AMPAR	α-amino-3-hydroxyl-5-methyl-4-isoxazole-propionate receptor
APV	D-2-amino-5-phosphonopentanoic
AR	Adrenergic receptor
BLA	Basolateral amygdala
BNST	Bed nucleus of the stria terminalis
CaMKII	Calcium-calmodulin kinase II
cAMP	Cyclic adenosine monophosphate
CeA	Central amygdala
CMS	Chronic mild stress
CNIH	Cornichon-like protein
CRF1	CRH receptor 1
CRH	Corticotropin releasing hormone
CS	Conditioned stimulus
DA	Dopamine
DR	Dorsal raphe
DREADD	Designer receptors exclusively activated by designer drugs
EPN	Entopeduncular nucleus
GABA	γ-aminobutyric acid
GAD	Glutamic acid decarboxylase
GAT	GABA transporter
HPA	Hypothalamic-pituitary-adrenal
LC	Locus coeruleus
LDTg	Laterodorsal tegmental nucleus
LHA	Lateral hypothalamic area
LHb	Lateral habenula
LPO	Lateral preoptic area
LTD	Long-term depression
LTP	Long-term potentiation
mEPSC	Miniature excitatory postsynaptic current
NAc	Nucleus accumbens
NE	Norepinephrine
NLGN	Neuroligin
NMDAR	N-methyl-D-aspartate receptor
NRXN	Neurexin
PFC	Prefrontal cortex
PKA	Protein kinase A
PKC	Protein kinase C

PP2A	Protein phosphatase 2A
PTSD	Posttraumatic stress disorder
PVN	Paraventricular nucleus
RMTg	Rostromedial tegmental nucleus
TARP	Transmembrane AMPAR regulatory protein
US	Unconditioned stimulus
vGLUT	Vesicular glutamate transporter
vHb	Ventral habenula
VTA	Ventral tegmental area

List of contents

List of figures

List of boxes

Chapter 1: Introduction

We are part of a society in which resources are limited and competition for opportunities is commonplace. Stress is thus our lifelong companion. Far from being a unimodal phenomenon, the stressors that we encounter come in different flavors. For instance, the governmental directives to enforce a lockdown during the Covid-19 pandemic do not leave much room for alternatives, hence why the recent worldwide situation represents an example of uncontrollable or inescapable stress. On the other hand, writing a thesis under a deadline is stressful for PhD candidates, who throughout the years learn to organize their schedule ahead of time in order to dilute the pressure and maximize their chances of success. The latter is an example of controllable or escapable stress, since actions may be taken to cope with the situation. Importantly, whether we perceive a particular stressor as controllable or uncontrollable has major clinical implications. Indeed, active coping is proposed as a beneficial approach to tackle neuropsychiatric conditions (LeDoux and Gorman, 2001), while inescapable stressors are instead at the basis of depressive symptoms and cognitive deficits (Maier and Watkins, 2005). Moreover, the perceived controllability over daily aversive events negatively correlates with the clinical severity of mental disorders (Kushner et al., 1993). Therefore, from a translational perspective, there is the need to understand how the brain encodes various forms of stress and what are the ethological repercussions of such encoding. This knowledge would allow us to establish causal links between brain alterations and behaviors, both in adaptive and pathological contexts, potentially paving the way for new therapeutic interventions.

I present my doctoral thesis during an exciting period for the field of neuroscience. At this moment, there are straightforward tools designed to monitor dynamics of neuronal activity, assess synaptic function, and modulate the efficacy of communication across precise cellular ensembles. First and foremost, it is currently possible to do all of the above in a region-specific manner. Among the various brain structures susceptible to stress, my work focuses on the lateral habenula (LHb). We decided to study this nucleus based on several different grounds: (1) LHb neurons are excited by multiple stressors and aversive events (Matsumoto and Hikosaka, 2009), (2) they contribute to a wide range of behavioral manifestations, both in pathological and physiological contexts (Li et al., 2013; Lecca et al., 2017), (3) they undergo a broad array of experience-dependent synaptic alterations, many of which are linked to specific behavioral functions (Li et al., 2011; Lecca et al., 2016; Tchenio et al., 2017), and (4) they control the activity of the ventral tegmental area (VTA) and raphe nuclei, two important structures for the execution of motivated behaviors and dysregulated in mood disorders (Wang and Aghajanian, 1977; Stern et al., 1979; Christoph et al., 1986). Despite these accumulating data, whether various forms of stress differentially modulate behavior through divergent synaptic plasticity in LHb neurons remains unknown.

Throughout the introduction, I will first describe the physiological response to stress and the current models that are available in the laboratory to study such a phenomenon. After commenting on the links between stress and neuropsychiatric conditions, I will move on to the brain encoding of stress and highlight several structures that have been at the forefront of the field over recent years. I will finally introduce the anatomical and functional principles of the habenular complex, underscoring the importance of studying

glutamatergic synaptic transmission – the common denominator across the two projects of my PhD work. In particular, the first article studies how the habenular encoding of escapable stressors instructs avoidance strategies (Trusel et al., 2019), while the second manuscript concentrates on how inescapable stress shapes habenular function in order to drive reward-seeking deficits (Nuno-Perez et al., 2021). Let us commence.

1.1 How does the body respond to stress?

Most physiological characterizations of the bodily response to stress, regardless of its controllability, have been performed in rodent models. These studies have defined stress as the state by which intrinsic or extrinsic stimuli, referred to as stressors, disrupt the homeostatic state of an individual at the hormonal, physiological and behavioral level (Herman et al., 2016). The physiological response to stress is bimodal (**Figure 1**). First, stressors are perceived by sensory organs and then relayed through the brainstem into cholinergic pre-ganglionic neurons in the spinal cord, eventually driving the release of epinephrine and norepinephrine (NE) from the adrenal medulla. This signaling pathway is characterized by its fast temporal dynamics and comprises the sympathetic adreno-medullary system, which orchestrates fight-or-flight responses that typically result in increased heart rate and augmented blood glucose (Goldstein, 1987). In parallel to the rapid activation of the adreno-medullary system, stress perception can be more slowly relayed into central sensory pathways, by triggering the release of corticotropin releasing hormone (CRH) from parvocellular neurons in the paraventricular nucleus (PVN) of the hypothalamus (Vale et al., 1981). CRH then reaches the anterior pituitary through the hypophysial portal circulation, where it interacts with CRH receptor 1 (CRF1) in order to drive the release of adrenocorticotropic hormone (ACTH) into the circulatory system (Engler et al., 1989). Systemic ACTH ultimately drives the synthesis and secretion of glucocorticoids (i.e., cortisol and corticosterone) from the adrenal cortex, which sends a negative feedback to the PVN and anterior pituitary to suppress CRH and ACTH synthesis (Canny et al., 1989). The recognition of mineralocorticoid and glucocorticoid receptors in virtually every organ system, including the brain, affects patterns of gene expression and is hence accountable for the long-term physiological changes induced by stress (Sapolsky et al., 2000). This second cascade of events is referred to as the hypothalamic-pituitary-adrenal (HPA) axis. Bearing in mind the physiological response to stress, we will now move on to common paradigms that are available to induce it in the laboratory.

1.2 Animal models of stress

There are multiple experimental procedures capable of inducing stress in rodent models (**Box 1**). Throughout my PhD thesis, we will systematically model stress with the electric foot-shock paradigm, which consists of delivering electric discharges to the animal through a metal grid on the floor. The origin of this paradigm goes back to 1908, when Yerkes and Dodson revealed that mice would avoid contexts associated with foot-shock delivery. Interestingly, the higher was the intensity of the stimulus, the faster the animals would develop such avoidance responses (Yerkes and Dodson, 1908). Most of the initial characterization of the behavioral reactions to acute foot-shock stimuli was performed in rats. It was

reported that electric discharges below 0.3 mA suppress locomotion and induce mild flinching responses, whereby animals move their limbs and tail without absolute change in body position (Kimble, 1955; Levine, 1966). Conversely, stimuli above 0.5 mA lead to robust jumping and motivated escape responses (Campbell and Masterson, 1969). The inherent stress of foot-shock experience not only contains a physical component, given the mechanical perception of pain, but also induces a psychological response in the form of negative emotional reactions (Pynoos et al., 1996). In fact, the emotional component of the paradigm is so important that it can lead to long-lasting behavioral adaptations even in the absence of repetitive exposure (Louvart et al., 2005; Louvart et al., 2006).

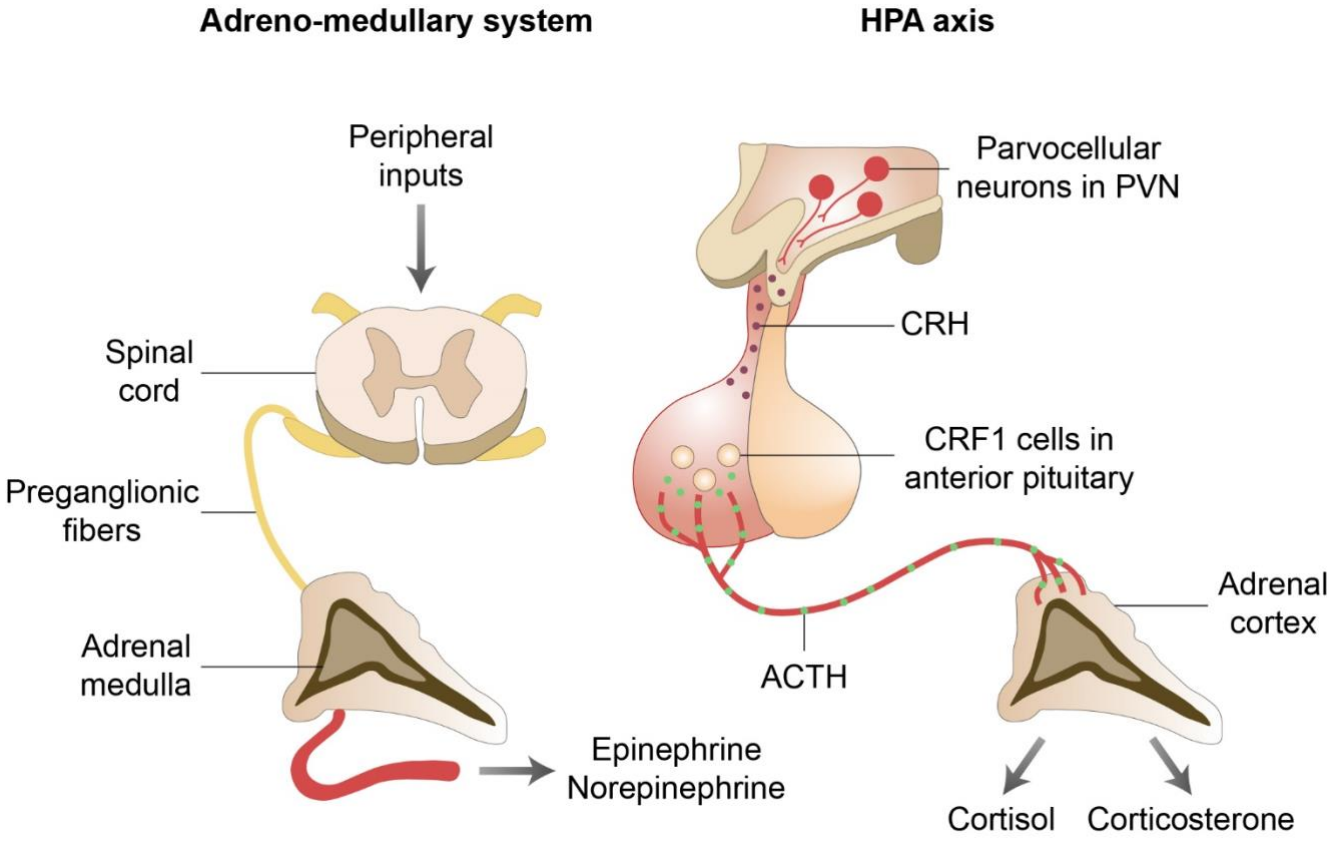

Figure 1. The bodily response to stress. The adreno-medullary system involves pre-ganglionic neurons in the spinal cord, which receive peripheral inputs and in turn induce the release of epinephrine and NE from the adrenal medulla. Alternatively, the HPA axis is based on the release of CRH from PVN neurons into the anterior pituitary, leading to the increase in systemic ACTH concentrations and the eventual release of glucocorticoids from the adrenal cortex.

We believe the foot-shock paradigm has several advantages. First of all, foot-shock delivery triggers the canonical stress response leading to increased plasma levels of epinephrine and NE, and augmented central and peripheral concentration of the stress hormones CRH, ACTH and glucocorticoids (Handa et al., 1994; Weinstock et al., 1998; Iwasaki-Sekino et al., 2009). This paradigm thereby results in the concurrent engagement of the sympathetic adreno-medullary cascade and the HPA axis, both hallmarks of naturally occurring stress episodes. Secondly, the properties of the paradigm can be easily tuned in terms of foot-shock duration and intensity, enabling a straightforward optimization of the settings aligned to the nature

Box 1 | Common models of stress in rodents

Preclinical models are fundamental to the comprehension of physiological alterations after stress exposure, as well as to the screening of pharmacotherapies aiming to alleviate pathological behaviors. Initial paradigms of stress, pioneered by Hans Selye in the 1950s, focused on the adaptations to physical experiences. Eventually, John Mason widened the range of noxious stimuli in order to study the contribution of adverse emotional reactions. This distinction, still valid today, renders two classes of stress models: physical and psychological.

Physical stress paradigms compromise the homeostatic state of animals by modifying the environmental conditions:

- Immobilization stress leads to the total prevention of movement by fixing the four limbs of the animal and blocking any neck torsion. A milder version of this model is restraint stress, which hinders movement to a lesser extent by introducing the animal inside a plastic tube. In both paradigms, rodents typically struggle and try to regain movement during the initial phases, but eventually decide to remain motionless. These paradigms are predominantly of physical nature, but a psychological dimension is also in place (claustrophobic-like). The main drawback of these models is the impossibility to tune the intensity of the experience.
- Forced swim stress is often used as a readout for the helpless state or behavioral despair of the animal. Nonetheless, this paradigm was initially developed to drive the stress response by introducing the animal inside a cylinder filled with water, which will render a swimming response that reflects an attempted escape. This procedure has been heavily criticized due to its cruelty.
- Stress through food and water deprivation is frequently used to motivate performance during reward-guided behaviors. However, one must be aware that either manipulation represents a source of stress for the animal. Indeed, these stressors are frequently included in the repertoire of the chronic mild stress paradigm.
- Thermogenic stress consists in exposing rodents to cold temperatures, either inside a water tank or a freezer. This model is efficient for modeling acute stress, but under chronic schedules the body adapts to these thermal changes and the stress response is heavily compromised.

Alternatively, psychological stress paradigms compromise the homeostatic state of animals by inducing a negative emotional response:

- Social defeat stress includes a physical and a psychological component. The former arises from direct encounters with aggressive and dominant strains of rodents. The latter becomes prominent after introducing the aggressor and aggressed animals in the same cage, blocking any physical interaction but maintaining the perception of sensory cues (i.e., odor, sound and vision).
- Sleep deprivation can be achieved through dysregulation of day-night cycles. In particular, sleep is disrupted by keeping intense lighting conditions overnight, allowing only a brief period of darkness during the day. Despite being effective to model acute stress, animals adapt to new day-night schedules upon repetitive exposure.
- Neonatal isolation consists in separating the pups from their mother and litter during the weaning period, repetitively but during short periods of time. This paradigm results in the activation of the HPA axis without prominent growth defects.
- Predatory stress involves the exposure to innate predatory cues including fox urine, cat feces or looming stimuli. Acutely, these encounters drive motivated escape responses and are therefore appropriate to study the sympathetic adreno-medullary system.
- Noise-induced stress is considered relevant for modern human ambiences and is induced through the exposure to background noises of high intensity. Animals show habituation to repetitive noise exposure, thereby rendering it unsuitable for modeling chronic stress.

of the experiment (Bali and Jaggi, 2015). This versatility allows the paradigm to be employed in different configurations of severity (mild or intense), regularity (acute or chronic) and contingency (escapable or inescapable). Moreover, in contrast to a wide variety of alternative stressors, animals do not habituate to repetitive foot-shock exposure, and therefore desensitization is not a confounding variable (Van den Berg et al., 1998; Hajós-Korcsok et al., 2003). Lastly, several therapeutic approaches with clinical validity in depressive patients are capable of alleviating depressive-like symptoms in preclinical models subjected to unpredictable foot-shocks, thereby supporting the translational power of this paradigm. Examples of such translational approaches include administration of the antidepressant drug imipramine, treatment with deep brain stimulation, and regular practice of physical exercise (Chourbaji et al., 2005; Greenwood et al., 2007; Li et al., 2011).

We asserted above that the foot-shock paradigm is versatile and able to accommodate several experimental designs. This is a crucial aspect for my PhD thesis, since my ultimate goal is to compare brain alterations induced by escapable versus inescapable stress. I will now refer to two important variations of the foot-shock paradigm.

1.2.1 The active avoidance paradigm

The gold standard for modeling escapable stressors via foot-shock delivery is the active avoidance paradigm (LeDoux et al., 2017). It enables animals to avoid a harmful stimulus (unconditioned stimulus, US, foot-shock) through the exploitation of a preceding sensory cue (conditioned stimulus, CS, tone). This process is complex and first requires a diminished contextual fear response, which hinders Pavlovian conditioning and goal-directed actions (Miller, 1948; Mowrer, 1951). An association might then be learnt between the sensory cue, which acquires predictive value, and the subsequent aversive outcome. Finally, animals learn to instrumentally exploit this association by triggering a motor action during the cue presentation, ultimately leading to the avoidance of the foot-shock stimulus (Krypotos et al., 2015). Much of the research on active avoidance focuses on the phenomena of emotional processing and fear encoding. According to such a fear-centered framework, the CS-US association enables the cue itself to become aversive, triggering a fear response that the animal tries to reduce by avoiding (Dinsmoor, 2001). However, an alternative reward-centered theory posits that any avoidance process conducive to seeking safety should be perceived as a positive outcome, by virtue of the violation of aversive expectation (Ilango et al., 2012). In fact, it is still a matter of much debate whether the execution of escape responses is primarily driven by the emotional or the rewarding centers of the brain.

1.2.2 The unpredictable foot-shock paradigm

Inescapable stressors can be modeled with the unpredictable foot-shock paradigm, whereby animals are subjected to a series of electric discharges with randomized intervals (Kim and Seo, 2013). In contrast to the active avoidance task, which prompts an action to escape from future stressors and thus promotes survival, inescapable foot-shock exposure engages fear reactions and drives emotional states that are detrimental to the well-being of the animal (Overmier and Seligman, 1967; Drugan et al., 1997). Indeed, a single foot-shock stimulus of high intensity (1.5-2 mA) is sufficient to trigger long-lasting behavioral

deficits, including social avoidance and anxiety – a framework employed to model posttraumatic stress disorder (PTSD) (Siegmund and Wotjak, 2007). Alternatively, repetitive foot-shock exposure across several sessions drives behavioral despair, learning deficits and anhedonia, altogether more evocative of depressive-like symptoms (Vollmayr et al., 2004; Li et al., 2011). The prominent interaction between stress and pathological states will be further developed in the next section.

Box 2 | Preclinical models of stress are often employed to induce depressive states

The race to develop suitable models of depression is governed by the aspiration of reaching three levels of translational validity. The first level, known as face validity, tries to establish a comparable symptomatology to the human condition. The second aspect, coined as construct validity, aims at obtaining rodent models with a similar etiology and biological basis. Lastly, predictive validity focuses on the development of laboratory models that are responsive to treatments employed in clinical contexts. The four models that are considered to fulfil such criteria are discussed below.

- The learned helplessness model of depression, first described by Solomon in the 1960s, consists in subjecting rodents to two sessions of inescapable foot-shock exposure at randomized intervals. Approximately a fifth of the experimental animals, referred to as susceptible, acquire a helpless phenotype that is reminiscent of humans giving up in the face of adversity. Together with such behavioral despair, susceptible subjects also display anhedonia, loss of sexual appetite, reduced body weight, and spatial memory deficits. Interestingly, a systematic inbreeding of susceptible animals leads to a congenital form of depression. The depressive-like symptoms can be reversed by short-term treatments with tricyclic antidepressants, hence rendering the predictive validity of the model.
- The chronic mild stress paradigm (CMS), perhaps considered the most relevant for the human condition, was conceived in order to tackle the common desensitization phenomenon that follows repetitive exposure to most stressors. First developed by Katz and Willner, CMS exposes rodents to a combination of low-intensity stressors throughout extended periods of time. Examples of such stressors include tilting of the cage, food or water deprivation, cohousing with a high number of littermates, and disruption of day-night cycles. This paradigm is anxiogenic and leads to behavioral despair, anhedonia and cognitive deficits. The symptomatology of CMS animals is treatable with pharmacological approaches commonly employed in the clinic.
- The paradigm of social defeat stress acknowledges the fact that most stressors in current human contexts are of social nature. Every day for up to two weeks, experimental rodents are exposed to brief bouts of aggressive interactions against dominant males, followed by long-lasting periods of sensory perception (i.e., odor, sound and vision) without direct physical contact. Less than half of the animals subjected to the paradigm are susceptible to developing anhedonia. Susceptible subjects can be effectively treated with antidepressants and broad-spectrum benzodiazepines. A major drawback of this model is that it can only be used with males, since females do not evoke aggressive responses from dominant strains of rodents.
- Maternal separation consists in separating pups from their mother and litter during the two weeks of early postnatal development, evocative of human cases of child neglect. This paradigm leads to persistent HPA hyperactivity and multiple behavioral deficits including anxiety, helplessness and memory deficits. As with the models presented above, these behavioral symptoms can be reversed after protracted treatment with antidepressants.

1.3 Stress and brain pathology

The foot-shock paradigm is not the only model of stress capable of promoting the development of neuropsychiatric disorders. Several of the stress models discussed above, when experienced in a protracted fashion, lead to pathological states including anxiety and, more prominently, depression (**Box 2**) (Willner et al., 1987; Kudryavtseva et al., 1991; Berton et al., 2006; Aisa et al., 2007; Erburu et al., 2015; Lukkes et al., 2017). It is worthy of note that the comorbidity between stress and neuropsychiatric conditions is often observed in the clinic as well (Kendler et al., 1998; Swaab et al., 2005). Thus, despite the sources of stress may differ across species, the response to stress and the subsequent alterations in brain function remain similar. This supports the construct validity of preclinical models (Vollmayr and Gass, 2013). I will now discuss the link between stress and mental illness, with a particular focus on depression and PTSD (**Figure 2**).

1.3.1 Depression

Pioneering evidence linking stress with distinct neuropsychiatric disorders came from genetic studies. Mice carrying a knockout mutation for corticosteroid receptors, solely in excitatory neurons of the forebrain, display reduced levels of anxiety and despair (Tronche et al., 1999). Conversely, the emulation of the stress response by overexpression of glucocorticoid receptors exerts anxiogenic effects and induces the emergence of helplessness and despair – behavioral adaptations which can be rescued by administration of antidepressant drugs (Wei et al., 2004). Similarly, intracerebroventricular CRH administration induces anxiety and depressive-like phenotypes (Valdez et al., 2002; Heinrichs and Koob, 2004). These seminal studies demonstrate that opposite manipulations of the central response to stress can bidirectionally modulate pathological behaviors, thus setting the grounds for considering HPA hyperactivation as a contributing factor for mood disorders (Brown et al., 2004; de Kloet et al., 2005).

Supporting the translational validity of such a theory, exposure to chronic stressors in humans leads to systemic increases in cortisol levels, concomitantly with anxiety episodes and memory deficits typically observed in depressive patients (Lupien et al., 1998; Wolf et al., 2001; Lenze et al., 2012). Interestingly, similar cognitive impairments are present during the aftermath of pituitary cancers that result in hypercortisolemia (i.e., Cushing disease) (Starkman et al., 1992; Nieman, 2018). These independent results indicate that the brain dysfunction and subsequent behavioral maladaptations, rather than being defined by the sources of stress, are governed by HPA hyperactivation and the resulting increase in glucocorticoid signaling. Further connecting stress with brain pathology, patients with depression exhibit augmented concentrations of cortisol in the urine and, as concluded from postmortem tissue, increased CRH labeling in hypothalamic PVN neurons (Carroll et al., 1976; Purba et al., 1996). Moreover, HPA hyperdrive is a common biomarker of both chronic stress and depression, and remission from depression is often followed by relapse in those patients with abnormal HPA reactivation (Aguilera, 1994; Zobel et al., 2001; Pariante and Lightman, 2008). Altogether, we conclude that stress precipitates the emergence of depressive states, both in humans and preclinical models.

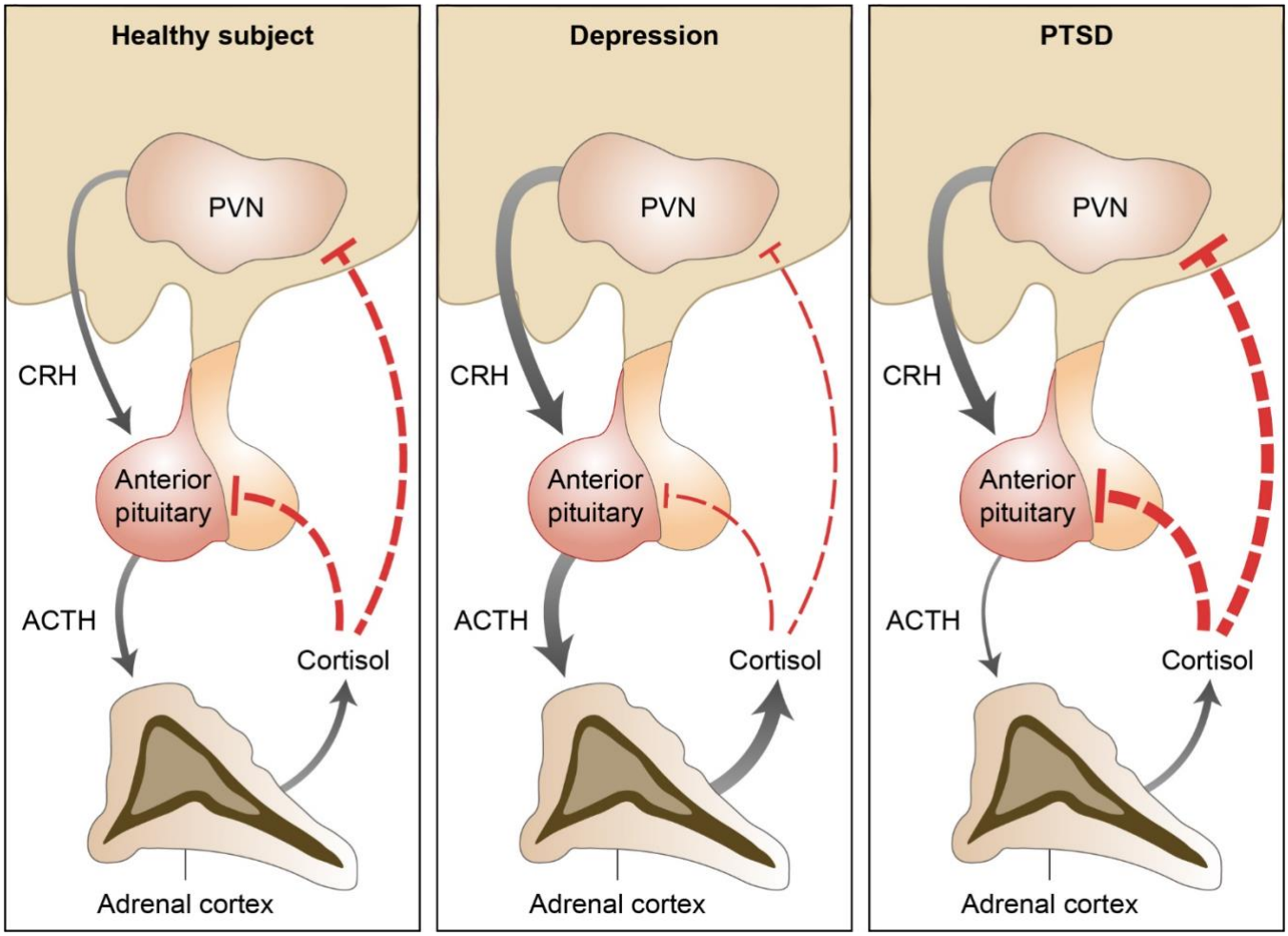

Figure 2. The HPA axis is differentially dysregulated in depression and PTSD. In healthy subjects, cortisol secretion exerts a negative feedback loop onto hypothalamic CRH secretion and pituitary ACTH synthesis. This negative interaction is hampered in patients with depression, thereby leading to increased production of CRH and ACTH, as well as higher cortisol concentrations. The situation is more complex in PTSD patients. Despite their negative feedback is potentiated, PTSD subjects display higher CRH synthesis, which does not translate into higher ACTH synthesis because of the downregulation of CRF1 in the pituitary.

1.3.2 Posttraumatic stress disorder

Links between PTSD, a neurological syndrome that results from an intense traumatic experience, and aberrant stress responses have also been established. In particular, excessive CRH activity is part of the etiology of the disease. In preclinical models, CRH administration is sufficient to drive the emergence of PTSD-like symptoms, including abnormal startle reflexes following acoustic stimuli, disruption of sleep cycles, and heightened fear responses (Laryea et al., 2012). Moreover, activation of CRF1 in limbic brain structures potentiates basal and stress-driven anxiety, and leads to negative emotional reactions (Henckens et al., 2016). Conversely, knockout mice for CRF1 display low sensitivity to stress and milder anxious phenotypes than control littermates (Contarino et al., 1999; Bale et al., 2002). On the clinical side, PTSD patients show increased glucocorticoid receptor levels in the blood, as well as higher CRH concentrations in the cerebrospinal fluid (Yehuda et al., 1991; Yehuda et al., 1995; Bremner et al., 1997; Baker et al., 1999; Sautter et al., 2003). Importantly, a study showed that urine cortisol levels in veterans from the Vietnam

War were lower than those observed in patients with major depressive disorder, hence reflecting a clinical signature that differentiates the two syndromes (Mason et al., 1986). Perhaps the most reproducible biomarker in PTSD patients is the hyperactivity of the negative feedback that systemic cortisol levels exert over ACTH secretion in the pituitary, yet it remains unclear whether such a phenomenon is a result of PTSD per se, or rather reflects a genetic predisposition for developing the syndrome (Smith et al., 1989; Heim et al., 2001). An additional alteration of the HPA axis in PTSD subjects is the apparent downregulation of CRF1 in the pituitary, as evidenced by decreased ACTH secretion following CRH administration (Yehuda et al., 2004; Ströhle et al., 2008).

Collectively, these rodent and human studies highlight the face validity of preclinical models to study the bodily response to stress, and underscore the complex interactions between stress and brain function. The close resemblance between the stress response in humans and rodents, the prevailing comorbidity between stress exposure and neuropsychiatric conditions, and the conserved efficacy of numerous clinical treatments across species, indicate that current models carry certain translational value. However, there are obvious limitations to the properties of present stress paradigms, since it is virtually impossible to model human experiences with precision in laboratory animals. A better understanding of the neuronal circuits of stress might prove useful to develop better paradigms, that more closely resemble the brain alterations observed in humans after stress exposure.

1.4 Brain encoding of stressful experience

In this section, I will describe how stress is encoded in the brain by means of different forms of synaptic plasticity (**Box 3**), and the communication across specific neuronal populations. Stress exposure affects a wide variety of brain regions. For the purpose of conciseness, I will highlight brain structures that have been in the vanguard of the field during recent years. My selection includes prominent constituents of the limbic system, the monoaminergic nuclei, and recently evolved cortical areas (Sapolsky, 2003; McEwen and Morrison, 2013; Mahar et al., 2014; Douma and de Kloet, 2020).

1.4.1 Amygdala

The central subdivision of the amygdala (CeA) contains CRH neurons that project to the hypothalamic PVN, where the stress response is coordinated, hence suggesting a role in the regulation of the HPA axis (Marcilhac and Siaud, 1997). Along these lines, restraint stress increases amygdalar CRH expression, and corticosterone delivery specifically in the CeA exerts CRF1-dependent anxiogenic effects (Kalin et al., 1994; Myers et al., 2005; Shekhar et al., 2005; Callahan et al., 2013). Furthermore, knockdown or overexpression of CRH in CeA neurons desensitizes or potentiates anxiety-like behaviors after acute stress exposure, respectively (Regev et al., 2012; Callahan et al., 2013). CeA neurons, apart from containing CRH, also express markers of inhibitory transmission (Carta et al., 2008; Gafford et al., 2012; Heldt et al., 2012). At inhibitory synapses, CRH administration or the paradigm of chronic mild stress (CMS) potentiate the release of γ-aminobutyric acid (GABA), and increase the connectivity across CeA neurons (Kang-Park et al., 2015; Partridge et al., 2016). An important CeA input is the basolateral amygdala (BLA), mainly

consisting of glutamatergic neurons (McDonald, 1996; Kim et al., 2016; Kim et al., 2017). Similar to CeA, BLA neurons undergo stress-driven synaptic plasticity at inhibitory synapses. More specifically, the tonic inhibitory transmission onto BLA neurons is decreased upon chronic immobilization, foot-shock exposure, or protracted CRF1 activation (Rainnie et al., 2004; Liu et al., 2014). Besides these adaptations at inhibitory synapses, BLA neurons undergo changes in excitatory transmission as well. Chronic restraint stress results in dendritic hypertrophy, together with the potentiation of glutamatergic connections through changes in subunit composition and phosphorylation state of α-amino-3-hydroxyl-5-methyl-4-isoxazole-propionate receptors (AMPAR) (Yi et al., 2017). Similarly, formation of stress-related memories relies on presynaptic potentiation of glutamate release and postsynaptic increase in AMPAR levels (McKernan and Shinnick-Gallagher, 1997; Rumpel et al., 2005). Further contributing to the overall enhancement of BLA excitatory synapses, acute stressors prevent the induction of AMPAR depression through endogenous cannabinoid signaling (Li et al., 2018). Overall, the decrease in tonic inhibition and the potentiation of excitatory synapses result in stress-driven hyperactivity of BLA neurons (Sharp, 2017).

Box 3 | Forms of synaptic plasticity

Stressful experience triggers patterns of neuronal activity and eventually modifies the efficacy and strength of synaptic transmission across brain regions. According to their behavioral repercussions, these experience-dependent alterations can either be adaptive, for example in the context of learning to escape from a neutral stimulus that turns into a threat (Wenzel et al., 2018), or maladaptive, for instance leading to the manifestation of stress-driven anhedonia (Pignatelli et al., 2020). Depending on the timeline for induction and expression, synaptic plasticity can be further categorized as short-term or long-term (Citri and Malenka, 2008). Short-term plasticity occurs through milliseconds or minutes and is normally associated with transient adaptations to sensory stimuli, ephemeral adjustments of behavioral states, and the formation of memories with transitory nature (Abbott and Regehr, 2004). Given its fast temporal dynamics, short-term plasticity is often expressed via the alteration of calcium levels within presynaptic terminals and the modulation of neurotransmitter release probability (Dobrunz and Stevens, 1997; Jackman et al., 2016). Alternatively, any synaptic tuning that leads to sustained behavioral changes or durable memory traces is considered a form of long-term plasticity (Takeuchi et al., 2014). By contrast with the presynaptic locus of short-term alterations, these long-term variants are usually expressed through the modification of the number and conductance of neurotransmitter receptors within postsynaptic compartments (Whitlock et al., 2006; Penn et al., 2017).

1.4.2 Locus coeruleus

Most stimuli that trigger the HPA cascade also drive the activation of neurons in the locus coeruleus (LC) – the principal source of the neuromodulator NE in the brain. Foot-shock exposure, restraint, noise-induced stress, forced swim and water deprivation, among others, are all manipulations able to activate LC neurons and increase NE metabolites in LC-innervated cortical areas (Abercrombie and Jacobs, 1988; Britton et al., 1992; Smagin et al., 1995; Chen and Sara, 2007; Valentino and Van Bockstaele, 2008). Following acute stress, NE release from LC neurons induces an anxious state in order to increase attention to sensory stimuli, facilitate coping behaviors, and enable the association between the context and the noxious experience (Berridge and Waterhouse, 2003; Sara and Bouret, 2012). LC neurons display either tonic or phasic firing activity at baseline (Aston-Jones and Cohen, 2005; Carter et al., 2010). Under stressful

conditions, however, the frequency of tonic firing increases and this results in anxious phenotypes (Curtis et al., 1997; Page and Abercrombie, 1999; Snyder et al., 2012). Optogenetic induction of tonic firing in LC neurons is anxiogenic in the absence of stress, hence indicating a causal link between tonic firing and maladaptive behaviors. Moreover, the neuronal population that triggers these anxious phenotypes expresses CRF1, and receives direct synaptic inputs from CRH neurons located in the CeA (McCall et al., 2015). Finally, the LC also releases NE onto BLA neurons that express β-adrenergic receptors (AR), a connection that further contributes to the emergence of negative emotional states and anxious behaviors after stress exposure (**Figure 3**) (Siuda et al., 2015; McCall et al., 2017).

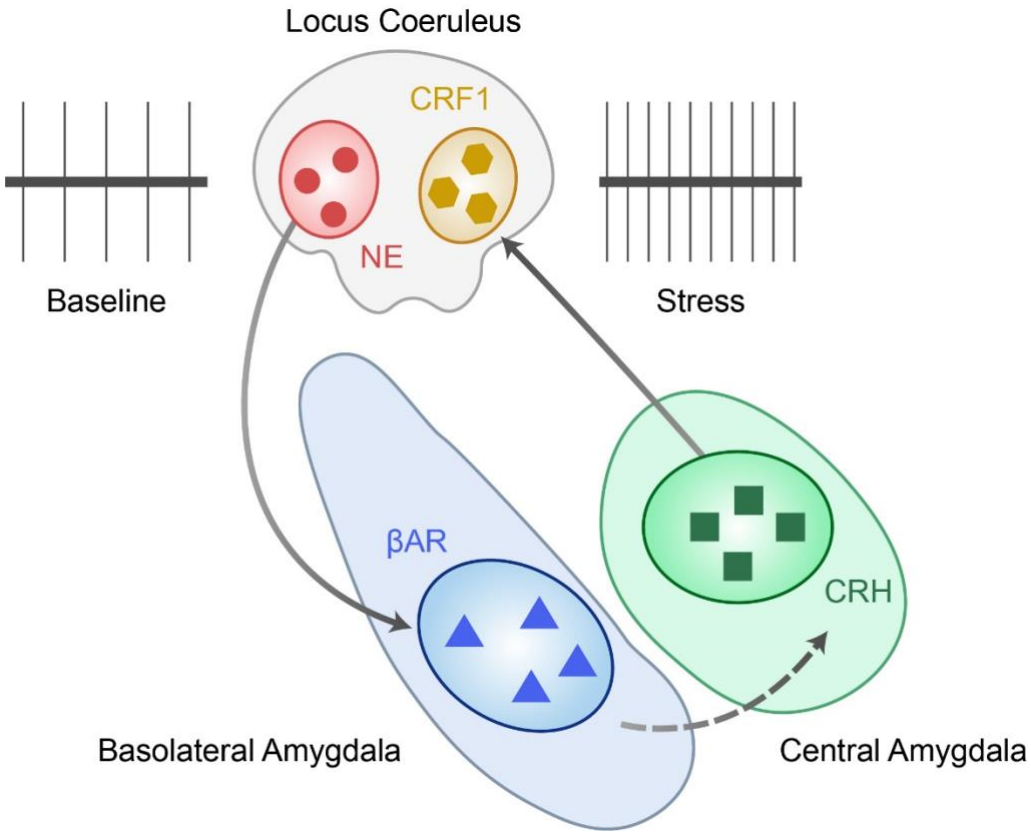

Figure 3. Stress encoding in amygdalo-noradrenergic circuits. Stress drives the CeA release of CRH onto CRF1 neurons in the LC, leading to the emergence of anxious behaviors. At the same time, acute stressors increase the frequency of tonic firing in noradrenergic LC neurons, which contact BLA neurons expressing β-ARs, further promoting adverse emotional states. The BLA also activates the CeA, despite this connection has not been studied in the context of stress-driven LC adaptations.

1.4.3 Paraventricular nucleus

The hypothalamic PVN releases CRH into the anterior pituitary and is thus a critical node for the HPA orchestration (Herman et al., 2003; Ulrich-Lai and Herman, 2009). However, apart from controlling endocrine response to stress, PVN neurons shape stress-driven behaviors as well (De Marco et al., 2016). In zebrafish, stress intensity positively correlates with the activity levels of individual CRH cells, the size of the recruited CRH population, and the degree of stress-driven locomotion (Vom Berg-Maurer et al., 2016). In mice, foot-shock exposure drives bursting modes of firing activity in CRH neurons, an adaptation

that is partially prevented by simultaneous delivery of sucrose rewards (Kim et al., 2019; Yuan et al., 2019). Furthermore, increased activity of CRH neurons following the presentation of predatory cues can predict the occurrence of escape behaviors (Daviu et al., 2020). Acute stressors drive a stereotypical set of behaviors like grooming and enhanced locomotor activity, and the emergence of this behavioral repertoire depends on the activation of CRH neurons projecting to the lateral hypothalamic area (LHA) (Füzesi et al., 2016). Moreover, engagement of CRH neuronal activity is required for the social transmission of stress into partner mice who observe how littermates experience noxious stimuli. This social transmission of stress relies on the short-term potentiation of excitatory synapses in PVN neurons (Sterley et al., 2018). Further linking hypothalamic neurons to stress-driven behavioral alterations, mice with a conditional deletion of CRH solely in PVN neurons exhibit anxiolytic phenotypes under stressful conditions (Ramot et al., 2017; Zhang et al., 2017).

1.4.4 Prefrontal cortex

Neurons in the prefrontal cortex (PFC), an evolutionarily recent brain region involved in higher order cognitive processes, are susceptible to stress (Miller, 2000). In young animals, forced swim stress and acute periods of restraint potentiate the glutamatergic transmission mediated by AMPARs and N-methyl-D-aspartate receptors (NMDAR). These alterations, which occur in the absence of presynaptic modulation of glutamate release probability, depend on the activation of glucocorticoid receptors and the subsequent modulation of receptor trafficking through the GTPase Rab4. Moreover, this mechanism is required for the stress-driven improvement in working memory tasks (Yuen et al., 2009; Yuen et al., 2011). Contrasting with the effects of acute stressors at young ages, protracted restraint stress and the CMS paradigm lead to the depression of AMPAR and NMDAR transmission, together with deficits in object recognition. These maladaptive effects are mediated by degradation of AMPAR and NMDAR subunits through ubiquitination (Yuen et al., 2012). Therefore, at young ages, acute and chronic stressors lead to opposite synaptic and behavioral alterations (**Figure 4**). Nonetheless, in adult stages, both acute and chronic stressors impair PFC function and drive similar cognitive impairments. The mechanisms underlying these adaptations involve the hyperactive engagement of dopamine (DA) and NE signaling. Indeed, activation of D1-DA receptors and β1-ARs stimulates adenylyl cyclases, which potentiate the production of the second messenger cyclic adenosine monophosphate (cAMP). This signaling pathway opens hyperpolarizing HCN channels within dendrites, ultimately weakening excitatory inputs onto PFC neurons (Murphy et al., 1996; Chen et al., 2001; Ramos et al., 2005; Arnsten, 2009; Wahl-Schott and Biel, 2009). Furthermore, α1-ARs promote the opening of hyperpolarizing SK channels and facilitate the activation of protein kinase C (PKC), whose inhibition is protective against stress-driven cognitive deficits (Birnbaum et al., 1999; Hagenston et al., 2008; Hains et al., 2009). Altogether, these studies prove that stress-driven effects in PFC function and cognition largely depend on the properties of the stressor and the age of the animal.

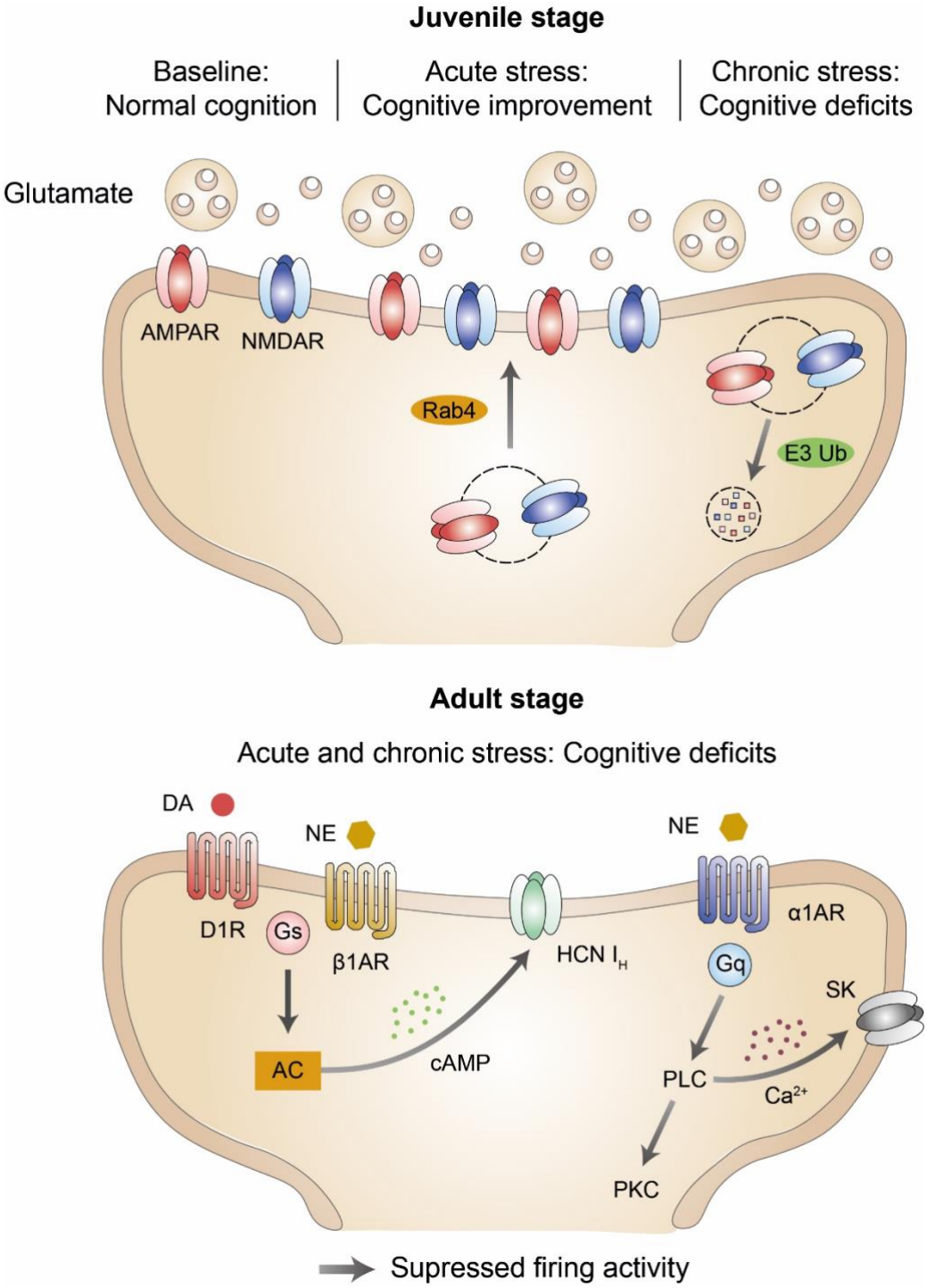

Figure 4. Synaptic and behavioral adaptations in the PFC are determined by the age of the animal and the chronicity of the stressor. In juvenile rodents, acute stressors enhance cognitive performance by potentiating AMPAR and NMDAR transmission in a Rab4-dependent fashion. Conversely, chronic stressors drive cognitive deficits via degradation of glutamate receptors through E3 ubiquitin ligases (E3 Ub). In adult animals, the stress-driven activation of metabotropic D1-DA receptors and β1-ARs increases cAMP production by adenylyl cyclases (AC), thereby activating hyperpolarizing HCN-mediated currents. Moreover, the concomitant activation of α1-ARs stimulates phospholipase C (PLC). This enzyme activates PKC and triggers the opening of calcium-dependent SK channels, further contributing to neuronal hyperpolarization. Altogether, these metabotropic events result in cognitive deficits after stress exposure.

1.4.5 Ventral tegmental area

DA neurons located in the VTA, the rewarding center of the brain, project mainly to the nucleus accumbens (NAc) and PFC (Lammel et al., 2012). Exposure to acute stressors, including foot-shock and tail pinch, increases DA levels in the PFC and biases behavioral manifestations towards aversion (Sorg and Kalivas, 1993; Vander Weele et al., 2018). In the NAc, however, DA dynamics undergo an initial increase, related to novelty encoding and facilitation of active coping behaviors, followed by a long-lasting reduction, related to the disruption of defensive responses in inescapable contexts (Douma and de Kloet, 2020). These biphasic dynamics go along with the existence of two different DA neuronal populations within the VTA. Dorsolateral DA neurons decrease their firing following acute stress exposure, and undergo phasic rebound excitation upon the termination of the experience (Mantz et al., 1989; Guarraci and Kapp, 1999; Brischoux et al., 2009; Navratilova et al., 2012). Conversely, ventromedial VTA DA neurons are excited by stress exposure (Anstrom and Woodward, 2005; Anstrom et al., 2009; Cohen et al., 2012). With respect to chronic stressors, protracted restraint stress or social defeat increase the spontaneous and burst firing of DA neurons, both in brain slices and *in vivo*, and favor long-term potentiation (LTP) of NMDAR glutamatergic transmission (Krishnan et al., 2007; Cao et al., 2010; Stelly et al., 2016). Providing a mechanistic link to the manifestation of stress-driven behavioral adaptations, mice resilient to social defeat do not exhibit such an increase in firing activity. Interestingly, optogenetic induction of phasic firing activity in NAc-projecting VTA DA neurons of resilient mice is capable of rendering a susceptible phenotype (Chaudhury et al., 2013). However, these data contrast with the observation that excitation of VTA DA neurons innervating the NAc is protective, rather than facilitating, against the development of susceptible phenotypes (Tye et al., 2013). These seemingly opposite results may be explained by the circuit specificities of the populations that were manipulated in either study.

1.4.6 Dorsal raphe nucleus

Studies in freely behaving cats, following exposure to high-intensity noises, did not detect increases in firing rate of neurons located in the dorsal raphe nucleus (DR) – the main source of the neuromodulator serotonin in the brain (Wilkinson and Jacobs, 1988). Similarly, in anesthetized rats, bright flashes of light do not excite DR neurons (Mosko and Jacobs, 1974). Nonetheless, certain noxious stimuli, including foot-shocks and aggressive interactions, do engage DR activation and disrupt the typical rhythmicity of action potential discharge, hence leading to bursting firing patterns (Walletschek and Raab, 1982; Schweimer and Ungless, 2010). Similarly, acute stressors trigger the expression of early markers of neuronal activity in the DR (Grahn et al., 1999; Takase et al., 2004; Commons, 2008). This increase in activity after acute stress exposure follows a circuit logic. Indeed, while amygdala-projecting DR neurons are excited by foot-shocks, as assessed by fiber photometry, those projecting to cortical areas are instead inhibited (Ren et al., 2018). These data contrast with earlier microdialysis studies, showing that acute stressors increase serotonin levels in the DR and several efferent regions, including PFC and amygdala (Sheikh et al, 2007; Mo et al., 2008). Importantly, the foot-shock-driven increase in brain serotonin levels is long-lasting when the stressor is inescapable, while it is rather brief when the stressor can be avoided (Amat et al., 2005). As opposed to acute stressors, CMS decreases the spontaneous firing activity and serotonin levels in the DR (Bekris et al., 2005; Kang et al., 2005; Bambico et al., 2009). Collectively, these studies suggest that acute and chronic stressors modulate serotonin signaling in the brain through modulation of neuronal activity within the DR.

1.4.7 Bed nucleus of the stria terminalis

Neurons in the anteroventral region of the bed nucleus of the stria terminalis (BNST), also known as extended amygdala, project to the PVN where the stress response is organized (Sawchenko and Swanson, 1983; Radley et al., 2009). These connections are mainly inhibitory, but excitatory and CRH efferents have also been elucidated (Cullinan et al., 1993; Moga and Saper, 1994). Lesions of the anterior BNST subdivision disrupt the activity of the HPA axis, thus suggesting a positive modulation of the endocrine response to stress (Spencer et al., 2005; Choi et al., 2007). Conversely, lesions of the posterior BNST increase CRH synthesis in the PVN, and further facilitate the HPA engagement following acute and chronic stressors (Choi et al., 2008). These observations suggest a region-specific modulation of the HPA axis by the BNST. In addition to the PVN projection, BNST neurons also project to the VTA. Glutamatergic BNST-to-VTA neurons are excited by foot-shock stimuli, whereas their GABAergic counterparts are inhibited by acute stress exposure. At the behavioral level, the former connection is anxiogenic, while the latter is anxiolytic and reduces fear responses (Jennings et al., 2013). Based on their electrophysiological properties, neurons in the BNST can be subdivided in three distinct types (I/II/III), and chronic stress drives cell type-specific adaptations in excitatory synaptic transmission. In particular, while types I and II undergo a change in AMPAR subunit composition, type III instead displays a facilitated LTP induction (Dabrowska et al., 2013; Daniel et al., 2019). These synaptic adaptations contribute to stress-induced behavioral adaptations, since delivery of AMPAR antagonists into the BNST exerts anxiolytic effects and reduces the sensitivity to foot-shock (Walker and Davis, 1997; Davis and Walker, 2014). Moreover, forced swim stress and predatory odors engage the activation of neurons in both the dorsal and ventral BNST subdivisions (Briand et al., 2010; Butler et al., 2016). These data highlight the vast heterogeneity of BNST neuronal populations, and support their differential susceptibility to stress.

In summary, I have discussed how stressful experiences are encoded across different brain regions. There are other areas, like the hippocampus and striatum, whose susceptibility to stress is also prominent (Dias-Ferreira et al., 2009; McEwen et al., 2016). However, they are out of the scope of my thesis work, since they are not embedded in the habenular neurocircuitry. In fact, most of the regions commented above are anatomically connected with the LHb, either as inputs or outputs. My doctoral work focuses on this epithalamic structure because habenular neurons are activated by stressors of different nature (Matsumoto and Hikosaka, 2009), and they control a multitude of motivated behaviors in both physiology and pathology (Li et al., 2013; Lecca et al., 2017). Moreover, LHb synapses undergo various forms of experience-dependent plasticity with important behavioral implications (Li et al., 2011; Lecca et al., 2016; Tchenio et al., 2017). Throughout the next section, I will discuss the anatomical and functional characteristics of habenular neurons, together with their susceptibility to stress.

1.5 Spotlight on the lateral habenula

1.5.1 Anatomy and function

My PhD thesis focuses on stress encoding within the LHb, an evolutionarily ancient limbic region identified in virtually all vertebrate species (Bianco and Wilson, 2009). The widespread interest in this structure is based on the fact that LHb neurons control the firing activity of two important neuromodulatory centers of the brain (i.e., VTA DA neurons, and serotonin neurons of the raphe) (Wang and Aghajanian, 1977; Stern et al., 1979; Christoph et al., 1986; Matsumoto and Hikosaka, 2007). Hence, the habenular complex bears a strategic position to regulate diverse motivational and cognitive functions. Most LHb neurons are glutamatergic, as proven by the expression of messenger RNA encoding for vesicular glutamate transporter 2 (vGLUT2) and vGLUT3 (Herzog et al., 2004; Brinschwitz et al., 2010; Aizawa et al., 2012). However, a small proportion of medially located LHb neurons are positive for GABAergic markers, such as glutamic acid decarboxylase 2 (GAD2) and GABA transporter 1 (GAT1) (Zhang et al., 2016; Zhang et al., 2018c). These inhibitory neurons have been proposed as a source of local inhibition for the surrounding population of glutamatergic cells (Flanigan et al., 2020; Webster et al., 2020). The resting membrane potential of LHb neurons is considerably more depolarized in comparison to cortical areas, and determines their firing patterns to a great extent (Weiss and Veh, 2011). Indeed, while hyperpolarized membrane potentials often go along with bursting spike discharges, depolarized voltages render either tonic firing or silent LHb neurons (**Figure 5**) (Yang et al., 2018).

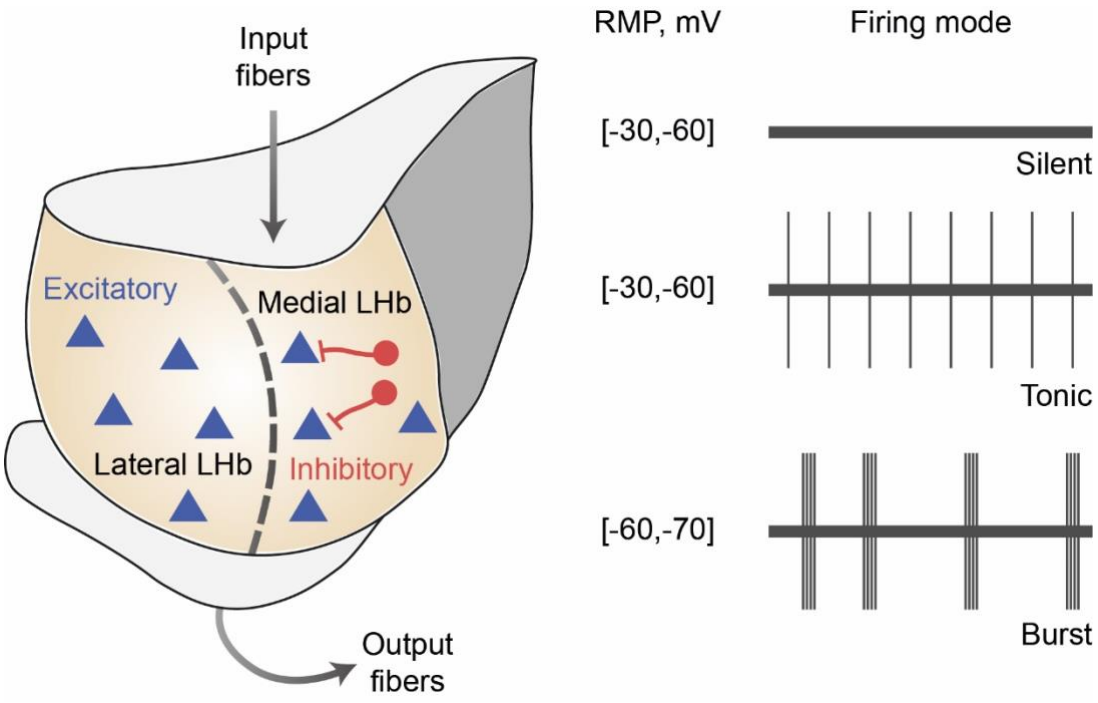

Figure 5. Coronal schematic of the lateral habenula. Most LHb neurons are glutamatergic, while the medial subdivision of this nucleus contains a minimal proportion of GABAergic neurons, which provide local inhibition. Notably, the mode of action potential discharge in LHb neurons depends on the resting membrane potential (RMP). Hyperpolarized RMPs are associated with bursting activity, while tonic and silent neurons often exhibit more depolarized RMPs.

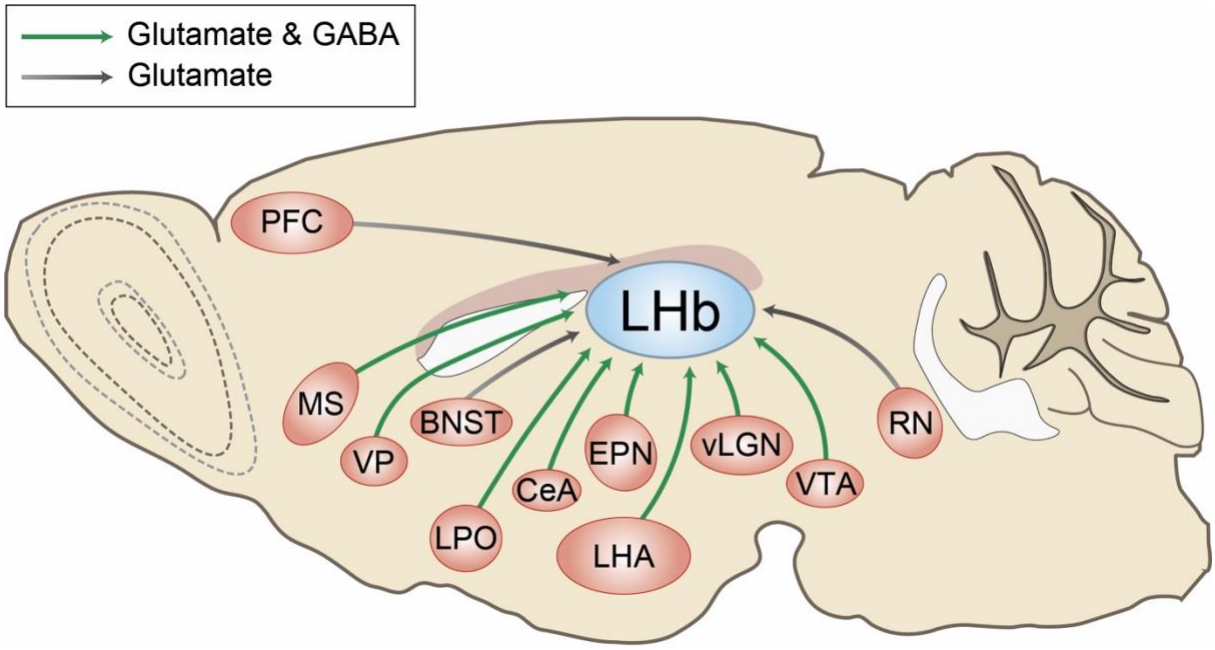

Figure 6. Upstream connectivity into the lateral habenula. The ventral tegmental area (VTA), and entopeduncular nucleus (EPN) corelease glutamate and GABA from the same terminals. The medial septum (MS), ventral pallidum (VP), lateral preoptic area (LPO), central amygdala (CeA), ventral lateral geniculate nucleus (vLGN), and lateral hypothalamic area (LHA) release glutamate and GABA either from separate neuronal populations, or without a proven corelease from the same terminals. The prefrontal cortex (PFC), bed nucleus of the stria terminalis (BNST), and raphe nuclei (RN) are excitatory inputs.

Through a conglomerate of fiber tracts known as stria medullaris, the LHb receives both excitatory and inhibitory inputs from a wide range of limbic structures including the LHA, lateral preoptic area (LPO), BNST, ventral lateral geniculate nucleus, CeA, diagonal band of Broca, PFC, ventral pallidum, and medial septum (**Figure 6**) (Warden et al., 2012; Golden et al., 2016; Stamatakis et al., 2016; Barker et al., 2017; Knowland et al., 2017; Zahm et al., 2017; Zhang et al., 2018a; Huang et al., 2019; Lazaridis et al., 2019; Zhou et al., 2019). In addition, LHb neurons are targeted by GABAergic and glutamatergic terminals from the murine entopeduncular nucleus (EPN), a main output of the basal ganglia and equivalent to the primate globus pallidus internus (Shabel et al., 2012). Finally, the habenular complex receives reciprocal connections from the monoaminergic brain centers whose firing is under habenular control, namely the VTA and raphe nuclei. Despite the expression of DA and serotonin receptors in LHb neurons, the neuromodulatory component of these synapses is yet to be studied in detail (Pompeiano et al., 1994; Aizawa et al., 2012; Muzerelle et al., 2016; Zhang et al., 2018b). Accordingly, the habenular monoaminergic inputs are considered glutamatergic and GABAergic in nature (Stamatakis et al., 2013; Root et al., 2014a; Root et al., 2014b; Yoo et al., 2016; Szőnyi et al., 2019). Overall, independently of the anatomical source of glutamate, excitation of LHb neurons is associated with the emergence of internal aversive states, as concluded from real-time place preference paradigms (Shabel et al., 2012; Root et al., 2014a; Lecca et al., 2017; Faget et al., 2018; Tooley et al., 2018). On the other hand, preference for particular contexts can be developed by silencing the presynaptic excitatory tone, or by activating presynaptic GABA release onto LHb neurons (Stamatakis et al., 2013; Stamatakis et al., 2016; Barker et al., 2017). Thus, we can conclude that excitation of LHb neurons is aversive, while their inhibition is rewarding. Despite the simple model of

excitation-aversion and inhibition-reward, there are instances in which distinct LHb inputs specialize into discrete physiological roles. For example, while hypothalamic inputs negatively regulate food consumption and are required for the execution of escape behaviors, EPN neurons signal the discrepancy between expected and actual outcomes (i.e., reward prediction error) (Stamatakis et al., 2016; Stephenson-Jones et al., 2016; Lecca et al., 2017).

The LHb targets different brain regions through an efferent pathway named fasciculus retroflexus (**Figure 7**). The most prominent output bundle emanates from the lateral aspect of the LHb, which excites GABAergic neurons in the rostromedial tegmental nucleus (RMTg) (Jhou et al., 2009b; Brinschwitz et al., 2010; Meye et al., 2016). In turn, activation of the RMTg negatively modulates the firing activity of VTA DA neurons and putative serotonin neurons in the raphe nuclei (Jhou et al., 2009a; Jhou et al., 2009b; Lecca et al., 2012; Li et al., 2019b). Besides this indirect pathway via the RMTg, excitatory terminals from medially located LHb neurons synapse directly onto GABAergic neurons of the VTA and raphe nuclei, hence reinforcing the RMTg-mediated inhibition of DA and serotonin signaling (Omelchenko et al., 2009; Brinschwitz et al., 2010; Sego et al., 2014). Furthermore, the habenular complex innervates raphe serotonin neurons and PFC-projecting VTA DA neurons (Lammel et al., 2012; Zhou et al., 2017). Less conventional LHb output regions include the noradrenergic LC, LHA, laterodorsal tegmental nucleus (LDTg) and several thalamic areas (Herkenham and Nauta, 1979; Quina et al., 2015; González et al., 2016; Namboodiri et al., 2016). However, with the exception of one study showing the functional excitation of GABAergic LDTg neurons following optogenetic activation of habenular axons (Yang et al., 2016), these alternative output structures remain poorly understood.

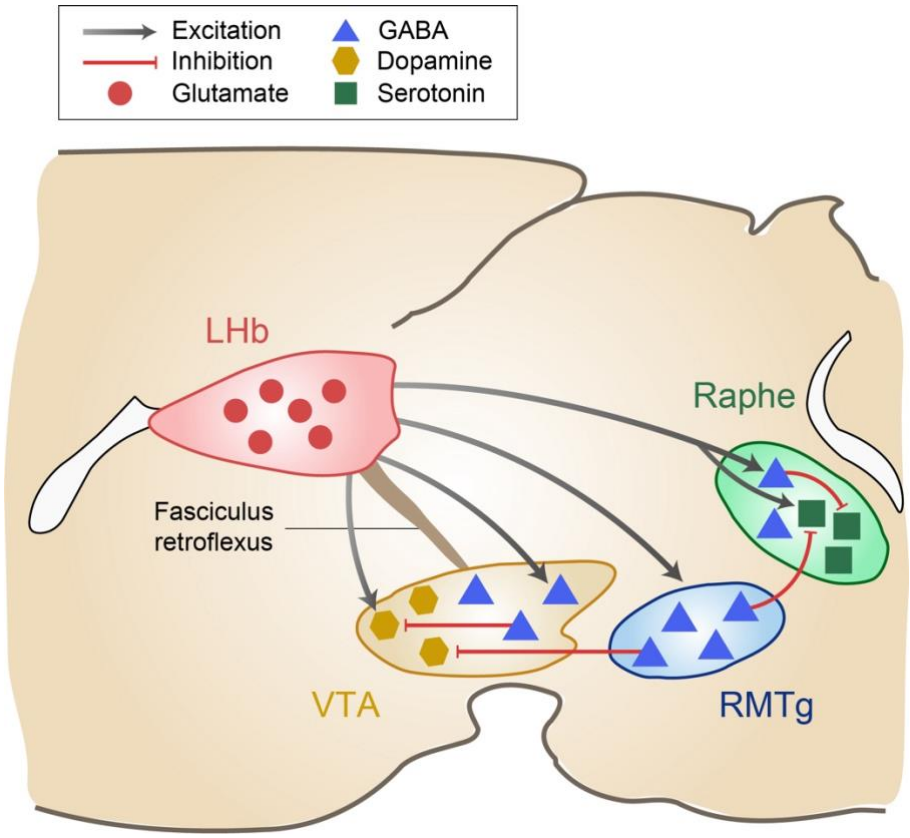

Figure 7. Downstream connectivity from the lateral habenula. LHb neurons send afferents to inhibitory neurons in the RMTg, which in turn inhibit DA neurons in the VTA and serotonin neurons in the raphe nuclei. Besides this indirect control of monoaminergic regions, the LHb innervates GABAergic neurons in both the VTA and raphe, thus reinforcing the inhibition of the DA and serotonin brain signaling. Lastly, LHb neurons synapse onto DA and serotonin neurons in the VTA and raphe, respectively.

Altogether, the upstream and downstream connectivity of the habenular complex predicts the central role of LHb neurons in stress encoding. This is the focus of the next section.

1.5.2 Stress encoding in habenular neurons

Pioneering work from Matsumoto and Hikosaka revealed that primate LHb neurons are phasically excited by the absence of an expected reward – a situation defined as reward omission (Matsumoto and Hikosaka, 2007). The authors further reported that the firing activity of LHb neurons similarly increases upon unexpected exposure to acute stressors (e.g., air puffs), as well as cues predicting imminent aversive stimuli (Matsumoto and Hikosaka, 2009). The habenular patterns of induced neuronal activity thus mirror those of VTA DA neurons (Schultz et al., 1993; Hollerman and Schultz, 1998). Emphasizing these contrasting scenarios, the LHb has earnt the designation of the "antireward" center of the brain. Since these seminal studies were conceived, LHb neurons have been reported to be consistently activated, as assessed by calcium imaging and early markers of neuronal activity, by a wide range of additional stressors including electrical foot-shocks, physical restraint, chemically-induced malaise, social defeat, maternal deprivation, and predatory odors and contours (Wirtshafter et al., 1994; Wang et al., 2017a; Lecca et al., 2017; Shabel et al., 2019). Importantly, the learned and congenital models of depression lead to chronic increases in the firing activity of LHb neurons, suggesting that their synaptic drive is persistently enhanced (Li et al., 2011; Li et al., 2013). In a milder paradigm based on 19 unpredictable foot-shocks, the aversive experience drives habenular hyperactivity and potentiates the LHb-to-RMTg connectivity (Stamatakis and Stuber, 2012). A similar phenomenon is observed in murine models of protracted maternal deprivation during infancy, physical restraint stress, and CMS (Tchenio et al., 2017; Yang et al., 2018; Cerniauskas et al., 2019). Several mechanisms contribute to the emergence of stress-driven hyperactivity in LHb neurons (**Figure 8**): (1) increased glutamate release probability from presynaptic terminals projecting onto AMPAR synapses (Li et al., 2011); (2) increased levels of βCaMKII protein within postsynaptic compartments, thereby leading to potentiated AMPAR expression and function (Li et al., 2013); (3) augmented levels of the inwardly-rectifying potassium channel Kir4.1 in astrocytes, thus facilitating NMDAR-dependent bursting modes of firing activity (Cui et al., 2018); (4) increased activity of protein phosphatase 2A (PP2A), hence reducing the postsynaptic accumulation of metabotropic $GABA_B$ receptors and ultimately weakening the habenular inhibitory tone (Lecca et al., 2016, Tchenio et al., 2017); (5) decreased GABA release from EPN terminals (Shabel et al., 2014); and (6) increased expression of the multifunctional protein p11, which interacts with various effectors such as serotonin receptors and ion channels (Seo et al., 2018). Independent rescue of these subcellular alterations prevents the manifestation of depressive-like symptoms, including anhedonia and behavioral despair. These data prove that habenular synaptic plasticity is required for the manifestation of behavioral deficits after stress exposure.

Inhibitory transmission in LHb neurons is important for the regulation of tonic firing activity and is dysregulated in pathological conditions (Lecca et al., 2016), but no evidence thus far supports its behavioral relevance during phasic encoding of stressful stimuli. Conversely, excitatory transmission has been linked with both tonic and phasic regulation of habenular firing activity, the latter in the context of reward omission encoding and threat-driven escape behaviors (Lecca et al., 2017; Shabel et al., 2019). Whilst we cannot rule out behavioral implications of GABAergic transmission during phasic stress encoding (Congiu et al., 2019), my PhD thesis focuses on glutamatergic synapses. In the next section, I will introduce ionotropic excitatory transmission, and place emphasis on the most relevant AMPAR and NMDAR properties.

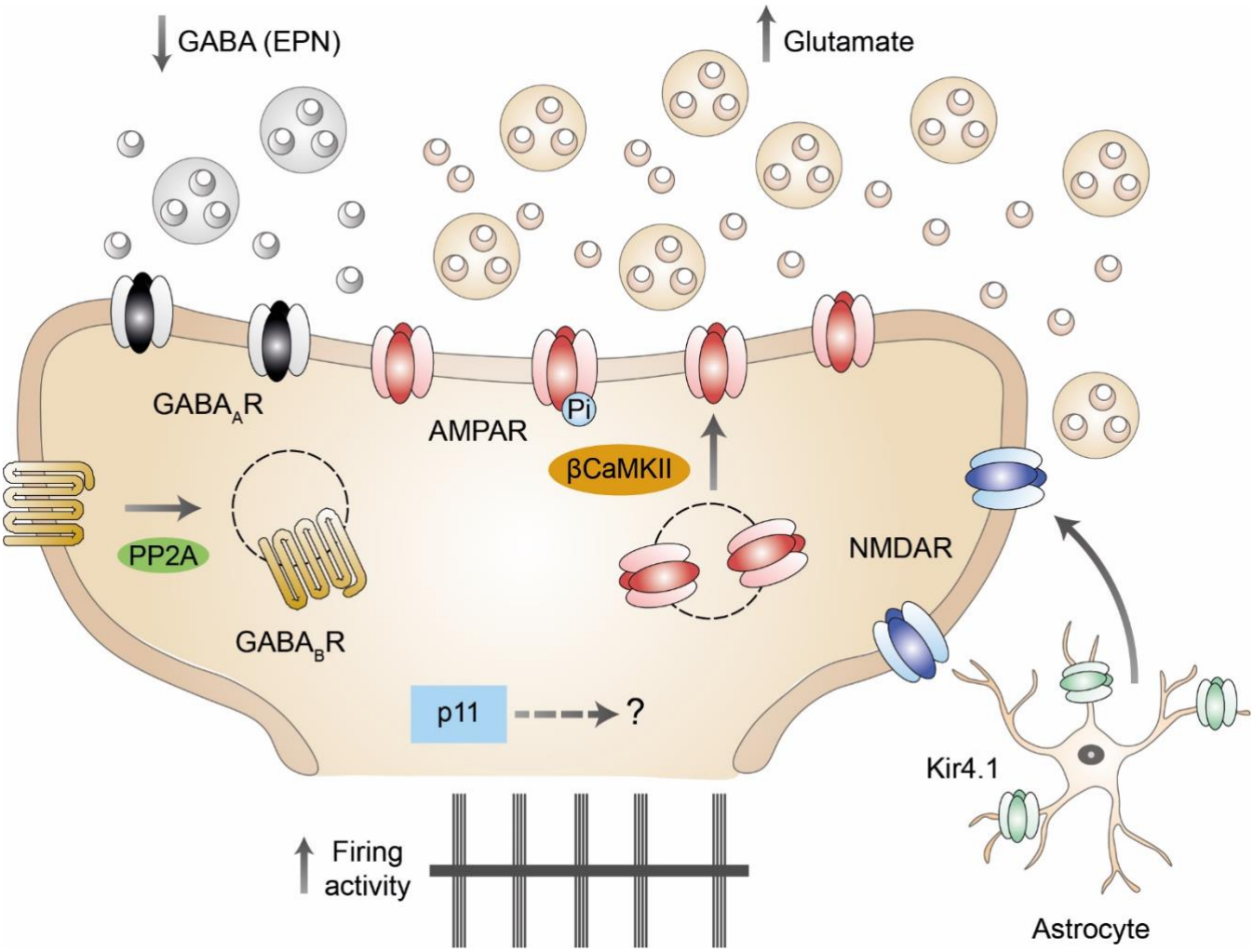

Figure 8. Different mechanisms contribute to LHb hyperactivity after inescapable stress exposure. At excitatory synapses: increased glutamate release, enhanced AMPAR function mediated by βCaMKII overexpression, and NMDAR-dependent bursting activity via astrocytic Kir4.1 overexpression. At inhibitory synapses: decreased GABA release from EPN terminals, and PP2A-mediated endocytosis of $GABA_B$ receptors. Lastly, p11 contributes to LHb hyperactivity through unknown mechanisms.

1.6 Properties of glutamate receptors

1.6.1 AMPA receptors

A fundamental mechanism for the modulation of synaptic strength is the modification of the number, composition, or biophysical properties of AMPARs within postsynaptic compartments (Huganir and Nicoll, 2013). These glutamate-gated receptors are constituted by the combination of alternative subunits (GluA1-GluA4) (Hollmann and Heinemann, 1994). Four of these subunits assemble into the core functional channel, which is permeable to sodium and, under certain conditions, calcium (**Figure 9**) (Linden et al., 1993; Vandenberghe et al., 2000). AMPAR opening takes place when the ligand glutamate is released from presynaptic terminals, driving the flow of extracellular cations into the postsynaptic compartment in favor of their electrochemical gradient (Bennay et al., 2008). The resulting neuronal depolarization, above a certain threshold, triggers the generation of action potentials (Andreasen and Lambert, 1998; Schöne et al., 2012). Importantly, the AMPAR calcium permeability is lost when the GluA2 subunit is present, due to the electrostatic repulsion induced by a positively-charged arginine residue located in the channel pore (Geiger et al., 1995; Swanson et al., 1997). This arginine residue concomitantly prevents the blockade of the cytoplasmic face of the channel by intracellular polyamines, a phenomenon that accounts for the linear current-voltage relationship of the GluA2-containing AMPARs (Kamboj et al., 1995; Liu and Cull-Candy, 2000). This biophysical property deeply contrasts with the inward rectification observed at positive potentials in GluA2-lacking and calcium-permeable AMPARs, where the arginine residue is replaced by a non-charged glutamine (Burnashev et al., 1992a). Calcium-permeable AMPARs, the predominant subtype in LHb neurons, are of particular importance because their levels are modulated during physiological processes such as LTP (Maroteaux and Mameli, 2012). Moreover, these receptors are characterized by faster inactivation kinetics and larger conductance, contributing to the overall enhancement of synaptic transmission (Clem and Huganir, 2010).

The biophysical properties of AMPARs are finely tuned according to various forms of posttranslational modifications within their intracellular carboxy-terminal tail (Lussier et al., 2015). For example, GluA1 phosphorylation at Serine-831 (calcium-calmodulin kinase II, CaMKII) or Serine-845 (protein kinase A, PKA) results in higher single-channel conductance, greater open probability, and enhanced targeting and retention to postsynaptic densities (Mammen et al., 1997; Barria et al., 1997; Derkach et al., 1999; Man et al., 2007). The degree and nature of the AMPAR posttranslational modifications largely depend on the sequence and length of their cytoplasmic tail. In this regard, AMPAR subunits can be categorized as long-tailed or short-tailed. The former includes GluA1, GluA4 and a long splicing form of GluA2 (GluA2L), while the latter includes GluA2, GluA3 and a short splicing form of GluA4 (GluA4S) (Shepherd and Huganir, 2007). The distinction between these two AMPAR forms has important physiological consequences. Indeed, while the levels of long-tailed AMPARs are extensively modulated by changes in network activity, for example upon LTP induction, the short-tailed variants go through constitutive cycling within synaptic compartments (Hayashi et al., 2000; Shi et al., 2001).

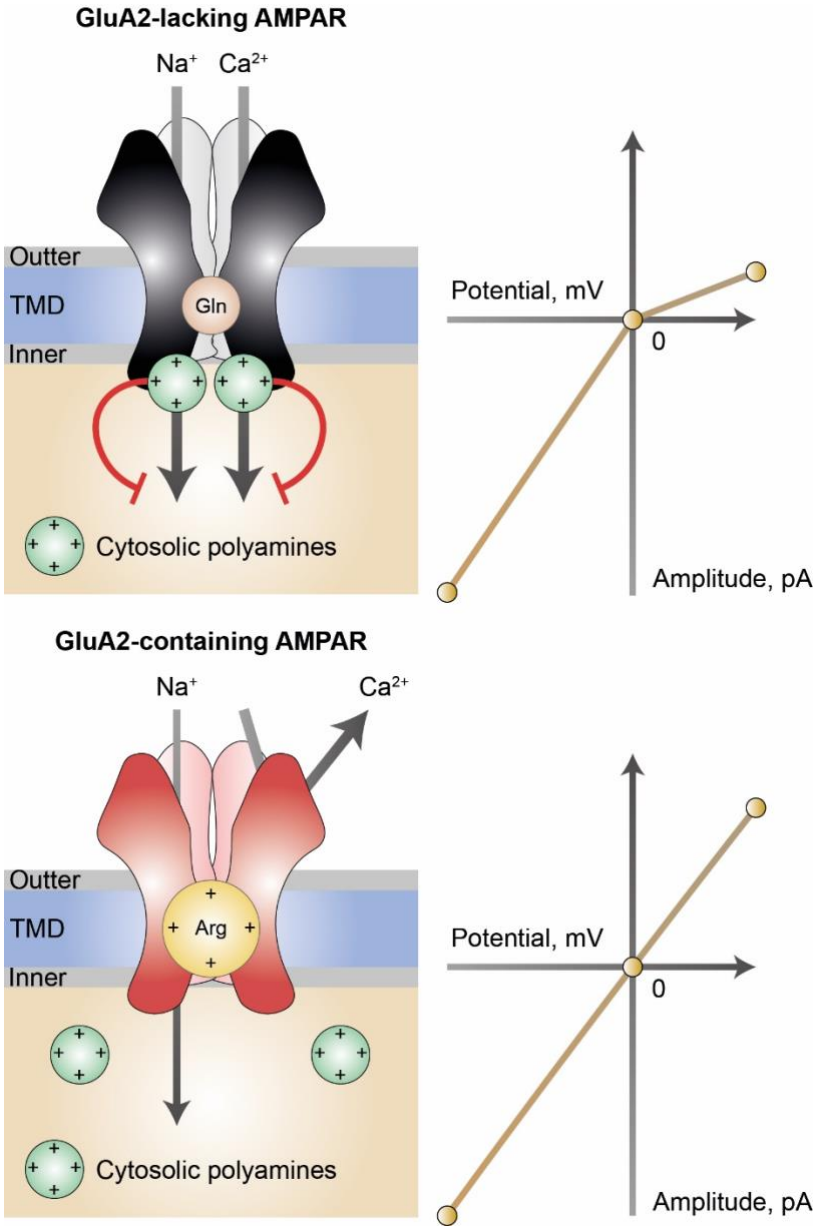

Figure 9. AMPAR subunit composition dictates the biophysical properties of the channel. In GluA2-lacking AMPARs, the neutral glutamine residue (Gln) within the channel transmembrane domain (TMD) allows the influx of bivalent calcium ions, and maximizes the influx of monovalent sodium ions. Given the absence of charge in the Gln side chains, cytosolic polyamines can interact with the intracellular face of the channel at positive potentials, hence rendering the inward rectification in current-voltage relationship. Conversely, in GluA2-containing AMPARs, Gln is replaced by a positively-charged arginine (Arg). This substitution impedes the influx of calcium ions, diminishes the influx of sodium ions, and prevents the interaction of polyamines with the channel TMD, ultimately explaining the linear current-voltage relationship of these receptors.

Besides the role of posttranslational modifications, the AMPAR properties are regulated based on their dynamic interactions with auxiliary subunits. The principal families of accessory proteins are the transmembrane AMPAR regulatory proteins (TARP) and cornichon-like proteins (CNIH) (Tomita et al., 2003; Schwenk et al., 2009). AMPARs might interact with up to four auxiliary subunits, and TARPs and CNIHs compete for the same binding sites (Straub and Tomita, 2012; Herring et al., 2013). Both protein families lead to slower decay kinetics upon AMPAR interaction, and thereby potentiate glutamatergic transmission (Cho et al., 2007; Herring et al., 2013). TARP subunits contain an intracellular carboxy-terminal tail capable of interacting with PSD95 and additional scaffolding proteins typical of excitatory synapses, as well as with membrane lipids (Nicoll et al., 2006; Bats et al., 2007). Such interactions contribute to AMPAR stabilization at postsynaptic compartments, thus explaining why TARP-devoid synapses display low AMPAR levels (Chen et al., 2000; Fukaya et al., 2006). Similarly, CNIH depletion from synapses leads to decreased AMPAR transmission (Herring et al., 2013).

AMPAR trafficking, defined as the mobilization across different subcellular pools, is also susceptible to modulation. Two GTPase families of the Ras superfamily, Rac and Rab, are particularly important for the regulation of AMPAR dynamics. These enzymes hydrolyze GTP into GDP and, in the process, release energy that can be employed in diverse cellular processes (Ridley et al., 2003; Hausser and Schlett, 2019). Examples of such processes include vesicle formation, movement and fusion, as well as trafficking of vesicular cargo (e.g., AMPAR). The GTPase Rac1 has been linked to postsynaptic AMPAR clustering and spine formation during synaptogenesis, and also contributes to the expression of LTP (Wiens et al., 2005; Haditsch et al., 2009). In the case of Rab proteins, a more complex picture emerges. During LTP, AMPARs are transferred from endosomal compartments into extrasynaptic sites within dendritic spines, a process mediated by Rab11, to subsequently be mobilized to synapses in a Rab8-dependent fashion (Gerges et al., 2004; Brown et al., 2007). During the opposite phenomenon of long-term depression (LTD), Rab5 mediates the internalization of synaptic AMPARs into early endosomes (Brown et al., 2005). These early endosomes can then be degraded through the lysosomal pathway, in a process governed by Rab7, or reintroduced into dendrites via the Rab11 recycling pathway (Fernández-Monreal et al., 2012).

I have discussed above the biophysical properties of AMPARs and their three principal sources of modulation (posttranslational modifications, interaction with auxiliary subunits, and trafficking). I will now explain the key features of the complementary NMDAR transmission.

1.6.2 NMDA receptors

These receptors are tightly involved in gating diverse mechanisms of neuronal plasticity, by which timely changes in network activity culminate in long-term alterations of synaptic structure and function (Paoletti et al., 2013). There are various NMDAR subunits (GluN1, GluN2A-D and GluN3A-B) (Traynelis et al., 2010). Four of these subunits assemble into the core functional channel, which is permeable to sodium and calcium (Burnashev et al., 1992b; Yu and Salter, 1998). NMDAR tetramers always contain two GluN1 subunits, whereas the remaining combinations of GluN2 and GluN3 are specific to brain region, neuronal subtype, and even cellular localization (Monyer et al., 1994; Fritschy et al., 1998; Kumar and Huguenard, 2003). Heterodimeric tetramers have identical non-GluN1 subunits, while heterotrimeric variants are composed of disparate non-GluN1 subunits (Sheng et al., 1994). The most abundant NMDAR assemblies throughout the mature brain are heterodimeric GluN1/2A, heterodimeric GluN1/2B, and heterotrimeric GluN1/2A/2B (Al-Hallaq et al., 2007; Rauner and Köhr, 2011).

Several biophysical properties are unique to NMDARs. First, despite being gated by glutamate, glycine is required as co-agonist for enabling the channel opening (Johnson and Ascher, 1987). Second, NDMARs display high permeability for calcium (MacDermott et al., 1986). Third, NMDAR conductance is greatly diminished at negative potentials, due to the channel blockade by magnesium ions (Coan and Collingridge, 1985). This observation, apart from explaining why most NMDAR electrophysiological studies are performed at positive potentials, also justifies non-linear integrations detected within dendritic spines (Branco et al., 2010). Lastly, the decay of NMDAR currents is protracted due to the slow kinetics of glutamate unbinding – a crucial phenomenon for the integration of temporally adjacent inputs across nearby synapses (Lester et al., 1990; Vergnano et al., 2014). As with AMPARs, NMDAR subunit composition also

influences the biophysical properties of the channel. Heterodimeric GluN2A and GluN2B receptors show greater sensitivity to magnesium blockade, higher single-channel conductance, and augmented calcium permeability when compared to heterodimeric GluN2C and GluN2D receptors (Siegler Retchless et al., 2012). Furthermore, GluN2A subunits confer high open probability and fast deactivation kinetics, the latter due to their relatively low affinity to glutamate and glycine (Vicini et al., 1998; Erreger et al., 2005).

1.6.3 NMDAR-dependent AMPAR plasticity

Despite the fact that NMDARs might undergo plasticity of their own, their primary function is ascribed to providing the calcium source for gating AMPAR adaptations (Kwon and Castillo, 2008; Rebola et al., 2008; Harnett et al., 2009). For example, while synapses in hippocampal mossy fibers lack the ability to undergo AMPAR LTP under basal conditions, an increase in NMDAR levels unmasks this plasticity (Rebola et al., 2011). The direction of NMDAR-driven AMPAR plasticity, either LTP or LTD, is governed by the extent and kinetics of the postsynaptic calcium transient (**Figure 10**) (Lüscher and Malenka, 2012). Large calcium transients are required for LTP induction, a process that is facilitated by the simultaneous engagement of presynaptic glutamate release and postsynaptic depolarization (Crair and Malenka, 1995; Isaac et al., 1997). Under these circumstances, the magnesium blockade is released from the NMDAR pore and calcium ions can extensively permeate through the channel. Calcium then leads to the activation of CaMKII, the kinase responsible for increasing the single-channel conductance of AMPARs and driving their synaptic insertion (Benke et al., 1998; Derkach et al., 1999; Shi et al., 1999; Lisman et al., 2002). By contrast with LTP, LTD takes place in the absence of postsynaptic depolarization. Under these conditions, magnesium greatly diminishes calcium influx through NMDARs (Jahr and Stevens 1993; Sabatini et al., 2002). The modest increase in cytoplasmic calcium concentrations is not sufficient to activate CaMKII, but successfully stimulates the phosphatase calcineurin, among others, which displays high affinity for calcium (Lisman 1989; Mulkey et al., 1994). As a result, the dephosphorylation of AMPARs reduces single-channel conductance and promotes their endocytosis via clathrin-coated vesicles (Lüscher et al., 1999). Importantly, LTP- and LTD-driven changes in AMPAR biophysical properties and trafficking dynamics are concomitant with opposite structural changes. Indeed, while LTP is associated with spine enlargement and appearance, LTD leads to spine shrinkage and collapse (Toni et al., 2001; Matsuzaki et al., 2004; Nägerl et al., 2004; Zhou et al., 2004). Altogether, the combination of functional and structural alterations accounts for the final modulation of synaptic strength.

Whether NMDAR-dependent calcium influx leads to LTP or LTD is influenced by NMDAR subunit composition. Certain studies have suggested that heterodimeric GluN2A receptors are required for LTP, while their GluN2B counterparts are instead required for LTD (Sakimura et al., 1995; Sprengel et al., 1998; Liu et al., 2004; Brigman et al., 2010). However, extensive evidence diminishes the validity of such a simplistic scenario, in favor of a more comprehensive framework (Tang et al., 1999; Barria and Malinow, 2005). It is currently accepted that both heterodimeric GluN2A and heterotrimeric GluN2A/2B receptors are important for LTP induction (Müller et al., 2009). The former ensures a large calcium transient due to the high open probability, while the latter provides a scaffolding complex to recruit important proteins for LTP (e.g., CaMKII) (Erreger et al., 2005; Foster et al., 2010; Halt et al., 2012). Supporting the contribution of GluN2B to LTP, increasing GluN2B/2A ratio broadens the range of stimulation frequencies conducive to LTP, while narrowing the range for LTD (Kopp et al., 2006; Yashiro and Philpot, 2008).

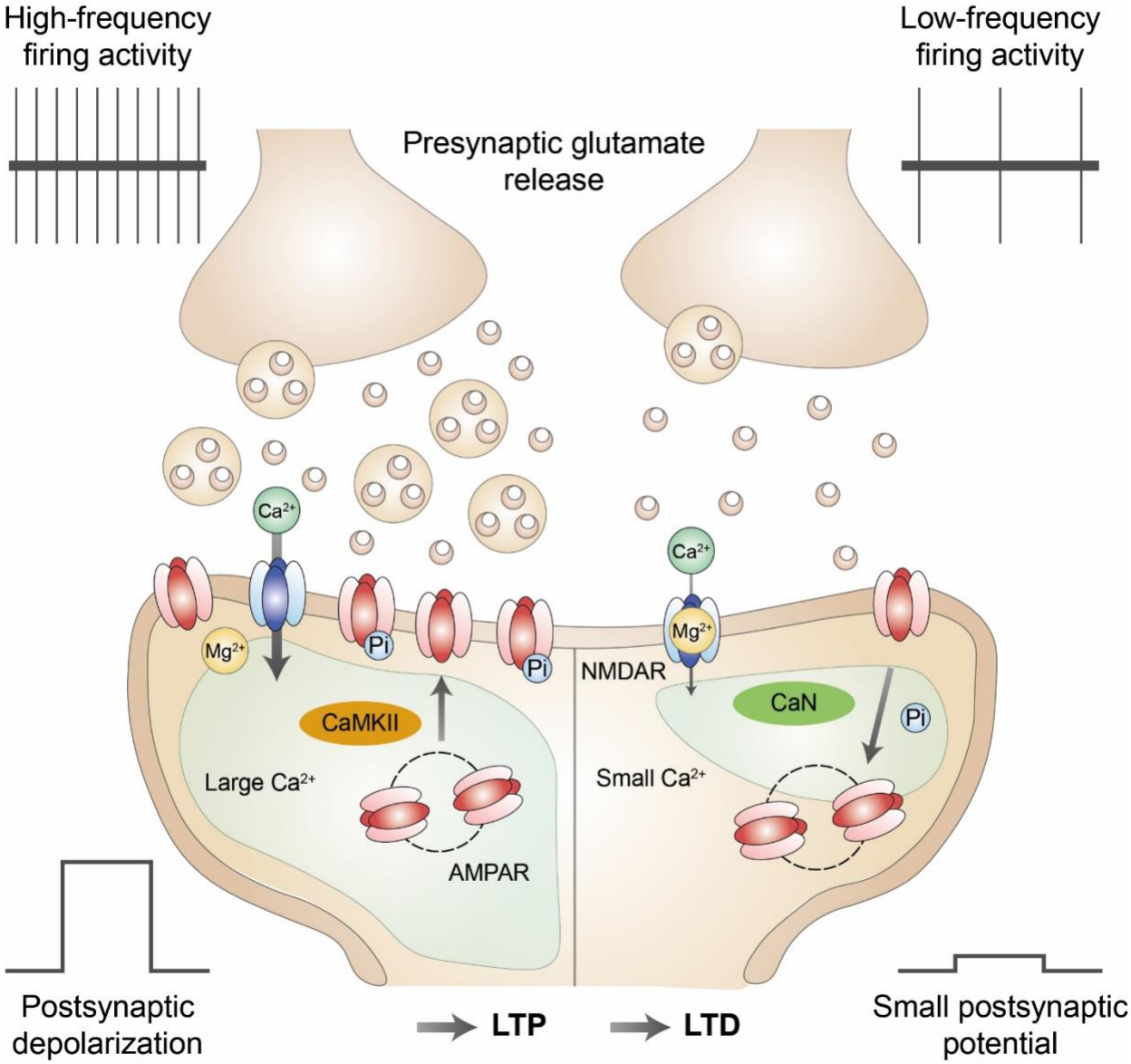

Figure 10. NMDAR-dependent LTP/LTD are triggered by different subcellular mechanisms. LTP occurs through the coincident detection of high-frequency glutamate release from presynaptic terminals and postsynaptic depolarization. Under these circumstances, the NMDAR magnesium block is relieved and calcium can permeate extensively into the dendrite. This results in the activation of CaMKII, thus driving AMPAR insertion into the membrane and increasing their conductance through phosphorylation. LTD, on the other hand, is achieved through the low-frequency stimulation of glutamate release. In the absence of postsynaptic depolarization, calcium influx through NMDARs is vastly reduced. This triggers a small postsynaptic calcium signal, sufficient to activate the protein the phosphatase calcineurin (CaN), thereby promoting AMPAR endocytosis and decreasing their conductance through dephosphorylation.

Apart from the NMDAR subunit composition, additional factors modulate the NMDAR-dependent synaptic plasticity of AMPAR transmission. LTP is regulated by interactions between diverse cell-adhesion molecules, including neuroligins (NLGN1-4) and neurexins (NRXNα-β). Postsynaptic NLGNs are located within dendritic spines, and they act as the ligands of presynaptic NRXN proteins (Südhof, 2008). Several lines of evidence support the contribution of these proteins to synaptic plasticity. Functional and structural variants of NMDAR-dependent LTP, classically triggered by high-frequency stimulation in hippocampal pyramidal neurons, rely upon the interaction between NLGN1 and NRXNβ (Jiang et al., 2017; Wu et al., 2019). Interestingly, despite NLGN3 not being a requirement for LTP, gain-of-function mutations enhance the extent of potentiation (Etherton et al., 2011). Moreover, a certain sequence of alternative splicing must be removed from presynaptic NRXN proteins in order to enable LTP induction (Aoto et al., 2013). The role of NLGN and NRXN in synaptic depression remains to be characterized, although a recent study reported the lack of AMPAR LTD following the reduction in NLGN1 levels (Dang et al., 2018). Therefore, we can conclude that NMDAR-dependent plasticity of AMPAR transmission is influenced by interactions between pre- and postsynaptic adhesion molecules.

Overall, I have highlighted the most relevant characteristics of AMPAR and NMDAR transmission at excitatory synapses. The subunit composition of these receptors is a key determinant of their biophysical properties at baseline. However, a richness of additional players come into the picture in order to facilitate a more sophisticated tuning, especially in the case of AMPARs. Lastly, we have discussed the interaction between both families of receptors, underscoring the NMDAR role in the induction of AMPAR synaptic plasticity.

The next two chapters encompass the results of my doctoral work. In the second chapter, where I participated in the category of collaborator, we elucidated the synaptic and circuit mechanisms required for avoidance learning during escapable stress exposure (Trusel et al., 2019). In the third chapter, which contains most of the effort and energy required for the completion of my thesis, we unraveled synaptic plasticity rules that underlie reward-seeking deficits after exposure to inescapable stressors (Nuno-Perez et al., 2021).

Chapter 2: Assessing the role of LHb neurons during avoidance learning

The odor of expired meals prompts us to discard them at the expense of consumption, an action that protects us from sickness. This is an example where the association between a predictive sensory cue and a negative outcome triggers an instrumental action in order to avoid harmful stimuli. While the neuronal underpinnings for cue-punishment association have been extensively studied during fear conditioning, the synaptic correlates of threat prediction and escape are poorly understood (Maren et al., 2013; LeDoux et al., 2017). LHb neurons respond to negative outcomes and are required for innate escape behaviors (Lecca et al., 2017). Similarly, following a conditioning period, sensory cues preceding an aversive stimulus lead to habenular excitation (Matsumoto and Hikosaka, 2007). These data raise the possibility that cue-punishment associations in LHb neurons may support motor execution during avoidance learning. In terms of circuitry, the habenular complex receives extensive excitatory afferents from several brain structures, including the LHA, EPN and the medial VTA (Shabel et al., 2012; Stamatakis et al., 2013; Stamatakis et al., 2016). These inputs guide motivated behaviors and undergo experience-dependent alterations (Shabel et al., 2014; Lecca et al., 2017; Park et al., 2017; Tchenio et al., 2017). However, whether synaptic plasticity within discrete habenular circuits is required for avoidance learning remains unknown.

In the present study, we first employed fiber photometry to measure calcium dynamics as a proxy for neuronal activity in LHb neurons, as mice were trained in an active avoidance paradigm. This approach revealed that avoidance learning leads to the progressive recruitment of habenular excitation during the presentation of foot-shock-predictive cues. My contribution to this article was important during the second part of the study, where I performed whole-cell patch-clamp recordings in acute brain slices at different phases of avoidance learning (Figure 2, S2 and 3). These recordings led us to conclude that (1) cue-outcome associations drive a transient potentiation of AMPAR synapses – a phenomenon that occludes expression of NMDAR-dependent LTP, and arises specifically at LHA-to-LHb connections, and (2) the incidence of avoidance responses positively correlates with the strength of habenular excitatory synapses – a critical finding to establish the causal link between synaptic plasticity and action execution. Finally, combining optogenetic manipulations with the modulation of synaptic efficacy, we demonstrated that effective avoidance learning depends on reliable hypothalamic signals and intact AMPAR synapses in LHb neurons. Altogether, these observations broaden our understanding of how the brain encodes the avoidance of escapable stressors via instrumental cue-punishment associations.

The following section includes the manuscript related to this topic, as published in Neuron.

Report

Neuron

Punishment-Predictive Cues Guide Avoidance through Potentiation of Hypothalamus-to-Habenula Synapses

Highlights

- Punishments and punishment-predictive cues excite LHb neurons
- Avoidance learning strengthens hypothalamus-to-LHb excitation
- Hypothalamic inputs and AMPAR potentiation underlie avoidance

Authors

Massimo Trusel, Alvaro Nuno-Perez, Salvatore Lecca, ..., Takuya Takahashi, Francesco Ferraguti, Manuel Mameli

Correspondence

manuel.mameli@unil.ch

In Brief

Learning to predict a threat is crucial for survival. Trusel et al. identify the plasticity of neural circuit elements within the lateral habenula as a mechanism instrumental in guiding anticipation and avoidance of external aversive events.

Trusel et al., 2019, Neuron *102*, 120–127
April 3, 2019
https://doi.org/10.1016/j.neuron.2019.01.025

CellPress

CellPress

Neuron
Report

Punishment-Predictive Cues Guide Avoidance through Potentiation of Hypothalamus-to-Habenula Synapses

Massimo Trusel,[1] Alvaro Nuno-Perez,[1] Salvatore Lecca,[1] Harumi Harada,[3] Arnaud L. Lalive,[1] Mauro Congiu,[1] Kiwamu Takemoto,[4] Takuya Takahashi,[4] Francesco Ferraguti,[3] and Manuel Mameli[1,2,5,*]
[1]Department of Fundamental Neuroscience, University of Lausanne, 1005 Lausanne, Switzerland
[2]Inserm, UMR-S 839, 75005 Paris, France
[3]Department of Pharmacology, Medical University of Innsbruck, 6020 Innsbruck, Austria
[4]Department of Physiology, Graduate School of Medicine, Yokohama City University, 236-0004 Yokohama, Japan
[5]Lead Contact
*Correspondence: manuel.mameli@unil.ch
https://doi.org/10.1016/j.neuron.2019.01.025

SUMMARY

Throughout life, individuals learn to predict a punishment via its association with sensory stimuli. This process ultimately prompts goal-directed actions to prevent the danger, a behavior defined as avoidance. Neurons in the lateral habenula (LHb) respond to aversive events as well as to environmental cues predicting them, supporting LHb contribution to cue-punishment association. However, whether synaptic adaptations at discrete habenular circuits underlie such associative learning to instruct avoidance remains elusive. Here, we find that, in mice, contingent association of an auditory cue (tone) with a punishment (foot shock) progressively causes cue-driven LHb neuronal excitation during avoidance learning. This process is concomitant with the strengthening of LHb AMPA receptor-mediated neurotransmission. Such a phenomenon occludes long-term potentiation and occurs specifically at hypothalamus-to-habenula synapses. Silencing hypothalamic-to-habenulainputs or optically inactivating postsynaptic AMPA receptors within the LHb disrupts avoidance learning. Altogether, synaptic strengthening at a discrete habenular circuit transforms neutral stimuli into salient punishment-predictive cues to guide avoidance.

INTRODUCTION

The sound of a fire alarm guides a rapid action to immediately ensure safety. This is an instance where associating environmental cues to aversive events grants individuals to predict and avoid threats, a primary strategy for survival. Neurons in the lateral habenula (LHb) are instrumental in processing aversive events and guide innate escape behaviors. Unexpected punishments or disappointment phasically excite LHb neurons (Lecca et al., 2017; Matsumoto and Hikosaka, 2007; Wang et al., 2017). Importantly, after conditioning, punishment-predictive external cues are also efficient in driving LHb neuronal excitation (Matsumoto and Hikosaka, 2007). This suggests that the LHb may support cue-punishment learning. Such process is instrumental for adaptive behavioral strategies, including avoidance, a cardinal mechanism allowing individuals to prevent the predicted punishment (LeDoux et al., 2017).

Glutamatergic inputs from brain structures, including the lateral hypothalamus (LH), the medial ventral tegmental area (mVTA), and the entopeduncular nucleus of the basal ganglia (EPN) increase LHb neuronal activity and guide aversive behaviors (Root et al., 2014; Stamatakis et al., 2016; Shabel et al., 2012). Importantly, such excitatory synapses can undergo activity-dependent synaptic plasticity (Valentinova and Mameli, 2016). Moreover, in pathological conditions, pre- and postsynaptic modifications of glutamatergic neurotransmission alter LHb neuronal output and ultimately underlie depressive-like states (Lecca et al., 2016; Li et al., 2011; Meye et al., 2015). Altogether, this evidence supports the notion that synaptic plasticity at discrete inputs onto LHb synapses tunes LHb neurons firing and is causal for specific behavioral outcomes.

Long-term potentiation (LTP) of excitatory transmission is crucial for learning processes and enables neuronal networks to represent a memory (Nabavi et al., 2014). Yet, whether synaptic adaptations within habenular circuits represent a cellular substrate for associative learning occurring during avoidance remains poorly understood.

Here, we examined whether cue-punishment associations and the subsequent cue-driven avoidance (1) engage LHb neuronal dynamics and (2) require pathway-specific synaptic plasticity.

RESULTS

Punishment-Predictive Cues Excite LHb Neurons during Avoidance Learning

Aversive events or their predictors lead to a time-locked phasic excitation of LHb neurons (Matsumoto and Hikosaka, 2007). Here, we examined the progression of LHb neuronal dynamics throughout cue-punishment association and avoidance learning.

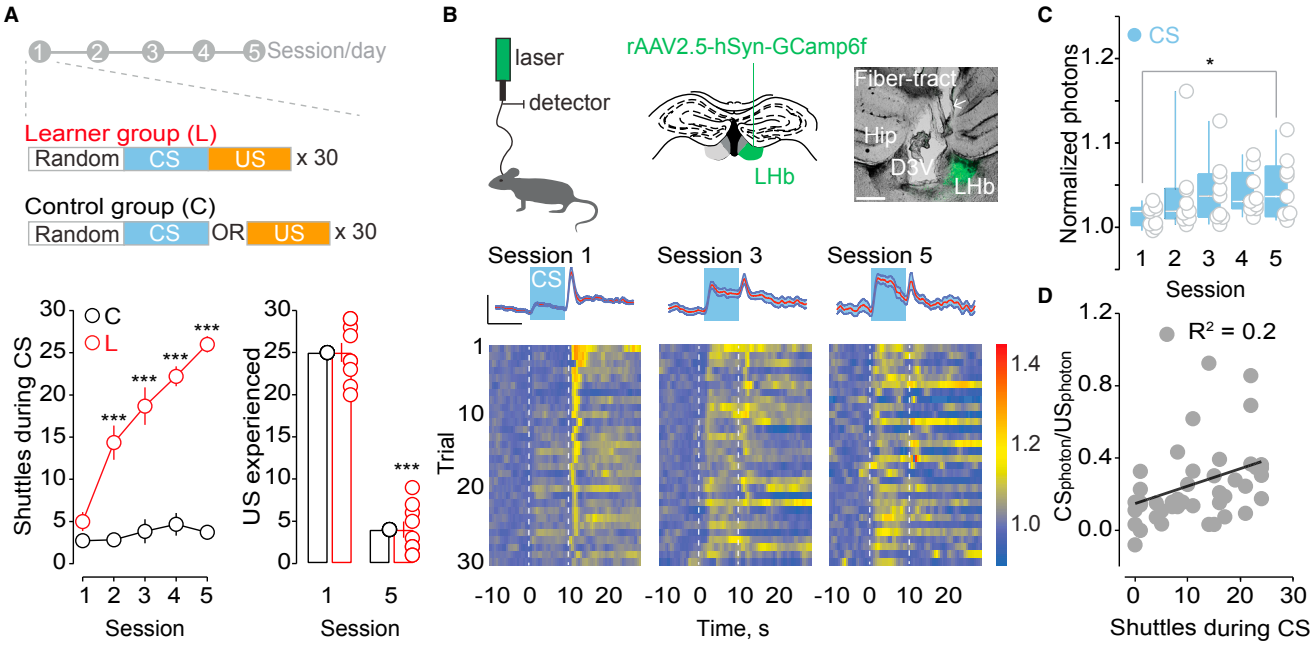

Figure 1. Excitation of LHb Neurons by Aversion-Predictive Cues Develops during Avoidance Learning

(A) Behavioral protocol; time course and bar graph with scatterplot illustrating avoidance rate along 5 sessions (controls [C], [black] $n_{animals}$ = 7, learners [L], [red] $n_{animals}$ = 9; two-way repeated-measures ANOVA, main effect of training protocol, session, and interaction, ***p < 0.001; % US received: session 1, C = 100%, L = 83.4% ± 3.8%; session 5, C = 100% ± 0%, L = 13.3% ± 3.2%, L: session 1 versus session 5, t test, t_{8} = 18.4, ***p < 0.001).

(B) Protocol, injection site, and image illustrating GCamP6f expression in the LHb (500 μm); sample heatmap and traces (100 photons; 10 s) of normalized fluorescence signal after CS (0–10 s, blue) and US (onset 10 s) across the 30 trials on days 1, 3, and 5.

(C) Box and scatterplot summarizing the normalized fluorescence (max photons/baseline) upon CS across sessions (n = 9; repeated measures [RM] one-way ANOVA; Dunnett's D1 versus D5; q_{8} = 3.3; *p = 0.03).

(D) Scatterplot and correlation analysis for avoidance scores and the CS-US fluorescence across the sessions (n = 9; Spearman r = 0.448; *p = 0.047; R^2 represents the goodness of fit).

Data are represented with boxplots (median and quartiles) or mean ± SEM. See also Figure S1.

To model cue-punishment associative learning and subsequent cue-guided avoidance, we employed a two-way active avoidance task (LeDoux et al., 2017). During 5 sessions (1 session/day; 30 trials/session), mice experienced a tone (conditioned stimulus [CS], 10 s) followed by a foot shock (unconditioned stimulus [US]). Foot-shock delivery would stop if mice crossed compartments (shuttles; Figure S1A). We examined avoidance learning by computing goal-directed shuttles during the CS. Mice progressively improve their shuttling performance, thereby preventing shock occurrence (learner group [L]; Figure 1A). In contrast, control mice received similar amount of foot shocks and tones (compared to L-mice), but CS and US were never contingent (control group, [C]; Figure 1A).

To examine LHb neurons' activity during avoidance learning, we employed photometric analysis of calcium-mediated fluorescent transients—used as a proxy for neuronal activity (Lecca et al., 2017). We virally expressed the fluorescent Ca^{2+} sensor GCaMP6f unilaterally in the LHb and implanted a multimodal fiber optic above the injection site to collect the emitted photons (Figures 1B and S1B). Post hoc analysis indicated that ~69% (2,596/3,729 neurons; 4 mice) of the LHb neuronal population expressed GCaMP6f and was glutamatergic (i.e., EAAC1+; Figures S1C and S1D).

During the first training session, calcium fluorescent transients were time locked to foot-shock delivery, with minimal transients evoked during CS presentation (Figures 1A and 1B). During subsequent training days, while cue-punishment association and cue-driven shuttles progressed, fluorescent transients were typically observed in response to both foot shock and CS onset (day 3; Figures 1B, 1C, and S1E). The CS-driven phasic fluorescent responses, measured at the peak, gradually developed over the sessions to become, at day 5, significantly larger than day 1 (Figure 1C). CS-driven fluorescent transients were learning driven and GCamp6f mediated, as they were absent across the five sessions in control mice and GFP-only-expressing learner animals (Figures S1E and S1F). In contrast, the amplitude of US-driven transients remained comparable across training sessions, supporting the stability over time of the photometric signal (Figures S1E and S1G–S1I). Consistently, the ratio $CS_{photons}/US_{photons}$ at each session from individual learner mice correlated with the number of shuttle events during the CS (Figure 1D). Finally, single-unit recordings in awake mice corroborated that CS-driven LHb neurons excitation occurs in learner, but not control, mice (Figure S1J). Altogether, these data indicate that the transition from neutral to punishment-valued cues during avoidance learning associates with cue-evoked LHb neuronal excitation.

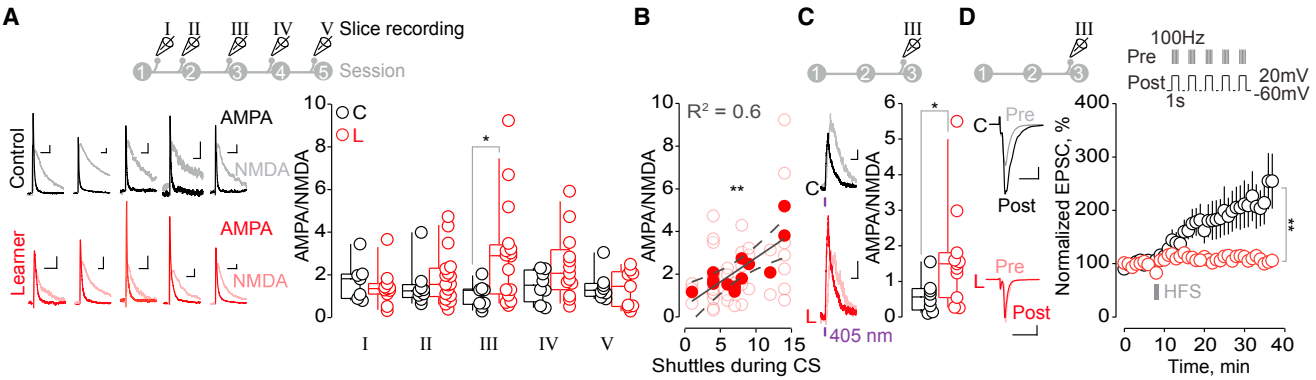

Figure 2. Transient Synaptic Potentiation onto LHb Neurons during Avoidance

(A) Timeline and sample traces (10 pA; 20 ms) representing AMPAR and NMDAR-EPSCs (+40 mV). Box and scatterplot of the AMPAR/NMDAR ratios (session I, 1 h after session 1: C [black] 1.7 ± 0.4, $n_{cells/animals}$ = 7/3; L [red] 1.6 ± 0.4, $n_{cells/animals}$ = 7/3; t test, t_{12} = 0.29, p > 0.05; II, 24 h after session 1: C 1.5 ± 0.3, $n_{cells/animals}$ = 9/3; L 1.8 ± 0.3, $n_{cells/animals}$ = 18/4; t test, t_{25} = 0.87, p > 0.05; III, 24 h after session 2: C 1.1 ± 0.2, $n_{cells/animals}$ = 10/6; L 3.0 ± 0.6, $n_{cells/animals}$ = 16/7; t test, t_{24} = 2.5, *p = 0.02; IV, 24 h after session 3: C 1.5 ± 0.3, $n_{cells/animals}$ = 8/2; L 2.4 ± 0.4, $n_{cells/animals}$ = 13/2; t test, t_{19} = 1.58, p > 0.05; V, 24 h after session 4: C 1.5 ± 0.2, $n_{cells/animals}$ = 8/4; L 1.4 ± 0.3, $n_{cells/animals}$ = 9/4; t test, t_{15} = 0.26, p > 0.05).

(B) Avoidance scores plotted in function of AMPAR/NMDAR ratios (learners, empty circles, single cells; filled circles, average value/mouse; session I, II, and III; correlation value/mouse; Spearman r = 0.766, **p = 0.003, R^2 represents the goodness of fit).

(C) Same as (A) but with MNI-glutamate uncaging (C [black] 0.6 ± 0.2, $n_{cells/animals}$ = 8/2; L [red] 1.7 ± 0.4, $n_{cells/animals}$ = 11/3; Mann-Whitney, U = 19, *p = 0.04).

(D) Amplitude versus time plot and sample traces (50 pA; 10 ms) of EPSCs before (light line) and after (dark line) HFS-pairing protocol (average $EPSC_{34\text{-}36\ min}$: C [black], 208.1 ± 38.4 $n_{cells/animals}$ = 7/3; L [red], 107.5 ± 11.8, $n_{cells/animals}$ = 7/3; t test, t_{12} = 2.5, **p = 0.03).

Data are represented with boxplots (median and quartiles) or mean ± SEM. See also Figure S2.

Avoidance Learning and Synaptic Potentiation in the LHb

Potentiation of excitatory synapses represents a neurobiological substrate underlying the association between cues and salient experiences. Accordingly, LTP may support the emergence of cue-valued excitation of midbrain dopamine neurons during reward-prediction learning (Stuber et al., 2008).

We therefore tested the prediction that synaptic strengthening of excitatory transmission onto LHb neurons represents a core mechanism for cue-driven avoidance learning. To examine excitatory synaptic transmission onto LHb neurons along the progression of avoidance learning, we performed *ex vivo* patch-clamp experiments in LHb-containing acute slices from control and learner mice. Evoked excitatory postsynaptic currents (EPSCs) were recorded at different timings during the training—∼1 h after session one (I) and 24 h after sessions one (II), two (III), three (IV), and four (V; Figure 2A). Bath application of the NMDAR antagonist D-2-amino-5-phosphonopentanoate (AP5) and digital subtraction allowed the isolation of synaptically evoked AMPA- and NMDA-mediated currents (+40 mV; Figure 2A). This permitted computing the NMDAR ratio, a validated proxy for postsynaptic strengthening of excitatory transmission (Meye et al., 2015). The AMPAR/NMDAR ratio significantly, but transiently, augmented in learner mice compared to control mice (Figure 2A). Namely, it was larger 24 h after training session two (III) and positively correlated with avoidance performance (Figures 2A and 2B). However, AMPAR/NMDAR ratios were lower and comparable between experimental groups 24 h after sessions three and four, as well as after session one, indicating the transient nature of this plasticity (Figure 2A).

The increased AMPAR/NMDAR ratio detected 24 h after session two can occur via enhanced AMPAR function and/or number or alternatively via reduction of NMDAR function and/or number (Mameli et al., 2011). To probe the contribution of each glutamate receptor type during avoidance learning, we used uncaging of MNI-glutamate onto LHb dendrites. At +40 mV, a brief (1.5 ms) flash of 405-nm UV light evoked a composite response (AMPAR and NMDAR mediated). Isolation of AMPARs and NMDARs currents unraveled higher AMPAR/NMDAR ratios in learner mice, similarly to the results obtained with extracellular stimulation (Figure 2C). Comparison of AMPAR and NMDAR absolute currents revealed a significant upward shift of AMPAR-EPSCs amplitudes, while NMDAR responses remained comparable across experimental groups (Figure S2A). Avoidance learning (at session III) did not alter EPSCs evoked by high-frequency trains of synaptic stimulation, indicating unaltered presynaptic glutamate release (Figure S2B). Altogether, these data suggest that cue-punishment association, and the consequent development of avoidance, occurs along with a postsynaptic potentiation of AMPAR-dependent transmission onto LHb neurons. We reasoned that, if learning requires such an LTP-like process, animals undergoing avoidance learning would show occluded LTP *in vitro*. Pairing high-frequency extracellular stimulation with postsynaptic depolarization (1 s at 20 mV) led to LTP in slices from control (and naive) mice (Figures 2D and S2C). This phenomenon required NMDARs, as it was abolished by the presence of the NMDAR antagonist AP5 (Figure S2C). The pairing protocol failed, however, to induce LTP in slices obtained from mice undergoing avoidance learning (III; Figure 2D). Altogether, cue-punishment association and avoidance occur along with transient LTP of postsynaptic AMPAR transmission.

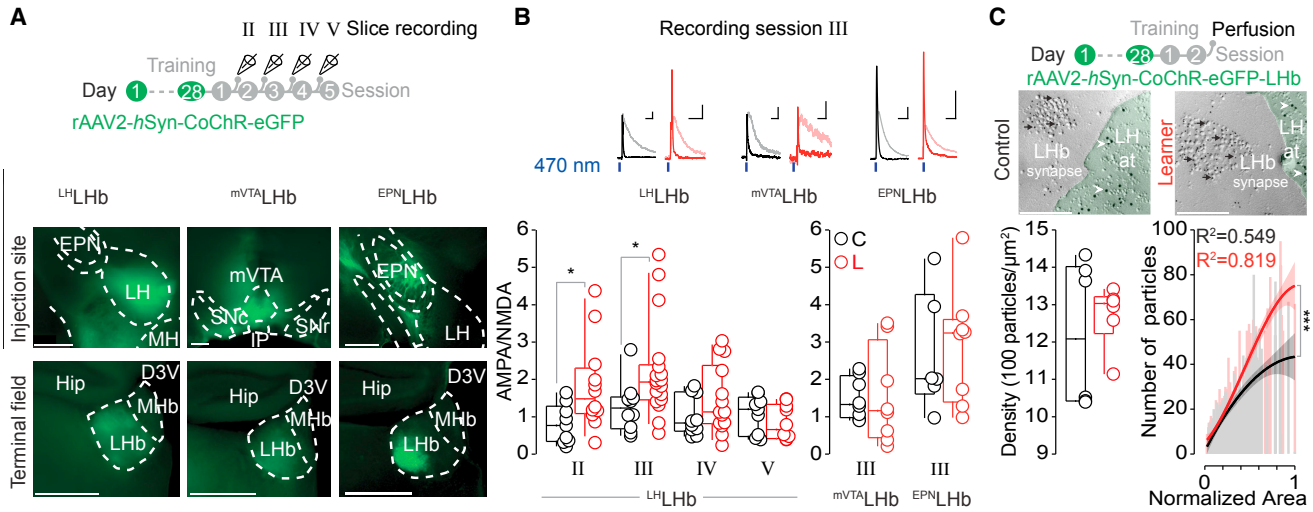

Figure 3. Learning-Driven Potentiation at Hypothalamic-to-Habenula Projections

(A) Timeline and representative images for CoChR expression in LH, mVTA, EPN, and LHb terminals (500 μm).

(B) Sample traces at session III (LH 50 pA, 20 ms, mVTA, 10 pA, 20 ms; EPN 50 pA, 20 ms); box- and scatterplot of the optical AMPA/NMDA ratios (LH, session II: C 0.8 ± 0.2, $n_{cells/animals}$ = 9/2; L 1.8 ± 0.3, $n_{cells/animals}$ = 12/2; $t_{19\ =}$ 2.4, p = 0.03; session III: C 1.3 ± 0.2, $n_{cells/animals}$ = 10/5; L 2.2 ± 0.3, $n_{cells/animals}$ = 18/6; t test, $t_{26\ =}$ 2.2, p = 0.04; session IV: C 1.0 ± 0.2, $n_{cells/animals}$ = 10/2; L 1.5 ± 0.2, $n_{cells/animals}$ = 14/2; t test, $t_{22\ =}$ 1.4, p > 0.05; session V: C 1.1 ± 0.2, $n_{cells/animals}$ = 9/2; L 0.8 ± 0.1, $n_{cells/animals}$ = 10/2; t test, $t_{17\ =}$ 1.0, p > 0.05; mVTA, session III: C [black] 1.5 ± 0.2, $n_{cells/animals}$ = 8/5; L [red] 1.6 ± 0.5, $n_{cells/animals}$ = 8/4; t test, $t_{14\ =}$ 0.13, p > 0.05; EPN, session III: C 2.7 ± 0.7, $n_{cells/animals}$ = 6/3; L 2.9 ± 0.6, $n_{cells/animals}$ = 8/3; t test, $t_{12\ =}$ 0.3, p > 0.05).

(C) Timeline and representative images of freeze-fracture replica immunolabeling for AMPARs at LH-to-LHb synaptic contacts (200 nm). Portion of a LH axon terminal (protoplasmic face in light green, 10 nm gold particle of CoChR-GFP, white arrowheads) apposed to an LHb dendritic shaft. AMPARs (5 nm gold particles, black arrows) were observed in the postsynaptic membrane specialization (PSD). Box and scatterplot of averaged density (5-nm gold particles/μm^2; C [black], 1,220.6 ± 79, $n_{counts/animals}$ = 179/6; L [red], 1,272.3 ± 33.5, $n_{counts/animals}$ = 192/6; Mann-Whitney, U = 18, p > 0.05).

Data are represented with boxplots (median and quartiles). Third-order polynomial fitting of AMPARs number versus normalized PSD area is shown (control versus learners, $n_{animals}$ = 6/group; $F_{4,361\ =}$ 15, p < 0.001, R^2 indicates goodness of fit). See also Figure S2.

Pathway Specificity of Avoidance-Learning-Driven Plasticity

The lateral hypothalamus (LH), the medial VTA (mVTA), and the entopeduncular nucleus (EPN) (1) project glutamate-releasing axons to the LHb, (2) activate AMPARs and NMDARs, and (3) promote LHb neuronal firing to drive aversive behaviors (Root et al., 2014; Shabel et al., 2012; Stamatakis et al., 2016). Importantly, unexpected punishments engage the LH-to-LHb pathway to trigger LHb neuronal excitation (Lecca et al., 2017). We examined the possibility that synaptic potentiation in the LHb during avoidance also presents circuit specificity. To this end, we virally expressed the excitatory opsin CoChR (CoChR-EGFP; Klapoetke et al., 2014) into the LH, mVTA, or the EPN (Figure 3A). Whole-cell recordings within the fluorescent terminal fields in the LHb, from all these inputs, confirmed the excitatory nature of opto-currents (Figures 3B and S2D). 24 h after training session one and two (II and III), AMPAR/NMDAR ratios at LH-LHb synapses were significantly larger in learner compared to control mice, matching the initial progression of avoidance learning. Instead, optically driven mVTA- and EPN-LHb AMPAR/NMDAR ratios were comparable between groups (Figures 3B and S2E). Notably, AMPARs/NMDARs in control condition were highly variable across inputs, indicating pathway-specific postsynaptic properties. In addition, a fear-conditioning protocol, where CS-US association occurs but in an inescapable condition, failed to change LH-LHb AMPAR/NMDAR ratios (Figure S2F).

We find that an optical-high frequency stimulation (HFS) protocol at LH inputs paired with postsynaptic depolarization employing the fast opsins CoChR and Chrimson (Klapoetke et al., 2014) led to LTP in control mice (Figure S2G). This phenomenon was absent at EPN inputs and occluded in learner mice (Figures S2G and S2H). These data support the notion that (1) at LH-LHb synapses, AMPAR/NMDAR ratio increases along with LTP (Figure S2I) and (2) learning-driven AMPAR potentiation is circuit specific.

To corroborate these results and visualize the locus of expression for avoidance-driven AMPAR potentiation, we employed freeze-fracture replica immunolabeling (Schönherr et al., 2016). Combined with infusion of rAAV2-hSyn-CoChR-EGFP, this approach allows the quantification of membrane AMPARs specifically at synapses formed by LH axons to LHb postsynaptic neurons (Figure 3C). AMPARs (GluA1–4) gold immunolabeling showed no overall difference in density between learner and control mice. However, in learner mice (24 h after session 2), a larger fraction of particles (receptors) within the broader postsynaptic membrane specialization (PSD) areas was observed compared to control animals (Figure 3C). Altogether, this suggests that a larger postsynaptic membrane pool of AMPARs underlies the potentiation of LH-to-LHb excitatory synapses during avoidance learning.

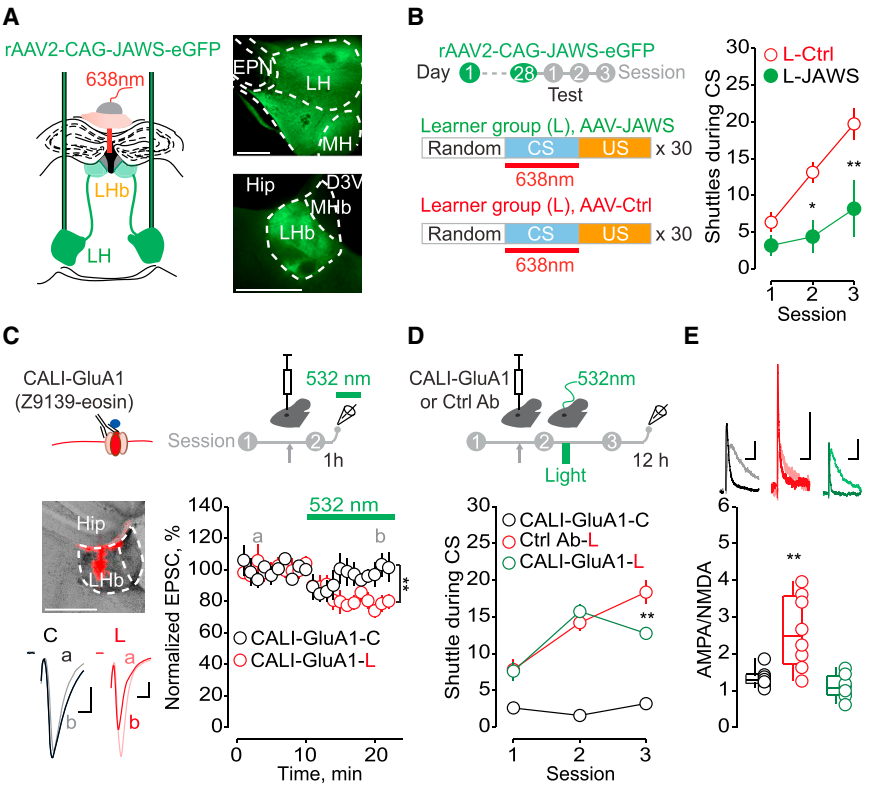

Figure 4. Avoidance Learning Requires LH-to-LHb Projections and AMPARs Potentiation

(A) Fiber implant and infusion of rAAV-CAG-JAWS-EGFP; representative images for JAWS expression (500 μm).

(B) Training protocol and behavioral performance during training (learners-control virus [L-Ctrl] [red, n = 8], learners-JAWS [L-JAWS] [green, n = 5]; two-way repeated-measures ANOVA, main effect of virus, session, and interaction [$F_{2,\ 22} = 3.8$; $p = 0.04$]).

(C) Schematic of CALI approach. Amplitude versus time plot of EPSCs (50 pA, 10 ms) before (light) and after (dark) light exposure (532 nm; average $EPSC1_{8–22\ min}$: CALI-GluA1-C [black] 98.2 ± 3.7 $n_{cells/animals}$ = 6/4; CALI-GluA1-L [red] 79.7 ± 1.9, $n_{cells/animals}$ = 6/4; t test, $t_{10} = 4.4$, **p = 0.01).

(D) Timeline of avoidance performance (infusion 4 h prior session 2; light 1 h post-session 2). Average shuttles during CS at session 3 are as follows: control mice CALI-GluA1 (CALI-GluA1-C) (black) 3.2 ± 0.7; learner mice control antibody (Ctrl-Ab-L) (red) 18.3 ± 1.6; learner mice CALI-GluA1 (CALI-GluA1-L) (green) 12.8 ± 0.7; one-way ANOVA $F_{(2,16)} = 47$, **p < 0.01.

(E) Sample traces (20 pA; 20 ms) representing AMPAR and NMDAR-EPSCs 12 h after behavioral testing. Box- and scatterplot of the AMPAR/NMDAR ratios are shown (CALI-GluA1-C 1.3 ± 0.8, $n_{cells/animals}$ = 8/3; Ctrl-Ab-L 2.6 ± 0.3, $n_{cells/animals}$ = 8/2; CALI-GluA1-L 1.1 ± 0.1, $n_{cells/animals}$ = 8/3; one-way ANOVA $F_{(2,21)} = 13.78$, **p < 0.01).

Data are represented with boxplots (median and quartiles) or mean ± SEM. See also Figure S3.

Required Circuit and Mechanism for Avoidance Learning

We next aimed to probe the necessity of LH inputs for avoidance learning. We tested LH-to-LHb projections requirement by optically reducing their function. We transduced LH neurons with a light-driven chloride pump (orange-red spectrum of activation) via infusion of rAAV2-JAWS-EGFP (Figure 4A). 4 weeks later, we prepared acute brain slices and found that 584-nm light reduced EPSCs within the LHb (Figure S3A). Next, we recorded foot-shock-driven LH-dependent LHb excitation using single units in anesthetized mice (Lecca et al., 2017). Light at 638 nm reduced foot-shock excitation in JAWS-expressing mice, but not in GFP-control animals (Figure S3B). These experiments also revealed that light off failed to induce any rebound excitation (Figure S3B). Thus, JAWS activation efficiently reduces presynaptic function of LH terminals onto the LHb. Next, we chronically implanted JAWS-expressing mice with a single fiber optic directed just above the LHb (Figure S3C). We reasoned that breaking the contingency between CS and US by functionally limiting LH-LHb projections would impair the formation of punishment-predictive cues. Shining light at 638 nm to silence LH-to-LHb terminals during CS presentation reduced avoidance learning (Figure 4B). This highlights the necessary role of the LH-LHb projection for the acquisition of avoidance behavioral strategy.

Although this provides insights for the circuit requirement of avoidance, it leaves open the existence of causality between AMPAR strengthening and behavior. We predicted that synaptic potentiation of AMPARs is an essential mechanism for avoidance learning. To test this, we employed chromophore-assisted light inactivation with eosin (CALI) to inactivate GluA1-containing AMPARs with precise temporal and spatial resolution (Takemoto et al., 2017). Monoclonal antibodies against an extracellular domain of GluA1 (236–286 amino acids [aas]) chemically labeled with eosin produce oxygen singlets in response to 532-nm laser light, thereby damaging synaptic GluA1-AMPARs (CALI-GluA1) (Takemoto et al., 2017). Notably, CALI-GluA1 efficiently targets and impairs newly inserted AMPARs, which represent a receptor pool more labile and less anchored to the scaffolding complex (Malinow and Malenka, 2002; Takemoto et al., 2017). To examine the efficiency of CALI-GluA1 in the LHb, we locally infused the antibody in control and learner mice 4–5 h prior session two (Figure 4C). 1 h after session two, we found that continuous 532-nm laser light onto slices reduced AMPAR currents solely in learner mice (Figure 4C). This suggests that CALI-GluA1 rapidly and efficiently diminishes AMPAR transmission in animals undergoing avoidance learning. Therefore, this intervention offers an opportunity to test causality between strengthened AMPAR transmission and avoidance learning with fine temporal and spatial precision.

In order to achieve this, we initially trained a set of mice during session one. The following day, the same mice underwent infusion of either CALI-GluA1 or a control antibody (anti-Myc-eosin, Ctrl-Ab) into the LHb (Takemoto et al., 2017). Mice were then

implanted with a fiber optic and experienced training session two (Figure S3D). 1 h post-training, we exposed the injected area to 532 nm continuous illumination. The following day, mice were tested on session day three (Figure 4D). All injected animals ("learners") progressively increased avoidance performance during the initial two sessions (Figure 4D). Illumination left the progression of learning intact in mice infused with Ctrl-Ab. In contrast, CALI-GluA1-L mice failed to further improve their avoidance performance and exhibited a significant reduction in cue-driven avoidance compared to Ctrl-Ab-L mice. CALI-GluA1 did not affect the behavior of control mice (Figure 4D). When examining AMPAR/NMDAR ratio in LHb-containing slices from these same animals, we found that Ctrl-Ab-L mice exhibited high AMPAR/NMDAR ratios. In contrast, CALI-GluA1-L mice presented a significantly lower AMPAR/NMDAR, comparable to those from CALI-GluA1 control mice. Altogether, this indicates that GluA1-mediated synaptic potentiation in the LHb is a requirement for proper avoidance.

DISCUSSION

LHb neurons respond to unpredicted punishments. Here, we show that also punishment-predictive cues excite LHb neuronal population during avoidance learning. This phenomenon parallels the expression of an LTP-like process at lateral hypothalamic-to-LHb excitatory synapses, a synaptic substrate necessary for avoidance.

Synaptic Basis of Avoidance

We describe that, during avoidance learning, a transient enhancement of excitatory synaptic transmission onto LHb neurons occurs as a result of AMPAR enrichment at LH-to-LHb synapses. In addition, LHb neurons of learner mice did not show, in contrast to control animals, HFS-LTP in acute brain slices. This suggests that, during the steep initial phase of avoidance learning, LH-to-LHb excitatory synapses undergo potentiation. Such synaptic potentiation, however, does not occur during CS-US association in an inescapable context, an encoding primarily mediated by amygdala neuronal populations (Ciocchi et al., 2010).

Short-term and long-term changes in excitatory transmission within the LHb are also instrumental for punishment-mediated innate escape as well as for behavioral despair in depressive states (Lecca et al., 2017; Li et al., 2013). Altogether, these data highlight the contribution of glutamatergic transmission for precise LHb-dependent neuronal encoding, ultimately leading to avoidance learning.

A feature of this study is the input-specific expression of avoidance learning-induced plasticity. Afferents from the LH, the mVTA, and the EPN onto the LHb contribute to aversion processing and are sufficient to drive aversive behaviors (Root et al., 2014; Shabel et al., 2012; Stamatakis et al., 2016). The avoidance-learning-mediated adaptations, including the increase in AMPAR/NMDAR ratio, occlusion of LTP, and higher AMPARs membrane expression, specifically occur at LH-to-LHb synapses. In addition, silencing LH-to-LHb terminals diminishes avoidance behaviors. What renders the LH-to-LHb an essential substrate for avoidance? cAMP responsive element binding protein (CREB) phosphorylation, crucial for learning processes, occurs during avoidance in the hypothalamus (Saha and Datta, 2005; Won and Silva, 2008). Furthermore, impairment of the orexin signaling in the hypothalamus disrupts taste-aversion learning (Mediavilla et al., 2011). Lastly, LH neurons mediate unpredicted foot-shock-driven LHb neuronal excitation, and their terminal activation in LHb guides real-time place aversion (Lecca et al., 2017). Altogether, LH-driven excitatory transmission onto LHb neurons represents a fundamental substrate contributing to the encoding of both unpredicted aversion and prediction of punishment. Glutamate release onto LHb neurons remains unaffected during progression of learning, suggesting the absence of plastic mechanisms in upstream structures. However, the induction mechanisms (i.e., coincident detection and/or precise firing patterns) endowing LH terminals to establish synaptic potentiation onto LHb synapses remain yet to be clarified. Recent data point to the medial septum as a source of sensory information to the LHb (Zhang et al., 2018). Neuromodulators are released during salient experiences in several brains structures, including the LHb (Lecca et al., 2014). These may represent two potential gating candidates to mechanistically trigger the LTP-like processes that guide avoidance learning. Our data do not rule out a potential contribution of (1) alternative inputs impinging onto the LHb and (2) other types of neurotransmission during discrete phases of avoidance.

The local and temporally restricted inactivation of GluA1-AMPARs resets synaptic strengthening, thereby impairing avoidance behavior. This supports a causal role of AMPAR-mediated potentiation for establishing cue-punishment association and subsequent avoidance learning. Notably, we report that CALI-GluA1 mediates reduction of EPSCs solely in the learner group. This is consistent with previous results suggesting that AMPARs participating to synaptic potentiation during learning are more susceptible to inactivation (Takemoto et al., 2017). This may result from LTP-driven insertion of labile AMPAR pools or unsilencing of silent synapses (Groc et al., 2006; Malinow, 2003). Altogether, these results favor the notion that punishment-predictive memories can form through AMPAR-mediated LTP-like processes.

Evolution of Plasticity during Prediction Learning

A signature of the reported synaptic potentiation during avoidance is its transient nature, as it occurs during a restricted time window, namely during the steepest portion of cue-punishment learning. During this phase, mice exhibited the largest change in number of avoidances compared to the previous session. Therefore, such synaptic plasticity may facilitate cue-punishment association and the consequent acquisition of avoidance. However, the extent of synaptic potentiation, reflected by the AMPAR/NMDAR ratio, returned back to baseline levels at later sessions. This inverted U-shape of learning-driven potentiation suggests that this process may not contribute to the maintenance of the learned avoidance behavior. It is therefore plausible that persistent cue-punishment memories are mediated by different mechanisms within the LHb or stored elsewhere than the LHb (i.e., monoaminergic nuclei; Wenzel et al., 2018). Notably, such phenomenon presents striking similarities with cue-reward

learning in dopamine neurons of the VTA (Stuber et al., 2008). In the midbrain, transient synaptic strengthening of AMPAR neurotransmission has been proposed as a leading substrate to enable reward prediction.

Altogether, these data support that, in the LHb, and more broadly within neuronal circuits of motivation, the transient enhancement in synaptic strength during the acquisition of avoidance (or reward) learning may transform neutral stimuli into punishment- (or reward-) predictive stimuli. This provides insights on how the brain resolves novel cue-stimulus associations.

STAR★METHODS

Detailed methods are provided in the online version of this paper and include the following:

- KEY RESOURCES TABLE
- CONTACT FOR REAGENT AND RESOURCE SHARING
- EXPERIMENTAL MODEL AND SUBJECT DETAILS
- METHOD DETAILS
  - Stereotactic injections
  - Slice electrophysiology
  - *In vivo* electrophysiology
  - Histology and immunofluorescence
  - Freeze fracture replica immunolabeling
  - Immunoparticles quantification
  - Fiber photometry
  - Behavioral testing
  - Drugs
- QUANTIFICATION AND STATISTICAL ANALYSIS

SUPPLEMENTAL INFORMATION

Supplemental Information includes three figures and can be found with this article online at https://doi.org/10.1016/j.neuron.2019.01.025.

ACKNOWLEDGMENTS

We thank M. Carta, D. Dupret, L. Neukomm, F.J. Meye, and the members of the Mameli laboratory for comments on the manuscript. We thank the Bellone and Tan laboratories for viral constructs and technical assistance. This work was supported by the Austrian Science Fund Sonderforschungsbereich grant F44-17 to F.F., ERC StG SalienSy 335333, the Swiss National Funds 31003A, and Vaud Canton to M.M.

AUTHOR CONTRIBUTIONS

M.T. and M.M. conceptualized the project and performed and analyzed the electrophysiological recordings and behavior. M.T. and S.L. performed and analyzed *in vivo* photometry data. A.N.-P. performed electrophysiological recordings. A.L.L. and M.C. performed *in vivo* electrophysiology experiments. H.H. and F.F. performed and analyzed the electron microscopy data. K.T. and T.T. provided tools for CALI. M.M. and M.T. wrote the manuscript with the help of all authors.

DECLARATION OF INTERESTS

The authors declare no competing interests.

Received: July 20, 2018
Revised: November 23, 2018
Accepted: January 14, 2019
Published: February 11, 2019

REFERENCES

Ciocchi, S., Herry, C., Grenier, F., Wolff, S.B., Letzkus, J.J., Vlachos, I., Ehrlich, I., Sprengel, R., Deisseroth, K., Stadler, M.B., et al. (2010). Encoding of conditioned fear in central amygdala inhibitory circuits. Nature *468*, 277–282.

Groc, L., Gustafsson, B., and Hanse, E. (2006). AMPA signalling in nascent glutamatergic synapses: there and not there! Trends Neurosci. *29*, 132–139.

Klapoetke, N.C., Murata, Y., Kim, S.S., Pulver, S.R., Birdsey-Benson, A., Cho, Y.K., Morimoto, T.K., Chuong, A.S., Carpenter, E.J., Tian, Z., et al. (2014). Independent optical excitation of distinct neural populations. Nat. Methods *11*, 338–346.

Lecca, S., Meye, F.J., and Mameli, M. (2014). The lateral habenula in addiction and depression: an anatomical, synaptic and behavioral overview. Eur. J. Neurosci. *39*, 1170–1178.

Lecca, S., Pelosi, A., Tchenio, A., Moutkine, I., Lujan, R., Hervé, D., and Mameli, M. (2016). Rescue of GABAB and GIRK function in the lateral habenula by protein phosphatase 2A inhibition ameliorates depression-like phenotypes in mice. Nat. Med. *22*, 254–261.

Lecca, S., Meye, F.J., Trusel, M., Tchenio, A., Harris, J., Schwarz, M.K., Burdakov, D., Georges, F., and Mameli, M. (2017). Aversive stimuli drive hypothalamus-to-habenula excitation to promote escape behavior. eLife *6*, e30697.

LeDoux, J.E., Moscarello, J., Sears, R., and Campese, V. (2017). The birth, death and resurrection of avoidance: a reconceptualization of a troubled paradigm. Mol. Psychiatry *22*, 24–36.

Li, B., Piriz, J., Mirrione, M., Chung, C., Proulx, C.D., Schulz, D., Henn, F., and Malinow, R. (2011). Synaptic potentiation onto habenula neurons in the learned helplessness model of depression. Nature *470*, 535–539.

Li, K., Zhou, T., Liao, L., Yang, Z., Wong, C., Henn, F., Malinow, R., Yates, J.R., 3rd, and Hu, H. (2013). βCaMKII in lateral habenula mediates core symptoms of depression. Science *341*, 1016–1020.

Malinow, R. (2003). AMPA receptor trafficking and long-term potentiation. Philos. Trans. R. Soc. Lond. B Biol. Sci. *358*, 707–714.

Malinow, R., and Malenka, R.C. (2002). AMPA receptor trafficking and synaptic plasticity. Annu. Rev. Neurosci. *25*, 103–126.

Mameli, M., Bellone, C., Brown, M.T., and Lüscher, C. (2011). Cocaine inverts rules for synaptic plasticity of glutamate transmission in the ventral tegmental area. Nat. Neurosci. *14*, 414–416.

Matsumoto, M., and Hikosaka, O. (2007). Lateral habenula as a source of negative reward signals in dopamine neurons. Nature *447*, 1111–1115.

Mediavilla, C., Cabello, V., and Risco, S. (2011). SB-334867-A, a selective orexin-1 receptor antagonist, enhances taste aversion learning and blocks taste preference learning in rats. Pharmacol. Biochem. Behav. *98*, 385–391.

Meye, F.J., Valentinova, K., Lecca, S., Marion-Poll, L., Maroteaux, M.J., Musardo, S., Moutkine, I., Gardoni, F., Huganir, R.L., Georges, F., and Mameli, M. (2015). Cocaine-evoked negative symptoms require AMPA receptor trafficking in the lateral habenula. Nat. Neurosci. *18*, 376–378.

Nabavi, S., Fox, R., Proulx, C.D., Lin, J.Y., Tsien, R.Y., and Malinow, R. (2014). Engineering a memory with LTD and LTP. Nature *511*, 348–352.

Root, D.H., Mejias-Aponte, C.A., Qi, J., and Morales, M. (2014). Role of glutamatergic projections from ventral tegmental area to lateral habenula in aversive conditioning. J. Neurosci. *34*, 13906–13910.

Saha, S., and Datta, S. (2005). Two-way active avoidance training-specific increases in phosphorylated cAMP response element-binding protein in the dorsal hippocampus, amygdala, and hypothalamus. Eur. J. Neurosci. *21*, 3403–3414.

Schönherr, S., Seewald, A., Kasugai, Y., Bosch, D., Ehrlich, I., and Ferraguti, F. (2016). Combined optogenetic and freeze-fracture replica immunolabeling to examine input-specific arrangement of glutamate receptors in the mouse amygdala. J. Vis. Exp., 53853.

Shabel, S.J., Proulx, C.D., Trias, A., Murphy, R.T., and Malinow, R. (2012). Input to the lateral habenula from the basal ganglia is excitatory, aversive, and suppressed by serotonin. Neuron *74*, 475–481.

Stamatakis, A.M., Van Swieten, M., Basiri, M.L., Blair, G.A., Kantak, P., and Stuber, G.D. (2016). Lateral hypothalamic area glutamatergic neurons and their projections to the lateral habenula regulate feeding and reward. J. Neurosci. *36*, 302–311.

Stuber, G.D., Klanker, M., de Ridder, B., Bowers, M.S., Joosten, R.N., Feenstra, M.G., and Bonci, A. (2008). Reward-predictive cues enhance excitatory synaptic strength onto midbrain dopamine neurons. Science *321*, 1690–1692.

Takemoto, K., Iwanari, H., Tada, H., Suyama, K., Sano, A., Nagai, T., Hamakubo, T., and Takahashi, T. (2017). Optical inactivation of synaptic AMPA receptors erases fear memory. Nat. Biotechnol. *35*, 38–47.

Valentinova, K., and Mameli, M. (2016). mGluR-LTD at excitatory and inhibitory synapses in the lateral habenula tunes neuronal output. Cell Rep. *16*, 2298–2307.

Wang, D., Li, Y., Feng, Q., Guo, Q., Zhou, J., and Luo, M. (2017). Learning shapes the aversion and reward responses of lateral habenula neurons. eLife *6*, e23045.

Wenzel, J.M., Oleson, E.B., Gove, W.N., Cole, A.B., Gyawali, U., Dantrassy, H.M., Bluett, R.J., Dryanovski, D.I., Stuber, G.D., Deisseroth, K., et al. (2018). Phasic dopamine signals in the nucleus accumbens that cause active avoidance require endocannabinoid mobilization in the midbrain. Curr. Biol. *28*, 1392–1404.e5.

Won, J., and Silva, A.J. (2008). Molecular and cellular mechanisms of memory allocation in neuronetworks. Neurobiol. Learn. Mem. *89*, 285–292.

Zhang, G.W., Shen, L., Zhong, W., Xiong, Y., Zhang, L.I., and Tao, H.W. (2018). Transforming sensory cues into aversive emotion via septal-habenular pathway. Neuron *99*, 1016–1028.e5.

STAR★METHODS

KEY RESOURCES TABLE

REAGENT or RESOURCE	SOURCE	IDENTIFIER
Antibodies		
Anti-NeuN mouse	Millipore	Cat# MAB377; RRID: AB_2298772
647-Alexa anti-mouse	Invitrogen	Cat# A-21247; RRID: AB_141778
Anti-GAD67 mouse	Millipore	Cat# MAB5406; RRID: AB_2278725
Anti-EAAC1 goat	Millipore	Cat# MAB1520; RRID: AB_90732
panAMPA	Frontiers Science Company	Cat#: panAMPAR-GP-Af580-1
Anti-GFP Rabbit	Invitrogen	Cat#: A11122; RRID AB_221569
Goat anti-guinea pig IgG-5nm Gold particle	British Biocell International	Cat#: EM.GFAR5
Goat anti-rabbit IgG-10nm Gold particle	British Biocell International	Cat#: EM.GAR10
Bacterial and Virus Strains		
rAAV2.5–*h*Syn–CoChR–eGFP	UNC Vector Core	N/A
AAV5-*h*Syn-Chrimson-tdTomato	Addgene	Cat#: 59171
rAAV2.2–CAG–JAWS–GFP	Vector biolabs	N/A
rAAV2.5–*h*Syn–GCaMP6f	Addgene	Cat#: 100837
rAAV2.1–CAG–tdTomato	Addgene	Cat#: 59462
Chemicals, Peptides, and Recombinant Proteins		
Anti-GluA1-Eosin (Cali-GluA1)	Gift of T. Takahashi	
Anti-Myc-eosin (Control)	Gift of T. Takahashi	
D-AP5	Hello Bio	Cat#: HB0225
Picrotoxin	Hello Bio	Cat#: HB0506
NBQX disodium salt	Hello Bio	Cat#: HB0443

CONTACT FOR REAGENT AND RESOURCE SHARING

Further information and requests for resources and reagents should be directed to and will be fulfilled by the Lead Contact, Manuel Mameli (manuel.mameli@unil.ch).

EXPERIMENTAL MODEL AND SUBJECT DETAILS

Male naive mice (C57Bl6/J; 4–12 weeks) were group-housed (three to five per cage) on a 12:12 h light cycle (lights on at 7 a.m.) with food and water *ad libitum*. All procedures aimed to fulfill the 3R criterion and were approved by the Veterinary Offices of Vaud (Switzerland; License VD3171).

METHOD DETAILS

Stereotactic injections

Mice were anesthetized with ketamine (150 mg kg^{-1}) and xylazine (100 mg kg^{-1}) (Veterinary office University of Lausanne) and were placed on a stereotactic frame (Kopf, Germany). Bilateral injections obtained through a glass needle of 200-400 nL volume were performed at a rate of approximately 100 nL min^{-1}. The injection pipette was withdrawn from the brain 10 min after the infusion. Injections were performed using the following coordinates: lateral hypothalamus (LH: −1.25 mm posterior to bregma, 0.95 mm lateral, −5.1 mm ventral from pia); entopeduncular nucleus (EPN: −1.25 mm posterior to bregma, 1.80 mm lateral, −4.65 mm ventral); medial VTA (mVTA: −2.2 mm posterior to bregma, 0.3 mm lateral, −4.8 mm ventral); lateral habenula (LHb: −1.35 mm posterior to bregma, 0.45 mm lateral, −3.1 mm ventral).

Animals were allowed to recover for a minimum of 3 weeks before the recordings.

Viral constructs employed in the study: rAAV2.5–*h*Syn–CoChR–eGFP (University of North Carolina viral vector core, USA; titer: 1×10^{12} gc/ml); AAV5-*h*Syn-Chrimson-tdTomato (University of Pennsylvania viral vector core; titer: 7×10^{12} gc/ml). rAAV2.2–CAG–JAWS–GFP (Vector biolabs, USA; titer: 7×10^{12} gc/ml); rAAV2.5–*h*Syn–GCaMP6f, rAAV2.1–CAG–tdTomato (University of

Pennsylvania viral vector core; titer: 5×10^{12} gc/ml and 1.19×10^{13} gc/ml). The injection sites were examined for all experiments and only data from animals with correct injections were included.

Slice electrophysiology

The mice were anesthetized (ketamine/xylazine; 150 mg/100 mg kg^{-1}), sacrificed, and their brains were transferred in ice-cold carbogenated (95% O_2/5% CO_2) solution, containing (in mM) choline chloride 110; glucose 25; $NaHCO_3$ 25; $MgCl_2$7; ascorbic acid 11.6; sodium pyruvate 3.1; KCl 2.5; NaH_2PO_4 1.25; $CaCl_2$0.5. Coronal brain slices (250 μm thickness) were prepared and transferred for 10 min to warmed solution (34°C) of identical composition, before they were stored at room temperature in carbogenated artificial cerebrospinal fluid (ACSF) containing (in mM) NaCl 124; $NaHCO_3$ 26.2; glucose 11; KCl 2.5; $CaCl_2$ 2.5; $MgCl_2$ 1.3; NaH_2PO_4 1. During recordings, slices were immersed in ACSF and continuously superfused at a flow rate of 2.5 mL min^{-1} at 30°C. Neurons were patch-clamped using borosilicate glass pipettes (2.7–4 MΩ; Phymep, France) under an Olympus-BX51 microscope (Olympus, France). For voltage or current clamp recordings, signal was amplified, filtered at 5 kHz and digitized at 10 kHz (Multiclamp 200B; Molecular Devices, USA). Data were acquired using Igor Pro with NIDAQ tools (Wavemetrics, USA). Access resistance was continuously monitored with a −4 mV step delivered at 0.1 Hz. Experiments were discarded if the access resistance increased by more than 20% during the recording.

Extracellular stimulation from AMPI ISO-Flex stimulator was delivered through glass electrodes placed in the LHb.

Light stimulation (470 nm 1 ms for CoChR experiments, 584 nm continuous for JAWS experiments) was delivered with a LED (CoolLed, UK) illumination system. We systematically tested for direct optically-driven currents (100 msec light) sporadically observed in regions receiving afferent inputs from the site of injection. In case a direct photo-current was found the cell was discarded.

A 532 nm laser (Integrated Optics, Lithuania) was used in the experiments for the in-vitro validation and in-vivo activation (2 min light exposure) of the CALI strategy. For glutamate uncaging (4-methoxy-7-nitroindolinyl-caged L-glutamate 200μM, Tocris), a single-path photolysis head was connected to a solid-state laser (Rapp Optolectronics, Germany; 405 nm, duration 0.5 ms, diameter 3–5μm).

All recordings were made in voltage-clamp configuration, in picrotoxin-containing ACSF (100 μM). The stimulation intensity (electrical and light) was titered to obtain currents between ± 50-300 pA. AMPAR/NMDAR ratios of evoked EPSC were obtained by AMPAR-EPSC +40 mV/NMDAR-EPSCs at +40 mV. I_{AMPAR} and I_{NMDAR} were pharmacologically isolated by the application of APV (100 μM), NBQX (20 μM), and by subsequent identification of the individual currents via digital subtraction. CALI and JAWS in-vitro validation experiments were performed in voltage clamp mode at −50 mV and light was applied continuously until the end of the experiment. The internal medium consisted of (in mM) cesium methanesulfonate 120, CsCl 10, HEPES 10, EGTA 10, creatine phosphate 5; Na2ATP 4; Na3GTP 0.4.

Long-term plasticity experiments were performed at −60 mV with an internal solution contained the following (in mM): K-gluconate 140; KCl 5; HEPES 10; EGTA 0.2; MgCl2 2; Na2ATP 4; Na3GTP 0.3; and creatine-phosphate 10. For the measurement of AMPAR-$EPSC_{-60\ mV}$/NMDAR-$EPSCs_{+40\ mV}$ before and after the LTP protocol, we used an internal solution containing the following (in mM): cesium methanesulfonate 130; 15 CsCl, 10 HEPES, 0.2 EGTA, 10 Creatine Phosphate, 4 ATP-Mg, 0.3 GTP-Na. The induction protocol for long-term plasticity consisted of 5 trains of 1 s stimulation at 100 Hz, delivered at 0.1Hz, paired with somatic depolarization (+20 mV).

Data collection and analysis for the electrophysiology experiments were not performed blind to the conditions of the experiments.

In vivo electrophysiology

Recordings under anesthesia

For the JAWS validation *in vivo*, mice previously injected in the LH with rAAV2-CAG-JAWS-eGFP were anesthetized using isoflurane (Univentor, Malta. Induction: 2%; maintenance: 1%–1.5%) and placed in the stereotaxic apparatus (Kopf, Germany). Their body temperature was maintained at 36 ± 1°C using a feedback-controlled heating pad (CMA 450 Temperature controller, USA). An optrode was lowered at the coordinates of LHb. Each cell was tested for its response to repetitive (every 5 s) shocks (0.5 s, 1.5 - 2 mA) delivered to the hind paw contralateral to the recording side. If excited the Fs response was re-tested while simultaneously shining the light (638nm, 10mW, 4 s). PSTHs and raster plots were built from 30 to 60 shocks and displayed using 10 ms bin width. A cell was considered excited when the mean number of action potentials/bin (bin length = 10 ms) in at least one of the four epochs (50 ms per epoch) after the shock inset was 2 times the Standard Deviation (SD) higher than baseline levels (the average number of action potentials/bin in the 2 s period before the shock). The duration of the response was calculated from the latency to the first of at least 5 consecutive bins not different than the baseline + 2SD. The magnitude of the response was obtained subtracting the baseline firing rate to the firing during the duration of the shock response.

At the end of each experiment, the electrode placement was determined with an iontophoretic deposit of pontamine sky blue dye (1 mA, continuous current for 5 min). Brains were then rapidly removed and fixed in 4% paraformaldehyde solution. The position of the electrodes was identified with a microscope on coronal section sections (100 μm). Only recordings in the correct area were considered for analysis.

For awake *in vivo* recordings, mice were implanted with a custom stainless steel headbar for head fixation. The scalp was removed and skull scraped clean and dry using a scalpel. LHb sites (AP, lateral, in mm, from bregma: −1.4, 0.45) were marked with sharpie pen

on the skull and covered with a drop of silicone elastomer (Kwik-Cast; WPI). Cyanoacrylate glue (Vetbond, 3M) was lightly dabbed on the skull. Then, the headbar was levelled flat and lowered to touch lambda, covered with dental adhesive (C and B Metabond, Parkell) and secured with dental cement (Jetkit, Lang). Only a thin layer of cement was applied above the marked VM sites.

After at least 3 days of recovery, mice were habituated to head fixation in a 3-cm-wide acrylic cylinder for 10 min twice a day. In parallel, mice were trained for four days in the active avoidance paradigm. After the fourth training session, mice were anesthetized, dental cement and silicone above LHb were removed, and holes were drilled on the marked LHb locations. The craniotomy was then covered *in silico*ne elastomere. The next day, mice were headfixed for recordings, instead of the last behavior session.

After headfixation, the craniotomy was exposed and and electrode was lowered in the LHb (DV 2.3-3.2, from brain, in mm). Single unit activity was recorded extracellularly using glass micropipettes filled with 2% Chicago sky blue dissolved in 0.5 M sodium acetate (impedance 5-15 MΩ). Signal was filtered (band-pass 500–5000 Hz), pre-amplified (DAM80, WPI, Germany), amplified (Neurolog System, Digitimer, UK) and displayed on a digital storage oscilloscope (OX 530, Metrix, USA). Experiments were sampled on- and offline by a computer connected to CED Power 1401 laboratory interface (Cambridge Electronic Design, Cambridge, UK) running the Spike2 software (Cambridge Electronic Design).

Single units were isolated and after recording baseline activity (3 minutes), each cell was tested for its response to CS presentation (25kHz, 80dB, 4 s duration, random interval of 5-30 s, 6 to 12 trials; recordings per single mouse lasted < 90 min) delivered by a speaker placed nearby the mouse. PSTHs and raster plots were built using 100 ms bin normalized to a window of 2 s baseline. For each cell we calculate the modulation index (CS firing – baseline firing / CS firing + baseline firing). A cell was considered excited or inhibited when the modulation index was larger than 0.1 or lower than −0.1, respectively.

Histology and immunofluorescence

Mice were anaesthetized and transcardially perfused with 4% paraformaldehyde (w/v) in 0.1 M phosphate buffered saline (PBS; pH 7.4). Coronal sections (100 μm) were cut with a vibratome. To examine fiber placement and for injection sites examination, we used an epifluorescent microscope (Zeiss) with a 5x and 10x objective. For immunofluorescence, the brain slices were incubated for 48h at 4°C in mouse anti-NeuN antibody (1:500, MAB377 Millipore) in PBS containing 0.3% Triton X and 5% normal goat serum. After extensive washes in PBS, the slices were incubated for 24h at 4°C with 647-Alexa-coupled secondary anti-mouse antibody (1:1000, Invitrogen). Images of the lateral habenula (3 fields/mouse) were acquired using a confocal microscope (TCS SP5 AOBS TANDEM, Leica) with a 20X objective. The number of GCaMP6f and NeuN-positive neurons was counted. To identify the nature of cells expressing GCaMP6f, antigen retrieval was performed by incubating the brain slices in 50mM Na-citrate solution at 80°C for 30 minutes. Slices were rinsed, incubated 1h in a solution containing 0.3% Triton X and 5% normal goat serum, and then for 48h at 4°C in a cocktail of mouse anti-GAD67 antibody (1:250, MAB5406 Millipore) and goat anti-EAAC1 (1:250, MAB1520 Millipore) in PBS containing 5% normal goat serum. After extensive washes in PBS, the slices were incubated for 24h at 4°C with 555-Alexa-coupled secondary anti-goat antibody, and then 647-Alexa-coupled secondary anti-mouse antibody (1:1000, Invitrogen). Images of the LHb were acquired using a confocal microscope (TCS SP5 AOBS TANDEM, Leica) with a 20X and a 63X immersion objective. ImageJ software (version 1.6, https://imagej.nih.gov/ij/) was used for image processing.

Freeze fracture replica immunolabeling

Anesthetized mice were perfused transcardially using a peristaltic pump at a flow rate of 5 ml/min with 25 mM phosphate buffered saline solution (PBS) for 1 min, followed by ice cold 1% paraformaldehyde (PFA) and 15% saturated picric acid in 0.1 M phosphate buffer (PB) for 7 min. Coronal slices (130 mm thick) were cut using a vibrating microslicer (VT1000, Leica, Vienna, Austria) in 0.1 M PB. A region of the LHb was trimmed from the slices and immersed in graded glycerol (10%–30% in 0.1 M PB) at 4°C overnight and frozen by a high pressure freezing machine (HPM 010; BAL-TEC, Balzers, Liechtenstein). Frozen samples were fractured using a double-replica table at −115°C and replicated by carbon deposition (5 nm thick), carbon-platinum (2 nm) and carbon (15 nm) with a freeze-fracture replica machine (BAF060; BAL-TEC). Tissue debris were dissolved with shaking at 80°C for 20 h in a solution containing 15 mM Tris-HCl (pH 8.3), 20% sucrose, and 2.5% SDS. The replicas were washed three times in 50 mM Tris-buffered saline (TBS, pH 7.4) containing 0.05% bovine serum albumin (BSA), 0.1% Tween-20, and 0.05% sodium azide and blocked with 5% BSA in washing buffer for 1 h at room temperature. Subsequently, they were incubated with primary antibodies for 3 overnights at 15°C. The primary antibodies were: guinea pig polyclonal IgG raised against the 717-754 amino acid residues common to all AMPAR subunits (diluted 1:200, Frontier Science Co. Ltd, Hokkaido, Japan, cat. no. panAMPAR-GP-Af580-1) and rabbit polyclonal IgG raised against the green fluorescent protein (GFP) from the jellyfish *Aequorea victoria* (diluted 1:1,000, Molecular Probes-Invitrogen, cat. no. A11122, Lot. no. 1356608). Antigen-antibody complexes were identified using secondary antibodies against the species of the first antibody and conjugated to gold particles of different size: goat anti-guinea pig IgG conjugated with 5 nm gold particles and goat anti-rabbit IgG conjugated with 10 nm gold particles (both diluted 1:30, British Biocell International, Cardiff, UK). Incubation was carried out overnight at 15°C. The labeled replicas were examined using a transmission electron microscope (CM-120; Philips).

Immunoparticles quantification

Images of excitatory postsynaptic specializations (PSD), identified by the presence of intramembrane particle (IMP) clusters on the exoplasmic face (E-face) accompanied by the protoplasmic face (P-face) of the presynaptic plasma membrane labeled by GFP immunoparticles, were captured at a magnification of 88,000 with a digital camera (Morada, Soft Imaging System; SIS). The PSD was

demarcated freehand and the area was measured using the iTEM (SIS) or FIJI software (distributed under the General Public License). Immunoparticles within the PSD and those located outside but within 30 nm from the edge of the PSD were regarded as synaptic labeling, considering possible deviations of the immunoparticle from the antigen. The majority of analysis was performed on dendritic shafts as under our experimental conditions the vast majority of LHb spines were fractured at the neck and the PSD could not be exposed. Sampling and analysis of AMPAR density was performed by an investigator blind of the experimental groups. Data from both full and partial synapses were used since there was no significant difference ($p = 0.31$, unpaired t test) in AMPAR density.

Fiber photometry

The fiber photometry measurements in this study were carried out by the ChiSquare χ^2-200 system (ChiSquare Biomaging, Brookline, MA). Briefly, blue light from a 473-nm picosecond-pulsed laser (at 50 MHz; pulse width ~80 ps FWHM) was delivered to the sample through a single mode fiber. Fluorescence emission from the tissue was collected by a multimode fiber. The singlemode and multimode fibers were arranged side by side in a ferrule that is connected to a detachable multimode fiber implant. The emitted photons collected through the multimode fiber pass through a bandpass filter (FF01-550/88, Semrock) to a single-photon detector. Photons were recorded by the time-correlated single photon counting (TCSPC) module (SPC-130EM, Becker and Hickl, GmbH, Berlin, Germany) in the ChiSquare χ^2-200 system. Online analysis of photon counting was systematically employed to determine whether the fiber probe was correctly placed to detect fluorescent changes (photon count > 300 photons). The experiments were replicated two to three times in the laboratory with different batches of mice.

Behavioral testing

Active avoidance

Behavioral tests were performed during the light phase. The active avoidance procedure (AA) was performed using a modified version of the Ugo Basile shuttle box apparatus. We substituted the door separating the two portions of the apparatus with two separate walls in order to allow the passage of optical fibers reaching the animal's head. The animals were handled daily by the experimenter for 3 days before the start of the behavioral tests. Mice were habituated to the testing room for a minimum of 30 minutes, and then a minimum of 10 minutes to the testing chamber. The training protocol consisted of a maximum of 5 sessions, 30 trials per session, 1 session/day. The protocol consisted in a random inter-trial interval (ITIs, min 20 s max 40 s) followed by a 10 s ≈70dB 5Khz tone (conditioning stimulus, CS), immediately followed by a 0.3 mA footshock (unconditioned stimulus, US) delivered through the metallic floor grid. The foot shock had a maximal duration set to 25 s and was terminated when the animal shuttled to the opposite compartment, or prevented if the animal shuttled during the delivery of the CS. For electrophysiological experiments, the animals exposed to the training were excluded from further testing if they failed to avoid at least 5 trials during session 2. Control animals were subjected to a pattern of US designed to mimick the average experience of the learner group on each specific session (1 to 5). The total duration of foot shock experienced in each session was scattered in episodes of 1, 2 or 3 s, and delivered not contingently to the US. For the control protocol, both CS and US were not-stoppable by shuttling to the opposite compartment.

For experiments employing JAWS *in vivo*, light was provided through a laser-coupled fiber optic at 638 nm. Light was applied during the entire presentation of the CS at a power of 15 mW at the tip of the fiber. For experiments using CALI (site of injection identified with flurobeads), a fiber optic delivered light (532 nm, 60 mW, 2 minutes) above the LHb.

Fear conditioning

Animals underwent a fear conditioning procedure. Briefly, the animals were conditioned in the apparatus used for active avoidance. On the first day, they experienced 4 presentations of the CS (total CS duration of 30 s, 7.5 kHz, 80 dB; inter-trial interval: 20–180 s). On day 2 the CS was paired with a US (1 s foot shock, 0.6 mA, 5 CS+/US pairings; inter-trial interval: 20–180 s) at the offset of the CS. The animals were sacrificed for recordings 24h after the conditioning.

Drugs

The drugs were obtained from Sigma (Switzerland), Tocris (Bristol, UK) and Hellobio (Bristol, UK). With the exception of picrotoxin and NBQX (DMSO, 0.01% final bath concentration), all drugs were dissolved in purified water.

QUANTIFICATION AND STATISTICAL ANALYSIS

Online and offline analysis for electrophysiological data were performed using Igor Pro-6 (Wavemetrics, USA). Sample size was predetermined on the basis of published studies, experimental pilots and in-house expertise. Animals were randomly assigned to experimental groups. Compiled data are always reported and represented as boxplots (median and quartiles) or mean ± SEM, with single data points plotted (single cell for electrophysiology and single animal for behavioral experiments). Animals or data points were not excluded from analyses unless noted. Data distribution was tested for normality. When applicable, statistical tests were one-way ANOVAs, two-way ANOVAs, paired or unpaired t test. In case of not-normally distributed data, we used the Mann-Whitney and Friedman non-parametric test. Curve fitting was statistically tested with Pearson or Spearman tests. Testing was always performed two-tailed with $\alpha = 0.05$.

Neuron, Volume *102*

Supplemental Information

Punishment-Predictive Cues Guide Avoidance through Potentiation of Hypothalamus-to-Habenula Synapses

Massimo Trusel, Alvaro Nuno-Perez, Salvatore Lecca, Harumi Harada, Arnaud L. Lalive, Mauro Congiu, Kiwamu Takemoto, Takuya Takahashi, Francesco Ferraguti, and Manuel Mameli

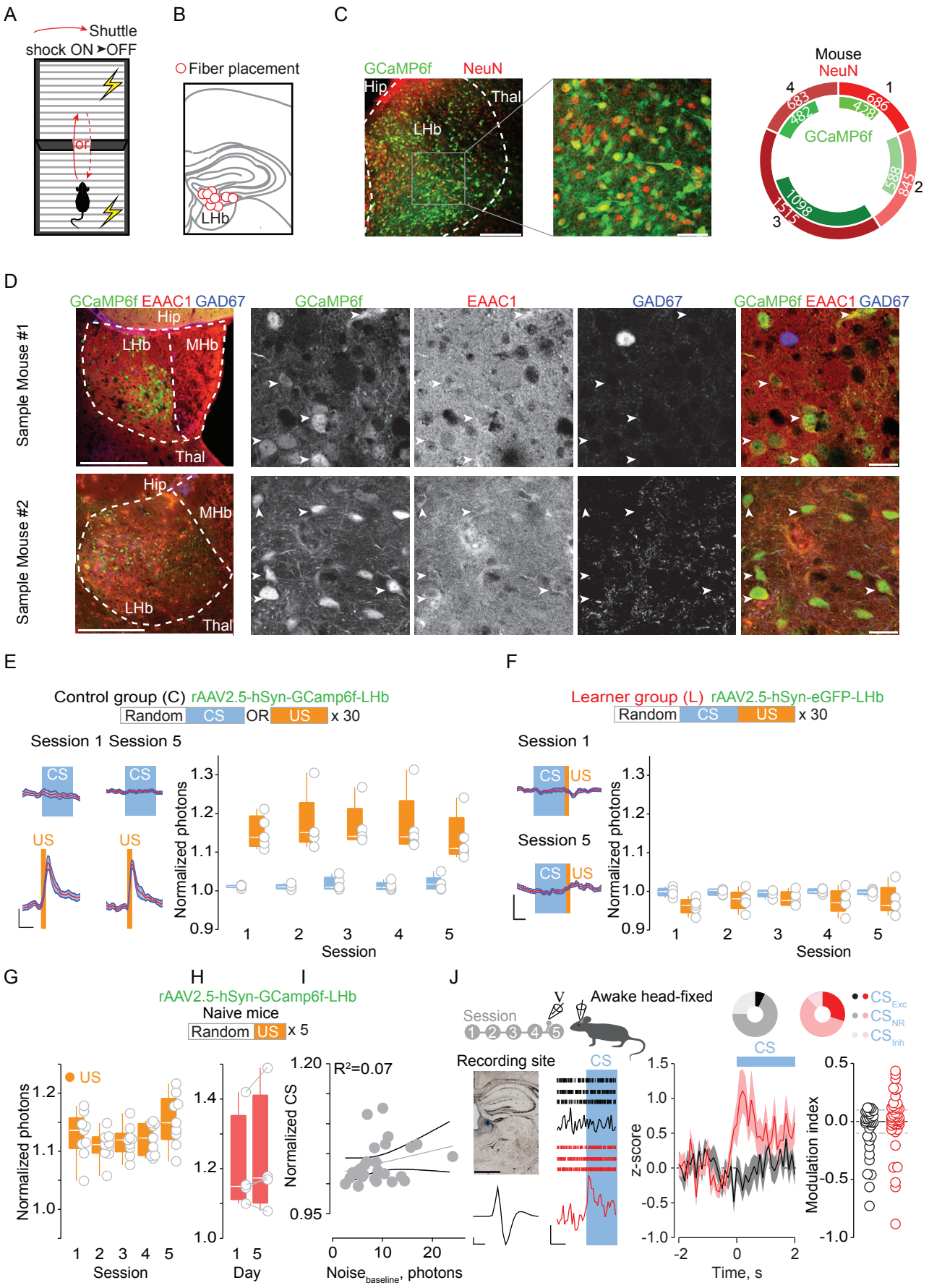

Trusel et al., Figure S1

Figure S1. Analysis of GCaMP6f signal in the LHb. Related to Figure 1.

(**A**) Schematic representation of the two-way active avoidance behavioral test. Two identical compartments are separated by two walls, leaving a passage for the mouse to cross. After the CS onset, the mouse can stop the delivery of the footshock (through the electrified floor) by crossing the walls and reaching the opposite compartment.

(**B**) Schematic of a LHb-containing coronal section including the approximate sites of fibers placement (red circles, N=9).

(**C**) Representative image and magnification of GCaMP6f (green) and NeuN staining (red) in the LHb (scalebar: main=200µm, inset=50 µm). Plot reporting the total number of NeuN positive (outer circle, red) and the cells exhibiting GCaMP6f co-staining (inner circle, green) in 4 mice (black numbers, 3 LHb slices/mouse).

(**D**) Representative images (scalebar 250µm) and magnification (scalebar 20µm) of LHb slices displaying GCaMP6f expression (green), co-stained with the glutamatergic marker EAAC1 (red) and the GABAergic marker GAD67 (blue) in 2 different representative mice (scalebar: main=250µm, inset=20 µm). White arrowheads point to GCaMP6f neurons visibly co-stained with EAAC1, but not GAD67.

(**E**) Sample traces, box and scatter plot reporting the unchanged photon number measured across all sessions in control-trained mice infused with $rAAV_{2.5}$-hSyn-GCaMP6f in LHb upon the delivery of the CS (N=5, RM One-way ANOVA Dunnett's D1 vs D5 q_4=0.95 p>0.05) and US (N=5, RM One-way ANOVA Dunnett's D1 vs D5 q_4=0.87 p>0.05).

(**F**) Sample traces, box and scatter plot reporting the unchanged photon number measured across all sessions in learner mice infused with $rAAV_{2.5}$- hSyn-eGFP in LHb upon the delivery of the CS (N=5, RM One-way ANOVA Dunnett's D1 vs D5 q_4=0.17 p>0.05) and US (N=5, RM One-way ANOVA Dunnett's D1 vs D5 q_4=0.96 p>0.05).

(**G**) Box and scatter plot reporting the unchanged normalized photon number measured across all sessions upon the delivery of US in Learner mice (US, N=9, RM One-way ANOVA Dunnett's D1 vs D5 q_8=0.49 p>0.05).

(**H**) Box and scatter plot reporting the unchanged photon number measured in naïve mice only exposed to 5 US at day 1 and 5 (N=4, average of 5 trials/mouse/day; t-test t_6=0.8 p>0.05).

Data are represented with box plots (median and quartiles).

(**I**) Normalized CS plotted in function of the photon noise at baseline for the learner group (correlation value/mouse; Spearman r=0.362, p>0.05, R^2 represents the goodness of fit).

(**J**) Timeline of awake head-fixed *in vivo* recordings, recording site (scalebar 1mm) and representative action potential (scalebar 0.2mV, 5ms). Raster plot (3 trials) and PSTH (10 trials) from a sample recording in a control and a learner mouse. Averaged z-score for all recordings in controls and learner mice (Controls: $n_{cells}/_{animals}$=41/2 vs Learners: $n_{cells}/_{animals}$=50/4; RM Two-way ANOVA, Controls vs Learners, $F_{1,73}$=2.63, p=0.02). Pie charts representing the distribution of CS-excited, CS-non-responding and CS-inhibited neurons (Controls: CS_{Exc}=3, CS_{NR}=28, CS_{Inh}=10; Learners: CS_{Exc}=15, CS_{NR}=29, CS_{Inh}=6; X^2 t_2=8.2, p=0.02). Related scatter plot of the modulation index representing deviation of differential CS responses from zero (arbitrary cutoff set at ±0.1).

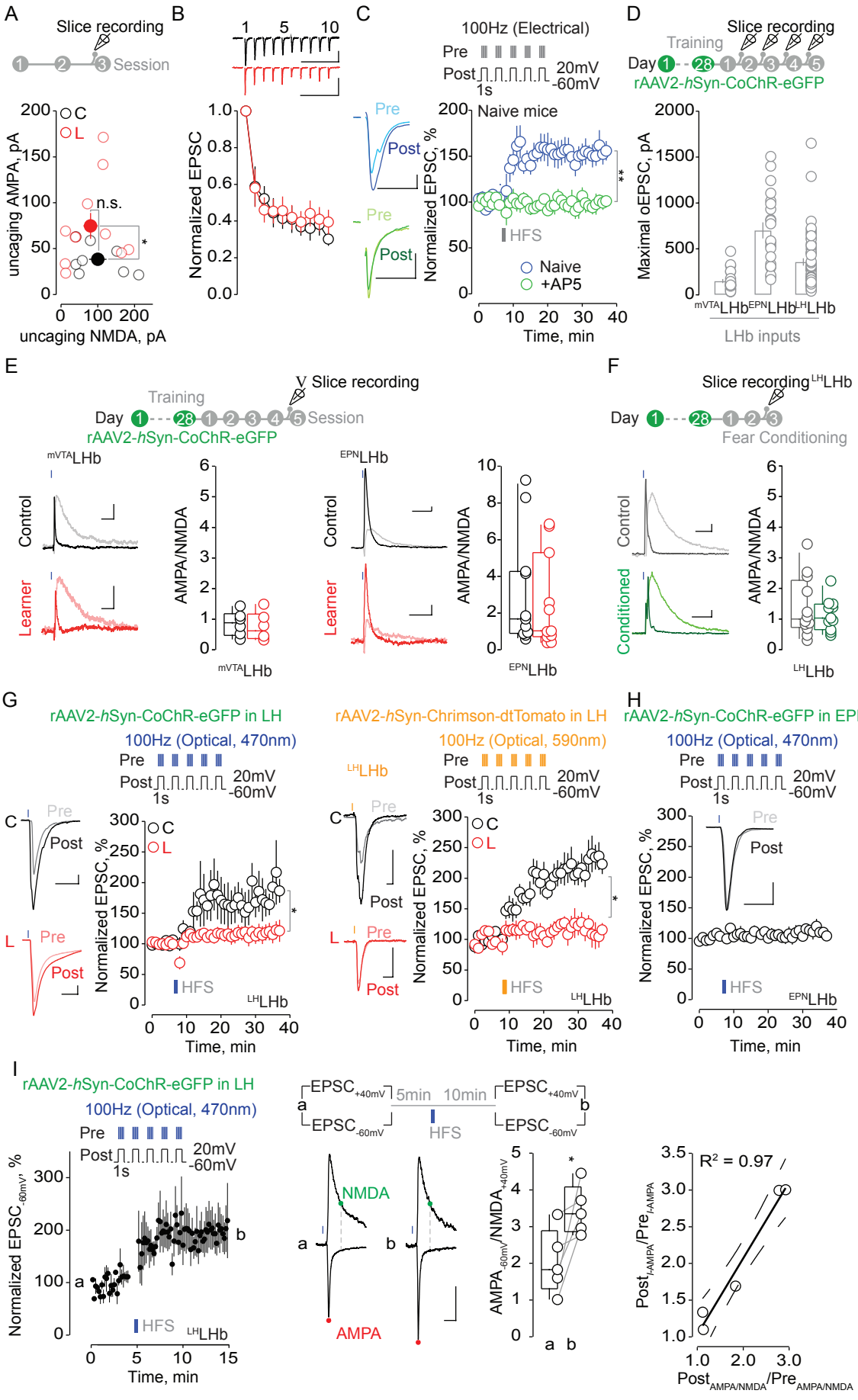

Trusel et al., Figure S2

Figure S2. Properties of excitatory transmission and synaptic plasticity within the LHb. Related to Figure 2 and Figure 3.

(**A**) Correlation plot of AMPAR and NMDAR absolute current amplitudes evoked by MNI-Glutamate uncaging (NMDAR: controls 100.3±23.8, learners 80.6±18.9, t-test, t_{17}=0.6547 p>0.05; AMPAR: controls 38.5±5.8, learners 74.8±13.7, t-test, t_{17}=2.148 *p=0.0464; controls (C, black) $n_{cells}/_{animals}$=8/2; learners (L, red) $n_{cells}/_{animals}$=11/3).

(**B**) Sample traces and plot reporting the amplitude of trains (10 consecutive 20Hz pulses) of electrically-evoked EPSCs, normalized to the first EPSC (Two-Way Anova, $F_{1,22}$=0.67, p>0.05; controls (C, black) $n_{cells}/_{animals}$=12/7; learners (L, red) $n_{cells}/_{animals}$=12/7).

(**C**) Amplitude versus time plot of normalized EPSCs, and sample traces (50 pA, 10 ms) of EPSCs before (light line) and after (dark line) the conditioning protocol (HFS) in LHb-containing slices from naïve animals in presence or absence of the NMDAR antagonist APV (average $EPSC_{34\text{-}36\ min}$: naïve (blue), 154±11.8, $n_{cells}/_{animals}$=6/4; +APV (green), 94.9±7.9, $n_{cells}/_{animals}$=6/3; t-test, t_{10}=4.165 **p=0.0019).

(**D**) Box- and scatter plot reporting the maximal optically-induced current recorded during the optogenetic *ex-vivo* experiments with CoChR. Connectivity rate from subset of recordings: $n_{cellsEPSC}/n_{total}$, LH-LHb 50/50, EPN-LHb 18/18, mVTA 27/34.

(**E**) Experimental timeline and sample traces (20 pA, 20 ms) representing the AMPAR and NMDAR currents (+40 mV). Box and scatter plot of the AMPAR/NMDAR ratios 24 hours after session 4 at mVTA and EPN inputs (V, mVTA: controls (C, black) 0.9±0.2, $n_{cells}/_{animals}$=6/2; learners (L, red) 0.8±0.42, $n_{cells}/_{animals}$=6/2; t-test, t_{10}=0.4 p>0.05. V, EPN: controls (C, black) 3.1±0.9, $n_{cells}/_{animals}$=11/2; learners (L, red) 2.5±0.8, $n_{cells}/_{animals}$=11/2; t-test, t_{20}=0.46 p>0.05).

(**F**) Experimental timeline and sample traces (20 pA, 20 ms) representing the AMPAR and NMDAR currents (+40 mV). Box and scatter plot of the AMPAR/NMDAR ratios at LH inputs 24 hours after a fear conditioning session (controls (gray) 1.4±0.3, $n_{cells}/_{animals}$=7/3; conditioned (green) 1.1±0.2; t-test, t_{21}=0.7 p>0.05).

(**G**) Amplitude versus time plot of normalized EPSCs, and sample traces (50 pA, 20 ms) of light-evoked EPSCs before (light line) and after (dark line) the LTP protocol (HFS) in LHb-containing slices from animals expressing the opsins CoChR and Chrimson in the LH (CoChR; average $EPSC_{34\text{-}36min}$: controls (C, black), 186.2±25.9, $n_{cells}/_{animals}$=9/6; learners (L, red), 116.4±12.3, $n_{cells}/_{animals}$=9/4; t-test, t_{16}=2.297 *p=0.0355. Chrimson; average $EPSC_{34\text{-}36min}$: controls (C, black), 225.2±26.3, $n_{cells}/_{animals}$=6/2; learners (L, red), 113.5±17.3, $n_{cells}/_{animals}$=3/2; t-test, t_7=2.8 *p=0.03).

Data are represented as mean±SEM.

(**H**) Amplitude versus time plot of normalized EPSCs, and sample traces (100 pA, 20 ms) of light-evoked EPSCs before (light line) and after (dark line) the LTP protocol (HFS) in LHb-containing slices from animals expressing the opsins CoChR in the EPN (controls (C, black), average $baseline_{2\text{-}7min}$: 102.2±1.6, average $EPSC_{34\text{-}36min}$: 106.3±10.62, $n_{cells}/_{animals}$=7/2; t-test, t_{12}=0.38 p>0.05).

(**I**) Amplitude versus time plot of normalized EPSCs, and sample traces (50 pA, 20 ms) of light-evoked AMPAR (-60 mV) and AMPAR+NMDAR (+40 mV) EPSCs before (a) and after (b) the LTP protocol (HFS) in LHb-containing slices from animals expressing the opsin CoChR in the LH (naive (black), average $baseline_{1\text{-}4min}$: 102.9±0.6, average $EPSC_{10\text{-}15min}$: 205.4±31.86, $n_{cells}/_{animals}$=5/2; t-test, t_8=3.2 p=0.01). Box plot and scatter plot for AMPAR/NMDAR ratios before (a) and after (b) LTP together with a correlation plot between EPSC amplitude and AMPAR/NMDAR ratio (pre:1.8±0.4, post: 3.0±1.3, $n_{cells}/_{animals}$=5/2; Pre vs post paired t-test, t_6=3.0 *p=0.02). Scatter plot and correlation analysis for fold-change of I_{AMPA} (post/pre-HFS), and the fold-change of the AMPAR/NMDAR (post/pre-HFS) (n=5, Pearson r=0.986, p=0.002, R^2 represents the goodness of fit).

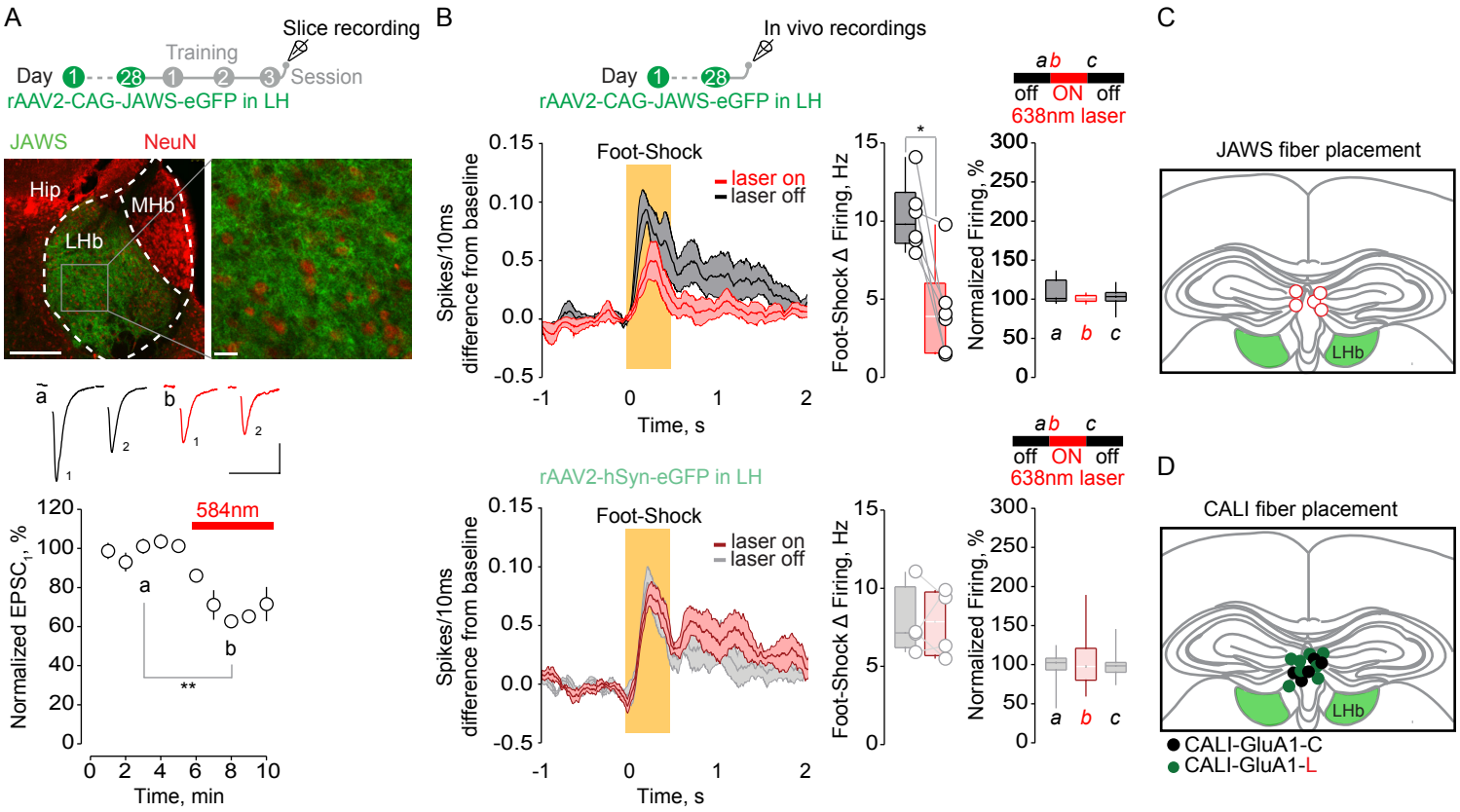

Trusel et al., Figure S3

Figure S3. Validation of silencing and inactivation tools in the LHb. Related to Figure 4.

(**A**) Experimental timeline and sample image depicting JAWS-expressing fibers from LH in the LHb (green) and NeuN staining (red) (scalebar, main, 200 µm, inset, 20 µm). Amplitude versus time plot of normalized EPSCs evoked by extracellular stimulation in the LHb in mice expressing the inhibitory opsin JAWS in the LH, and sample traces (100 pA, 20 ms), before (a, black) and after (b, red) the 584 nm light application (a: 99.5±0.3, b: 71.3±1.5, $n_{cells}/_{animals}$=4/1, paired t-test, t_3=9.978 **p=0.0021).

(**B**) Peristimulus time histogram (PSTH) for footshock-evoked excitation (Fs, 0.5 s, 3mA, ISI: 5 s) reporting average spike counting for Fs-excited LHb neurons before and during exposure to 638 nm light in animals infused with $rAAV_2$-CAG-JAWS-eGFP (Top) or $rAAV_2$-hSyn-eGFP (Bottom). Box plots graph and scatter plot for shock-driven activity without/with light delivery ($rAAV_2$-CAG-JAWS-eGFP: laser off (black) 10.3±0.9, laser ON (red) 4.2±1.2, $n_{cells}/_{animals}$=6/3; t-test, t_5=3.96 *p=0.01. $rAAV_2$-hSyn-eGFP: laser off (black) 7.7±1.1, laser ON (red) 7.6±1.1, $n_{cells}/_{animals}$=4/2; t-test, t_3=0.037 p>0.05). Box plots referring to averaged firing activity during 1 second prior light ON (a), during light (b) and immediately after light off ($rAAV_2$-CAG-JAWS-eGFP: laser off (a, black) 96.3±5.5, laser ON (b, red) 106.8±10.7, laser off (c, black) 100.2±7.1 $n_{cells}/_{animals}$=20/3; Friedman test, p>0.05. $rAAV_2$-hSyn-eGFP: laser off (a, gray) 107.8±4.9, laser ON (b, pink) 101.6±1.5, laser off (c, gray) 102.5±4.0 $n_{cells}/_{animals}$=10/2; Friedman test, p>0.05).

Data are represented with box plots (median and quartiles).

(**C**) Schematic of a LHb-containing coronal section including the approximate sites of fibers placement (red circles, N=5) for *in vivo* JAWS experiments.

(**D**) Schematic of a LHb-containing coronal section including the approximate sites of fibers placement relative to the CALI *in-vivo* experiment (black circles, N=8, CALI-GluA1-C, green circles, N=8, CALI-GluA1-L).

Chapter 3: Probing the LHb contribution to cognitive processes

Reward seeking is a fundamental cognitive process shared by most animal species. In many instances, natural environments are dynamic and associative rules between actions and outcomes are labile. Therefore, the brain relies on neuronal computations in order to ensure the attainment of positive outcomes despite changes in contextual properties (White et al., 2013). The manifestation of this phenomenon, known as cognitive flexibility, has long been attributed to prefrontal networks (Ragozzino, 2007). Indeed, diverse PFC regions are associated with behavioral adaptations during value-based decision-making, collectively integrating costs and benefits from past actions in order to instruct future decisions (Euston et al., 2012; Friedman et al., 2015; Murray and Rudebeck, 2018). However, subcortical contributions to these cognitive processes remain poorly understood.

The habenular complex is emerging as an important contributor to cognitive flexibility. In the Morris water maze, LHb lesions leave intact the behavior during early acquisition trials, when there is no expectation about the whereabouts of the safe position, while impairing the performance upon changes in the platform location (Thornton and Davies, 1991; Lecourtier et al., 2004). In maze paradigms designed for reward seeking, habenular inactivation increases the error incidence specifically during reversal training (Baker et al., 2015; Baker et al., 2017). Moreover, LHb dysfunction leads to the loss of reward biases when deciding between outcomes of dynamic cost and magnitude (Stopper and Floresco, 2014). Importantly, these cognitive processes, as well as the function of LHb neurons, are susceptible to stress. For example, chronic stressors favor habit formation by desensitizing subjects to shifts in outcome value (Dias-Ferreira et al., 2009), and concomitantly promote a plethora of synaptic adaptations in LHb neurons (Li et al., 2011; Cerniauskas et al., 2019). Taken together, these observations open the possibility that habenular synaptic adaptations might account for the manifestation of stress-driven cognitive deficits. This is the focus of the present study.

First, we modeled reward-guided behaviors using a T-maze paradigm. By monitoring population calcium dynamics, we showed that LHb neurons exhibit phasic transients of activity time-locked to the omission of expected rewards (i.e., error). These calcium signals are required to minimize the error incidence in favor of obtaining rewards, thereby supporting cognitive performance. We then demonstrated that acute stressors increase the number of errors during the task, and reduce AMPAR transmission in LHb neurons. This synaptic adaptation occurs simultaneously at multiple glutamatergic inputs, including the LHA, EPN, BNST and medial VTA. Finally, by integrating behavioral data after diverse manipulations aiming to modulate synaptic strength, we proved that stress-driven reductions in LHb AMPAR transmission are both sufficient and required for the manifestation of cognitive deficits. In summary, the present study indicates that a subcortical synaptic mechanism, vulnerable to stress, underlies behavioral performance in the context of reward seeking.

The following section includes the manuscript related to this topic, as published in Neuron.

Neuron

Report

Stress undermines reward-guided cognitive performance through synaptic depression in the lateral habenula

Graphical Abstract

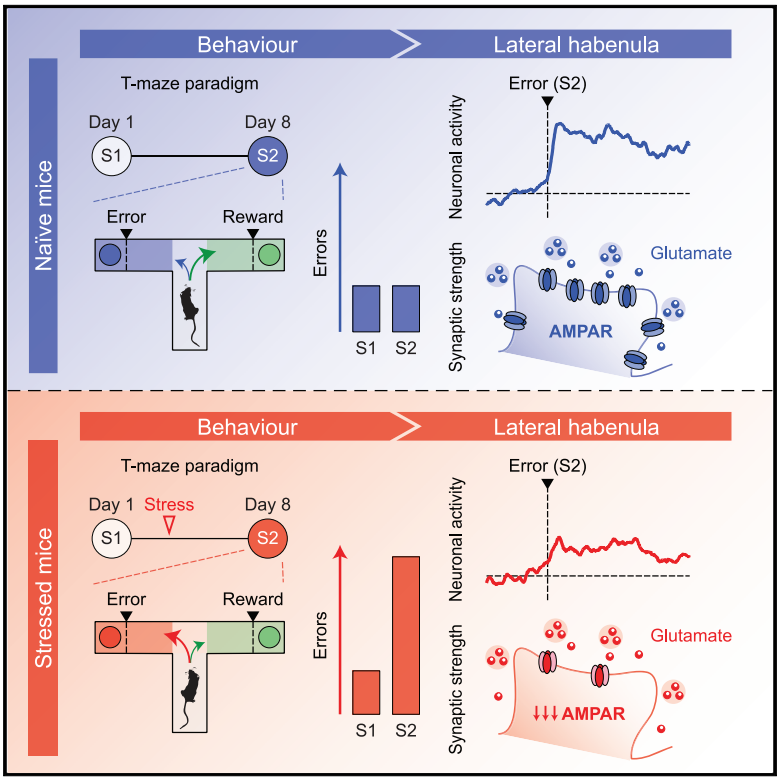

Highlights

- A specific phase during an appetitive cognitive task engages LHb neuronal dynamics
- The strength of excitatory synapses in LHb neurons predicts cognitive performance
- Stress triggers cognitive impairments and disrupts LHb neuronal activity
- Deficits in reward-guided behaviors require a decrease in LHb AMPAR transmission

Authors

Alvaro Nuno-Perez, Massimo Trusel, Arnaud L. Lalive, ..., Mariano Soiza-Reilly, Claudia Bagni, Manuel Mameli

Correspondence

manuel.mameli@unil.ch

In Brief

Effective evaluation of costs and benefits is fundamental for survival and vulnerable to stress. Nuno-Perez et al. show that the strength of AMPAR transmission within the mouse lateral habenula governs the incidence of non-rewarded choices in a reward-guided task. Stress weakens habenular excitatory synapses and consequently augments non-rewarded decisions.

Nuno-Perez et al., 2021, Neuron *109*, 947–956
March 17, 2021
https://doi.org/10.1016/j.neuron.2021.01.008

CellPress

Neuron

CellPress
OPEN ACCESS

Report

Stress undermines reward-guided cognitive performance through synaptic depression in the lateral habenula

Alvaro Nuno-Perez,[1] Massimo Trusel,[1] Arnaud L. Lalive,[1] Mauro Congiu,[1] Denise Gastaldo,[1] Anna Tchenio,[1] Salvatore Lecca,[1] Mariano Soiza-Reilly,[2] Claudia Bagni,[1] and Manuel Mameli[1,3,4,*]

[1]The Department of Fundamental Neuroscience, The University of Lausanne, 1005 Lausanne, Switzerland
[2]IFIBYNE, The University of Buenos Aires, Buenos Aires, Argentina
[3]Inserm, UMR-S 839, 75005 Paris, France
[4]Lead contact
*Correspondence: manuel.mameli@unil.ch
https://doi.org/10.1016/j.neuron.2021.01.008

SUMMARY

Weighing alternatives during reward pursuit is a vital cognitive computation that, when disrupted by stress, yields aspects of neuropsychiatric disorders. To examine the neural mechanisms underlying these phenomena, we employed a behavioral task in which mice were confronted by a reward and its omission (i.e., error). The experience of error outcomes engaged neuronal dynamics within the lateral habenula (LHb), a subcortical structure that supports appetitive behaviors and is susceptible to stress. A high incidence of errors predicted low strength of habenular excitatory synapses. Accordingly, stressful experiences increased error choices while decreasing glutamatergic neurotransmission onto LHb neurons. This synaptic adaptation required a reduction in postsynaptic AMPA receptors (AMPARs), irrespective of the anatomical source of glutamate. Bidirectional control of habenular AMPAR transmission recapitulated and averted stress-driven cognitive deficits. Thus, a subcortical synaptic mechanism vulnerable to stress underlies behavioral efficiency during cognitive performance.

INTRODUCTION

The willingness to obtain a reward prompts goal-directed behaviors whose execution relies on the online deployment of cognitive processes (Halassa and Kastner, 2017). Events compromising the homeostatic state of individuals, defined here as stress, imperil such reward-guided cognitive capacities (Friedman et al., 2017). The prefrontal cortex contributes to cognitive functions, yet how subcortical neuronal systems govern these aspects in physiological and pathological conditions remains elusive (Arnsten, 2015).

The epithalamic lateral habenula (LHb) conveys reward and aversive signals to monoaminergic brain centers, including the mesolimbic dopamine system (Lecca et al., 2014; Matsumoto and Hikosaka, 2007). LHb neurons participate in cognitive processes by shaping decision-making and retrieval of spatial memories (Baker et al., 2015; Mathis et al., 2015; Stopper and Floresco, 2014). Importantly, lesion or pharmacological manipulations of the habenular complex suggest a role for the LHb in guiding choice selection during cognitive performance (Baker et al., 2017; Lecourtier et al., 2004; Thornton and Evans, 1984). For instance, upon the modification of environmental contingencies, perturbing habenular function prevents rodents from updating their decisions in a T-maze paradigm (Nielson and McIver, 1966). Hence, LHb neurons integrate a range of internal and external information to support fitness during cognitive performance.

Exposure to stressors aberrantly increases neuronal activity, promotes long-lasting synaptic adaptations, and induces transcriptional remodeling within the LHb (Cerniauskas et al., 2019; Cui et al., 2018; Lecca et al., 2016; Li et al., 2011). These cellular alterations are instrumental for the emergence of behavioral phenotypes typical of mood disorders (Hu et al., 2020). Stress can concomitantly drive suboptimal decision-making, a hallmark of neuropsychiatric conditions such as anxiety and depression (Friedman et al., 2017; Schwabe and Wolf, 2009; Sousa and Almeida, 2012). However, whether causality exists between neuronal plasticity within the LHb and stress-driven cognitive deficits remains to be addressed.

Here, we combined photometric analysis of calcium signals, slice electrophysiology, and LHb-specific manipulations of excitatory synaptic transmission to establish that (1) LHb neurons participate in a distinct phase of an appetitive task associated with a negative outcome, (2) habenular synaptic strength is predictive for cognitive performance, and (3) stress-driven synaptic depression in LHb neurons is instrumental for the expression of cognitive deficits.

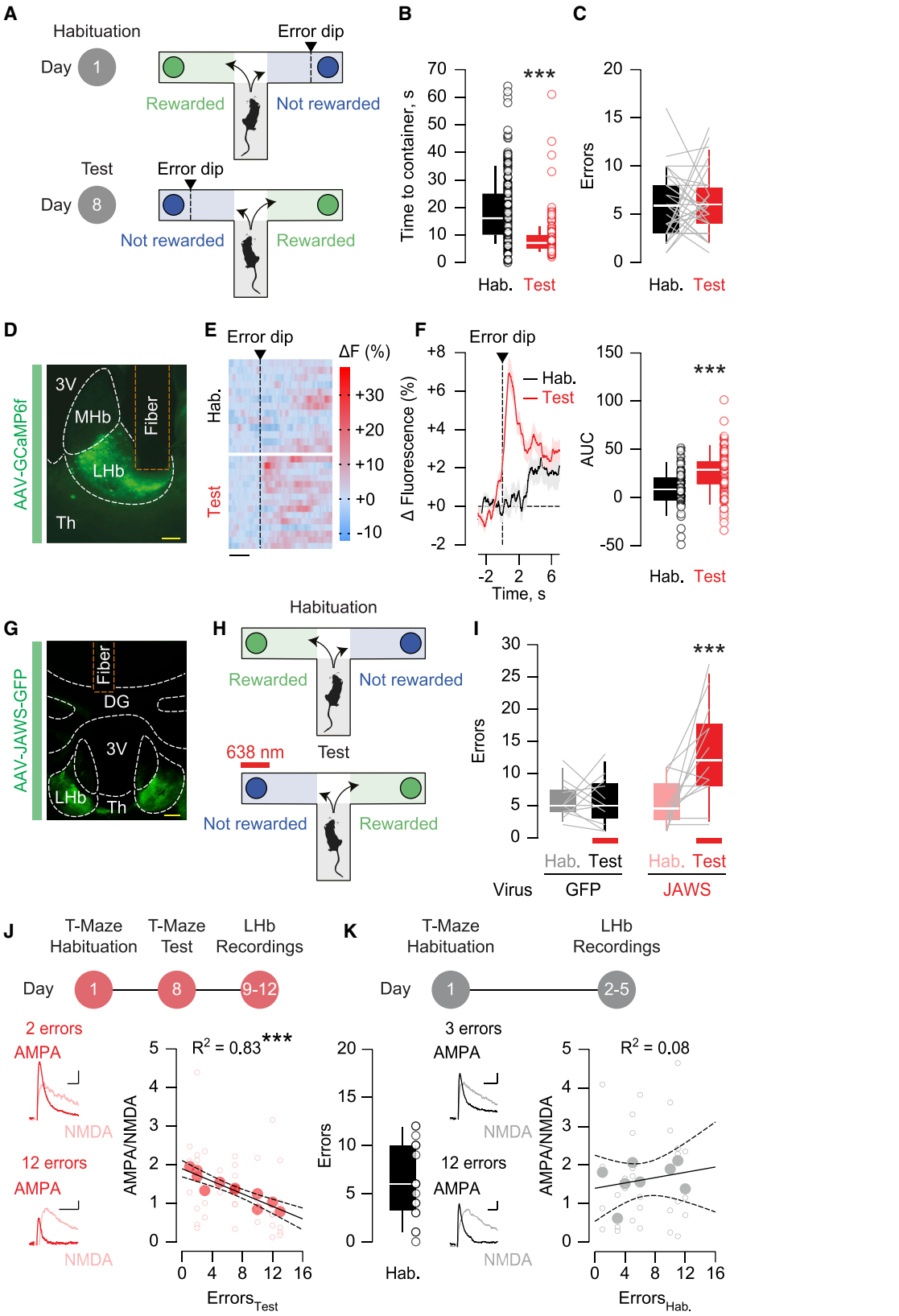

(legend on next page)

RESULTS

Excitatory transmission onto LHb neurons as a substrate for cognitive performance

We designed a reward-guided task using a T-maze paradigm in which food-restricted mice choose between two alternative arms throughout consecutive trials (Friedman et al., 2017). One arm was systematically baited with a food reward (chow, 10 mg), whereas the opposite remained non-baited. Mice were first exposed to the T-maze during the habituation session (day 1) and re-exposed one week later during the test session (day 8), when arm outcomes were inverted (Figure 1A). Sessions were terminated whenever mice chose the rewarded arm 5 consecutive times, or after 35 trials if the completion criterion was not attained. Mice reached the container located at the end of the arms more rapidly during the test session compared with habituation, suggesting the emergence of a goal-directed behavior (Figure 1B). The performance, as measured by the number of head dips into the non-rewarded container (henceforth errors), was comparable across sessions (Figure 1C). Therefore, mice coped efficiently with the switch in outcome position. Moreover, the distribution and preference of reward choices were similar during habituation and the test session (Figures S1A–S1D), suggesting that mice did not simply develop a strategy to avoid the session termination and maximize caloric intake.

The LHb participates in cognitive processes, as well as the encoding of reward omission, but whether specific phases of the T-maze paradigm engage LHb neurons is unknown (Matsumoto and Hikosaka, 2007; Stopper and Floresco, 2014). To test this, we injected a GCaMP6f-expressing adeno-associated virus (AAV; $rAAV_{2.5}$-hSyn1-GCaMP6f) in the LHb to monitor population calcium dynamics with fiber photometry (Figures 1D, S1E, and S1F) (Cui et al., 2014). After increasing the number of trials within a session for analytical and statistical purposes (see STAR Methods), we detected LHb fluorescence transients time-locked to head dips into the non-rewarded container (Figures 1E and 1F). Such calcium signals emerged during early trials of the test session and were smaller in the absence of arm switch (Figures S1G and S1H). In contrast, reward dips led to comparable fluorescence changes across sessions (Figures S1I and S1J). The dichotomy between transients recorded after error and reward dips was conserved when calcium signals were aligned to entry into the respective arms (Figures S1K and S1L). Finally, optical silencing of LHb neurons ($rAAV_8$-hSyn1-JAWS-GFP), which was time locked to error dips during the test session, increased the error incidence compared with control animals (Figures 1G–1I and S1M–S1P). Hence, a distinct phase associated with a negative outcome recruits timely LHb neuronal activity to instruct choice selection during the reward-guided task.

The LHb is defined as a disappointment brain center, and synaptic adaptations of excitatory transmission within this nucleus underlie behaviors in response to negative experiences (Shabel et al., 2019; Trusel et al., 2019). We thereby examined the strength of excitatory synaptic transmission in LHb neurons, after mice experienced reward and error outcomes in the T-maze task. We prepared LHb-containing acute slices and recorded AMPA/NMDA ratios (AMPA/NMDA) as a proxy for postsynaptic efficacy after the test session at day 8 (Lüthi and Lüscher, 2014). The analysis revealed a negative correlation between number of errors performed at day 8 and AMPA/NMDA (Figure 1J). Such a correlation was absent when AMPA/NMDA was recorded after the habituation session (Figure 1K). Altogether, these data demonstrate that encountering the non-rewarded outcome recruits LHb neurons and that excitatory synaptic strength at LHb synapses is predictive for mouse performance in the reward-guided task.

Stress drives cognitive deficits and weakens habenular excitatory transmission

A stressful experience leads to maladaptive shifts in cognitive performance and triggers plasticity of excitatory synaptic transmission in LHb neurons (Friedman et al., 2017; Li et al., 2011). We employed a stressful challenge known to perturb LHb function by subjecting mice to a single session of unpredictable foot shocks one day after the habituation session of the T-maze

Figure 1. Excitatory transmission onto LHb neurons guides cognitive performance during the T-maze task

(A) Schematic of the behavioral paradigm.

(B) Boxplots and scatterplots of the time to reach the arm containers (habituation, black: n = 28 mice/140 trials, 20.02 ± 1.006; test session, red: n = 29 mice/144 trials, 8.688 ± 0.5951). Mann-Whitney test (U = 2,602, ***p < 0.001).

(C) Boxplots and scatterplots of the error incidence (habituation, black: n = 31 mice, 5.839 ± 0.6258; test session, red: n = 31 mice, 6.29 ± 0.5888).

(D) Representative injection site of AAV-GCaMP6f and fiber implantation (scale bar: 100 μm). 3V, third ventricle; M/LHb, medial/lateral habenula; Th, thalamus.

(E) Single-mouse heatmap of LHb fluorescence aligned to entry into the non-rewarded container (error dip; scale bar: 2 s).

(F) Time course of the average LHb fluorescence aligned to entry into the non-rewarded container (error dip). Boxplots and scatterplots of the area under the curve (AUC) (habituation, black: n = 5 mice/40 trials, 8.191 ± 3.429; test session, red: n = 5 mice/74 trials, 25.86 ± 2.758). Mann-Whitney test (U = 830, ***p < 0.001).

(G) Representative injection site of AAV-JAWS and fiber implantation (scale bar: 200 μm). DG, dentate gyrus.

(H) Schematic of the behavioral paradigm. Red light during the test session, aligned to entry into the non-rewarded container.

(I) Boxplots and scatterplots of the error incidence in GFP mice (black: n = 12 mice, 5.75 ± 0.7739 during habituation and 5.75 ± 1.021 during test) and JAWS mice (red: n = 13 mice, 5.154 ± 0.972 during habituation and 13 ± 2.044 during test). Two-way repeated-measure ANOVA ($F_{1,23}$ = 8.306) with Sidak correction (***p < 0.001, habituation versus test).

(J) Experimental timeline. Example traces of AMPA/NMDA after the test session (scale bars: 10 pA and 10 ms). Correlation plot between AMPA/NMDA and error incidence of the test session (open circles: individual values; closed circles: single-mouse averages; n = 11 mice/43 cells). Pearson correlation (R^2 = 0.833, $F_{1,9}$ = 44.89, ***p < 0.001).

(K) Experimental timeline. Boxplots and scatterplots of the error incidence during habituation (n = 16 mice, 5.313 ± 0.7113). Example traces of AMPA/NMDA after habituation (scale bars: 10 pA and 5 ms). Correlation plot between AMPA/NMDA and error incidence during habituation (open circles: individual values; closed circles: single-mouse averages; n = 8 mice/33 cells). Pearson correlation (R^2 = 0.0838, $F_{1,6}$ = 0.5486, p = 0.487).

Data are represented with heatmaps, boxplots (median and quartiles), or mean ± SEM. See also Figure S1.

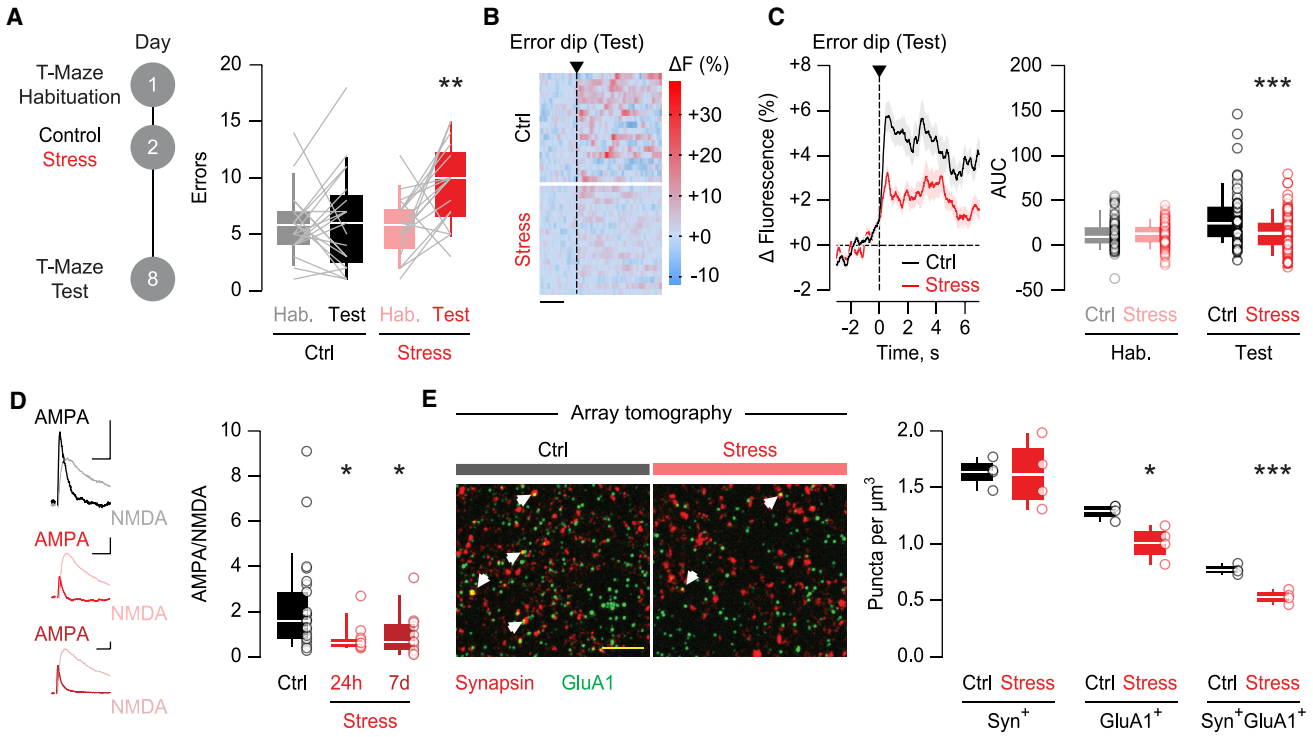

Figure 2. Stress triggers cognitive deficits and reduces AMPAR transmission in LHb neurons

(A) Experimental timeline. Boxplots and scatterplots of the error incidence (control, black: n = 20 mice, 5.8 ± 0.6633 during habituation and 6.05 ± 1.006 during test; stress, red: n = 17 mice, 5.706 ± 0.6847 during habituation and 9.353 ± 0.895 during test). Two-way repeated-measure ANOVA ($F_{1,35}$ = 6.297) with Sidak correction (**p < 0.01, habituation versus test).

(B) Single-mouse heatmap of LHb fluorescence aligned to entry into the non-rewarded container (error dip) during the test session (scale bar: 2 s).

(C) Time course of the average LHb fluorescence aligned to entry into the non-rewarded container (error dip) during the test session. Boxplots and scatterplots of the AUC (control, black: n = 5 mice/69 trials, 12.549 ± 1.987 during habituation; n = 5 mice/76 trials, 30.331 ± 3.363 during test; stress, red: n = 5 mice/70 trials, 12.276 ± 1.57 during habituation; n = 5 mice/91 trials, 14.841 ± 2.144 during test). Two-way ANOVA ($F_{1,302}$ = 10.56) with Sidak correction (***p < 0.001, control versus stress).

(D) Example traces of AMPA/NMDA (scale bars: 30 pA and 10 ms). Boxplots and scatterplots of AMPA/NMDA (control, black: n = 6 mice/26 cells, 2.105 ± 0.4023; stress, light red: 24 h, n = 4 mice/13 cells, 0.76 ± 0.1717; dark red: 7 days, n = 3 mice/12 cells, 0.9567 ± 0.2753). One-way ANOVA ($F_{2,48}$ = 4.042) with Holm-Sidak correction (*p < 0.05, comparisons against control).

(E) Array tomography images obtained from single 100-nm slices immunolabeled against Synapsin (red) and GluA1 (green) (scale bar: 5 μm). White arrows indicate representative puncta showing co-localization of both markers. Boxplots and scatterplots of the number of puncta per cubic micrometer (control, black: n = 4 mice, 1.633 ± 0.0615 for Synapsin, 1.289 ± 0.0319 for GluA1 and 0.769 ± 0.0207 for Synapsin/GluA1; stress, red: n = 4 mice, 1.616 ± 0.1474 for Synapsin, 1.01 ± 0.0723 for GluA1 and 0.5303 ± 0.0282 for Synapsin/GluA1). Unpaired Student's t test (GluA1: t_6 = 3.525, *p < 0.05; Synapsin/GluA1: t_6 = 6.828, ***p < 0.001). Data are represented with heatmaps, boxplots (median and quartiles), or mean ± SEM. See also Figures S2 and S3.

task (Stamatakis and Stuber, 2012). One week later, mice performed a greater number of errors during the test session, in contrast with control animals (Figure 2A). Accordingly, stress-exposed mice shifted their choice from reward-to-reward toward reward-to-error transitions (Figures S2A and S2B). Moreover, mice from all experimental groups reached the container located at the end of the arms more rapidly during the test session (Figure S2C), suggesting that a stressful experience compromises reward-guided behaviors without affecting the motivational component. The cognitive deficits following stress exposure, together with the result of the optical silencing of LHb neurons (Figure 1I), leads to the prediction that stress disrupts LHb calcium dynamics during head dips into the non-rewarded container. Indeed, compared with control animals, stress-exposed mice exhibited smaller fluorescence transients aligned to error dips during the test session (Figures 2B, 2C, S2D, and S2E). The extent of calcium signals negatively correlated with single-mouse error incidence (Figure S2F). Altogether, these results suggest that stress concomitantly impairs reward-guided behaviors and error-driven LHb neuronal activity.

Inspired by the negative correlation between error incidence and AMPA/NMDA in the LHb (Figure 1J), we hypothesized that stress-exposed mice would exhibit weaker excitatory synaptic transmission than their control counterparts. AMPA/NMDA from LHb neurons diminished in acute brain slices prepared 24 h and 7 days after stress exposure (Figure 2D). Generalizing this finding to stressors of a different nature, AMPA/NMDA decreased similarly 24 h after a single session of restraint stress (Figure S3A). To identify the expression mechanism of this plasticity, we employed quantitative array tomography to visualize habenular AMPA receptors (AMPARs; GluA1) and NMDA receptor (NMDAR) subunits (GluN1). Stress decreased the density of synaptic GluA1

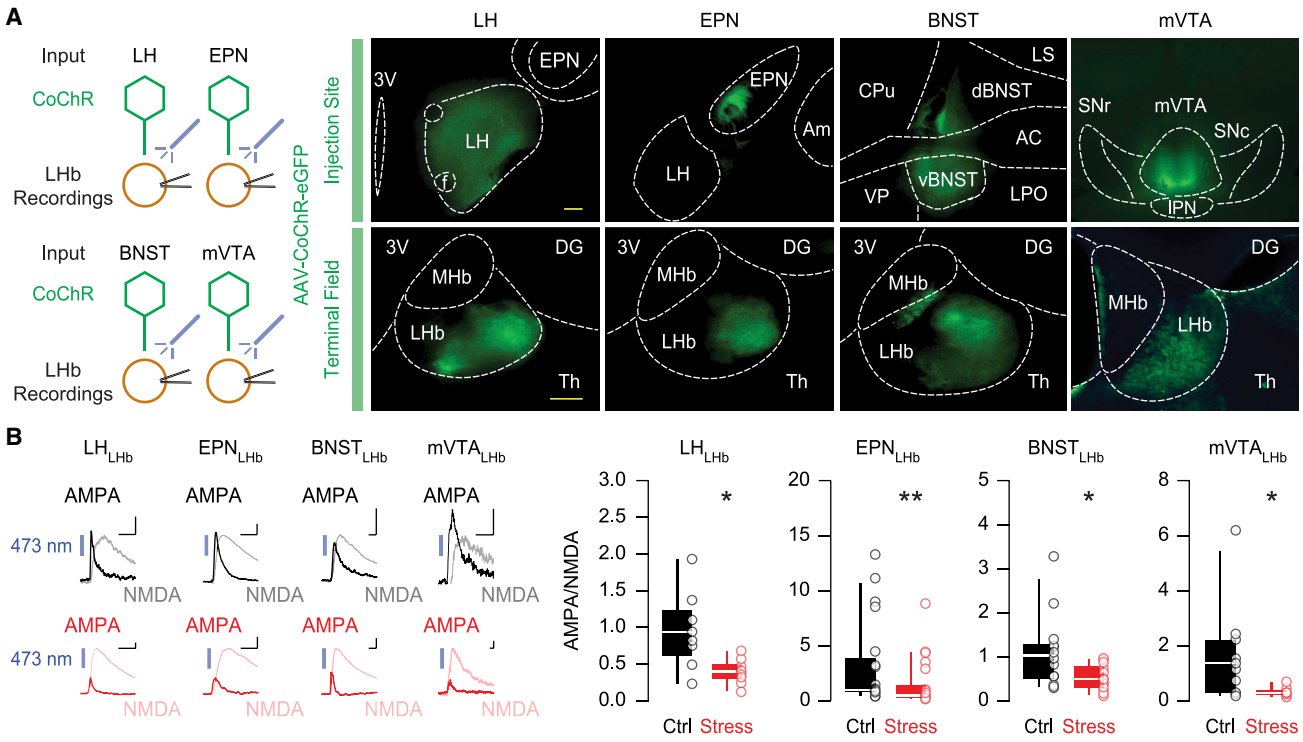

Figure 3. Stress-driven depression of habenular AMPAR transmission is not input-specific

(A) Schematic of the experimental design. Representative injection sites of AAV-CoChR (top, scale bar: 200 μm) and the corresponding terminal field within the LHb (bottom, scale bar: 100 μm). LH, lateral hypothalamus; f, fornix; EPN, entopeduncular nucleus; Am, amygdala; CPu, caudate putamen; VP, ventral pallidum; LS, lateral septum; d/vBNST, dorsal/ventral bed nucleus of the stria terminalis; AC, anterior commissure; LPO, lateral preoptic area; SNr/c, substantia nigra pars reticulata/compacta; mVTA, medial ventral tegmental area; IPN, interpeduncular nucleus.

(B) Example traces of input-specific AMPA/NMDA (scale bars: 50 pA and 10 ms for LH, EPN, and BNST; 10 pA and 10 ms for mVTA). Boxplots and scatterplots of AMPA/NMDA (control, black: LH, n = 2 mice/8 cells, 0.9538 ± 0.1864; EPN, n = 5 mice/20 cells, 3.164 ± 0.8938; BNST, n = 4 mice/13 cells, 1.102 ± 0.235; mVTA, n = 3 mice/10 cells, 1.633 ± 0.5646; stress, red: LH, n = 3 mice/9 cells, 0.3944 ± 0.0559; EPN, n = 7 mice/22 cells, 1.431 ± 0.4577; BNST, n = 5 mice/13 cells, 0.5162 ± 0.0799; mVTA, n = 2 mice/8 cells, 0.3113 ± 0.0636). Mann-Whitney test (LH: U = 10; EPN: U = 110; BNST: U = 41.5; mVTA: U = 12.5) (**p < 0.01, *p < 0.05). Data are represented with boxplots (median and quartiles) or mean ± SEM. See also Figure S3.

without affecting GluN1 puncta, pointing to AMPAR downscaling as the main underlying mechanism for stress-induced AMPA/NMDA reduction (Figures 2E and S3B). Reinforcing this idea, stress lowered AMPA/NMDA and AMPAR currents evoked by single-photon (S)-α-Amino-2,3-dihydro-4-methoxy-7-nitro-δ-oxo-1H-indole-1-pentanoic acid (MNI)-glutamate uncaging, as well as the frequency and amplitude of AMPAR, but not NMDAR, excitatory postsynaptic currents (EPSCs) (Figures S3C–S3E). Finally, stress decreased the AMPAR rectification index and sensitivity to the GluA2-lacking AMPAR blocker NASPM without affecting currents evoked by stimulation with high-frequency trains (Figures S3F–S3H). Thus, although we cannot rule out changes in NMDAR transmission, a stressful experience produces maladaptive reward-guided behaviors, together with a postsynaptic reduction in GluA1 AMPAR at LHb synapses.

Circuit basis of stress-driven AMPAR plasticity

We next examined whether stress-driven synaptic depression follows a circuit-specific rule or occurs widely throughout the LHb. LHb neurons receive glutamatergic inputs from different brain regions, including the lateral hypothalamus (LH), the entopeduncular nucleus (EPN) of the basal ganglia, the bed nucleus of the stria terminalis (BNST), and the medial ventral tegmental area (mVTA) (Lazaridis et al., 2019; Root et al., 2014; Shabel et al., 2012; Stamatakis et al., 2016). To investigate input-specific efficacy of glutamatergic neurotransmission, we independently injected a *Chloromonas oogama* channelrhodopsin (CoChR)-encoding AAV (rAAV$_{2.5}$-hSyn1-CoChR-eGFP) in the LH, EPN, BNST, or mVTA (Figure 3A) (Trusel et al., 2019). Recording input-specific AMPA/NMDA in the LHb revealed a reduction in synaptic strength at all inputs probed 24 h after stress exposure (Figure 3B). Input-specific stimulation with high-frequency trains displayed no alteration in presynaptic function at any input except for the mVTA, which reflected a reduction in release probability following stress exposure (Figure S3I) (Cerniauskas et al., 2019). Therefore, a stressful experience weakens AMPAR transmission onto LHb neurons, regardless of the anatomical source of glutamate.

Establishing causality between stress-driven synaptic depression and cognitive deficits

Is the stress-driven weakening of habenular excitatory transmission required for the increased error incidence in the T-maze task? Initially, we aimed to emulate the stress-driven synaptic

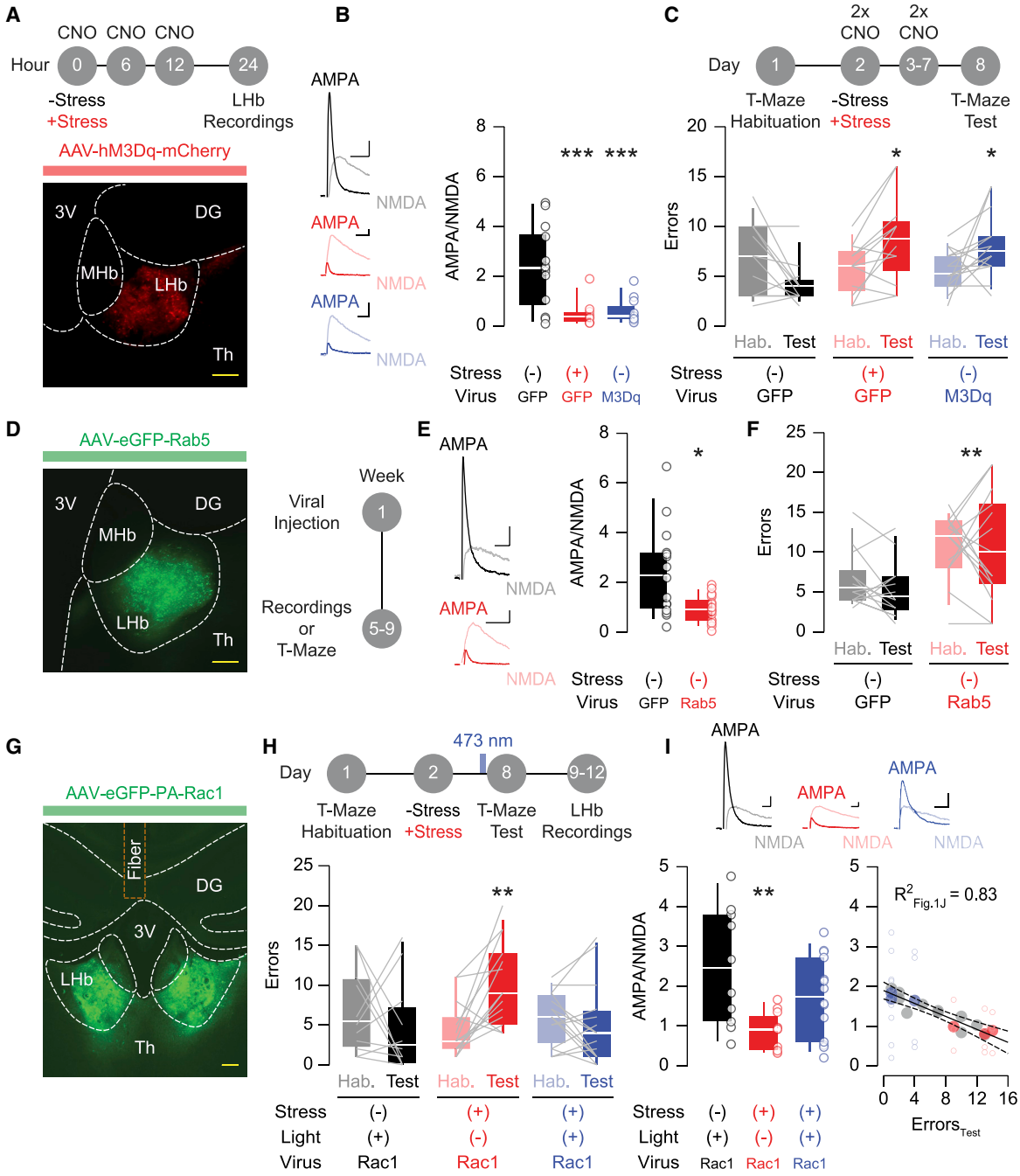

Figure 4. Reduction and potentiation of habenular AMPAR transmission mimics and rescues stress-driven cognitive deficits

(A) Experimental timeline. Representative injection site of AAV-hM3Dq (scale bar: 100 μm).

(B) Example traces of AMPA/NMDA (scale bars: 30 pA and 10 ms). Boxplots and scatterplots of AMPA/NMDA from control/GFP mice (black: n = 3 mice/13 cells, 2.353 ± 0.4565), stress/GFP mice (red: n = 3 mice/11 cells, 0.4818 ± 0.1509), and control/M3Dq mice (blue: n = 3 mice/12 cells, 0.5575 ± 0.1453). One-way ANOVA ($F_{2,33}$ = 12.18) with Holm-Sidak correction (***p < 0.001, comparisons against control/GFP).

(C) Experimental timeline. Boxplots and scatterplots of the error incidence in control/GFP mice (black: n = 12 mice, 6.833 ± 1.043 during habituation and 4.167 ± 0.6134 during test), stress/GFP mice (red: n = 12 mice, 5.75 ± 0.7295 during habituation and 8.75 ± 1.262 during test), and control/M3Dq mice (blue: n = 15 mice, 5.533 ± 0.5152 during habituation and 8 ± 0.8338 during test). Two-way repeated-measure ANOVA ($F_{1,36}$ = 2.342) with Sidak correction (*p < 0.05, habituation versus test).

(D) Representative injection site of AAV-Rab5 (scale bar: 100 μm). Experimental timeline.

(E) Example traces of AMPA/NMDA (scale bars: 25 pA and 10 ms). Boxplots and scatterplots of AMPA/NMDA (GFP, black: n = 3 mice/15 cells, 2.391 ± 0.4619; Rab5, red: n = 5 mice/20 cells, 0.938 ± 0.116). Mann-Whitney test (U = 74.5, *p < 0.05).

(legend continued on next page)

adaptation by capitalizing on the concept of homeostatic downscaling, whereby prolonged neuronal hyperactivity reduces the strength of synaptic transmission (Pan-Vazquez et al., 2020; Pati et al., 2019; Turrigiano, 2008). We injected an hM3Dq-encoding AAV (rAAV$_{8.2}$-hSyn1-hM3Dq-mCherry) into the LHb, allowing neuronal depolarization after exposure to the specific ligand clozapine N-oxide (CNO) (Figures S4A and S4B). Repeated intraperitoneal CNO administration, throughout one day or six consecutive days, decreased AMPA/NMDA and the amplitude of miniature EPSCs 12 h after the last CNO exposure, reproducing the stress-driven synaptic depression (Figures 4A, 4B, and S4C). Consequently, two daily CNO administrations in the intervening days between habituation and test session increased the number of errors at day 8 of the T-maze task (Figure 4C). Hence, LHb-specific weakening of excitatory synapses is sufficient to recapitulate stress-driven maladaptations in reward-guided performance.

However, homeostatic downscaling remains an indirect intervention to reduce excitatory synaptic transmission. Rab5 and Rac1 are small guanosine triphosphatases (GTPases) that weaken and potentiate AMPAR expression and function, respectively (Brown et al., 2005; Wright et al., 2020). Viral Rab5 overexpression within the LHb (rAAV$_{8.2}$-hSyn1-eGFP-Rab5) reduced AMPA/NMDA and increased the number of errors during the reward-guided task, simulating stress-driven synaptic adaptation and subsequent behavioral impairment (Figures 4D–4F and S4A). A drawback of this manipulation is the weak temporal control of Rab5 overexpression, because the reduction in AMPAR transmission occurs before the behavioral assessment. To overcome this limitation, we virally delivered a photoactivatable (PA) version of Rac1 in the LHb (rAAV$_{8.2}$-hSyn1-eGFP-PA-Rac1), which enables the potentiation of AMPAR transmission to be spatially and temporally restricted (Wright et al., 2020). Blue light exposure (473 nm) potentiated AMPAR currents onto LHb neurons in acute brain slices (Figure S4D). We then transduced PA-Rac1 in the LHb and concomitantly implanted an optic fiber above the site of injection (Figures 4G, S4A, and S4E). Animals underwent habituation and were (or not) exposed to stimulation with blue light at day 8, immediately before the test session (1 Hz, 40 minutes). Stress-exposed mice subjected to blue light performed a similar number of errors as the control group, in contrast with their stressed counterparts not exposed to blue light (Figures 4H and S4F). We then recorded *ex vivo* AMPA/NMDA from a cohort of these mice. Although PA-Rac1 overexpression in the absence of light left unaltered the stress-driven reduction in AMPA/NMDA, *in vivo* Rac1 photoactivation normalized this parameter (Figure 4I). Interestingly, the resulting AMPA/NMDA values fell within a linear regression comparable with that of the naive mice in Figure 1J (Figures 4I and S4G). These data reinforce a scenario in which the strength of excitatory synapses in LHb neurons predicts the error incidence during the test session of the reward-guided task.

DISCUSSION

The LHb represents a core neuronal substrate for aversive behaviors, depressive symptoms, and coping strategies (Hu et al., 2020). Furthermore, stress biases the LHb encoding of positive and negative stimuli, likely contributing to pathological states (Shabel et al., 2019). We highlight here an unconventional facet of LHb neurons by providing a synaptic foundation governing cognitive performance during appetitive behaviors.

A synaptic framework for cognitive performance

Despite the central role of cognitive computations during reward-guided choices, their neuronal underpinnings are a matter of debate. Within the mammalian brain, decisions are made not by single neuronal domains but by the collective dynamics of multiple brain circuits (Wang, 2008). Animal physiology and human functional imaging defined the activity and synaptic strength in the prefrontal cortex as instrumental contributors to the control of decision-making (Arnsten et al., 2012). In our study, we propose that excitatory synaptic transmission within a subcortical node is required for reward-guided cognitive performance. Namely, we show that the low strength of AMPAR transmission in LHb neurons predicts a high incidence of errors during reward pursuit. Stress-driven synaptic depression, as well as LHb optical silencing, drives cognitive deficits through the disruption of reward omission encoding. Our photometric analysis highlights that such a process emerges during the test session, coinciding with the time in which the association between context and reward is already in place (Cherng et al., 2020; Palumbo et al., 2020). Future studies will need to elucidate whether LHb synaptic strength and neuronal activity are universal for shaping the performance during cognitive processes of an alternative nature. This is a plausible scenario, because pharmacological blockade of habenular glutamate receptors compromises the retrieval of spatial memories (Mathis et al., 2015). NMDAR decrease and dendritic spine loss in the prefrontal cortex contribute to working-memory deficits (Arnsten et al., 2012; Hains et al., 2009). In the hippocampus, AMPAR reduction mediates the emergence of adaptive behaviors in spatial memory

(F) Boxplots and scatterplots of the error incidence (GFP, black: n = 13 mice, 6.538 ± 0.9715 during habituation and 5.231 ± 0.9881 during test; Rab5, red: n = 14 mice, 10.79 ± 1.1 during habituation and 10.43 ± 1.848 during test). Two-way repeated-measure ANOVA ($F_{1,25}$ = 9.965, **p < 0.01, GFP versus Rab5 interaction).
(G) Representative injection site of AAV-PA-Rac1 and fiber implantation (scale bar: 200 μm).
(H) Experimental timeline. Boxplots and scatterplots of the error incidence in PA-Rac1 mice subjected to control/light (black: n = 11 mice, 6.636 ± 1.591 during habituation and 4.545 ± 1.729 during test), stress/no-light (red: n = 14 mice, 4.429 ± 0.9061 during habituation and 10.36 ± 1.393 during test), and stress/light (blue: n = 15 mice, 5.933 ± 0.8421 during habituation and 5 ± 1.317 during test). Two-way repeated-measure ANOVA ($F_{1,37}$ = 0.9971) with Sidak correction (**p < 0.01, habituation versus test).
(I) Example traces of AMPA/NMDA (scale bars: 20 pA and 5 ms). Boxplots and scatterplots of AMPA/NMDA from a cohort of mice in (H) (black: control/light, n = 2 mice/10 cells, 2.454 ± 0.466; red: stress/no-light, n = 3 mice/11 cells, 0.8827 ± 0.1408; blue: stress/light, n = 3 mice/14 cells, 1.726 ± 0.2739). One-way ANOVA ($F_{2,32}$ = 5.882, **p < 0.01). Overlay of the stressed PA-Rac1 mice onto the correlation analysis of Figure 1J (open circles: individual values; closed circles: single-mouse averages; n = 6 mice/25 cells).
Data are represented with boxplots (median and quartiles) or mean ± SEM. See also Figure S4.

tasks (Awasthi et al., 2019). Therefore, synaptic depression of excitatory transmission throughout the brain may represent a common substrate to modulate diverse cognitive functions.

Mechanistic and circuit understanding of stress-driven cognitive deficits

Stressful life events constitute a key environmental risk factor for the development of neuropsychiatric disorders (Monroe and Harkness, 2005). In addition, stress exerts aberrant effects on the structure and function of excitatory synapses in multiple brain regions (Thompson et al., 2015). Both acute and chronic stressors perturb LHb function, yet this occurs through distinct mechanisms and by engaging diverse neuronal circuits (Cerniauskas et al., 2019; Knowland et al., 2017; Lecca et al., 2016; Li et al., 2011; Shabel et al., 2014). Our observation that a stressful experience drives AMPAR synaptic depression in LHb neurons supports the general framework whereby aberrant synaptic transmission underlies stress-driven behavioral deficits. However, specific examination of the NMDAR component after stress is necessary to understand the complete landscape of cellular adaptations at excitatory synapses. Notably, the induction mechanism of habenular AMPAR downscaling remains unknown. In zebrafish, prolonged stress engages the progressive recruitment of larger neuronal ensembles (Andalman et al., 2019). AMPAR two-photon monitoring at individual spines opens an opportunity to test whether stress-driven synaptic depression originates at discrete LHb neurons and synapses and subsequently spreads to neighboring ones (Roth et al., 2020).

The AMPAR depression described here lacks input specificity, thereby contrasting with the prevailing view that behavioral adaptations often rely on plasticity within precise neuronal circuits (LeGates et al., 2018; Pascoli et al., 2018; Zhou et al., 2019). However, our data do not rule out output circuit specificity. Accordingly, LHb innervation of neurons in the rostromedial tegmental nucleus mediates reward prediction error responses, positioning the LHb-to-midbrain projection as a novel element for cognitive performance (Li et al., 2019). The diverse LHb neuronal clusters emerging based on molecular diversity, as well as anatomical projection targets, might prove useful in defining whether stress-driven modifications follow a clear biological rule (Hashikawa et al., 2020; Wallace et al., 2020).

Altogether, the present work unravels the instrumental role of excitatory transmission within a subcortical node essential to avoid reward omissions, a fundamental module governing appetitive behaviors.

STAR★METHODS

Detailed methods are provided in the online version of this paper and include the following:

- KEY RESOURCES TABLE
- RESOURCE AVAILABILITY
  - Lead contact
  - Materials availability
  - Data and code availability
- EXPERIMENTAL MODEL AND SUBJECT DETAILS
- METHOD DETAILS
  - Stereotaxic surgeries
  - Stress paradigms
  - T-maze paradigm
  - Fiber photometry
  - Viral manipulations
  - Electrophysiology in acute brain slices
  - Glutamate uncaging
  - Single-unit recordings under anesthesia
  - Histology
  - Array tomography
- QUANTIFICATION AND STATISTICAL ANALYSIS

SUPPLEMENTAL INFORMATION

Supplemental Information can be found online at https://doi.org/10.1016/j.neuron.2021.01.008.

ACKNOWLEDGMENTS

We thank the Mameli laboratory, F.J. Meye, D. Jabaudon, J.A. Esteban, and C. Lüscher for their feedback on the manuscript. We thank the UZH Viral Vector Facility for technical support. We thank J.A. Esteban (CSIC, Madrid) for providing the Rab5 construct. This work was supported by a European Starting Grant (ERC SalienSy 335333), Swiss National Funding (31003A) to M.M., NCCR Synapsy (51NF40-158776), and Swiss National Funding (310030-182651/1) to C.B.

AUTHOR CONTRIBUTIONS

A.N.-P. performed and analyzed electrophysiological recordings and behavioral experiments. M.T., A.L.L., M.C., A.T., and M.M. helped with electrophysiology and behavior. S.L. assisted with photometric recordings. M.S.-R. performed and analyzed array tomography experiments. D.G. and C.B. conducted and analyzed biochemical studies. M.M. and A.N.-P. designed the study and wrote the manuscript with the help of all authors.

DECLARATION OF INTERESTS

The authors declare no competing interests.

Received: April 24, 2020
Revised: October 5, 2020
Accepted: January 8, 2021
Published: February 2, 2021

REFERENCES

Andalman, A.S., Burns, V.M., Lovett-Barron, M., Broxton, M., Poole, B., Yang, S.J., Grosenick, L., Lerner, T.N., Chen, R., Benster, T., et al. (2019). Neuronal Dynamics Regulating Brain and Behavioral State Transitions. Cell *177*, 970–985.e20.

Arnsten, A.F. (2015). Stress weakens prefrontal networks: molecular insults to higher cognition. Nat. Neurosci. *18*, 1376–1385.

Arnsten, A.F., Wang, M.J., and Paspalas, C.D. (2012). Neuromodulation of thought: flexibilities and vulnerabilities in prefrontal cortical network synapses. Neuron *76*, 223–239.

Awasthi, A., Ramachandran, B., Ahmed, S., Benito, E., Shinoda, Y., Nitzan, N., Heukamp, A., Rannio, S., Martens, H., Barth, J., et al. (2019). Synaptotagmin-3 drives AMPA receptor endocytosis, depression of synapse strength, and forgetting. Science *363*, 6422.

Baker, P.M., Oh, S.E., Kidder, K.S., and Mizumori, S.J. (2015). Ongoing behavioral state information signaled in the lateral habenula guides choice flexibility in freely moving rats. Front. Behav. Neurosci. *9*, 295.

Baker, P.M., Raynor, S.A., Francis, N.T., and Mizumori, S.J. (2017). Lateral habenula integration of proactive and retroactive information mediates behavioral flexibility. Neuroscience *345*, 89–98.

Brown, T.C., Tran, I.C., Backos, D.S., and Esteban, J.A. (2005). NMDA receptor-dependent activation of the small GTPase Rab5 drives the removal of synaptic AMPA receptors during hippocampal LTD. Neuron *45*, 81–94.

Cerniauskas, I., Winterer, J., de Jong, J.W., Lukacsovich, D., Yang, H., Khan, F., Peck, J.R., Obayashi, S.K., Lilascharoen, V., Lim, B.K., et al. (2019). Chronic Stress Induces Activity, Synaptic, and Transcriptional Remodeling of the Lateral Habenula Associated with Deficits in Motivated Behaviors. Neuron *104*, 899–915.e8.

Cherng, B.W., Islam, T., Torigoe, M., Tsuboi, T., and Okamoto, H. (2020). The Dorsal Lateral Habenula-Interpeduncular Nucleus Pathway Is Essential for Left-Right-Dependent Decision Making in Zebrafish. Cell Rep. *32*, 108143.

Chuong, A.S., Miri, M.L., Busskamp, V., Matthews, G.A., Acker, L.C., Sørensen, A.T., Young, A., Klapoetke, N.C., Henninger, M.A., Kodandaramaiah, S.B., et al. (2014). Noninvasive optical inhibition with a red-shifted microbial rhodopsin. Nat Neurosci *17*, 1123–1129.

Cui, G., Jun, S.B., Jin, X., Luo, G., Pham, M.D., Lovinger, D.M., Vogel, S.S., and Costa, R.M. (2014). Deep brain optical measurements of cell type-specific neural activity in behaving mice. Nat. Protoc. *9*, 1213–1228.

Cui, Y., Yang, Y., Ni, Z., Dong, Y., Cai, G., Foncelle, A., Ma, S., Sang, K., Tang, S., Li, Y., et al. (2018). Astroglial Kir4.1 in the lateral habenula drives neuronal bursts in depression. Nature *554*, 323–327.

Friedman, A., Homma, D., Bloem, B., Gibb, L.G., Amemori, K.I., Hu, D., Delcasso, S., Truong, T.F., Yang, J., Hood, A.S., et al. (2017). Chronic Stress Alters Striosome-Circuit Dynamics, Leading to Aberrant Decision-Making. Cell *171*, 1191–1205.e28.

Hains, A.B., Vu, M.A., Maciejewski, P.K., van Dyck, C.H., Gottron, M., and Arnsten, A.F. (2009). Inhibition of protein kinase C signaling protects prefrontal cortex dendritic spines and cognition from the effects of chronic stress. Proc. Natl. Acad. Sci. USA *106*, 17957–17962.

Halassa, M.M., and Kastner, S. (2017). Thalamic functions in distributed cognitive control. Nat. Neurosci. *20*, 1669–1679.

Hashikawa, Y., Hashikawa, K., Rossi, M.A., Basiri, M.L., Liu, Y., Johnston, N.L., Ahmad, O.R., and Stuber, G.D. (2020). Transcriptional and Spatial Resolution of Cell Types in the Mammalian Habenula. Neuron *106*, 743–758.e5.

Hu, H., Cui, Y., and Yang, Y. (2020). Circuits and functions of the lateral habenula in health and in disease. Nat. Rev. Neurosci. *21*, 277–295.

Knowland, D., Lilascharoen, V., Pacia, C.P., Shin, S., Wang, E.H., and Lim, B.K. (2017). Distinct Ventral Pallidal Neural Populations Mediate Separate Symptoms of Depression. Cell *170*, 284–297.e18.

Lazaridis, I., Tzortzi, O., Weglage, M., Märtin, A., Xuan, Y., Parent, M., Johansson, Y., Fuzik, J., Fürth, D., Fenno, L.E., et al. (2019). A hypothalamus-habenula circuit controls aversion. Mol. Psychiatry *24*, 1351–1368.

Lecca, S., Meye, F.J., and Mameli, M. (2014). The lateral habenula in addiction and depression: an anatomical, synaptic and behavioral overview. Eur. J. Neurosci. *39*, 1170–1178.

Lecca, S., Pelosi, A., Tchenio, A., Moutkine, I., Lujan, R., Hervé, D., and Mameli, M. (2016). Rescue of GABAB and GIRK function in the lateral habenula by protein phosphatase 2A inhibition ameliorates depression-like phenotypes in mice. Nat. Med. *22*, 254–261.

Lecourtier, L., Neijt, H.C., and Kelly, P.H. (2004). Habenula lesions cause impaired cognitive performance in rats: implications for schizophrenia. Eur. J. Neurosci. *19*, 2551–2560.

LeGates, T.A., Kvarta, M.D., Tooley, J.R., Francis, T.C., Lobo, M.K., Creed, M.C., and Thompson, S.M. (2018). Reward behaviour is regulated by the strength of hippocampus-nucleus accumbens synapses. Nature *564*, 258–262.

Li, B., Piriz, J., Mirrione, M., Chung, C., Proulx, C.D., Schulz, D., Henn, F., and Malinow, R. (2011). Synaptic potentiation onto habenula neurons in the learned helplessness model of depression. Nature *470*, 535–539.

Li, H., Vento, P.J., Parrilla-Carrero, J., Pullmann, D., Chao, Y.S., Eid, M., and Jhou, T.C. (2019). Three Rostromedial Tegmental Afferents Drive Triply Dissociable Aspects of Punishment Learning and Aversive Valence Encoding. Neuron *104*, 987–999.e4.

Lüthi, A., and Lüscher, C. (2014). Pathological circuit function underlying addiction and anxiety disorders. Nat. Neurosci. *17*, 1635–1643.

Mathis, V., Cosquer, B., Avallone, M., Cassel, J.C., and Lecourtier, L. (2015). Excitatory Transmission to the Lateral Habenula Is Critical for Encoding and Retrieval of Spatial Memory. Neuropsychopharmacology *40*, 2843–2851.

Matsumoto, M., and Hikosaka, O. (2007). Lateral habenula as a source of negative reward signals in dopamine neurons. Nature *447*, 1111–1115.

Monroe, S.M., and Harkness, K.L. (2005). Life stress, the "kindling" hypothesis, and the recurrence of depression: considerations from a life stress perspective. Psychol. Rev. *112*, 417–445.

Nielson, H.C., and McIver, A.H. (1966). Cold stress and habenular lesion effects on rat behaviors. J. Appl. Physiol. *21*, 655–660.

Palumbo, F., Serneels, B., Pelgrims, R., and Yaksi, E. (2020). The Zebrafish Dorsolateral Habenula Is Required for Updating Learned Behaviors. Cell Rep. *32*, 108054.

Pan-Vazquez, A., Wefelmeyer, W., Gonzalez Sabater, V., Neves, G., and Burrone, J. (2020). Activity-Dependent Plasticity of Axo-axonic Synapses at the Axon Initial Segment. Neuron *106*, 265–276.e6.

Pascoli, V., Hiver, A., Van Zessen, R., Loureiro, M., Achargui, R., Harada, M., Flakowski, J., and Lüscher, C. (2018). Stochastic synaptic plasticity underlying compulsion in a model of addiction. Nature *564*, 366–371.

Pati, S., Salvi, S.S., Kallianpur, M., Vaidya, B., Banerjee, A., Maiti, S., Clement, J.P., and Vaidya, V.A. (2019). Chemogenetic Activation of Excitatory Neurons Alters Hippocampal Neurotransmission in a Dose-Dependent Manner. eNeuro *6*, ENEURO.0124-19.2019.

Root, D.H., Mejias-Aponte, C.A., Zhang, S., Wang, H.L., Hoffman, A.F., Lupica, C.R., and Morales, M. (2014). Single rodent mesohabenular axons release glutamate and GABA. Nat. Neurosci. *17*, 1543–1551.

Roth, R.H., Cudmore, R.H., Tan, H.L., Hong, I., Zhang, Y., and Huganir, R.L. (2020). Cortical Synaptic AMPA Receptor Plasticity during Motor Learning. Neuron *105*, 895–908.e5.

Schwabe, L., and Wolf, O.T. (2009). The context counts: congruent learning and testing environments prevent memory retrieval impairment following stress. Cogn. Affect. Behav. Neurosci. *9*, 229–236.

Shabel, S.J., Proulx, C.D., Trias, A., Murphy, R.T., and Malinow, R. (2012). Input to the lateral habenula from the basal ganglia is excitatory, aversive, and suppressed by serotonin. Neuron *74*, 475–481.

Shabel, S.J., Proulx, C.D., Piriz, J., and Malinow, R. (2014). Mood regulation. GABA/glutamate co-release controls habenula output and is modified by antidepressant treatment. Science *345*, 1494–1498.

Shabel, S.J., Wang, C., Monk, B., Aronson, S., and Malinow, R. (2019). Stress transforms lateral habenula reward responses into punishment signals. Proc. Natl. Acad. Sci. USA *116*, 12488–12493.

Sousa, N., and Almeida, O.F. (2012). Disconnection and reconnection: the morphological basis of (mal)adaptation to stress. Trends Neurosci. *35*, 742–751.

Stamatakis, A.M., and Stuber, G.D. (2012). Activation of lateral habenula inputs to the ventral midbrain promotes behavioral avoidance. Nat. Neurosci. *15*, 1105–1107.

Stamatakis, A.M., Van Swieten, M., Basiri, M.L., Blair, G.A., Kantak, P., and Stuber, G.D. (2016). Lateral Hypothalamic Area Glutamatergic Neurons and Their Projections to the Lateral Habenula Regulate Feeding and Reward. J. Neurosci. *36*, 302–311.

Stopper, C.M., and Floresco, S.B. (2014). What's better for me? Fundamental role for lateral habenula in promoting subjective decision biases. Nat. Neurosci. *17*, 33–35.

Thompson, S.M., Kallarackal, A.J., Kvarta, M.D., Van Dyke, A.M., LeGates, T.A., and Cai, X. (2015). An excitatory synapse hypothesis of depression. Trends Neurosci. *38*, 279–294.

Thornton, E.W., and Evans, J.A. (1984). The effects of lesions of the habenula nucleus on lever press behaviour during a tandem operant schedule with contrasting response requirements. Behav. Brain Res. *12*, 327–334.

Trusel, M., Nuno-Perez, A., Lecca, S., Harada, H., Lalive, A.L., Congiu, M., Takemoto, K., Takahashi, T., Ferraguti, F., and Mameli, M. (2019). Punishment-Predictive Cues Guide Avoidance through Potentiation of Hypothalamus-to-Habenula Synapses. Neuron *102*, 120–127.e4.

Turrigiano, G.G. (2008). The self-tuning neuron: synaptic scaling of excitatory synapses. Cell *135*, 422–435.

Wallace, M.L., Huang, K.W., Hochbaum, D., Hyun, M., Radeljic, G., and Sabatini, B.L. (2020). Anatomical and single-cell transcriptional profiling of the murine habenular complex. eLife *9*, e51271.

Wang, X.J. (2008). Decision making in recurrent neuronal circuits. Neuron *60*, 215–234.

Wright, W.J., Graziane, N.M., Neumann, P.A., Hamilton, P.J., Cates, H.M., Fuerst, L., Spenceley, A., MacKinnon-Booth, N., Iyer, K., Huang, Y.H., et al. (2020). Silent synapses dictate cocaine memory destabilization and reconsolidation. Nat. Neurosci. *23*, 32–46.

Zhou, W., Jin, Y., Meng, Q., Zhu, X., Bai, T., Tian, Y., Mao, Y., Wang, L., Xie, W., Zhong, H., et al. (2019). A neural circuit for comorbid depressive symptoms in chronic pain. Nat. Neurosci. *22*, 1649–1658.

STAR★METHODS

KEY RESOURCES TABLE

REAGENT or RESOURCE	SOURCE	IDENTIFIER
Antibodies		
Anti-Synapsin-1 (rabbit)	Cell Signaling Technology	AB_2616578
Anti-GluA1 (mouse)	Millipore	AB_11212678
Anti-GluN1 (mouse)	Millipore	AB_94946
Donkey anti-rabbit Alexa Fluor 647	Jackson ImmunoResearch	AB_2492288
Donkey anti-mouse Alexa Fluor 488	Jackson ImmunoResearch	AB_2340846
Donkey anti-mouse Cy3	Jackson ImmunoResearch	AB_2340813
Virus strains		
$rAAV_{2.5}$-hSyn1-CoChR-eGFP	UNC Vector Core	N/A
$rAAV_{1/2}$-hSyn1-$ChR2_{H134R}$-eGFP	UZH Vector Facility	v221-1
$rAAV_{2.5}$-hSyn1-GCaMP6f	Gift from G. Keller (FMI, Basel)	N/A
$rAAV_{8}$-hSyn1-JAWS-GFP	Chuong et al., 2014	Addgene_65014
$rAAV_{8.2}$-hSyn1-hM3Dq-mCherry	UZH Vector Facility	v101-8
$rAAV_{8.2}$-hSyn1-eGFP-Rab5	UZH Vector Facility	v435-8
$rAAV_{8.2}$-hSyn1-eGFP-PA-Rac1	UZH Vector Facility	v371-8
$rAAV_{8.2}$-hSyn1-eGFP	UZH Vector Facility	v81-8
Chemicals, peptides, and recombinant proteins		
Picrotoxin	Hello Bio	HB0506
APV	Hello Bio	HB0225
NBQX disodium salt	Hello Bio	HB0443
MNI-caged L-glutamate	Hello Bio	HB0423
Tetrodotoxin citrate	Hello Bio	HB1035
NASPM trihydrochloride	Hello Bio	HB0441
Clozapine N-oxide dihydrochloride	Hello Bio	HB6149

RESOURCE AVAILABILITY

Lead contact

Further information and requests for resources and reagents should be directed to and will be fulfilled by the Lead Contact, Manuel Mameli (manuel.mameli@unil.ch).

Materials availability

This study did not generate new unique reagents.

Data and code availability

Original data for all figures and datasets in this paper are available upon request to the lead contact. This study did not generate new code.

EXPERIMENTAL MODEL AND SUBJECT DETAILS

Male mice were purchased from Janvier (C57BL6/J) and housed in groups of three-to-five per cage (4-12 weeks old). Food and water were provided *ad libitum* unless otherwise specified, and light-dark phases lasted 12 hours (from 7 a.m. to 7 p.m.). All procedures aimed to fulfil the 3R criterion (i.e., replacement, reduction and refinement) and were approved by the veterinary offices of Vaud (Switzerland; license VD3171).

METHOD DETAILS

Stereotaxic surgeries

4-6 week-old mice were anesthetized with ketamine (150 mg/kg) and xylazine (100 mg/kg) before bilateral injection of $rAAV_{2.5}$-hSyn1-CoChR-eGFP (titer = $1x10^{12}$ vg/mL) or $rAAV_{1/2}$-hSyn1-$ChR2_{H134R}$-eGFP (titer = $3.3x10^{13}$ vg/mL) in the lateral hypothalamus (AP −1.25 from bregma; ML ± 1.0; DV −5.1), entopeduncular nucleus (AP −1.2 from bregma; ML ± 1.8; DV −4.5), bed nucleus of the stria terminalis (AP +0.3 from bregma; ML ± 0.9; DV −4.55) or medial ventral tegmental area (AP −2 from bregma; ML ± 0.25; DV −4.6). Optogenetic recordings in acute brains slices were performed 3-4 weeks after stereotactic viral injection. $rAAV_{2.5}$-hSyn1-GCaMP6f (titer = $5x10^{12}$ vg/mL, 1:5 dilution), $rAAV_8$-hSyn1-JAWS-GFP (titer = $1.3x10^{13}$ vg/mL), $rAAV_{8.2}$-hSyn1-hM3Dq-mCherry (titer = $5.4x10^{12}$ vg/mL), $rAAV_{8.2}$-hSyn1-eGFP-Rab5 (titer = $6.4x10^{12}$ vg/mL), $rAAV_{8.2}$-hSyn1-eGFP-PA-Rac1 (titer = $1.2x10^{12}$ vg/mL) or $rAAV_{8.2}$-hSyn1-eGFP (titer = $9.4x10^{12}$ vg/mL) were injected in the LHb (AP −1.32 from bregma; ML ± 0.42; DV −2.8). Viral serotypes were chosen considering the level of expression and cell viability assessed in previous studies (Trusel et al., 2019). Optic fibers were concomitantly implanted for photometric experiments (Chi Square Bioimaging; DV −2.65), photoactivation of PA-Rac1 (Thorlabs; DV −2.3) and JAWS-driven optical silencing of LHb neurons (Thorlabs; DV −2.3). Mice were exposed to the T-maze task 3-4 weeks after surgery (7-10 week-old). Injection sites and fiber placements were checked for each animal, and mice with incorrect targeting were discarded from the analysis.

Stress paradigms

Foot-shock exposure

7-12 week-old mice were introduced in an operant conditioning chamber with a metal grid on the ground (Ugo Basile). Mice were subjected to a 20-minute session during which they received either 19 (stress) or 0 (control) unpredictable foot shocks with a randomized inter-shock interval of 1-90 s (1 mA intensity, 500 ms duration). Unless otherwise specified, mice were anesthetized for patch-clamp electrophysiology 24 hours after stress exposure. Alternatively, mice were exposed to the foot-shock paradigm 1 day after the habituation session and 6 days before the test session of the T-maze task.

Acute restraint stress

7-12 week-old mice were introduced inside a polyethylene tube (Falcon, 50 mL) during 1.5 hours. For control mice, the tube was introduced in their home cage. Recordings were performed 24 hours after the end of the session.

T-maze paradigm

The T-maze apparatus consisted of a central arm and two side arms (Ugo Basile). The maze was placed 65 cm above the floor. Arm dimensions were 5 cm width, 12 cm height and 35 cm length. One of the arms was systematically baited with a food reward (regular chow, 10 mg) while the opposite arm remained neutral (i.e., absence of reward). Mice were first exposed to the T-maze during the habituation session (day 1), and re-exposed one week later during the test session (day 8). During the latter, unless otherwise stated, arm outcomes were inverted. 48 hours before each session, mice were moved from their home cages to a new cage without food but with water *ad libitum*. Mice were habituated to the T-maze room for at least 1 hour before the commencement of each session. During the habituation and test session, 7-12 week-old mice were placed in the central arm at the beginning of every trial and subsequently chose between the two alternative side arms. When the whole body of the mouse was inside the chosen arm, the door was closed with a remote electronic system. Once the animal consumed the food reward or explored the non-rewarded container, the experimenter brought back the mouse to the home cage and baited, if needed, the rewarded arm with a fresh food pellet. Unless otherwise specified, both sessions were stopped whenever mice would choose the rewarded arm for 5 consecutive times, or after 35 trials provided the completion criterion was not reached. For photometric experiments, with analytical and statistical purposes, the number of errors and rewarded turns was increased by exposing mice to 50 trials in each session. Early and late error trials were categorized as those occurring within the first (0%–25%) and last quarter (75%–100%) during the test session, respectively. All sessions were recorded under infrared light (Noldus). For the calculation of the time needed to reach the container located at the end of the arms, the first 5 trials of the habituation and test session were used for each mouse. Transition probabilities were calculated on a single-mouse basis with the following formula, where $n_{i\rightarrow j}$ denotes the number of transitions between states (i.e., reward or error) and N represents the total amount of transitions:

$$P_{i\rightarrow j} = \frac{n_{i\rightarrow j}}{N} \Big/ \Big/ \sum P_{i\rightarrow j} = 1.$$

Fiber photometry

Experiments were performed with the χ^2-200 system (Chi Square Bioimaging). Blue light from a picosecond-pulsed laser was delivered to the LHb through a single-mode fiber (473 nm, 50 MHz, 80 picosecond full width at half maximum), whereas fluorescence emission was collected from the tissue with a multi-mode fiber. Both fibers were cannulated together throughout a cable, at the end of which a detachable ferrule was connected to the fiber implant located inside the mouse brain. FF01-550/88 bandpass filter was applied over the emitted photons collected by the multi-mode fiber (Semrock). Photons were recorded using a module of time-correlated single-photon counting SPC-130-EMN (Becker & Hickl GmbH). For consistency, calcium signals from all mice included in the present study were acquired using the same gain.

Viral manipulations

For the JAWS optical silencing (mice injected with rAAV$_8$-hSyn1-JAWS-GFP), red light (638 nm, 8 mW, continuous light) was shined during the test session aligned to the entry into the non-rewarded container, using a laser (MatchBox Integrated Optics) coupled to a Master-8 (AMPI) through a TTL system. Regarding the chemogenetic AMPAR downscaling *ex vivo* (mice injected with rAAV$_{8.2}$-hSyn1-hM3Dq-mCherry), three injections of clozapine N-oxide (CNO, 1 mg/kg) were administered intraperitoneally with a time separation of ±6 hours and, 12 hours after the last CNO injection, AMPA/NMDA recordings were performed (7-10 week-old mice). The timeline for these *ex vivo* recordings was chosen to examine the rapid repercussions of LHb hyperactivity driven by hM3Dq on excitatory transmission. For behavioral experiments, CNO was administered intraperitoneally twice per day (1 mg/kg) with a time separation of ±6 hours, during the intervening days between habituation and test session of the T-maze paradigm. In order to probe AMPAR transmission, the same timeline was used for *ex vivo* miniature EPSC recordings. For the photoactivation of PA-Rac1 (mice injected with rAAV$_{8.2}$-hSyn1-eGFP-PA-Rac1), mice were exposed to blue-light stimulation immediately prior to the test session (473 nm, 6-9 mW, 1 Hz, 150 ms pulses for 40 minutes), using a laser (Shanghai Dream Lasers Technology) coupled to a Master-8 (AMPI) through a TTL system. The same optical protocol was employed in acute brain slices to monitor AMPAR current amplitudes.

Electrophysiology in acute brain slices

7-12 week-old mice were anaesthetized with ketamine (150 mg/kg) and xylazine (100 mg/kg) prior to slice preparation. Coronal brain slices (thickness: 250 μm) containing the LHb were cut while immersed in ice-cold solution, bubbled with 95% O_2 and 5% CO_2 and containing the following reagents (in mM): Choline chloride (110); glucose (25); $NaHCO_3$ (25); $MgCl_2$ (7); ascorbic acid (11.6); sodium pyruvate (3.1); KCl (2.5); NaH_2PO_4 (1.25); and $CaCl_2$ (0.5). Slices were then allowed to recover for 1 hour at room temperature in artificial cerebrospinal fluid (ACSF) containing the following reagents (in mM): NaCl (124); $NaHCO_3$ (26.2); glucose (11); KCl (2.5); $CaCl_2$ (2.5); $MgCl_2$ (1.3); and NaH_2PO_4 (1). Borosilicate glass pipettes (Phymep; impedance: 2.5-4 MΩ) were filled with CsCl-based intracellular solution containing the following reagents (in mM): CsCl (130); NaCl (4); creatine phosphate (5); $MgCl_2$ (2); Na_2ATP (2); Na_3GTP (0.6); EGTA (1.1); HEPES (5); and spermine (0.1). Whole-cell voltage-clamp recordings were obtained from LHb neurons at 34°C with a perfusion flow rate of 2.5 mL/min. Throughout the recordings, electrical signal was filtered (5 kHz) and digitized (10 kHz) using MultiClamp 200B (Molecular Devices). Data acquisition was performed with Igor Pro and NIDAQ tools (Wave Metrics). Access resistance was continuously monitored with a voltage step of −4 mV (0.1 Hz). In electrical stimulation experiments, the electrode was introduced inside a glass pipette filled with ACSF and placed within the LHb to evoke EPSCs through an ISO-Flex stimulator coupled to a Master-8 (AMPI). For optogenetic experiments, EPSCs were evoked with an LED coupled to an Olympus-BX51 microscope delivering pulses of blue light (Cool LED; 473 nm, 5 mW, 1-10 ms duration). AMPAR currents, for the measurement of AMPA/NMDA (+40 mV), were pharmacologically isolated by bath application of picrotoxin (PTX, $GABA_AR$ antagonist; 100 μM) and D-2-amino-5-phosphonopentanoic acid (APV, NMDAR antagonist; 100 μM). NMDAR currents were calculated by subtraction analysis. AMPA/NMDA assessment was performed 1-4 days after T-maze in order to maximize the yield of recordings from the same cohort of animals employed for the behavioral experiments. AMPAR miniature EPSCs (−60 mV) were pharmacologically isolated with PTX and APV under bath application of tetrodotoxin (TTX, sodium channel blocker; 1 μM). NMDAR spontaneous EPSCs (−60 mV) were pharmacologically isolated with PTX and NBQX (AMPAR antagonist; 10 μM) in Mg^{2+}-free ACSF. EPSC trains were obtained at a frequency of 20 Hz in the presence of PTX and APV (−50 mV for electrical stimulation, −60 mV for input-specific). Timelines of AMPAR currents were recorded at −50 mV for NASPM-sensitivity experiments (30 μM) and at −60 mV for the photoactivation of PA-Rac1 (473 nm light, 1 Hz, 150 ms pulses), in the presence of PTX and APV. Whole-cell current-clamp recordings were performed to examine the CNO-induced depolarization (10 μM) in the presence of PTX, APV and NBQX. AMPAR rectification index (RI) was calculated under bath application of PTX and APV with the following formula, where I denotes current amplitude in pA:

$$RI = \frac{(-I_{-60}/I_{+40})}{(60/40)}$$

Glutamate uncaging

For MNI-glutamate uncaging (4-methoxy-7-nitroindolinyl-caged L-glutamate; 200 μM, Tocris), a single-path photolysis head was connected to a solid-state laser (Rapp OptoElectronic; 405 nm, 0.5 ms duration of optical pulse, 3-5 μm diameter of photolysis beam). Alignment of the laser path at the center of the recording chambers allowed localization of the photolysis area within the sample. The photolysis beam was positioned ± 80-100 μm away from the cell somata, side-by-side to a visualized dendrite. Optimization of laser photolysis was obtained by adjusting the position of the slice with respect to the laser beam, and the laser power was tuned (3-10 mW), in order to ensure that laser-evoked EPSCs yielded similar kinetics to those of synaptic EPSCs. AMPA/NMDA ratios were obtained by dividing the peak of AMPAR-EPSC (−60 mV) by the NMDAR-EPSC (+40 mV, ± 100 ms after onset when AMPAR-EPSC decayed).

Single-unit recordings under anesthesia

For the validation of rAAV$_8$-hSyn1-JAWS-GFP *in vivo*, 12 week-old mice were anesthetized with intranasal isoflurane (Univentor; 2% for induction, 1%–1.5% for maintenance) and placed onto a stereotaxic apparatus (Kopf Instruments). Their body temperature was maintained at 36°C using a feedback-controlled heating pad (CMA-450; Phymep). The scalp was retracted and a burr hole was drilled

above the LHb (AP −1.32 from bregma; ML ± 0.42; DV −2.8), for the placement of a recording electrode. Single-unit activity of spontaneous action potentials (minimal duration of recording epochs: 3 minutes), was recorded extracellularly using glass micropipettes (impedance: 5-15 MΩ), filled with 2% Chicago Sky Blue dissolved in 0.5 M sodium acetate. The signal was filtered (band-pass: 500-5000 Hz), pre-amplified (DAM80; WPI, Germany), amplified (Neurolog System; Digitimer, UK), and displayed on a digital storage oscilloscope (OX 530; Metrix, USA). Experiments were sampled online and offline by a computer connected to a laboratory interface (CED Power 1401; Cambridge Electronic Design, UK) running the Spike2 software (Cambridge Electronic Design, UK). Stable cells were subjected to 10 pulses of red light (638 nm, 8 mW, continuous light during 10 s). Raster plots and peri-stimulus time histograms were built using a bin width of 1 s.

Histology

Once the behavioral experiments were finished, animals were perfused transcardially with paraformaldehyde (4% PFA in 10 mM PBS). Brains were dissected out and kept at 4°C until slicing. A vibratome VT1000-S (Leica) was used to obtain coronal sections (100 μm). To corroborate proper fiber placement and injection site, we took images with an epi-fluorescent microscope (Zeiss). For optogenetic experiments, pictures were taken from the same slices in which electrophysiological recordings were performed.

Array tomography

Tissue preparation

7 week-old mice were anaesthetized with ketamine (150 mg/kg) and xylazine (100 mg/kg) and perfused transcardially with 4% PFA in 100 mM phosphate buffer (pH 7.4). Brains were dissected out, post-fixed in 4% PFA overnight at 4°C, and then equilibrated in 30% sucrose for 48 hours. Coronal tissue blocks containing both LHb nuclei were cut into 300 μm thick sections using a vibratome, and sections were subsequently processed for array tomography. Tissue sections were dehydrated in graded series of alcohol up to 70% ethanol (5 minutes each step at room temperature). Subsequently, the tissue was infiltrated in a 1:3 mixture of 70% ethanol and LRWhite resin (medium grade; Electron Microscopy Sciences) for 5 minutes, and then two times of 5 minutes in 100% LRWhite. The tissue was then infiltrated in LRWhite overnight at 4°C. On the following day, sections were flat-embedded between a glass slide (to provide a flat surface) and a sheet of ACLAR plastic (Electron Microcopy Sciences) to facilitate removal of the tissue section, and polymerized for 24 hours at 55°C. After embedding, the LHb was excised and mounted on EMBed blocks using a superglue for ultra-sectioning. Series of 25 100-nm sections were cut in ribbons using Jumbo Histo Diamond Knife (Diatome) and an ultra-microtome (UltraCut, Leica). The ribbons were mounted on glass coverslips coated with 0.1% gelatin and 0.01% chromium potassium sulfate, air-dried, placed on a hot plate (60°C) for 30 minutes, and then stored at room temperature until processing for immunofluorescence.

Immunofluorescence

Monoclonal antibodies were used to detect Synapsin-1 (rabbit, 1:200; Cell Signaling Technology; D12G5 XP, #5297), GluA1 (mouse, 1:200; Millipore; MAB2263, RH95) and GluN1 (mouse, 1:200; Chemicon; MAB363, 54.1). DAPI staining was included in each round for alignment purposes. Sections were then re-immunolabeled with a different set of antibodies and re-imaged in two rounds. For immunolabeling, sections were encircled with a hydrophobic barrier pen (ImmEdge, Vector Labs) and pre-incubated for 5 minutes in blocking solution (0.05% Tween, 0.1% bovine serum albumin in Tris buffer saline, pH 7.6). Subsequently, primary antibodies were diluted together in blocking solution and incubated with sections for 2 hours. Sections were thoroughly rinsed with PBS for three times, of 10 minutes each, using a plastic transfer pipette. Fluorescent-conjugated secondary antisera raised in donkey were used (anti-rabbit Alexa Fluor 647, anti-mouse Alexa Fluor 488 and anti-mouse Cy3; 1:200; Jackson ImmunoResearch). Secondary antisera were centrifuged at 13.000 rpm for 3 minutes before usage. Sections were incubated with the secondary antisera for 24 minutes and rinsed. Coverslips with sections were mounted on a glass slide using the SlowFade Gold Antifade Mountant with DAPI (Life Technologies) for imaging. After imaging, applied antibodies were eluted by incubating the sections with 0.02% SDS and 0.2 M NaOH in distilled water for 20 minutes. After two washes of 10 minutes with distilled water, coverslips were air-dried and placed on a hot plate (60°C) for 30 minutes. Upon re-immunolabeling, negative controls omitting primary antisera were run to corroborate the complete elution of primary antibodies.

Microscopy and image processing

Sections were imaged on a Leica DM6000 fluorescence microscope using an oil objective (Plan-Apochromat 63X/1.4 NA; Leica) and a CoolSNAP EZ camera. Serial images were processed, aligned and converted into stacks using Fiji software with *StackReg/MultiStackReg* plugins and DAPI staining. We analyzed 2 stacks per mouse of at least 20 images each. The quantitative analysis was done using sampling masks with average dimensions of 70 μm x 70 μm. Axon terminals were identified by the presence of Synapsin, and their relation to postsynaptic glutamate receptors was analyzed using the *Multiply* operation of the *Image Calculator* function. Resulting objects with overlapping voxels were then counted using the *Object Counter 3D* plugin, yielding density values (puncta per μm^3). Due to the high-resolution of array tomography, adjacent objects located in different synaptic compartments may not co-localize in the classic way, and their immunolabeled voxels may not overlap. To avoid these possible instances of under-detection in the quantitative analysis, we used the *Dilate* function to introduce a mask expansion in the size of one of the objects (< 0.2 μm). In the resulting dataset, we examined the presence of overlapping immunolabeled voxels. A mean density value was calculated per mouse.

QUANTIFICATION AND STATISTICAL ANALYSIS

Data analysis was performed using IGOR Pro (Wave Metrics) and Prism (GraphPad). Most data are represented using box and scatterplots depicting the median, 10%–90% confidence intervals and individual values. Correlation plots illustrate single-mouse means and, when appropriate, individual values. Results from fiber photometry are plotted on a single-mouse basis using heatmaps. For alternative plot representations, we show mean ± SEM. We employed the following statistical tests: Mann-Whitney test, Student's t test, one-way ANOVA and two-way ANOVA. Unless otherwise specified, tests are unpaired and two-tailed. *Post hoc* corrections for multiple comparisons were performed when appropriate (after one-way ANOVA and two-way ANOVA). Significance was conventionally set as ***$p < 0.001$, **$p < 0.01$ and *$p < 0.05$.

Neuron, Volume *109*

Supplemental information

Stress undermines reward-guided cognitive performance through synaptic depression in the lateral habenula

Alvaro Nuno-Perez, Massimo Trusel, Arnaud L. Lalive, Mauro Congiu, Denise Gastaldo, Anna Tchenio, Salvatore Lecca, Mariano Soiza-Reilly, Claudia Bagni, and Manuel Mameli

Nuno-Perez et al., Supplemental Figure 1

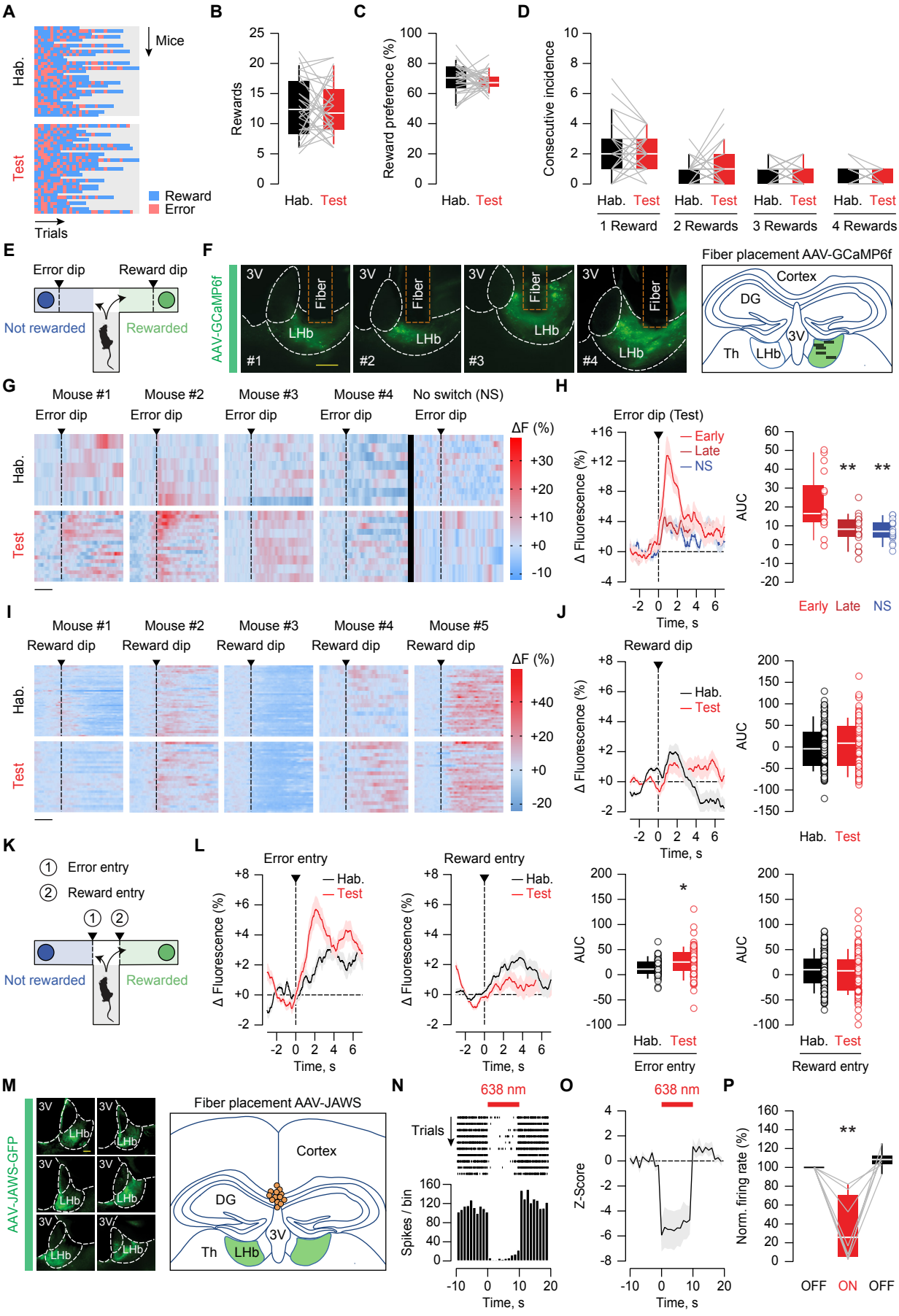

Figure S1. Behavioral, photometric and optogenetic analysis of LHb neurons during the T-maze task. Related to Figure 1.

(**A**) Single-mouse performance during habituation and test session (n=31 mice).

(**B**) Box and scatter plots of the reward incidence during habituation (black: n=31 mice, 12.74±0.8884) and test session (red: n=31 mice, 12.52±0.8137).

(**C**) Box and scatter plots of the reward preference during habituation (black: n=31 mice, 69.93±1.885) and test session (red: n=31 mice, 68.05±1.169).

(**D**) Box and scatter plots of the consecutive error incidence during habituation (black: n=31 mice, 2.0968±0.3172 for 1 error, 0.8387±0.1298 for 2 errors, 0.6774±0.1239 for 3 errors, and 0.3548±0.1075 for 4 errors) and test session (red: n=31 mice, 2.1613±0.2095 for 1 error, 1.2258±0.2268 for 2 errors, 0.5161±0.1279 for 3 errors, and 0.4194±0.0886 for 4 errors).

(**E**) Schematic of the behavioral task.

(**F**) Injection sites of AAV-GCaMP6f and fiber implantation above the site of injection (scale bar: 100 µm) in the cohort of mice employed for photometric experiments (Figure 1F). Coronal schematic depicting the approximate sites of fiber placement (black rectangles: n=5 mice).

(**G**) Single-mouse heat maps of LHb fluorescence aligned to the entry into the non-rewarded container (error dip) during habituation and test session (scale bar: 2 s).

(**H**) Time course of the average LHb fluorescence aligned to the entry into the non-rewarded container (error dip) during early and late trials of the test session, and during test trials in which the non-rewarded arm was not switched (NS). Box and scatter plots of the area under the curve (AUC) during early (light red: n=5 mice/17 trials, 21.8±3.769), late (dark red: n=5 mice/19 trials, 7.989±1.857) and no-switch trials during the test session (blue, NS: n=4 mice/15 trials, 7.274±1.517). One-way ANOVA ($F_{2,48}$=9.84) with Holm-Sidak correction (**p<0.01, comparisons against early).

(**I**) Single-mouse heat maps of LHb fluorescence aligned to the entry into the rewarded container (reward dip) during habituation and test session (scale bar: 2 s).

(**J**) Time course of the average LHb fluorescence aligned to the entry into the rewarded container (reward dip) during habituation and test session. Box and scatter plots of the area under the curve (AUC) during habituation (black: n=5 mice/186 trials, -0.3678±3.565) and test session (red: n=5 mice/149 trials, 5.404±4.376).

(**K**) Schematic of the behavioral task.

(**L**) Time course of the average LHb fluorescence during habituation and test session aligned to the entry into the non-rewarded and rewarded arms. Box and scatter plots of the area under the curve (AUC) during habituation (black: n=5 mice/46 trials, 13.6299±2.6152 for entry into non-rewarded arm; n=5 mice/186 trials, 10.1795±2.4401 for entry into rewarded arm) and test session (red: n=5 mice/74 trials, 25.0754±3.4268 for entry into non-rewarded arm; n=5 mice/150 trials, 4.3685±3.1677 for entry into rewarded arm). Mann-Whitney test (U=1228, *p<0.05).

(**M**) Representative injection sites of AAV-JAWS (scale bar: 100 µm) in the cohort of mice employed for behavioral experiments (Figure 1I). Coronal schematic depicting the approximate sites of fiber placement for the optical activation of JAWS (orange circles: n=13 mice).

(**N**) Raster plot and peri-stimulus time histogram of an example LHb neuron for the *in vivo* validation of JAWS photoactivation.

(**O**) Time course of the average z-score of spontaneous firing activity during red light treatment (n=2 mice/7 cells).

(**P**) Box and scatter plots of the normalized firing rate during (red: ON, 34.7±13.21) and after (black: OFF, 108.6±3.782) red light treatment (n=2 mice/7 cells). One-way repeated measures ANOVA ($F_{1.096,6.574}$=24.37) with Holm-Sidak correction (**p<0.01, ON versus OFF).

Data are represented with heat maps, box plots (median and quartiles) or mean±SEM.

Nuno-Perez et al., Supplemental Figure 2

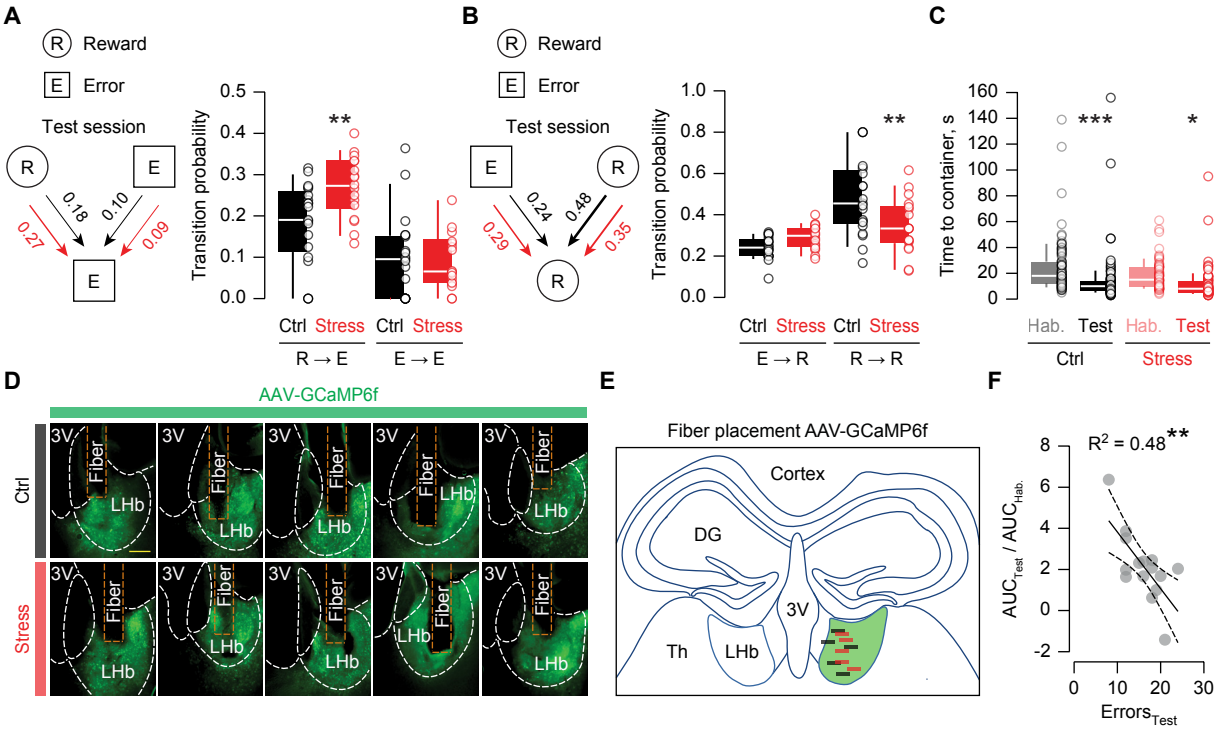

Figure S2. Behavioral and photometric analysis upon stress exposure. Related to Figure 2.

(**A**) Diagram displaying average transition probabilities to error choice during the test session. Box and scatter plots of transition probabilities to error choice in control (black: n=20 mice, 0.1817±0.02232 for R→E and 0.0973±0.02289 for E→E) and stressed mice (red: n=17 mice, 0.27±0.01914 for R→E and 0.08755±0.01605 for E→E). Two-way repeated measures ANOVA ($F_{1,35}$=3.214) with Sidak correction (**p<0.01, control versus stress).

(**B**) Diagram displaying average transition probabilities to reward choice during the test session. Box and scatter plots of transition probabilities to reward choice in control (black: n=20 mice, 0.241±0.01213 for E→R and 0.48±0.04154 for R→R) and stressed mice (red: n=17 mice, 0.2937±0.01448 for E→R and 0.3487±0.03276 for R→R). Two-way repeated measures ANOVA ($F_{1,35}$=3.214) with Sidak correction (**p<0.01, control versus stress).

(**C**) Box and scatter plots of the time to reach the arm containers in control (black: n=20 mice/100 trials, 23.87±2.015 during habituation; n=20 mice/100 trials, 13.56±1.877 during test) and stressed mice (red: n=15 mice/75 trials, 18.16±1.283 during habituation; n=17 mice/84 trials, 11.36±1.351 during test). Two-way ANOVA ($F_{1,355}$=23.7) with Sidak correction (***p<0.001, *p<0.05, habituation versus test).

(**D**) Injection sites of AAV-GCaMP6f and fiber implantation above the site of injection (scale bar: 100 µm) in the cohort of mice employed for photometric experiments (Figure 2C).

(**E**) Coronal schematic depicting the approximate sites of fiber placement (control: black rectangles, n=5 mice; stress: red rectangles, n=5 mice).

(**F**) Correlation plot between error incidence during the test session and LHb fluorescence aligned to the entry into the non-rewarded container (n=15 mice: 5 naïve mice from Figure 1F, 5 control mice from Figure 2C and 5 stressed mice from Figure 2C). Pearson correlation (R^2=0.4842, $F_{1,13}$=12.21, **p<0.01).

Data are represented with box plots (median and quartiles) or mean±SEM.

Nuno-Perez et al., Supplemental Figure 3

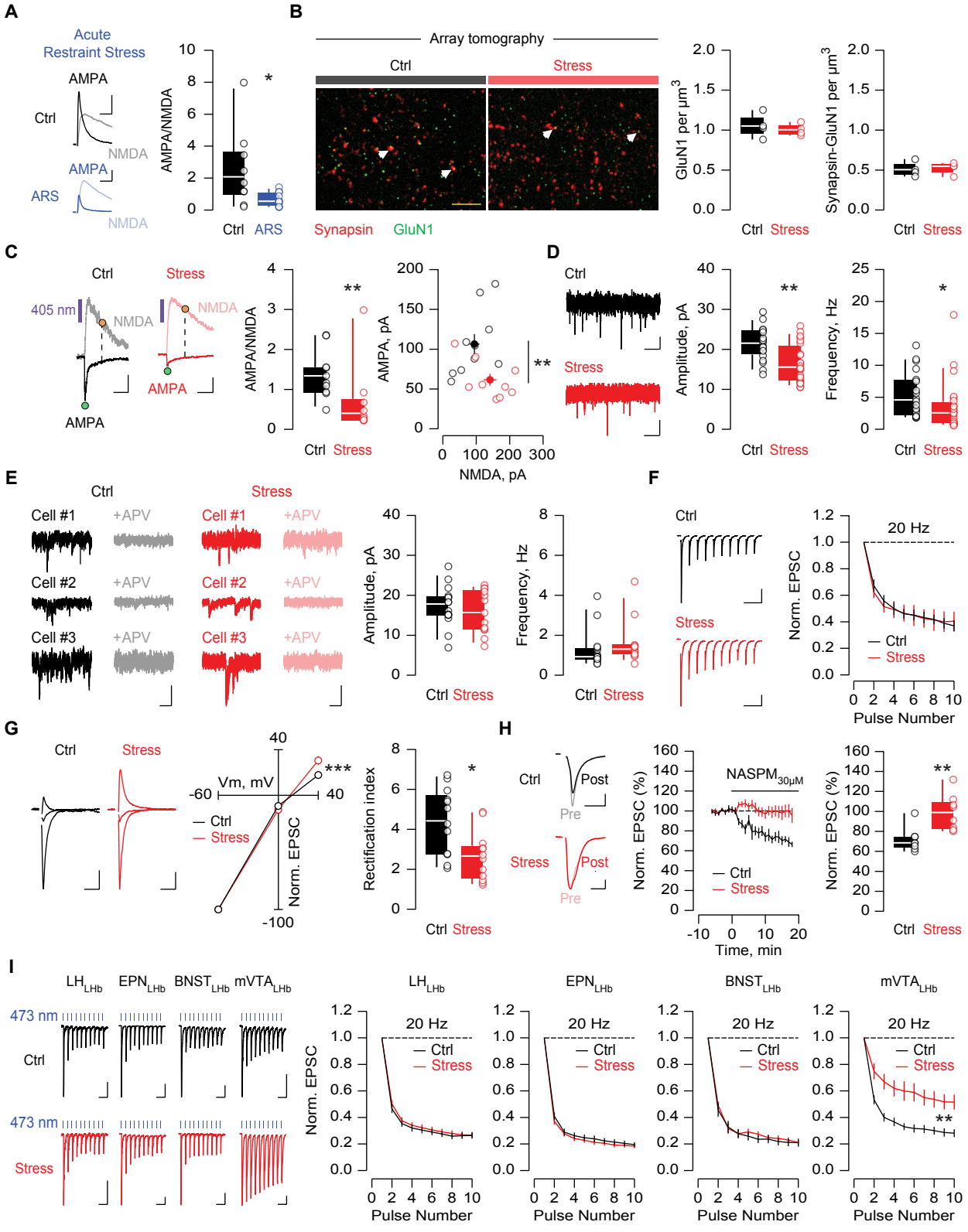

Figure S3. Stress reduces habenular AMPAR transmission. Related to Figure 2 and Figure 3.

(**A**) Example traces of AMPA/NMDA (+40 mV; scale bars: 50 pA, 10 ms). Box and scatter plots of AMPA/NMDA from control (black: n=2 mice/9 cells, 2.51±0.8158) and restrained mice (ARS, blue: n=3 mice/11 cells, 0.6564±0.1283). Mann-Whitney test (U=19, *p<0.05).

(**B**) Array tomography images obtained from single 100-nm slices immunolabeled against Synapsin (red) and GluN1 (green) (scale bar: 5 µm). White arrows indicate representative puncta showing co-localization of both markers. Box and scatter plots of the number of puncta per μm^3 in control (black: n=4 mice, 1.053±0.07596 for GluN1 and 0.5085±0.04607 for Synapsin/GluN1) and stressed mice (red: n=4 mice, 1.004±0.03689 for GluN1 and 0.5245±0.03795 for Synapsin/GluN1).

(**C**) Example traces of AMPA/NMDA with single-photon MNI-glutamate uncaging (-60/+40 mV; scale bars: 50 pA, 100 ms). Box and scatter plots of AMPA/NMDA from control (black: n=3 mice/10 cells, 1.372±0.1917) and stressed mice (red: n=2 mice/9 cells, 0.7061±0.2958). Scatter plot of absolute amplitudes in control (black: 106.4±13.28 for AMPAR and 94.29±15.79 for NMDAR) and stressed mice (red: 61.46±7.942 for AMPAR and 141.1±20.67 for NMDAR). Mann-Whitney test (U=13, **p<0.01).

(**D**) Example traces of AMPAR-mediated miniature EPSC recordings (mEPSC; -60 mV; scale bars: 10 pA, 250 ms). Box and scatter plots of mEPSC amplitude and frequency from control (black: n=3 mice/19 cells, 21.39±0.9497 for amplitude and 5.403±0.817 for frequency) and stressed mice (red: n=3 mice/23 cells, 16.5±1.003 for amplitude and 3.557±0.8387 for frequency). Mann-Whitney test (amplitude: U=98; frequency: U=127) (**p<0.01, *p<0.05).

(**E**) Example traces of NMDAR-mediated spontaneous EPSC recordings (sEPSC; -60 mV; scale bars: 20 pA, 100 ms), before and after bath application of the NMDAR antagonist APV. Box and scatter plots of sEPSC amplitude and frequency from control (black: n=2 mice/15 cells, 17.39±1.33 for amplitude and 1.279±0.2438 for frequency) and stressed mice (red: n=2 mice/13 cells, 15.8±1.495 for amplitude and 1.593±0.3034 for frequency).

(**F**) Example traces of AMPAR EPSC trains (-50 mV; scale bars: 50 pA, 100 ms). Plot of normalized EPSC amplitudes from control (black: n=2 mice/12 cells) and stressed mice (red: n=2 mice/12 cells).

(**G**) Example traces of AMPAR currents (-60/+0/+40 mV; scale bars: 50 pA, 10 ms). Current-voltage relationship, box and scatter plots of rectification index from control (black: n=2 mice/12 cells, 4.422±0.4847) and stressed mice (red: n=2 mice/12 cells, 2.663±0.359). Two-way repeated measures ANOVA ($F_{1,22}$=2.693) with Sidak correction (***p<0.001); Mann-Whitney test (U=28, *p<0.05).

(**H**) Example traces of AMPAR currents (-50 mV; scale bars: 50 pA, 5 ms). Time course, box and scatter plots of the NASPM sensitivity (30 µM) of AMPAR currents from control (black: n=3 mice/8 cells, 71.5±4.241) and stressed mice (red: n=3 mice/8 cells, 98.88±6.391). Mann-Whitney test (U=4, **p<0.01).

(**I**) Example traces of input-specific (Channelrhodopsin-2) AMPAR EPSC trains (-60 mV; scale bars: 50 pA, 100 ms). Plots of normalized EPSC amplitudes from control (black: LH, n=2 mice/24 cells; EPN, n=2 mice/29 cells; BNST, n=4 mice/34 cells; mVTA, n=2 mice/32 cells) and stressed mice (red: LH, n=3 mice/33 cells; EPN, n=2 mice/27 cells; BNST, n=2 mice/23 cells; mVTA, n=3 mice/43 cells). Two-way repeated measures ANOVA ($F_{1,73}$=10.59, **p<0.01, control versus stress interaction).

Data are represented with box plots (median and quartiles) or mean±SEM.

Nuno-Perez et al., Supplemental Figure 4

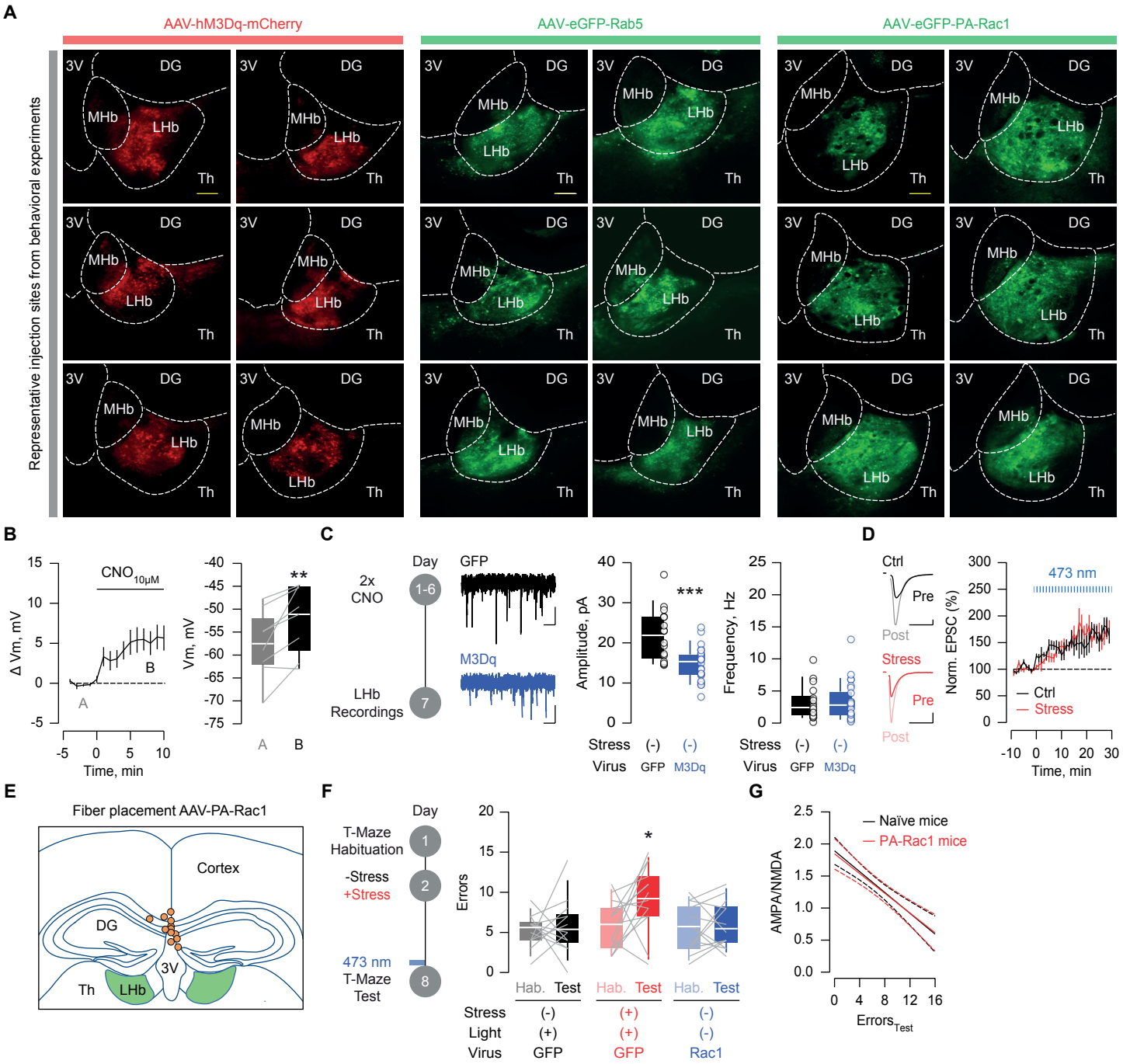

Figure S4. Validation of viral manipulations. Related to Figure 4.

(**A**) Representative injection sites of AAV-hM3Dq (scale bar: 100 μm), AAV-Rab5 (scale bar: 100 μm) and AAV-PA-Rac1 (scale bar: 50 μm) in the cohort of mice employed for behavioral experiments (Figure 4C, 4F and 4H).

(**B**) Time course of the change in membrane potential in LHb neurons upon bath application of CNO (10 μM). Box and scatter plots of the membrane potential before (grey: A, -57.53±2.643) and after (black: B, -52.06±2.654) CNO treatment (n=3 mice/8 cells). Paired student's t-test (t_7=3.536, **p<0.01).

(**C**) Experimental timeline. Example traces of AMPAR-mediated miniature EPSC recordings (mEPSC; -60 mV; scale bars: 10 pA, 250 ms). Box and scatter plots of mEPSC amplitude and frequency from GFP (black: n=2 mice/16 cells, 21.84±1.615 for amplitude and 3.097±0.6359 for frequency) and M3Dq mice (blue: n=3 mice/25 cells, 14.81±0.8312 for amplitude and 3.344±0.5879 for frequency). Mann-Whitney test (U=76, ***p<0.001).

(**D**) Example traces of AMPAR currents during the *ex vivo* validation of PA-Rac1 photoactivation (-60 mV; scale bars: 50 pA, 10 ms). Time course of the amplitude of AMPAR currents from control (black: n=2 mice/9 cells) and stressed mice (red: n=2 mice/7 cells), before and after blue light delivery (1 Hz, 150 ms). Two-way repeated measures ANOVA ($F_{38,532}$=6.577, ***p<0.001, time interaction).

(**E**) Coronal schematic depicting the approximate sites of fiber placement for the optical activation of PA-Rac1 (orange circles: n=12 mice).

(**F**) Experimental timeline. Box and scatter plots of the error incidence in GFP mice subjected to control/light (black: n=13 mice, 5.2308±0.5456 during habituation and 5.7692±0.9176 during test), GFP mice subjected to stress/light (red: n=14 mice, 5.9286±0.7657 during habituation and 9.2143±1.0747 during test) and PA-Rac1 mice subjected to control/no-light (blue: n=13 mice, 5.4615±0.7966 during habituation and 5.9231±0.7879 during test). Two-way repeated measures ANOVA ($F_{1,37}$=3.952) with Sidak correction (*p<0.05, habituation versus test).

(**G**) Overlay of the correlation analysis between error incidence and AMPA/NMDA from naïve (black, Figure 1J: R^2=0.833, $F_{1,9}$=44.89, ***p<0.001) and stressed PA-Rac1 mice (red, Figure 4I: R^2=0.9388, $F_{1,4}$=61.38, **p<0.01). Pearson correlation with test for slope comparison ($F_{1,13}$=0.06798, p=0.7984).

Data are represented with box plots (median and quartiles) or mean±SEM.

Chapter 4: Discussion

Taken together, the two studies included in my PhD thesis indicate that escapable and inescapable stressors induce opposite AMPAR plasticity in LHb neurons, thus causing divergent behavioral adaptations. In our first article, using the active avoidance paradigm as a model of escapable stress, we found that foot-shock-predicting cues gradually recruit LHb neurons throughout multiple training sessions. This phenomenon went together with the potentiation of AMPAR transmission specifically at LHA-to-LHb synapses. At the behavioral level, optogenetic silencing of LHA afferents during presentation of the CS, or prevention of habenular AMPAR potentiation, impaired avoidance responses. These results confirm the requirement of hypothalamic inputs, as well as excitatory LTP, for the adequate execution of active coping behaviors.

Conversely, our second study showed that inescapable foot-shock exposure weakens excitatory transmission at multiple LHb inputs, through the downregulation of AMPAR transmission. This adaptation hindered the excitation of LHb neurons upon omission of expected rewards during a cognitive T-maze task, ultimately resulting in abnormal choice selection by increasing the incidence of error outcomes. Notably, the normalization of synaptic strength following stress exposure prevented the manifestation of cognitive impairments. These data point to a subcortical synaptic mechanism, dysregulated by stress, that supports cognitive performance during reward seeking.

As a whole, my thesis provides a causal link between habenular synaptic plasticity and adaptations in motivated behaviors, both in the context of physiology (avoidance) and pathology (cognitive deficits). Our observations (1) support existing models whereby LHb function is an important contributor to goal-directed actions, (2) expand the collection of known circuits and synaptic mechanisms underlying these processes, and (3) provide a biological basis for their vulnerability to stress. Throughout the discussion, I will review these results within current frameworks, and highlight the future directions that could stem from my research.

4.1 Cellular mechanisms for stress-driven AMPAR plasticity

My doctoral work reveals that excitatory transmission in LHb neurons undergoes stress-driven plasticity, and the directionality of these adaptations depends on the properties of the stressor. Indeed, while escapable stressors potentiate habenular glutamatergic synapses, inescapable foot-shock exposure weakens synaptic strength. In both cases, the component affected by stressful experiences is AMPAR transmission. In the following section, I will present the potential mechanisms that may account for potentiation and depression of habenular AMPAR transmission.

4.1.1 Cellular mechanisms for AMPAR LTP

Our first study indicates that avoidance learning induces an LTP-like phenomenon, by which AMPARs are inserted into the postsynaptic compartment of LHA-receiving LHb neurons. This plasticity is specific for AMPAR transmission because (1) increased AMPAR labelling could be detected by freeze-fracture immunolabeling, and (2) glutamate uncaging revealed an increase in the amplitude of AMPAR currents, ruling out concomitant alterations in NMDAR transmission. The next paragraphs will describe the subcellular mechanisms that could lead to the potentiation of AMPAR transmission during avoidance learning (**Figure 11**).

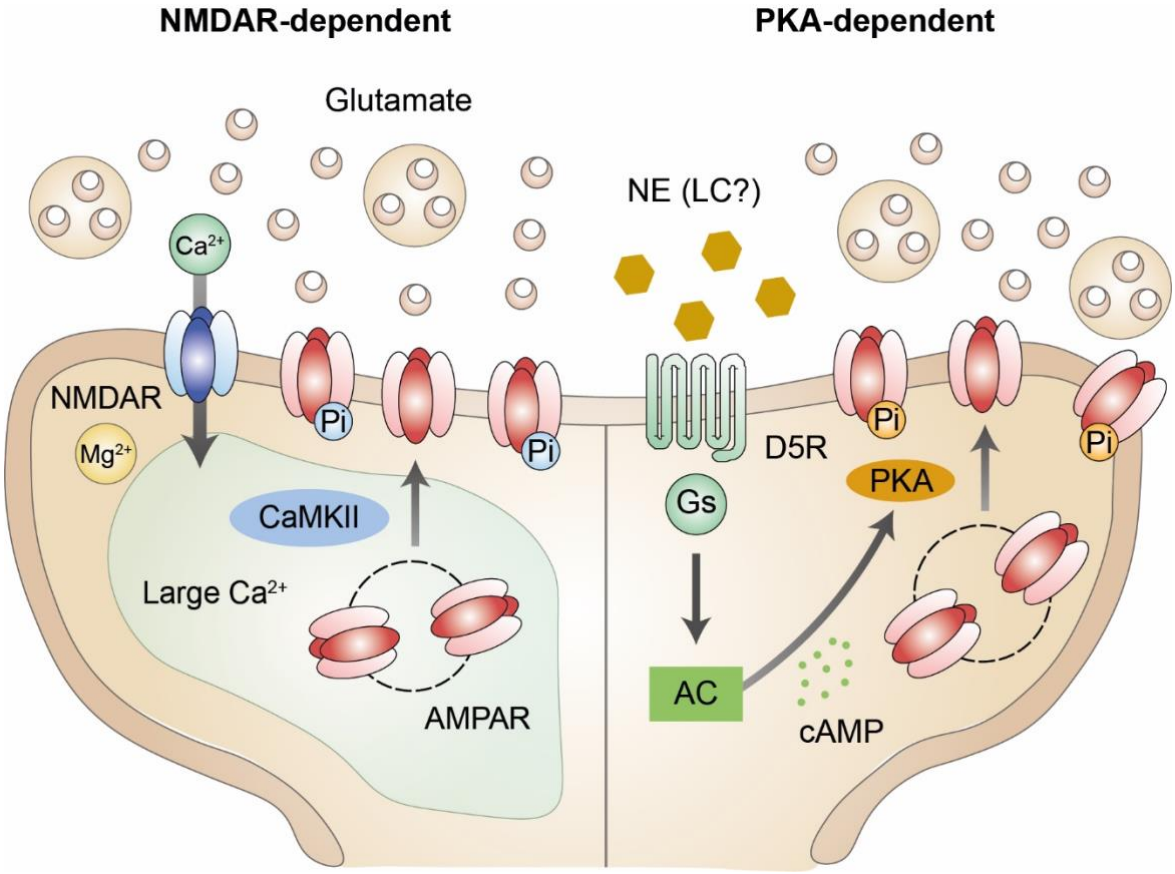

Figure 11. Proposed cellular mechanisms for the induction of LTP during avoidance learning. NMDAR-dependent potentiation is based on the removal of the magnesium block and the subsequent increase in postsynaptic calcium concentrations. These events lead to the activation of CaMKII, insertion of AMPARs into the membrane, and increases in their conductance through the phosphorylation of Serine-831. Alternatively, NE from LC neurons could activate D5-DA receptors. These metabotropic receptors drive cAMP production by adenylyl cyclases (AC) and thus activate PKA, which can phosphorylate Serine-845 of GluA1 subunits in order to increase AMPAR conductance and promote insertion of new receptors into the membrane.

4.1.1.1 NMDAR-dependent LTP

Different lines of evidence suggest that the observed AMPAR LTP depends on NMDAR activation. First, in acute brain slices of naïve mice, the protocol we employed for LTP induction consists of pairing high-frequency stimulation of presynaptic terminals with the postsynaptic depolarization of habenular neurons. This protocol has been extensively employed to trigger NMDAR-dependent LTP of AMPAR transmission (Lüscher and Malenka, 2012). Demonstrating that the resulting plasticity relies on NMDAR activation in our particular case, bath application of NMDAR antagonist D-2-amino-5-phosphonopentanoic (APV) prevented LTP induction. After three days of training, the increase in AMPA/NMDA ratio observed in learner mice occluded the expression of the APV-sensitive LTP. This occlusion phenomenon suggests a conserved induction mechanism between the LTP protocol elicited in brain slices, and the physiological AMPAR potentiation during avoidance learning. Moreover, if the physiological LTP is indeed NMDAR-dependent, habenular NMDAR blockade during avoidance learning should impair behavioral performance. Supporting this prediction, local APV infusion during avoidance training disrupts the execution of escape responses (**Appendix A**). Likewise, in the VTA, where NMDARs are required for AMPAR LTP during instrumental cue-outcome associations, *in vivo* local APV delivery compromises reward learning (Stuber et al., 2008).

The LTP occlusion seen in learner mice, together with the APV-mediated disruption of appropriate avoidance behaviors, indicate that NMDAR transmission is required for the physiological induction of the habenular AMPAR potentiation. However, the effects of APV on instrumental learning might be driven by the pharmacological repercussions on LHb neuronal firing, rather than the blockade of the NDMAR-driven plasticity per se. Similarly, the LTP occlusion could be reflecting the inability to insert more receptors into synaptic compartments because, after avoidance learning, postsynaptic densities might already be saturated with AMPARs that were incorporated through NMDAR-independent mechanisms. Hence, further evidence would be advantageous to strengthen the conclusion that the observed AMPAR LTP relies on NMDAR transmission.

NMDAR-dependent LTP needs the activation of CaMKII and the subsequent delivery of AMPARs into postsynaptic compartments (Shi et al., 1999). In LHb neurons, increased expression of βCaMKII is associated with AMPAR potentiation in pathological contexts (Li et al., 2013), thus opening the possibility that the same kinase might participate during the LTP triggered by avoidance learning. We could test this idea by performing western blotting in LHb extracts, which would allow us to measure βCaMKII levels. In order for this dataset to support the NMDAR dependency of LTP, learner mice should exhibit higher βCaMKII levels than their control counterparts. Alternatively, we could quantify the phosphorylation of Serine-831 in GluA1 subunits – the main substrate of the CaMKII enzymatic activity (Barria et al., 1997). Measurement of Serine-831 phosphorylation in the LHb has been achieved before, thereby supporting the feasibility of this approach (Meye et al., 2015). Increased phosphorylation levels of Serine-831 in learner mice, as compared to controls, would be required to support the NMDAR involvement in LTP induction. Furthermore, since AMPAR LTP through NMDAR and CaMKII activation relies on the synaptic delivery of receptors from extra-synaptic pools and intracellular vesicles, blocking habenular AMPAR trafficking

should in principle disrupt LTP expression and impair avoidance behaviors (Poncer et al., 2002; Rumpel et al., 2005). In order to prevent the experience-dependent delivery of AMPARs, and the subsequent execution of active coping strategies, we could capitalize on the viral overexpression of a truncated GluA1 form, only containing the receptor carboxy-terminal tail. This approach would preclude the trafficking of endogenous AMPARs across diverse subcellular compartments (Meye et al., 2015). Altogether, the combination of the experiments presented above would strongly reinforce the idea that AMPAR LTP resulting from avoidance learning depends on NMDAR transmission. Despite these predictions, one should be open to the possibility that AMPAR LTP does not rely on NMDAR activation alone, and additional processes may also contribute.

4.1.1.2 PKA-dependent LTP

Besides the phosphorylation of Serine-831 in GluA1, Serine-845 is associated with increased open probability and enhanced AMPAR retention within synaptic sites (Banke et al., 2000; Man et al., 2007). Notably, the phosphorylation of this residue is crucial for habenular LTP of excitatory transmission during cocaine withdrawal, thus indicating the physiological relevance of this mechanism (Meye et al., 2015). Serine-845 is phosphorylated by PKA, which is functional in LHb neurons and can be stimulated by cAMP through the activation of metabotropic G-protein coupled receptors (Syrovatkina et al., 2016; Authement et al., 2018). Importantly, LHb neurons express D5-DA receptors, whose activation engages the cAMP-producing pathway (Pivonello et al., 2007; Zhang et al., 2018c). Literature lacks evidence for DA release onto LHb neurons (Stamatakis et al., 2013), but endogenous noradrenergic signaling has been shown to activate DA receptors within the habenular complex (Root et al., 2015). The source of NE could be the LC, where we found fluorescently labeled cells after LHb injection of retrobeads (**Appendix B**). Considering that foot-shock stimuli excite neurons in the LC (Chen and Sara, 2007), we hypothesize that NE might be released during avoidance learning onto LHb neurons, potentially activating D5-DA receptors to stimulate PKA and ultimately phosphorylate Serine-845 in GluA1 subunits. Such a scenario could also contribute to the AMPAR potentiation observed in learner mice.

Altogether, I have highlighted the importance of NMDARs for the induction of the AMPAR LTP observed in learner mice. This scenario is supported by the occlusion of the NMDAR-dependent LTP in acute brain slices of learner mice, and by the disruption of escape behaviors after local APV administration. Moreover, in light of the previous description of alternative phenomena leading to LTP in LHb neurons (Meye et al., 2015), I decided to consider the PKA phosphorylation of Serine-845 as an additional process that could further strengthen habenular excitatory synapses. These two processes do not need to be mutually exclusive, and could act in concert in order to potentiate LHb synapses. Indeed, increased conductance through PKA-phosphorylated GluA1 could boost the postsynaptic depolarization and facilitate the removal of the NMDAR magnesium block, eventually enabling CaMKII-dependent LTP. I will now move on to the synaptic plasticity described in the third chapter of my PhD thesis, in the context of inescapable foot-shock exposure.

4.1.2 Cellular mechanisms for AMPAR LTD

Our second manuscript suggests that inescapable stress drives an LTD-like phenomenon, whereby AMPAR levels are reduced within postsynaptic compartments of LHb neurons. This plasticity is AMPAR-specific considering our data showing (1) decreased GluA1 levels through array tomography, (2) lower amplitude of AMPAR miniature excitatory postsynaptic currents (mEPSC), (3) diminished AMPAR currents evoked by glutamate uncaging, and (4) no change in GluN1 immunolabeling, or the amplitude of NMDAR currents. What are the cellular mechanisms responsible for inducing such plasticity?

Perhaps the most reproducible finding in the LHb field is the emergence of neuronal hyperactivity after stress exposure. This adaptation not only arises in the unpredictable foot-shock paradigm (Stamatakis and Stuber, 2012), but also in models of learned helplessness, maternal deprivation, CMS, and restraint stress (Li et al., 2011; Tchenio et al., 2017; Yang et al., 2018; Cerniauskas et al., 2019). When submitting mice to unpredictable foot-shocks, habenular hyperactivity depends on enhanced stimulation of PP2A, which leads to subsequent internalization of $GABA_B$ receptors (Lecca et al., 2016). Notably, one hour after foot-shock exposure, the increase in PP2A activity and the reduced $GABA_B$ receptor expression are already detectable, but the decline in AMPA/NMDA ratio and the reduction in mEPSC amplitude are not in place yet (Lecca et al., 2016). These data suggest that either the PP2A activation, or the subsequent neural hyperactivity, might be required for AMPAR reduction. This hypothesis could be tested by infusing the PP2A inhibitor LB-100 locally in the LHb, immediately after the foot-shock protocol – a manipulation that prevents the stress-driven neuronal hyperactivity (Lecca et al., 2016). 24 hours later, we could perform electrophysiological recordings and assess if the AMPAR LTD is manifest. If the weakening of excitatory synapses is not detectable, as we predict, either the PP2A stimulation or the resulting hyperactivity might be at the basis for the AMPAR reduction reported in our second study. In the next paragraphs, I will make a case for considering these stress-driven events as the trigger for AMPAR LTD.

4.1.2.1 ***PP2A-dependent LTD***

Conversely to LTP phenomena, which are linked to AMPAR phosphorylation, LTD processes are often associated with dephosphorylation events (Lisman, 1989; Mulkey et al., 1993; Lee et al., 1998; Wang and Gean, 1999; Lee et al., 2010; Lüscher and Malenka, 2012). We showed that the weakening of synaptic strength occurs primarily through downregulation of GluA1-containing AMPARs, on the grounds that foot-shock exposure decreased (1) AMPAR rectification index, (2) the sensitivity to NASPM (i.e., antagonist of calcium-permeable AMPARs), and (3) GluA1 immunolabelling. These results, together with the fact that habenular AMPARs are calcium-permeable, suggest that GluA1-containing AMPARs undergo LTD after stress exposure (Li et al., 2011; Maroteaux and Mameli, 2012; Meye et al., 2015; Li et al., 2017). Notably, PP2A can dephosphorylate GluA1 at threonine-840 during LTD (Delgado et al., 2007; Toda and Huganir, 2015), thus raising the possibility that the stress-driven increase in PP2A activity may be reducing GluA1 transmission through the dephosphorylation of this residue. Nonetheless, one must be cautious about the feasibility of such scenario, considering that the involvement of PP2A in AMPAR LTD was elucidated with pharmacological inhibitors that also affect the protein phosphatase PP1 (Delgado et al., 2007; Toda and Huganir, 2015). Therefore, alternative mechanisms need to be proposed.

4.1.2.2 Homeostatic downscaling of AMPAR transmission

The emergence of habenular hyperactivity depends on PP2A stimulation, and precedes the reduction in AMPAR transmission (Lecca et al., 2016). Accordingly, it is possible that the AMPAR LTD is not driven by the increase in PP2A activity per se, but by the resulting hyperactivity. The process by which activity levels in neuronal networks modulate synaptic strength is known as homeostatic scaling (Turrigiano, 2008). This framework posits that neurons adjust their responsiveness to presynaptic release of glutamate through the modulation of postsynaptic AMPARs. In the case of homeostatic downscaling, increases in network activity weaken excitatory synapses, as evidenced by the reduced mEPSC amplitude and decreased surface expression of AMPARs after protracted bicuculline treatment in culture (Lissin et al., 1998; O'Brien et al., 1998; Turrigiano et al., 1998; Watt et al., 2000). Designer receptors exclusively activated by designer drugs (DREADD) are commonly used to modulate the activity of neuronal populations in an acute fashion (Roth, 2016; Smith et al., 2016). However, one could conceive the idea of employing this technology with the aim of emulating the long-term effects of neuronal activity, including homeostatic scaling (Pan-Vazquez et al., 2020). In our study, we triggered the downscaling of habenular AMPARs through overexpression of the excitatory DREADD hM3Dq, whose activation reduced the AMPA/NMDA ratio similarly to stress. Along similar lines, foot-shock stimuli did not result in the weakening of excitatory transmission in LHb neurons, following protracted activation of the inhibitory DREADD hM4Di (**Appendix C**). These experiments suggest that stress-driven hyperactivity may be causative for the AMPAR downregulation reported here.

I would now like to speculate on the cellular mechanisms that may lead to homeostatic downscaling of habenular AMPAR transmission after stress exposure. Indeed, studies in cultured neurons hint at certain candidates (**Figure 12**). Focusing on GluA1-containing AMPARs, homeostatic downscaling promotes the ubiquitination of Lysine-868, and precludes the phosphorylation of Serine-845 through the dissociation of PKA from the postsynaptic density (Diering et al., 2014; Scudder et al., 2014; Widagdo et al., 2015). These posttranslational modifications trigger the internalization and degradation of GluA1 subunits. Furthermore, increased network activity facilitates the interaction between calmodulin and PSD95, thus resulting in the removal of the latter from synaptic compartments and the reduction of AMPAR anchoring (Chowdhury et al., 2018). Neuronal hyperactivity prompts the translocation of the cytoskeletal protein Arc into the nucleus, where it diminishes the transcription of the GluA1-encoding gene and trims AMPAR surface levels (Korb et al., 2013). Additionally, homeostatic downscaling involves the transient expression of Homer1a – an immediate early gene that enables agonist-independent activation of metabotropic glutamate receptors, and eventually results in AMPAR LTD (Hu et al., 2010). Finally, secretion of semaphorins and interaction with their neuropilin/plexin receptors contribute to the GluA1 reduction following increases in neuronal activity (Wang et al., 2017b). Altogether, we conclude that several mechanisms have been linked in culture with the homeostatic downscaling of calcium-permeable AMPARs, thereby validating its potential relevance for the habenular complex (Li et al., 2011; Maroteaux and Mameli, 2012). However, are these cellular processes relevant *in vivo*?

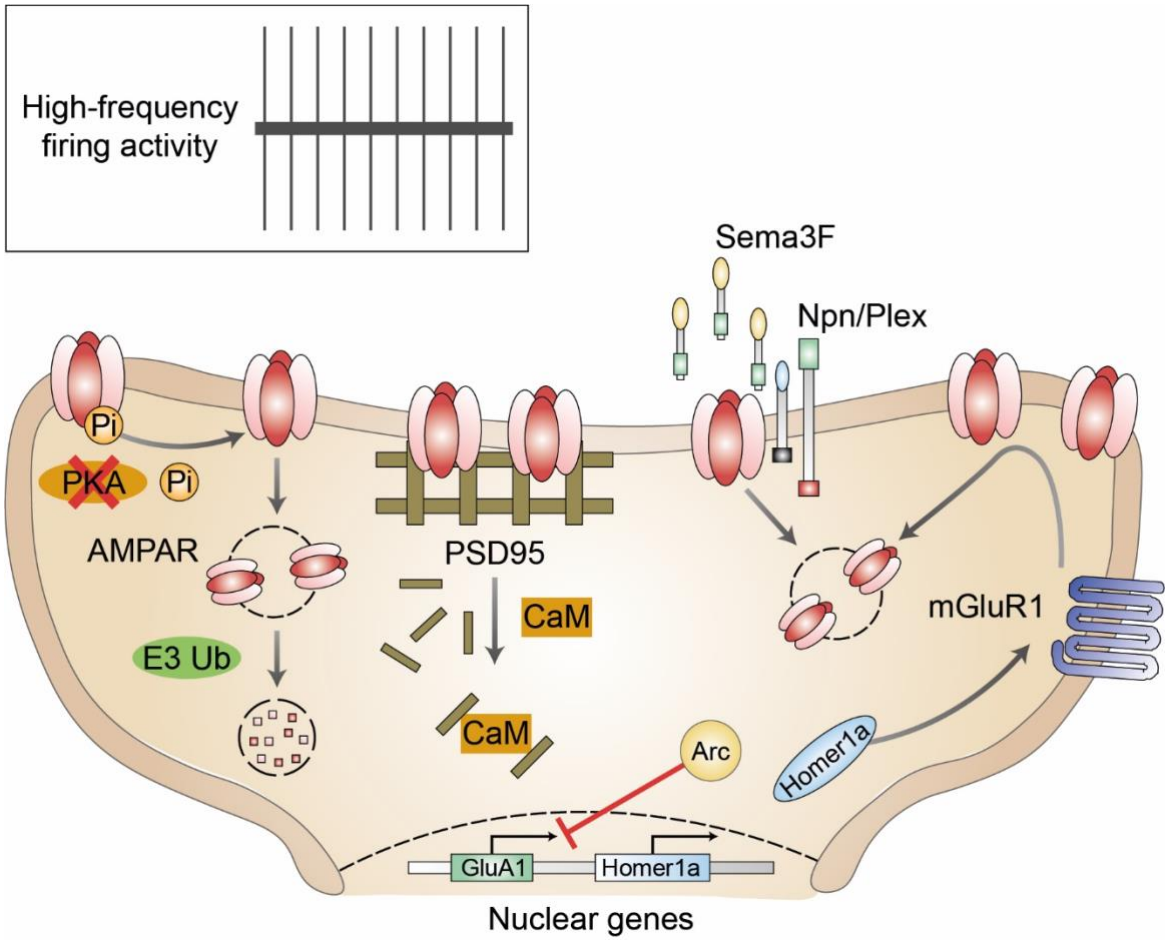

Figure 12. Diverse cellular mechanisms have been linked to the homeostatic downscaling of AMPAR transmission. PKA is detached from the postsynaptic density, thus decreasing AMPAR phosphorylation levels and promoting their endocytosis. Calmodulin (CaM) interacts with PSD95 and reduces AMPAR anchoring at synapses. Arc translocates to the nucleus and inhibits transcription of the GluA1-encoding gene. Transient expression of Homer1a activates metabotropic glutamate receptors and facilitates the endocytosis of AMPARs. Finally, semaphorin-3F is secreted by neurons and interacts with neuropilin-plexin receptors, ultimately resulting in AMPAR endocytosis.

Surprisingly, the field of homeostatic downscaling is in embryonic phases with respect to physiological conditions (Lee and Kirkwood, 2019). The primary visual cortex is possibly the singular exception to such statement, and might thus be useful to understand the cellular processes that are pertinent to the living brain (Desai et al., 2002). Exposure to visual stimuli after periods of dark rearing is used as the equivalent of bicuculline treatment in culture, and weakens AMPAR transmission accordingly (Goel et al., 2006; Goel and Lee, 2007; Torrado Pacheco et al., 2020). In cortical regions, activity-driven reductions in synaptic strength largely depend on Homer1a and Arc – two of the mechanisms described in cultured neurons (Gao et al., 2010; Diering et al., 2017; Chokshi et al., 2019). These commonalities indicate that the molecular pathways reported *in vitro* might similarly apply to physiological settings. Future studies need to evaluate whether these mechanisms participate during the habenular AMPAR downregulation reported in our second study.

In summary, I have presented evidence to support that LHb hyperactivity may account for the stress-driven decrease in AMPAR transmission. The direction of this plasticity contrasts with the potentiation of excitatory synapses during avoidance learning. Thus, we conclude that escapable and inescapable stressors trigger opposite synaptic plasticity in LHb neurons. The crucial distinction to emphasize here is that, while the execution of active coping behaviors goes along with potentiation of habenular synapses, pathological adaptations during reward seeking are rather associated with the depression of LHb excitatory transmission. The next paragraphs will focus on the circuit basis of the two motivated behaviors assessed in my doctoral work (i.e., avoidance learning and reward seeking).

4.2 Circuit mechanisms for adaptive behaviors

The second chapter of my PhD thesis focused on the neural underpinnings of an adaptive behavior that promotes survival, namely escape from noxious stimuli. In the third chapter, however, we diverted our attention to cognitive abnormalities that emerge after inescapable stress exposure, under the umbrella of pathological adaptations. Since these behavioral manifestations are fundamentally different, one would predict that the underlying neuronal circuits might be dissimilar as well, as we will discuss below.

4.2.1 Circuit mechanisms for avoidance learning

Our data support that the AMPAR LTP observed in learner mice relies on NMDAR transmission. An afferent structure, or several, must therefore provide sufficient glutamate release and postsynaptic depolarization to relieve the NMDAR magnesium block. Which inputs may be engaged during avoidance learning? We demonstrated (1) AMPAR enrichment in apposition to LHA terminals, (2) LHA-specific potentiation of LHb synapses, and (3) occlusion of NMDAR-dependent LTP precisely at LHA afferents. It is thus tempting to speculate that the LHA is the main source of excitation in LHb neurons during avoidance training. Further supporting the hypothalamic participation during active coping behaviors, silencing LHA afferents in LHb neurons disrupts escape responses following unpredictable foot-shocks or looming stimuli (Lecca et al., 2017). Avoidance learning also increases the expression of CREB in LHA neurons – a crucial substrate for the formation of cue-punishment associations (Saha and Datta, 2005; Won and Silva, 2008). Similarly, exposure to predatory cues elicits fleeing reactions and triggers LHA neuronal activity (Mendes-Gomes et al., 2020). Such escape responses activate LHA-projecting neurons in the BLA and CeA, pointing towards potential brain structures that might be upstream of the circuit evaluated in our present study (Chen et al., 2020; Weera et al., 2020).

Despite these accumulating data, it remains unclear during which phase of avoidance learning the LHA is involved. We disrupted the execution of avoidance responses by silencing hypothalamic inputs onto LHb neurons during the tone presentation, thereby suggesting that the LHA is crucial for CS encoding. Along similar lines, once the association is established between punishments and their predictive sensory cues, the CS presentation activates LHb-projecting neurons in the LHA (Lazaridis et al., 2019). Importantly, the LHA is not the only afferent structure that develops CS-driven responses during the formation of cue-outcome associations. Indeed, EPN and LPO neurons also increase their activity upon the cue presentation,

following a conditioning period (Stephenson-Jones et al., 2016; Barker et al., 2017). However, these data concerning cue-driven responses in the LHA, EPN and LPO apply to Pavlovian paradigms where no action can be executed to avoid harmful stimuli. Thus, in order to test the relevance of these inputs in the context of escape behaviors, we could measure calcium activity by fiber photometry during avoidance learning, at the level of LHA, EPN and LPO terminals within the LHb.

Provided that we find CS-driven transients with this approach, we might conceive two different alternatives: (1) LHA afferents are the exclusive source of glutamate release required for the emergence of CS-driven excitation (Lazaridis et al., 2019), or (2) additional inputs, including the EPN or LPO, contribute to strengthening habenular responses following the CS presentation (Stephenson-Jones et al., 2016; Barker et al., 2017). These slightly different scenarios have major physiological repercussions. If LHA alone is capable of orchestrating CS responses in the LHb, glutamate release should be sufficient to provide the postsynaptic depolarization necessary to relieve the NMDAR magnesium block, and the presynaptic source of glutamate for coincident detection. This is consistent with the idea that NMDAR-dependent LTP may happen even in absence of somatic spikes, based solely on dendritic plateau potentials (Gambino et al., 2014). Nonetheless, glutamate from the LHA might not be sufficient to activate NMDAR transmission in LHb dendritic spines (**Figure 13**). In this case, EPN/LPO-driven transients after the CS might provide the action potential generation required for the postsynaptic depolarization (Stephenson-Jones et al., 2016; Barker et al., 2017), and LHA might then act as a coincident detector to provide the presynaptic glutamate release. The latter scenario is consistent with Hebbian models of LTP induction, which require simultaneous release of glutamate from presynaptic terminals, and postsynaptic generation of firing activity (Crair and Malenka, 1995; Markram et al., 1997).

In conclusion, although we provide compelling data for the participation of LHA afferents during avoidance learning, future studies need to pinpoint the phase during which the hypothalamus is involved. Moreover, we cannot rule out the contribution of additional inputs, namely the EPN and LPO, which may also convey instructive signals onto LHb neurons during the CS presentation. A remarkable property of the AMPAR potentiation described here is the transitory nature. This deserves special attention, since it might have important implications at the circuit level, as we will explain below.

4.2.1.1 Temporal dynamics of avoidance learning

The LHA-specific potentiation of LHb glutamatergic synapses emerges after session 2, is maintained after session 3, and eventually reverses following session 4, at a time point when behavioral performance is maximal. It is worth mentioning that comparable dynamics have been documented in VTA neurons during instrumental learning based on cue-reward associations (Stuber et al., 2008). These commonalities imply that AMPAR LTP is important during the initial phases of instrumental training, when the learning rate is maximal and the associations between outcomes and predictive cues are labile. In other words, the potentiation of excitatory synapses is not linked to the manifestation of the learned behavior, but rather to its acquisition. In this regard, the LHb and VTA should not be conceived as structures devoted to memory storage, because the LTP is not in place anymore at late stages of training, despite the adequate execution of instrumental responses. Accordingly, it is possible that the transient plasticity within these regions may be important to relay the encoding of cue-outcome associations to downstream structures.

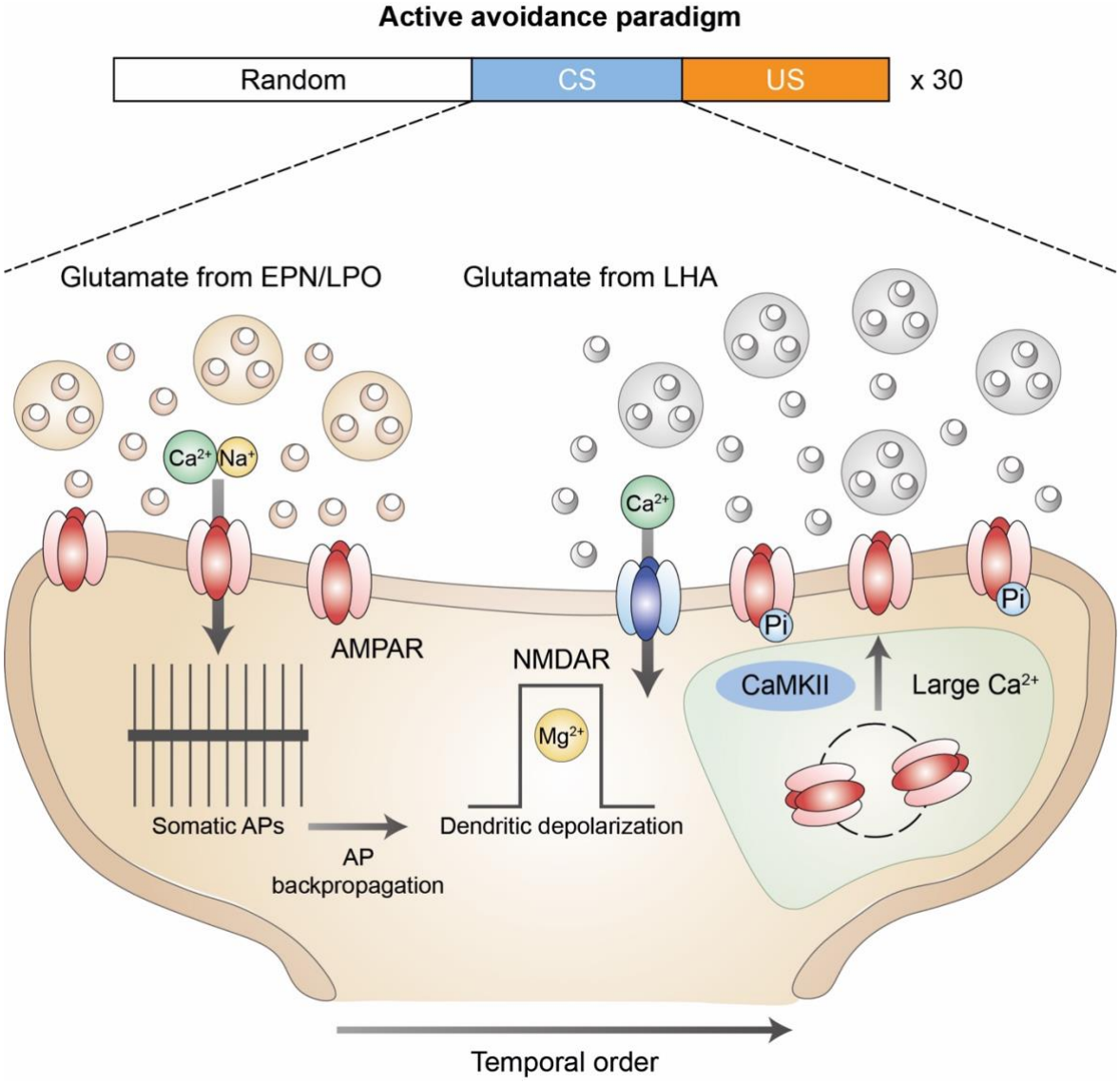

Figure 13. Model depicting the shared contribution of EPN/LPO and LHA inputs to LTP induction during CS presentation. Glutamate release from EPN/LPO terminals may drive the cation influx required to generate somatic action potentials, which could backpropagate into LHA-receiving dendrites in order to drive their depolarization. Upon depolarization, the NMDAR magnesium block is relieved, hence facilitating CaMKII-dependent LTP. *Note that, for illustration purposes, EPN/LPO and LHA are depicted as innervating the same dendritic compartment, but this might not be the case*.

What are the candidate brain areas that might receive the LHb instrumental information for further consolidation? The ventral habenula (vHb) in zebrafish, orthologue area of the mammalian LHb, follows similar neuronal dynamics throughout avoidance learning. The excitation during early phases of training is time-locked to US delivery, and signals get gradually transferred to the CS presentation across conditioning (Amo et al., 2014). These habenular neurons project to the raphe, and vHb-to-raphe inputs are both sufficient and necessary for the execution of escape responses. Therefore, the raphe nuclei may constitute the first set of output areas to receive the LHb encoding of cue-punishment associations (Lecca et al., 2017; Zhou et al., 2017). From there, information might be broadcasted to downstream structures targeted by

raphe axons, including the PFC, NAc and BLA (Van Bockstaele et al., 1993; Ren et al., 2018). Importantly, all these structures participate in avoidance learning. Predictive sensory cues trigger inhibitory responses in PFC neurons, and optogenetic disruption of these negative signals prevents the execution of escape responses (Diehl et al., 2018). These cue-inhibited PFC neurons project to the NAc, and photoactivation of PFC-to-NAc afferents during tone presentation disrupts avoidance learning (Diehl et al., 2020). Avoidance paradigms also activate neurons in the NAc shell division, and inactivation of this subpopulation promotes freezing while impairing active coping reactions (Ramirez et al., 2015). Lastly, BLA neurons convey instructive signals to the NAc during avoidance learning, since optogenetic and pharmacological inhibition of this pathway efficiently disrupts escape behaviors (Ramirez et al., 2015; Diehl et al., 2020).

In summary, we speculate that the transitory encoding of instrumental cue-punishment associations in LHb neurons might be relayed through the raphe nuclei onto diverse downstream structures, whose implication in avoidance learning is prominent. Despite our focus on this subcircuit, we cannot rule out that alternative LHb outputs are also important for the consolidation of avoidance learning. Indeed, punishment-predictive cues activate endocannabinoid signaling in the VTA, subsequently promoting DA release into NAc medium spiny neurons in order to facilitate the execution of escape responses (Wenzel et al., 2018). However, the role of LHb-to-VTA inputs in avoidance learning has not been proposed thus far, as opposed to the LHb-to-raphe pathway (Amo et al., 2014).

To experimentally assess the contribution of the LHb-to-raphe afferents in the consolidation of avoidance learning, we could design the following approach (**Figure 14**): (1) LHb injection of a high-titer adeno-associated virus 1 (AAV1), which has the ability to jump one synapse anterogradely (Zingg et al., 2017), encoding for Cre recombinase, and (2) raphe injection of a Cre-dependent AAV8, encoding for channelrhodopsin-2 or the inhibitory opsin JAWS. This design would allow us to target LHb-receiving cells in the raphe nuclei. First, we could analyze whether any of the aforementioned outputs (i.e., PFC, NAc and BLA) contain terminals emanating from the raphe. Once the relevant outputs are identified, we could perform electrophysiological recordings in order to study raphe-specific synaptic strength at these structures. By comparing control and learner mice following 5 days of training, once the LHb potentiation of excitatory transmission has faded, the presence of synaptic alterations would indicate which regions are potentially involved in the consolidation of avoidance learning. Finally, after candidate output areas have been identified, we could optically silence raphe terminals in these structures during the cue presentation, at late stages of training, to examine whether their contribution is required for the manifestation of consolidated escape behaviors. This approach has the potential to reveal the downstream structures onto which LHb neurons transfer the encoding of cue-punishments associations, for the consolidation of avoidance responses.

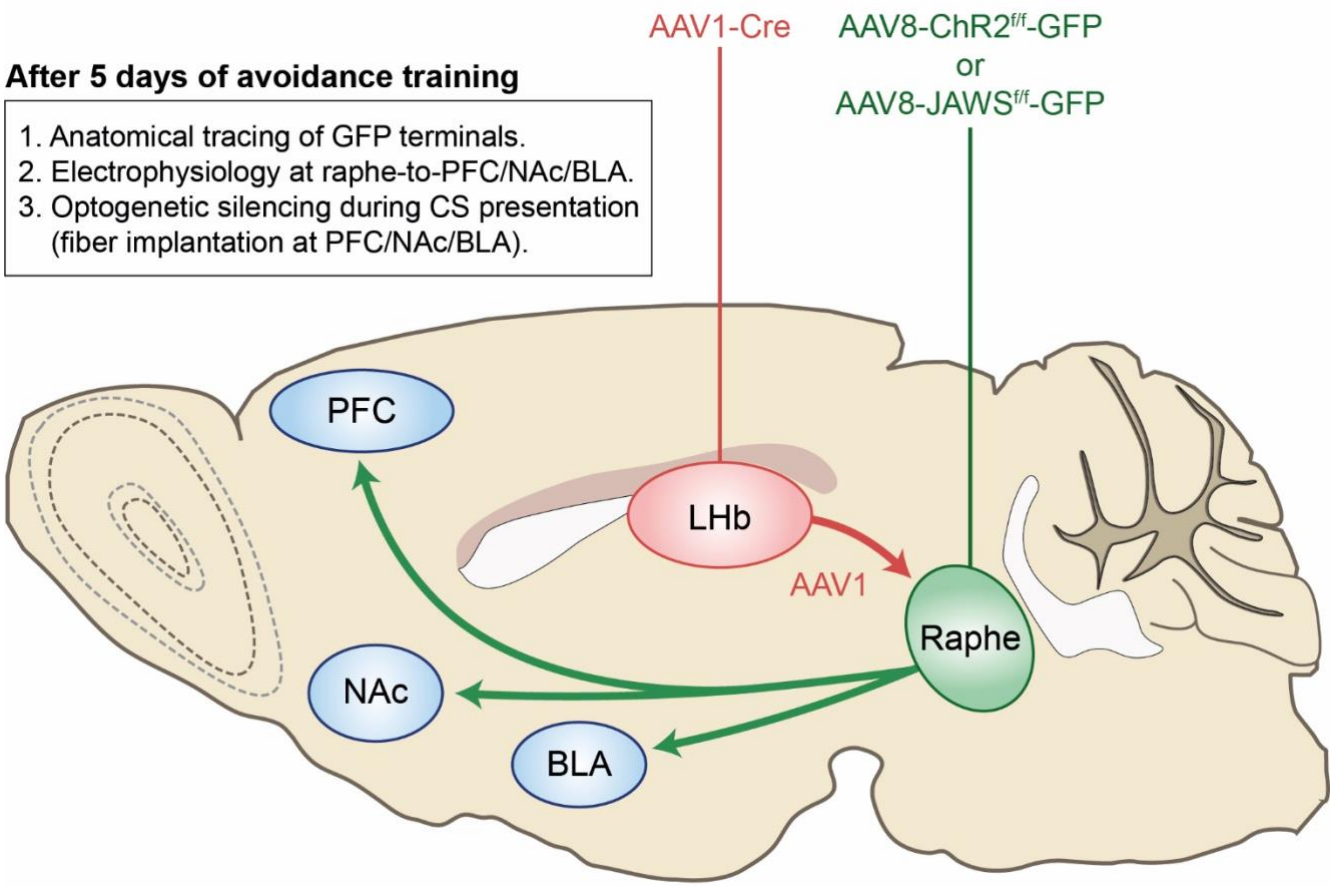

Figure 14. Experimental approach to probe the LHb output connectivity during the consolidation of avoidance learning. Injection of AAV1-Cre in the LHb would allow the virus to jump anterogradely into the raphe nuclei, where it may recombine with the LoxP sites flanking the ChR2- or JAWS-encoding sequence, thus allowing their expression. AAV8- ChR2 and AAV8-JAWS would be infused in different sets of mice. 3 weeks later, GFP labeling would be assessed in raphe outputs (PFC, NAc and BLA), in order to select the suitable candidates for further evaluation of the raphe-specific synaptic strength. Those outputs with synaptic alterations would be probed at the behavioral level (inhibition of raphe terminals during the CS presentation). These electrophysiological recordings and behavioral manipulations would be performed after 5 days of avoidance training, in order to ensure that the behavior is consolidated by the time of the experiment.

Collectively, I have explained the upstream and downstream connectivity of LHb neurons during avoidance learning. Based on literature, the LHA, EPN and LPO might be important inputs, while the raphe nuclei are potentially the most relevant outputs in the context of escape behaviors. The next section will aim attention at the LHb contribution and circuit basis of reward-guided cognitive processes, as evaluated by our second project.

4.2.2 Circuit mechanisms for reward-guided cognitive behaviors

The active avoidance paradigm is conceptually simple, since it can be broken down into essentially two aspects (CS and US encoding). However, the cognitive task employed during the second study is more complex and presents multiple phases worthy of consideration. These phases include decision-making at the level of the central arm, onset of exploration of the end-arm containers, and outcome valuation after reward consumption or omission. Thus, before going into the circuit basis of this behavior, we need to precisely formulate during which phase of the T-maze task the LHb is important.

4.2.2.1 The role of LHb during omission of expected rewards

Several lines of evidence indicate that synaptic strength in LHb neurons is crucial for encoding the absence of expected rewards (i.e., errors). We proved the instructive role of LHb during this phase through different observations: (1) fiber photometry revealed a phasic increase in neuronal activity, time-locked to entries into non-rewarded containers, (2) optical inhibition of LHb neurons during the same phase reduced reward choices in favor of errors, and (3) synaptic strength and the amplitude of the error-driven calcium signals negatively correlated with error incidence.

These accumulating data suggest that error-induced activity in LHb neurons acts as a disappointment signal to discourage the selection of error outcomes during future choices. This scenario is consistent with current models, whereby increases in habenular firing prompt the avoidance of associated contexts. Thus far, this notion had been supported by unrefined optical manipulations, whereby real-time place avoidance for particular compartments could be elicited by the tonic activation of habenular axons emanating from the ventral pallidum, EPN, LHA or VTA (Shabel et al., 2012; Root et al., 2014a; Lecca et al., 2017; Faget et al., 2018; Tooley et al., 2018). Notably, in our study, it is the phasic increase in activity during a well-defined phase that leads to the avoidance of a discrete context (i.e., the empty container). This transient of habenular activity is not present during habituation, when synaptic strength does not correlate with error incidence. Moreover, during the test session, the amplitude of error-driven transients gradually diminishes throughout successive trials. Altogether, these data suggest that the LHb is recruited when mice expect the realization of a positive outcome. The requirement of expectation for the habenular contribution to cognitive processes coheres with previous studies, in which LHb lesions impaired the update of cue-outcome associations specifically during reversal learning (Thornton and Davies, 1991; Lecourtier et al., 2004; Baker et al., 2015; Baker et al., 2017).

In our paradigm, the positive outcome expectation can be inferred from the reduction in the time required to reach the end-arm container, which indicates the existence of an association between the context and the reward. However, the paradigm is not sufficient to evoke a spatial memory of the food. This is evidenced by the fact that, during the test session, mice do not seem to systematically select the previously baited arm as their first choice. Thus, the present task is capable of eliciting a contextual association between the maze and the positive outcome, but it does not allow mice to remember the position of the reward. Nonetheless, we posit that contextual associations may be enough to promote a disappointment signal, since comparable increases in LHb neuronal activity can be elicited by reward omissions when mice

or monkeys are overtrained in reward-seeking paradigms (Matsumoto and Hikosaka, 2007; Matsumoto and Hikosaka, 2009; Shabel et al., 2019). These increases in habenular activity upon unexpected omissions are also detected in humans, thus raising the possibility that the synaptic mechanisms described here may have certain translational potential (Salas et al., 2010).

Putting all these observations together, we conclude that LHb neurons instruct choice selection by signaling reward omissions. This suggests strong candidates at the level of the upstream and downstream connectivity supporting behavioral performance during the reward-guided task.

4.2.2.2 Circuit mechanisms for reward omission

From a circuit standpoint, DA neurons in the VTA are inhibited by reward omissions, thereby responding with opposite dynamics to LHb neurons (Hollerman and Schultz, 1998; Takahashi et al., 2017). As a matter of fact, based on these mirroring scenarios, the habenular complex was proposed as the source of negative reward signals in the midbrain (Matsumoto and Hikosaka, 2007). Later studies backed up this conclusion. Habenular lesions impair reward omission-encoding signals in optogenetically-identified DA neurons, without affecting the emergence of inhibitory responses to aversive events or their predictive cues (Tian and Uchida, 2015). LHb neurons receive such omission-related signals from the EPN, as proven in rodents and monkeys (Hong and Hikosaka, 2008; Stephenson-Jones et al., 2016; Li et al., 2019a), and they transfer them to the VTA through inhibitory neurons in the RMTg (Hong et al., 2011; Li et al., 2019b). Although these results were drawn from Pavlovian paradigms, it remains possible that the same circuit is required for error-driven excitation of LHb neurons during the T-maze paradigm. To test this idea, we could employ anterograde and retrograde viral approaches to silence EPN-receiving, and RMTg-projecting, habenular neurons upon encountering the non-rewarded container during the test session (**Figure 15**). The prediction is that this manipulation would phenocopy the effects of the optogenetic inhibition of LHb neurons, thereby increasing the incidence of error choices, and further supporting the idea that synaptic strength within particular LHb circuits is crucial for cognitive performance. The notion of synaptic strength as a governing mechanism for cognitive processes is supported by literature, as illustrated in the next section.

4.2.2.3 Synaptic strength as a substrate for cognitive performance

Thus far, I have highlighted the habenular role during reward-guided behaviors at the physiological level. However, one of the main findings of our second study is that stress-driven reductions in synaptic strength are causative for the emergence of cognitive deficits. Indeed, stress exposure reduced habenular AMPAR transmission and triggered the same behavioral effects as the LHb optical silencing (i.e., increased error incidence). Most importantly, the weakening of excitatory synapses was concomitant with reductions in the amplitude of error-driven calcium signals, and bidirectional modulation of synaptic strength oppositely impacted on the number of error choices. All these data make us conclude that inescapable stressors drive aberrant decision-making by reducing the sensitivity of LHb neurons to the absence of expected rewards, suggesting that synaptic strength is an important contributor for cognitive performance. A recent publication reported the development of a radiolabeled compound with the ability to measure

AMPAR binding in the human brain, through positron emission tomography (Miyazaki et al., 2020). Our results set the prediction that PTSD patients, who experience traumatic events which are reminiscent of the unpredictable foot-shock paradigm, might display lower AMPAR binding than control subjects in the habenular complex.

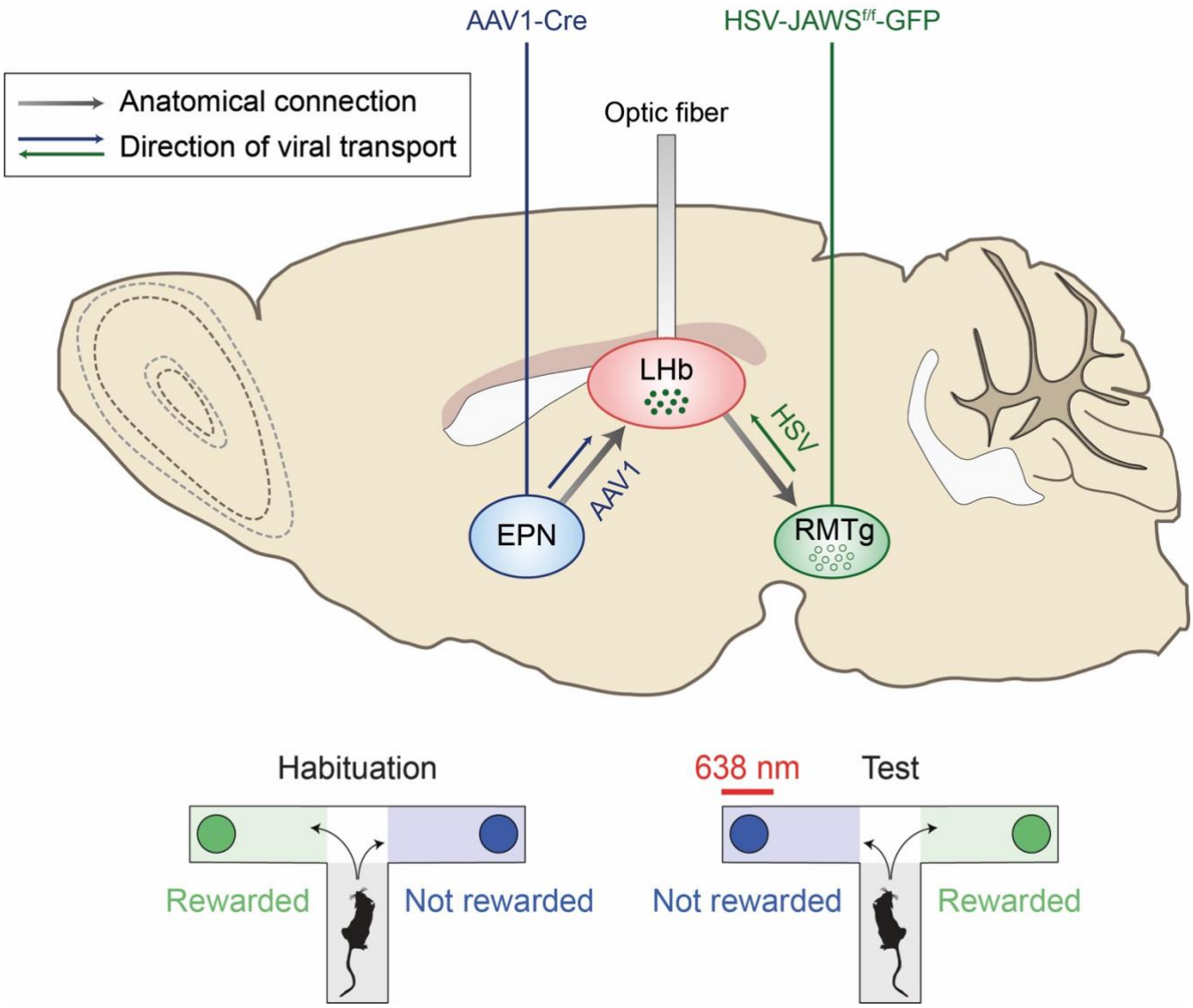

Figure 15. Experimental approach to study the EPN-to-LHb-to-RMTg circuit in the encoding of reward omission during the T-maze task. Injection of AAV1-Cre in the EPN would allow the virus to jump anterogradely into the LHb, while injection of HSV-JAWS$^{f/f}$ would allow the virus to be retrogradely transported into the LHb. Hence, the LoxP recombination would occur in EPN-receiving and RMTg-projecting habenular neurons. This subpopulation would be silenced by red light delivery through an optic fiber in the LHb, while encountering the non-rewarded container during the test session.

Interestingly, the comorbidity between weakened neural networks and cognitive deficits has been observed in additional brain structures. In the recently evolved PFC, the volume of NMDAR-containing dendritic arborizations positively correlates with single-monkey performance in working memory tasks (Goldman-Rakic, 1996; Dumitriu et al., 2010; Wang et al., 2013). Accordingly, stress drives prefrontal spine loss, reduces NMDAR transmission, and promotes deficits in working memory (Radley et al., 2006; Yuen et al., 2012). Therefore, reduced synaptic strength in both the LHb and PFC is associated with the emergence of cognitive impairments. The mechanisms underlying these similarities deserve special attention.

In LHb neurons, the reduction in synaptic strength after stress exposure is based on the decrease of AMPAR levels. In the PFC, however, stress drives the opening of hyperpolarizing channels in dendritic compartments through the activation of metabotropic DA and NE receptors (Murphy et al., 1996; Birnbaum et al., 1999). In the LHb, stress-driven deficits in reward seeking can be mimicked by the weakening of excitatory synapses, and rescued by potentiation of AMPAR transmission. Complementarily, in PFC neurons, working memory impairments can be emulated through the activation of catecholamine receptors, and prevented by the inhibition of hyperpolarizing conductances (Arnsten et al., 1999; Taylor et al., 1999; Wang et al., 2007; Vijayraghavan et al., 2007). Future research needs to assess whether these stress-driven alterations are interdependent, and whether they control specific or common aspects of cognitive behaviors. It is certainly possible that stressors result in cognitive deficits through synergistic actions on PFC and LHb neurons. Aberrant decision-making might be the aftermath of prefrontal synaptic alterations (Soares et al., 2012; Friedman et al., 2015; Friedman et al., 2017), while the insensitivity to value-based outcomes may be more related to the habenular AMPAR LTD reported here (Li et al., 2019b).

It is worth mentioning that a direct connection between PFC and LHb neurons has been proposed. At least in rats, the habenular complex receives glutamatergic inputs from PFC neurons (Kim and Lee, 2012). The activation of PFC-to-LHb afferents is associated with behavioral despair during stress exposure, and with the avoidance of associated contexts (Warden et al., 2012; Benekareddy et al., 2018). Yet, these findings need to be evaluated with caution, because the PFC faintly projects to the LHb, while heavily innervating the thalamic areas surrounding it (Gabbott et al., 2005; Kim and Lee, 2012). This opens the possibility that the optogenetic manipulations from previous studies were actually observing the behavioral effects of PFC-to-thalamus pathways (Warden et al., 2012; Benekareddy et al., 2018).

Altogether, my second study indicates that the strength of excitatory synapses in the LHb plays an important role during reward-guided behaviors, by shaping the responses of habenular neurons to encounters with the absence of anticipated rewards. Based on literature, the EPN is the most likely source of excitatory signals, which potentially result in the inhibition of VTA DA neurons via RMTg activation. Moreover, we highlighted the striking convergence between the PFC and LHb – two brain regions in which synaptic strength instructs the manifestation of cognitive behaviors.

4.3 Concluding remarks

My doctoral thesis illustrates the synaptic mechanisms by which stressors of different nature drive divergent consequences on behavior. We observed that AMPAR LTP promotes the avoidance of escapable stressors, while AMPAR LTD after inescapable stress exposure is at the basis of cognitive impairments. Our results cohere with earlier studies, in which opposite synaptic changes were shown to drive dissimilar behavioral adaptations. For example, LTP and LTD of excitatory transmission in hippocampal and BLA neurons lead to memory formation and forgetting (Nabavi et al., 2014; Choi et al., 2018; Awasthi et al., 2019).

The attempt to put together the findings from our two articles might shed light on the synaptic mechanisms behind certain clinical observations. Taking at face value the causative links between LHb synaptic strength and behavioral performance, we predict that mice exposed to the inescapable foot-shock paradigm may be impaired in the active avoidance task, at least until the AMPAR LTD is surmounted by potentiation. This would be an example in which uncontrollable stress disrupts the execution of coping behaviors. These preclinical predictions, based on our work, go in line with classical observations during the Second World War, when highly-skilled pilots underwent tragic accidents in the heat of battle due to operational errors (Broadbent, 1971). Moreover, from a clinical perspective, we could conceive the idea of overcoming stress-driven cognitive abnormalities (i.e., LTD) by embracing active coping strategies (i.e., LTP). This reasoning conforms to the therapeutic approach proposed for treating PTSD patients affected by the September 11 attacks in the World Trade Center (LeDoux and Gorman, 2001). Therefore, in order to tackle the cognitive impairments following inescapable stress, we could voluntarily challenge ourselves with mild stressors over which we might exert certain control.

Apart from these behavioral therapies for the prevention of stress-driven alterations, our results also support the utilization of pharmacological regimes to potentiate glutamatergic transmission. Ampakines are positive allosteric modulators of AMPAR transmission, capable of crossing the blood-brain barrier to boost synaptic function (Staubli et al., 1994; Lynch, 2004). These compounds are successful in ameliorating cognitive deficits in the context of aging and stress, but they exert effects at the whole-brain level (Lauterborn et al., 2016; Leem and Chang, 2017). Considering the absence of LHb-specific approaches in the clinical field, a situation likely to prevail in the forthcoming years, I would favor behavioral therapies over pharmacological treatments.

In the coming years, the field would certainly benefit from studies aiming to better delineate the circuit and molecular properties of distinct LHb subpopulations, required for the emergence of coping and pathological behaviors (Hashikawa et al., 2020; Wallace et al., 2020). These multiplex designs would allow us to characterize specific molecular markers, potentially druggable, embedded in discrete habenular circuits. Such an approach could result in the generation of new clinical tools, with the aim of reverting synaptic and behavioral alterations arising after stressful experiences that so commonly abound in modern societies (Cerniauskas et al., 2019).

Data appendix

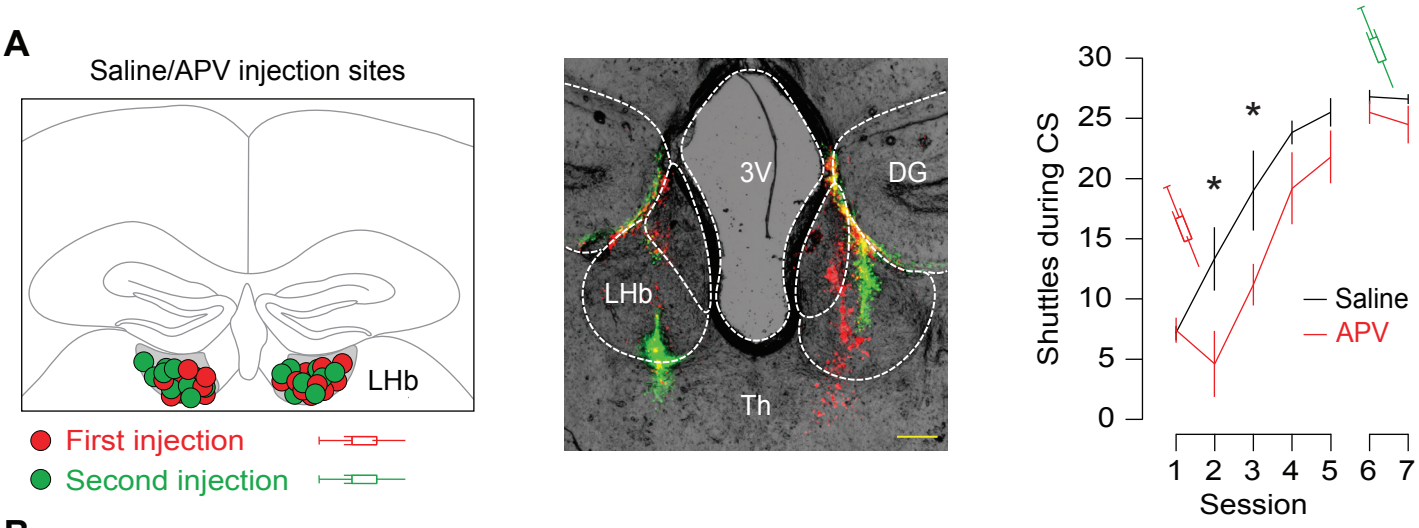

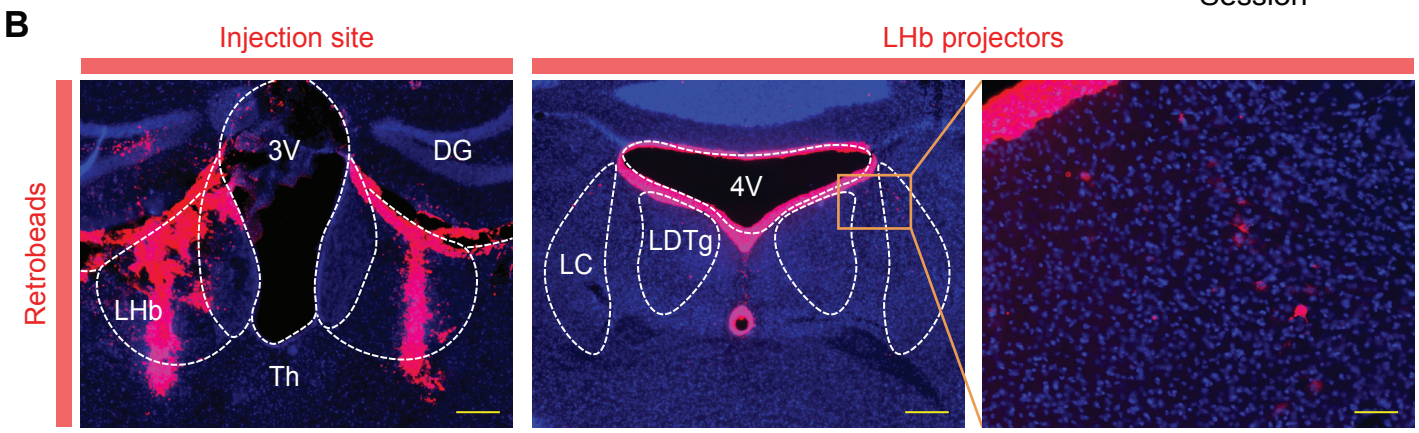

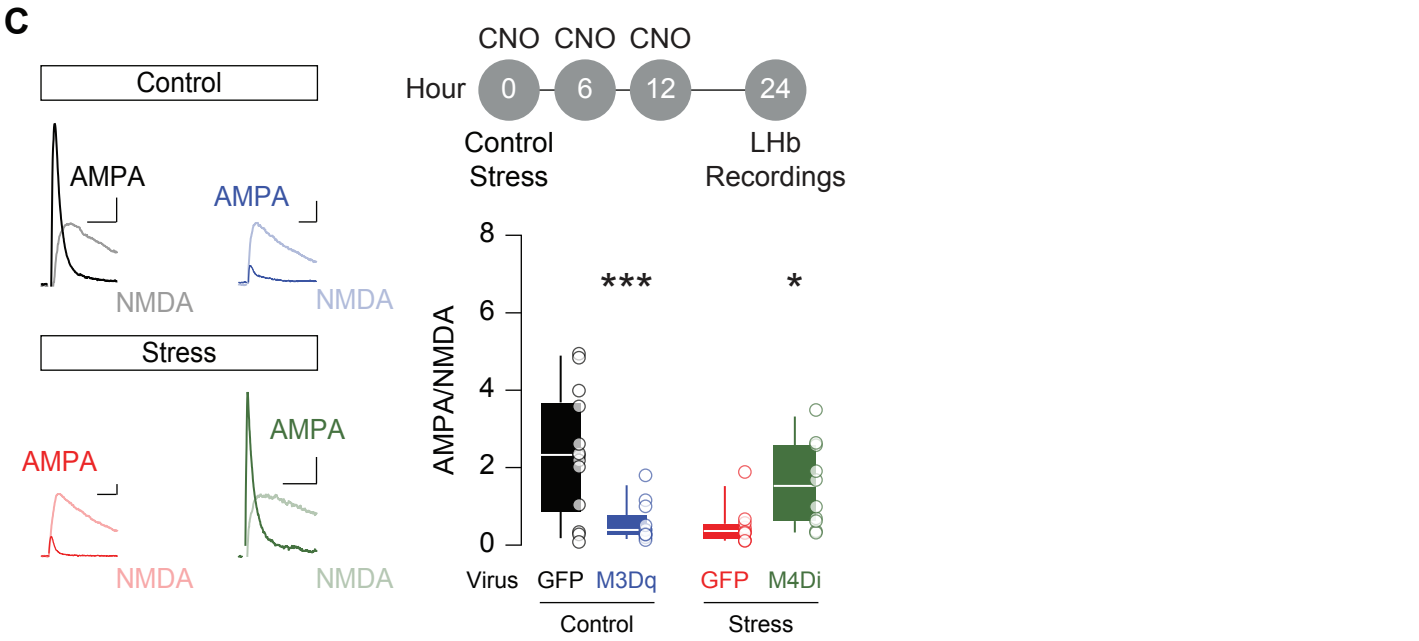

Data appendix.

(**A**) Coronal schematic depicting the approximate sites of saline/APV injection for NMDAR blockade during avoidance learning (red circles: first injection; green circles: second injection; n=6 saline and n=5 APV). Representative first (red) and second (green) infusion sites of APV (scale bar: 200 µm). Number of shuttles during CS presentation (i.e. avoidance responses) throughout the training. The first injection took place before session 2, while the second injection was performed prior to session 7. Two-way repeated measures ANOVA ($F_{1,9}$=2.888) with Holm-Sidak correction (*p<0.05, saline versus APV).

(**B**) Representative injection sites of fluorescent retrobeads in the LHb and corresponding projectors in the LC (scale bar: 200 µm for left and middle panels, 50 µm for right panel).

(**C**) Example traces of AMPA/NMDA (+40 mV; scale bars: 30 pA, 10 ms). Experimental timeline. Box and scatter plots of AMPA/NMDA from control/GFP (black: n=3 mice/13 cells, 2.353±0.4565), control/M3Dq mice (blue: n=3 mice/12 cells, 0.5575±0.1453), stress/GFP (red: n=3 mice/11 cells, 0.4818±0.1509) and stress/M4Di (green: n=3 mice/10 cells, 1.528±0.3496). Two-way ANOVA ($F_{1,42}$=1.376) with Holm-Sidak correction (***p<0.001, *p<0.05, comparisons against GFP).

List of publications

Research articles

- **Nuno-Perez, A.**, Trusel, M., Lalive, A. L., Congiu, M., Gastaldo, D., Tchenio, A., Lecca, S., Soiza-Reilly, M., Bagni, C., and Mameli, M. (2021). Stress undermines reward-guided cognitive performance through synaptic depression in the lateral habenula. Neuron 109, 947-956.
- Tan, D., **Nuno-Perez, A.**, Mameli, M., and Meye, F. J. (2019). Cocaine withdrawal reduces $GABA_BR$ transmission at entopeduncular nucleus - lateral habenula synapses. Eur J Neurosci 50, 2124-2133.
- Trusel, M., **Nuno-Perez, A.**, Lecca, S., Harada, H., Lalive, A. L., Congiu, M., Takemoto, K., Takahashi, T., Ferraguti, F., and Mameli, M. (2019). Punishment-Predictive Cues Guide Avoidance through Potentiation of Hypothalamus-to-Habenula Synapses. Neuron 102, 120-127.
- Maldonado, P. P., **Nuno-Perez, A.**, Kirchner, J. H., Hammock, E., Gjorgjieva, J., and Lohmann, C. (2020). Oxytocin Shapes Spontaneous Activity Patterns in the Developing Visual Cortex by Activating Somatostatin Interneurons. Curr Biol. S0960-9822(20)31532-3. The research related to this article was conducted during my Master's thesis, but part of the corresponding data analysis was performed while I was enrolled at the doctoral school.

Review articles

- **Nuno-Perez, A.**, Tchenio, A., Mameli, M., and Lecca, S. (2018). Lateral Habenula Gone Awry in Depression: Bridging Cellular Adaptations with Therapeutics. Front Neurosci 12, 485.

Previews

- **Nuno-Perez, A.**, and Mameli, M. (2020). In DA Club of Reinforcement: Glutamate, It's Your Birthday. Neuron 107, 765-767.

References

- Abbott, L. F., and Regehr, W. G. (2004). Synaptic computation. Nature 431, 796-803.
- Abercrombie, E. D., and Jacobs, B. L. (1988). Systemic naloxone administration potentiates locus coeruleus noradrenergic neuronal activity under stressful but not non-stressful conditions. Brain Res 441, 362-366.
- Aguilera, G. (1994). Regulation of pituitary ACTH secretion during chronic stress. Front Neuroendocrinol 15, 321-350.
- Aisa, B., Tordera, R., Lasheras, B., Del Río, J., and Ramírez, M. J. (2007). Cognitive impairment associated to HPA axis hyperactivity after maternal separation in rats. Psychoneuroendocrinology 32, 256-266.
- Aizawa, H., Kobayashi, M., Tanaka, S., Fukai, T., and Okamoto, H. (2012). Molecular characterization of the subnuclei in rat habenula. J Comp Neurol 520, 4051-4066.
- Al-Hallaq, R. A., Conrads, T. P., Veenstra, T. D., and Wenthold, R. J. (2007). NMDA di-heteromeric receptor populations and associated proteins in rat hippocampus. J Neurosci 27, 8334-8343.
- Amat, J., Baratta, M. V., Paul, E., Bland, S. T., Watkins, L. R., and Maier, S. F. (2005). Medial prefrontal cortex determines how stressor controllability affects behavior and dorsal raphe nucleus. Nat Neurosci 8, 365-371.
- Amo, R., Fredes, F., Kinoshita, M., Aoki, R., Aizawa, H., Agetsuma, M., Aoki, T., Shiraki, T., Kakinuma, H., Matsuda, M., Yamazaki, M., Takahoko, M., Tsuboi, T., Higashijima, S., Miyasaka, N., Koide, T., Yabuki, Y., Yoshihara, Y., Fukai, T., and Okamoto, H. (2014). The habenulo-raphe serotonergic circuit encodes an aversive expectation value essential for adaptive active avoidance of danger. Neuron 84, 1034-1048.
- Andreasen, M., and Lambert, J. D. (1998). Factors determining the efficacy of distal excitatory synapses in rat hippocampal CA1 pyramidal neurones. J Physiol 507, 441-462.
- Anstrom, K. K., and Woodward, D. J. (2005). Restraint increases dopaminergic burst firing in awake rats. Neuropsychopharmacology 30, 1832-1840.
- Anstrom, K. K., Miczek, K. A., and Budygin, E. A. (2009). Increased phasic dopamine signaling in the mesolimbic pathway during social defeat in rats. Neuroscience 161, 3-12.
- Aoto, J., Martinelli, D. C., Malenka, R. C., Tabuchi, K., and Südhof, T. C. (2013). Presynaptic neurexin-3 alternative splicing trans-synaptically controls postsynaptic AMPA receptor trafficking. Cell 154, 75-88.
- Arnsten, A. F. (2009). Stress signalling pathways that impair prefrontal cortex structure and function. Nat Rev Neurosci 10, 410-422.
- Arnsten, A. F., Mathew, R., Ubriani, R., Taylor, J. R., and Li, B. M. (1999). Alpha-1 noradrenergic receptor stimulation impairs prefrontal cortical cognitive function. Biol Psychiatry 45, 26-31.
- Aston-Jones, G., and Cohen, J. D. (2005). An integrative theory of locus coeruleus-norepinephrine function: adaptive gain and optimal performance. Annu Rev Neurosci 28, 403-450.
- Authement, M. E., Langlois, L. D., Shepard, R. D., Browne, C. A., Lucki, I., Kassis, H., and Nugent, F. S. (2018). A role for corticotropin-releasing factor signaling in the lateral habenula and its modulation by early-life stress. Sci Signal 11(520).
- Awasthi, A., Ramachandran, B., Ahmed, S., Benito, E., Shinoda, Y., Nitzan, N., Heukamp, A., Rannio, S., Martens, H., Barth, J., Burk, K., Wang, Y. T., Fischer, A., and Dean, C. (2019). Synaptotagmin-3 drives AMPA receptor endocytosis, depression of synapse strength, and forgetting. Science 363(6422).
- Baker, D. G., West, S. A., Nicholson, W. E., Ekhator, N. N., Kasckow, J. W., Hill, K. K., Bruce, A. B., Orth, D. N., and Geracioti, T. D. (1999). Serial CSF corticotropin-releasing hormone levels and adrenocortical activity in combat veterans with posttraumatic stress disorder. Am J Psychiatry 156, 585-588.
- Baker, P. M., Oh, S. E., Kidder, K. S., and Mizumori, S. J. (2015). Ongoing behavioral state information signaled in the lateral habenula guides choice flexibility in freely moving rats. Front Behav Neurosci 9, 295.
- Baker, P. M., Raynor, S. A., Francis, N. T., and Mizumori, S. J. (2017). Lateral habenula integration of proactive and retroactive information mediates behavioral flexibility. Neuroscience 345, 89-98.

- Bale, T. L., Picetti, R., Contarino, A., Koob, G. F., Vale, W. W., and Lee, K. F. (2002). Mice deficient for both corticotropin-releasing factor receptor 1 (CRFR1) and CRFR2 have an impaired stress response and display sexually dichotomous anxiety-like behavior. J Neurosci 22, 193-199.
- Bali, A., and Jaggi, A. S. (2015). Electric foot shock stress: a useful tool in neuropsychiatric studies. Rev Neurosci 26, 655-677.
- Bambico, F. R., Nguyen, N. T., and Gobbi, G. (2009). Decline in serotonergic firing activity and desensitization of 5-HT1A autoreceptors after chronic unpredictable stress. Eur Neuropsychopharmacol 19, 215-228.
- Banke, T. G., Bowie, D., Lee, H., Huganir, R. L., Schousboe, A., and Traynelis, S. F. (2000). Control of GluR1 AMPA receptor function by cAMP-dependent protein kinase. J Neurosci 20, 89-102.
- Barker, D. J., Miranda-Barrientos, J., Zhang, S., Root, D. H., Wang, H. L., Liu, B., Calipari, E. S., and Morales, M. (2017). Lateral Preoptic Control of the Lateral Habenula through Convergent Glutamate and GABA Transmission. Cell Rep 21, 1757-1769.
- Barria, A., and Malinow, R. (2005). NMDA receptor subunit composition controls synaptic plasticity by regulating binding to CaMKII. Neuron 48, 289-301.
- Barria, A., Derkach, V., and Soderling, T. (1997). Identification of the Ca^{2+}/calmodulin-dependent protein kinase II regulatory phosphorylation site in the alpha-amino-3-hydroxyl-5-methyl-4-isoxazole-propionate-type glutamate receptor. J Biol Chem 272, 32727-32730.
- Bats, C., Groc, L., and Choquet, D. (2007). The interaction between Stargazin and PSD-95 regulates AMPA receptor surface trafficking. Neuron 53, 719-734.
- Bekris, S., Antoniou, K., Daskas, S., and Papadopoulou-Daifoti, Z. (2005). Behavioural and neurochemical effects induced by chronic mild stress applied to two different rat strains. Behav Brain Res 161, 45-59.
- Benekareddy, M., Stachniak, T. J., Bruns, A., Knoflach, F., von Kienlin, M., Künnecke, B., and Ghosh, A. (2018). Identification of a Corticohabenular Circuit Regulating Socially Directed Behavior. Biol Psychiatry 83, 607-617.
- Benke, T. A., Lüthi, A., Isaac, J. T., and Collingridge, G. L. (1998). Modulation of AMPA receptor unitary conductance by synaptic activity. Nature 393, 793-797.
- Bennay, M., Langer, J., Meier, S. D., Kafitz, K. W., and Rose, C. R. (2008). Sodium signals in cerebellar Purkinje neurons and Bergmann glial cells evoked by glutamatergic synaptic transmission. Glia 56, 1138-1149.
- Berridge, C. W., and Waterhouse, B. D. (2003). The locus coeruleus-noradrenergic system: modulation of behavioral state and state-dependent cognitive processes. Brain Res Brain Res Rev 42, 33-84.
- Berton, O., McClung, C. A., Dileone, R. J., Krishnan, V., Renthal, W., Russo, S. J., Graham, D., Tsankova, N. M., Bolanos, C. A., Rios, M., Monteggia, L. M., Self, D. W., and Nestler, E. J. (2006). Essential role of BDNF in the mesolimbic dopamine pathway in social defeat stress. Science 311, 864-868.
- Bianco, I. H., and Wilson, S. W. (2009). The habenular nuclei: a conserved asymmetric relay station in the vertebrate brain. Philos Trans R Soc Lond B Biol Sci 364, 1005-1020.
- Birnbaum, S., Gobeske, K. T., Auerbach, J., Taylor, J. R., and Arnsten, A. F. (1999). A role for norepinephrine in stress-induced cognitive deficits: alpha-1-adrenoceptor mediation in the prefrontal cortex. Biol Psychiatry 46, 1266-1274.
- Branco, T., Clark, B. A., and Häusser, M. (2010). Dendritic discrimination of temporal input sequences in cortical neurons. Science 329, 1671-1675.
- Bremner, J. D., Licinio, J., Darnell, A., Krystal, J. H., Owens, M. J., Southwick, S. M., Nemeroff, C. B., and Charney, D. S. (1997). Elevated CSF corticotropin-releasing factor concentrations in posttraumatic stress disorder. Am J Psychiatry 154, 624-629.
- Briand, L. A., Vassoler, F. M., Pierce, R. C., Valentino, R. J., and Blendy, J. A. (2010). Ventral tegmental afferents in stress-induced reinstatement: the role of cAMP response element-binding protein. J Neurosci 30, 16149-16159.
- Brigman, J. L., Wright, T., Talani, G., Prasad-Mulcare, S., Jinde, S., Seabold, G. K., Mathur, P., Davis, M. I., Bock, R., Gustin, R. M., Colbran, R. J., Alvarez, V. A., Nakazawa, K., Delpire, E., Lovinger, D. M., and Holmes, A. (2010). Loss of GluN2B-containing NMDA receptors in CA1 hippocampus and cortex impairs long-term depression, reduces dendritic spine density, and disrupts learning. J Neurosci 30, 4590-4600.

- Brinschwitz, K., Dittgen, A., Madai, V. I., Lommel, R., Geisler, S., and Veh, R. W. (2010). Glutamatergic axons from the lateral habenula mainly terminate on GABAergic neurons of the ventral midbrain. Neuroscience 168, 463-476.
- Brischoux, F., Chakraborty, S., Brierley, D. I., and Ungless, M. A. (2009). Phasic excitation of dopamine neurons in ventral VTA by noxious stimuli. Proc Natl Acad Sci U S A 106, 4894-4899.
- Britton, K. T., Segal, D. S., Kuczenski, R., and Hauger, R. (1992). Dissociation between *in vivo* hippocampal norepinephrine response and behavioral/neuroendocrine responses to noise stress in rats. Brain Res 574, 125-130.
- Broadbent, D. (1971). Decision and Stress. Academic, London.
- Brown, E. S., Varghese, F. P., and McEwen, B. S. (2004). Association of depression with medical illness: does cortisol play a role. Biol Psychiatry 55, 1-9.
- Brown, T. C., Correia, S. S., Petrok, C. N., and Esteban, J. A. (2007). Functional compartmentalization of endosomal trafficking for the synaptic delivery of AMPA receptors during long-term potentiation. J Neurosci 27, 13311-13315.
- Brown, T. C., Tran, I. C., Backos, D. S., and Esteban, J. A. (2005). NMDA receptor-dependent activation of the small GTPase Rab5 drives the removal of synaptic AMPA receptors during hippocampal LTD. Neuron 45, 81-94.
- Burnashev, N., Monyer, H., Seeburg, P. H., and Sakmann, B. (1992a). Divalent ion permeability of AMPA receptor channels is dominated by the edited form of a single subunit. Neuron 8, 189-198.
- Burnashev, N., Schoepfer, R., Monyer, H., Ruppersberg, J. P., Günther, W., Seeburg, P. H., and Sakmann, B. (1992b). Control by asparagine residues of calcium permeability and magnesium blockade in the NMDA receptor. Science 257, 1415-1419.
- Butler, R. K., Oliver, E. M., Sharko, A. C., Parilla-Carrero, J., Kaigler, K. F., Fadel, J. R., and Wilson, M. A. (2016). Activation of corticotropin releasing factor-containing neurons in the rat central amygdala and bed nucleus of the stria terminalis following exposure to two different anxiogenic stressors. Behav Brain Res 304, 92-101.
- Callahan, L. B., Tschetter, K. E., and Ronan, P. J. (2013). Inhibition of corticotropin releasing factor expression in the central nucleus of the amygdala attenuates stress-induced behavioral and endocrine responses. Front Neurosci 7, 195.
- Campbell, B. A., and Masterson, F. A. (1969). Psychophysics of punishment. In: Punishment and aversive behavior, Campbell, B. A., and Church, R. M., Eds. (New York: Appleton-Century-Crofts).
- Canny, B. J., Funder, J. W., and Clarke, I. J. (1989). Glucocorticoids regulate ovine hypophysial portal levels of corticotropin-releasing factor and arginine vasopressin in a stress-specific manner. Endocrinology 125, 2532-2539.
- Cao, J. L., Covington, H. E., Friedman, A. K., Wilkinson, M. B., Walsh, J. J., Cooper, D. C., Nestler, E. J., and Han, M. H. (2010). Mesolimbic dopamine neurons in the brain reward circuit mediate susceptibility to social defeat and antidepressant action. J Neurosci 30, 16453-16458.
- Carroll, B. J., Curtis, G. C., Davies, B. M., Mendels, J., and Sugerman, A. A. (1976). Urinary free cortisol excretion in depression. Psychol Med 6, 43-50.
- Carta, A. R., Moreno, C. C., Cadoni, C., Tronci, E., and Di Chiara, G. (2008). Long-term increase in GAD67 mRNA expression in the central amygdala of rats sensitized by drugs and stress. Eur J Neurosci 27, 1220-1230.
- Carter, M. E., Yizhar, O., Chikahisa, S., Nguyen, H., Adamantidis, A., Nishino, S., Deisseroth, K., and de Lecea, L. (2010). Tuning arousal with optogenetic modulation of locus coeruleus neurons. Nat Neurosci 13, 1526-1533.
- Cerniauskas, I., Winterer, J., de Jong, J. W., Lukacsovich, D., Yang, H., Khan, F., Peck, J. R., Obayashi, S. K., Lilascharoen, V., Lim, B. K., Földy, C., and Lammel, S. (2019). Chronic Stress Induces Activity, Synaptic, and Transcriptional Remodeling of the Lateral Habenula Associated with Deficits in Motivated Behaviors. Neuron 104, 899-915.e8.
- Chaudhury, D., Walsh, J. J., Friedman, A. K., Juarez, B., Ku, S. M., Koo, J. W., Ferguson, D., Tsai, H. C., Pomeranz, L., Christoffel, D. J., Nectow, A. R., Ekstrand, M., Domingos, A., Mazei-Robison, M. S., Mouzon, E., Lobo, M. K., Neve, R. L., Friedman, J. M., Russo, S. J., Deisseroth, K., Nestler, E. J., and Han, M. H. (2013). Rapid regulation of depression-related behaviours by control of midbrain dopamine neurons. Nature 493, 532-536.
- Chen, F. J., and Sara, S. J. (2007). Locus coeruleus activation by foot shock or electrical stimulation inhibits amygdala neurons. Neuroscience 144, 472-481.
- Chen, L., Cai, P., Wang, R. F., Lu, Y. P., Chen, H. Y., Guo, Y. R., Huang, S. N., Hu, L. H., Chen, J., Zheng, Z. H., He, P., Zhang, B. F., Liu, J. Y., Wang, W. X., Li, H. Y., and Yu, C. X. (2020). Glutamatergic lateral hypothalamus promotes defensive behaviors. Neuropharmacology 178, 108239.

- Chen, L., Chetkovich, D. M., Petralia, R. S., Sweeney, N. T., Kawasaki, Y., Wenthold, R. J., Bredt, D. S., and Nicoll, R. A. (2000). Stargazin regulates synaptic targeting of AMPA receptors by two distinct mechanisms. Nature 408, 936-943.
- Chen, S., Wang, J., and Siegelbaum, S. A. (2001). Properties of hyperpolarization-activated pacemaker current defined by coassembly of HCN1 and HCN2 subunits and basal modulation by cyclic nucleotide. J Gen Physiol 117, 491-504.
- Cho, C. H., St-Gelais, F., Zhang, W., Tomita, S., and Howe, J. R. (2007). Two families of TARP isoforms that have distinct effects on the kinetic properties of AMPA receptors and synaptic currents. Neuron 55, 890-904.
- Choi, D. C., Furay, A. R., Evanson, N. K., Ostrander, M. M., Ulrich-Lai, Y. M., and Herman, J. P. (2007). Bed nucleus of the stria terminalis subregions differentially regulate hypothalamic-pituitary-adrenal axis activity: implications for the integration of limbic inputs. J Neurosci 27, 2025-2034.
- Choi, D. C., Furay, A. R., Evanson, N. K., Ulrich-Lai, Y. M., Nguyen, M. M., Ostrander, M. M., and Herman, J. P. (2008). The role of the posterior medial bed nucleus of the stria terminalis in modulating hypothalamic-pituitary-adrenocortical axis responsiveness to acute and chronic stress. Psychoneuroendocrinology 33, 659-669.
- Choi, J. H., Sim, S. E., Kim, J. I., Choi, D. I., Oh, J., Ye, S., Lee, J., Kim, T., Ko, H. G., Lim, C. S., and Kaang, B. K. (2018). Interregional synaptic maps among engram cells underlie memory formation. Science 360, 430-435.
- Chokshi, V., Gao, M., Grier, B. D., Owens, A., Wang, H., Worley, P. F., and Lee, H. K. (2019). Input-Specific Metaplasticity in the Visual Cortex Requires Homer1a-Mediated mGluR5 Signaling. Neuron 104, 736-748.e6.
- Chourbaji, S., Zacher, C., Sanchis-Segura, C., Dormann, C., Vollmayr, B., and Gass, P. (2005). Learned helplessness: validity and reliability of depressive-like states in mice. Brain Res Brain Res Protoc 16, 70-78.
- Chowdhury, D., Turner, M., Patriarchi, T., Hergarden, A. C., Anderson, D., Zhang, Y., Sun, J., Chen, C. Y., Ames, J. B., and Hell, J. W. (2018). Ca^{2+}/calmodulin binding to PSD-95 mediates homeostatic synaptic scaling down. EMBO J 37(1):122-138.
- Christoph, G. R., Leonzio, R. J., and Wilcox, K. S. (1986). Stimulation of the lateral habenula inhibits dopamine-containing neurons in the substantia nigra and ventral tegmental area of the rat. J Neurosci 6, 613-619.
- Citri, A., and Malenka, R. C. (2008). Synaptic plasticity: multiple forms, functions, and mechanisms. Neuropsychopharmacology 33, 18-41.
- Clem, R. L., and Huganir, R. L. (2010). Calcium-permeable AMPA receptor dynamics mediate fear memory erasure. Science 330, 1108-1112.
- Coan, E. J., and Collingridge, G. L. (1985). Magnesium ions block an N-methyl-D-aspartate receptor-mediated component of synaptic transmission in rat hippocampus. Neurosci Lett 53, 21-26.
- Cohen, J. Y., Haesler, S., Vong, L., Lowell, B. B., and Uchida, N. (2012). Neuron-type-specific signals for reward and punishment in the ventral tegmental area. Nature 482, 85-88.
- Commons, K. G. (2008). Evidence for topographically organized endogenous 5-HT-1A receptor-dependent feedback inhibition of the ascending serotonin system. Eur J Neurosci 27, 2611-2618.
- Congiu, M., Trusel, M., Pistis, M., Mameli, M., and Lecca, S. (2019). Opposite responses to aversive stimuli in lateral habenula neurons. Eur J Neurosci 50, 2921-2930.
- Contarino, A., Dellu, F., Koob, G. F., Smith, G. W., Lee, K. F., Vale, W., and Gold, L. H. (1999). Reduced anxiety-like and cognitive performance in mice lacking the corticotropin-releasing factor receptor 1. Brain Res 835, 1-9.
- Crair, M. C., and Malenka, R. C. (1995). A critical period for long-term potentiation at thalamocortical synapses. Nature 375, 325-328.
- Cui, Y., Yang, Y., Ni, Z., Dong, Y., Cai, G., Foncelle, A., Ma, S., Sang, K., Tang, S., Li, Y., Shen, Y., Berry, H., Wu, S., and Hu, H. (2018). Astroglial Kir4.1 in the lateral habenula drives neuronal bursts in depression. Nature 554, 323-327.
- Cullinan, W. E., Herman, J. P., and Watson, S. J. (1993). Ventral subicular interaction with the hypothalamic paraventricular nucleus: evidence for a relay in the bed nucleus of the stria terminalis. J Comp Neurol 332, 1-20.
- Curtis, A. L., Lechner, S. M., Pavcovich, L. A., and Valentino, R. J. (1997). Activation of the locus coeruleus noradrenergic system by intracoerulear microinfusion of corticotropin-releasing factor: effects on discharge rate, cortical norepinephrine levels and cortical electroencephalographic activity. J Pharmacol Exp Ther 281, 163-172.

- Dabrowska, J., Hazra, R., Guo, J. D., Dewitt, S., and Rainnie, D. G. (2013). Central CRF neurons are not created equal: phenotypic differences in CRF-containing neurons of the rat paraventricular hypothalamus and the bed nucleus of the stria terminalis. Front Neurosci 7, 156.
- Dang, R., Qi, J., Liu, A., Ren, Q., Lv, D., Han, L., Zhou, Z., Cao, F., Xie, W., and Jia, Z. (2018). Regulation of hippocampal long term depression by Neuroligin 1. Neuropharmacology 143, 205-216.
- Daniel, S. E., Menigoz, A., Guo, J., Ryan, S. J., Seth, S., and Rainnie, D. G. (2019). Chronic stress induces cell type-selective transcriptomic and electrophysiological changes in the bed nucleus of the stria terminalis. Neuropharmacology 150, 80-90.
- Davis, M., and Walker, D. L. (2014). Role of bed nucleus of the stria terminalis and amygdala AMPA receptors in the development and expression of context conditioning and sensitization of startle by prior shock. Brain Struct Funct 219, 1969-1982.
- Daviu, N., Füzesi, T., Rosenegger, D. G., Rasiah, N. P., Sterley, T. L., Peringod, G., and Bains, J. S. (2020). Paraventricular nucleus CRH neurons encode stress controllability and regulate defensive behavior selection. Nat Neurosci 23, 398-410.
- de Kloet, E. R., Joëls, M., and Holsboer, F. (2005). Stress and the brain: from adaptation to disease. Nat Rev Neurosci 6, 463-475.
- De Marco, R. J., Thiemann, T., Groneberg, A. H., Herget, U., and Ryu, S. (2016). Optogenetically enhanced pituitary corticotroph cell activity post-stress onset causes rapid organizing effects on behaviour. Nat Commun 7, 12620.
- Delgado, J. Y., Coba, M., Anderson, C. N., Thompson, K. R., Gray, E. E., Heusner, C. L., Martin, K. C., Grant, S. G., and O'Dell, T. J. (2007). NMDA receptor activation dephosphorylates AMPA receptor glutamate receptor 1 subunits at threonine 840. J Neurosci 27, 13210-13221.
- Derkach, V., Barria, A., and Soderling, T. R. (1999). Ca^{2+}/calmodulin-kinase II enhances channel conductance of alpha-amino-3-hydroxy-5-methyl-4-isoxazolepropionate type glutamate receptors. Proc Natl Acad Sci U S A 96, 3269-3274.
- Desai, N. S., Cudmore, R. H., Nelson, S. B., and Turrigiano, G. G. (2002). Critical periods for experience-dependent synaptic scaling in visual cortex. Nat Neurosci 5, 783-789.
- Dias-Ferreira, E., Sousa, J. C., Melo, I., Morgado, P., Mesquita, A. R., Cerqueira, J. J., Costa, R. M., and Sousa, N. (2009). Chronic stress causes frontostriatal reorganization and affects decision-making. Science 325, 621-625.
- Diehl, M. M., Bravo-Rivera, C., Rodriguez-Romaguera, J., Pagan-Rivera, P. A., Burgos-Robles, A., Roman-Ortiz, C., and Quirk, G. J. (2018). Active avoidance requires inhibitory signaling in the rodent prelimbic prefrontal cortex. Elife 7:e34657.
- Diehl, M. M., Iravedra-Garcia, J. M., Morán-Sierra, J., Rojas-Bowe, G., Gonzalez-Diaz, F. N., Valentín-Valentín, V. P., and Quirk, G. J. (2020). Divergent projections of the prelimbic cortex bidirectionally regulate active avoidance. Elife 9:e59281.
- Diering, G. H., Gustina, A. S., and Huganir, R. L. (2014). PKA-GluA1 coupling via AKAP5 controls AMPA receptor phosphorylation and cell-surface targeting during bidirectional homeostatic plasticity. Neuron 84, 790-805.
- Diering, G. H., Nirujogi, R. S., Roth, R. H., Worley, P. F., Pandey, A., and Huganir, R. L. (2017). Homer1a drives homeostatic scaling-down of excitatory synapses during sleep. Science 355, 511-515.
- Dinsmoor, J. A. (2001). Stimuli inevitably generated by behavior that avoids electric shock are inherently reinforcing. J Exp Anal Behav 75, 311-333.
- Dobrunz, L. E., and Stevens, C. F. (1997). Heterogeneity of release probability, facilitation, and depletion at central synapses. Neuron 18, 995-1008.
- Douma, E. H., and de Kloet, E. R. (2020). Stress-induced plasticity and functioning of ventral tegmental dopamine neurons. Neurosci Biobehav Rev 108, 48-77.
- Drugan, R. C., Basile, A. S., Ha, J. H., Healy, D., and Ferland, R. J. (1997). Analysis of the importance of controllable versus uncontrollable stress on subsequent behavioral and physiological functioning. Brain Res Brain Res Protoc 2, 69-74.

- Dumitriu, D., Hao, J., Hara, Y., Kaufmann, J., Janssen, W. G., Lou, W., Rapp, P. R., and Morrison, J. H. (2010). Selective changes in thin spine density and morphology in monkey prefrontal cortex correlate with aging-related cognitive impairment. J Neurosci 30, 7507-7515.
- Engler, D., Pham, T., Fullerton, M. J., Ooi, G., Funder, J. W., and Clarke, I. J. (1989). Studies of the secretion of corticotropin-releasing factor and arginine vasopressin into the hypophysial-portal circulation of the conscious sheep. I. Effect of an audiovisual stimulus and insulin-induced hypoglycemia. Neuroendocrinology 49, 367-381.
- Erburu, M., Cajaleon, L., Guruceaga, E., Venzala, E., Muñoz-Cobo, I., Beltrán, E., Puerta, E., and Tordera, R. M. (2015). Chronic mild stress and imipramine treatment elicit opposite changes in behavior and in gene expression in the mouse prefrontal cortex. Pharmacol Biochem Behav 135, 227-236.
- Erreger, K., Dravid, S. M., Banke, T. G., Wyllie, D. J., and Traynelis, S. F. (2005). Subunit-specific gating controls rat NR1/NR2A and NR1/NR2B NMDA channel kinetics and synaptic signalling profiles. J Physiol 563, 345-358.
- Etherton, M., Földy, C., Sharma, M., Tabuchi, K., Liu, X., Shamloo, M., Malenka, R. C., and Südhof, T. C. (2011). Autism-linked neuroligin-3 R451C mutation differentially alters hippocampal and cortical synaptic function. Proc Natl Acad Sci U S A 108, 13764-13769.
- Euston, D. R., Gruber, A. J., and McNaughton, B. L. (2012). The role of medial prefrontal cortex in memory and decision making. Neuron 76, 1057-1070.
- Faget, L., Zell, V., Souter, E., McPherson, A., Ressler, R., Gutierrez-Reed, N., Yoo, J. H., Dulcis, D., and Hnasko, T. S. (2018). Opponent control of behavioral reinforcement by inhibitory and excitatory projections from the ventral pallidum. Nat Commun 9, 849.
- Fernández-Monreal, M., Brown, T. C., Royo, M., and Esteban, J. A. (2012). The balance between receptor recycling and trafficking toward lysosomes determines synaptic strength during long-term depression. J Neurosci 32, 13200-13205.
- Flanigan, M. E., Aleyasin, H., Li, L., Burnett, C. J., Chan, K. L., LeClair, K. B., Lucas, E. K., Matikainen-Ankney, B., Durand-de Cuttoli, R., Takahashi, A., Menard, C., Pfau, M. L., Golden, S. A., Bouchard, S., Calipari, E. S., Nestler, E. J., DiLeone, R. J., Yamanaka, A., Huntley, G. W., Clem, R. L., and Russo, S. J. (2020). Orexin signaling in GABAergic lateral habenula neurons modulates aggressive behavior in male mice. Nat Neurosci 23, 638-650.
- Foster, K. A., McLaughlin, N., Edbauer, D., Phillips, M., Bolton, A., Constantine-Paton, M., and Sheng, M. (2010). Distinct roles of NR2A and NR2B cytoplasmic tails in long-term potentiation. J Neurosci 30, 2676-2685.
- Friedman, A., Homma, D., Bloem, B., Gibb, L. G., Amemori, K. I., Hu, D., Delcasso, S., Truong, T. F., Yang, J., Hood, A. S., Mikofalvy, K. A., Beck, D. W., Nguyen, N., Nelson, E. D., Toro Arana, S. E., Vorder Bruegge, R. H., Goosens, K. A., and Graybiel, A. M. (2017). Chronic Stress Alters Striosome-Circuit Dynamics, Leading to Aberrant Decision-Making. Cell 171, 1191-1205.e28.
- Friedman, A., Homma, D., Gibb, L. G., Amemori, K., Rubin, S. J., Hood, A. S., Riad, M. H., and Graybiel, A. M. (2015). A Corticostriatal Path Targeting Striosomes Controls Decision-Making under Conflict. Cell 161, 1320-1333.
- Fritschy, J. M., Weinmann, O., Wenzel, A., and Benke, D. (1998). Synapse-specific localization of NMDA and GABA(A) receptor subunits revealed by antigen-retrieval immunohistochemistry. J Comp Neurol 390, 194-210.
- Fukaya, M., Tsujita, M., Yamazaki, M., Kushiya, E., Abe, M., Akashi, K., Natsume, R., Kano, M., Kamiya, H., Watanabe, M., and Sakimura, K. (2006). Abundant distribution of TARP gamma-8 in synaptic and extrasynaptic surface of hippocampal neurons and its major role in AMPA receptor expression on spines and dendrites. Eur J Neurosci 24, 2177-2190.
- Füzesi, T., Daviu, N., Wamsteeker Cusulin, J. I., Bonin, R. P., and Bains, J. S. (2016). Hypothalamic CRH neurons orchestrate complex behaviours after stress. Nat Commun 7, 11937.
- Gabbott, P. L., Warner, T. A., Jays, P. R., Salway, P., and Busby, S. J. (2005). Prefrontal cortex in the rat: projections to subcortical autonomic, motor, and limbic centers. J Comp Neurol 492, 145-177.
- Gafford, G. M., Guo, J. D., Flandreau, E. I., Hazra, R., Rainnie, D. G., and Ressler, K. J. (2012). Cell-type specific deletion of GABA(A)α1 in corticotropin-releasing factor-containing neurons enhances anxiety and disrupts fear extinction. Proc Natl Acad Sci U S A 109, 16330-16335.
- Gambino, F., Pagès, S., Kehayas, V., Baptista, D., Tatti, R., Carleton, A., and Holtmaat, A. (2014). Sensory-evoked LTP driven by dendritic plateau potentials *in vivo*. Nature 515, 116-119.

- Gao, M., Sossa, K., Song, L., Errington, L., Cummings, L., Hwang, H., Kuhl, D., Worley, P., and Lee, H. K. (2010). A specific requirement of Arc/Arg3.1 for visual experience-induced homeostatic synaptic plasticity in mouse primary visual cortex. J Neurosci 30, 7168-7178.
- Geiger, J. R., Melcher, T., Koh, D. S., Sakmann, B., Seeburg, P. H., Jonas, P., and Monyer, H. (1995). Relative abundance of subunit mRNAs determines gating and Ca^{2+} permeability of AMPA receptors in principal neurons and interneurons in rat CNS. Neuron 15, 193-204.
- Gerges, N. Z., Backos, D. S., and Esteban, J. A. (2004). Local control of AMPA receptor trafficking at the postsynaptic terminal by a small GTPase of the Rab family. J Biol Chem 279, 43870-43878.
- Goel, A., and Lee, H. K. (2007). Persistence of experience-induced homeostatic synaptic plasticity through adulthood in superficial layers of mouse visual cortex. J Neurosci 27, 6692-6700.
- Goel, A., Jiang, B., Xu, L. W., Song, L., Kirkwood, A., and Lee, H. K. (2006). Cross-modal regulation of synaptic AMPA receptors in primary sensory cortices by visual experience. Nat Neurosci 9, 1001-1003.
- Golden, S. A., Heshmati, M., Flanigan, M., Christoffel, D. J., Guise, K., Pfau, M. L., Aleyasin, H., Menard, C., Zhang, H., Hodes, G. E., Bregman, D., Khibnik, L., Tai, J., Rebusi, N., Krawitz, B., Chaudhury, D., Walsh, J. J., Han, M. H., Shapiro, M. L., and Russo, S. J. (2016). Basal forebrain projections to the lateral habenula modulate aggression reward. Nature 534, 688-692.
- Goldman-Rakic, P. S. (1996). The prefrontal landscape: implications of functional architecture for understanding human mentation and the central executive. Philos Trans R Soc Lond B Biol Sci 351, 1445-1453.
- Goldstein, D. S. (1987). Stress-induced activation of the sympathetic nervous system. Baillieres Clin Endocrinol Metab 1, 253-278.
- González, J. A., Iordanidou, P., Strom, M., Adamantidis, A., and Burdakov, D. (2016). Awake dynamics and brain-wide direct inputs of hypothalamic MCH and orexin networks. Nat Commun 7, 11395.
- Grahn, R. E., Will, M. J., Hammack, S. E., Maswood, S., McQueen, M. B., Watkins, L. R., and Maier, S. F. (1999). Activation of serotonin-immunoreactive cells in the dorsal raphe nucleus in rats exposed to an uncontrollable stressor. Brain Res 826, 35-43.
- Greenwood, B. N., Strong, P. V., Dorey, A. A., and Fleshner, M. (2007). Therapeutic effects of exercise: wheel running reverses stress-induced interference with shuttle box escape. Behav Neurosci 121, 992-1000.
- Guarraci, F. A., and Kapp, B. S. (1999). An electrophysiological characterization of ventral tegmental area dopaminergic neurons during differential pavlovian fear conditioning in the awake rabbit. Behav Brain Res 99, 169-179.
- Haditsch, U., Leone, D. P., Farinelli, M., Chrostek-Grashoff, A., Brakebusch, C., Mansuy, I. M., McConnell, S. K., and Palmer, T. D. (2009). A central role for the small GTPase Rac1 in hippocampal plasticity and spatial learning and memory. Mol Cell Neurosci 41, 409-419.
- Hagenston, A. M., Fitzpatrick, J. S., and Yeckel, M. F. (2008). MGluR-mediated calcium waves that invade the soma regulate firing in layer V medial prefrontal cortical pyramidal neurons. Cereb Cortex 18, 407-423.
- Hains, A. B., Vu, M. A., Maciejewski, P. K., van Dyck, C. H., Gottron, M., and Arnsten, A. F. (2009). Inhibition of protein kinase C signaling protects prefrontal cortex dendritic spines and cognition from the effects of chronic stress. Proc Natl Acad Sci U S A 106, 17957-17962.
- Hajós-Korcsok, E., Robinson, D. D., Yu, J. H., Fitch, C. S., Walker, E., and Merchant, K. M. (2003). Rapid habituation of hippocampal serotonin and norepinephrine release and anxiety-related behaviors, but not plasma corticosterone levels, to repeated footshock stress in rats. Pharmacol Biochem Behav 74, 609-616.
- Halt, A. R., Dallapiazza, R. F., Zhou, Y., Stein, I. S., Qian, H., Juntti, S., Wojcik, S., Brose, N., Silva, A. J., and Hell, J. W. (2012). CaMKII binding to GluN2B is critical during memory consolidation. EMBO J 31, 1203-1216.
- Handa, R. J., Nunley, K. M., Lorens, S. A., Louie, J. P., McGivern, R. F., and Bollnow, M. R. (1994). Androgen regulation of adrenocorticotropin and corticosterone secretion in the male rat following novelty and foot shock stressors. Physiol Behav 55, 117-124.
- Harnett, M. T., Bernier, B. E., Ahn, K. C., and Morikawa, H. (2009). Burst-timing-dependent plasticity of NMDA receptor-mediated transmission in midbrain dopamine neurons. Neuron 62, 826-838.

- Hashikawa, Y., Hashikawa, K., Rossi, M. A., Basiri, M. L., Liu, Y., Johnston, N. L., Ahmad, O. R., and Stuber, G. D. (2020). Transcriptional and Spatial Resolution of Cell Types in the Mammalian Habenula. Neuron 106, 743-758.e5.
- Hausser, A., and Schlett, K. (2019). Coordination of AMPA receptor trafficking by Rab GTPases. Small GTPases 10, 419-432.
- Hayashi, Y., Shi, S. H., Esteban, J. A., Piccini, A., Poncer, J. C., and Malinow, R. (2000). Driving AMPA receptors into synapses by LTP and CaMKII: requirement for GluR1 and PDZ domain interaction. Science 287, 2262-2267.
- Heim, C., Newport, D. J., Bonsall, R., Miller, A. H., and Nemeroff, C. B. (2001). Altered pituitary-adrenal axis responses to provocative challenge tests in adult survivors of childhood abuse. Am J Psychiatry 158, 575-581.
- Heinrichs, S. C., and Koob, G. F. (2004). Corticotropin-releasing factor in brain: a role in activation, arousal, and affect regulation. J Pharmacol Exp Ther 311, 427-440.
- Heldt, S. A., Mou, L., and Ressler, K. J. (2012). *In vivo* knockdown of GAD67 in the amygdala disrupts fear extinction and the anxiolytic-like effect of diazepam in mice. Transl Psychiatry 2, e181.
- Henckens, M. J., Deussing, J. M., and Chen, A. (2016). Region-specific roles of the corticotropin-releasing factor-urocortin system in stress. Nat Rev Neurosci 17, 636-651.
- Herkenham, M., and Nauta, W. J. (1979). Efferent connections of the habenular nuclei in the rat. J Comp Neurol 187, 19-47.
- Herman, J. P., Figueiredo, H., Mueller, N. K., Ulrich-Lai, Y., Ostrander, M. M., Choi, D. C., and Cullinan, W. E. (2003). Central mechanisms of stress integration: hierarchical circuitry controlling hypothalamo-pituitary-adrenocortical responsiveness. Front Neuroendocrinol 24, 151-180.
- Herman, J. P., McKlveen, J. M., Ghosal, S., Kopp, B., Wulsin, A., Makinson, R., Scheimann, J., and Myers, B. (2016). Regulation of the Hypothalamic-Pituitary-Adrenocortical Stress Response. Compr Physiol 6, 603-621.
- Herring, B. E., Shi, Y., Suh, Y. H., Zheng, C. Y., Blankenship, S. M., Roche, K. W., and Nicoll, R. A. (2013). Cornichon proteins determine the subunit composition of synaptic AMPA receptors. Neuron 77, 1083-1096.
- Herzog, E., Gilchrist, J., Gras, C., Muzerelle, A., Ravassard, P., Giros, B., Gaspar, P., and El Mestikawy, S. (2004). Localization of VGLUT3, the vesicular glutamate transporter type 3, in the rat brain. Neuroscience 123, 983-1002.
- Hollerman, J. R., and Schultz, W. (1998). Dopamine neurons report an error in the temporal prediction of reward during learning. Nat Neurosci 1, 304-309.
- Hollmann, M., and Heinemann, S. (1994). Cloned glutamate receptors. Annu Rev Neurosci 17, 31-108.
- Hong, S., and Hikosaka, O. (2008). The globus pallidus sends reward-related signals to the lateral habenula. Neuron 60, 720-729.
- Hong, S., Jhou, T. C., Smith, M., Saleem, K. S., and Hikosaka, O. (2011). Negative reward signals from the lateral habenula to dopamine neurons are mediated by rostromedial tegmental nucleus in primates. J Neurosci 31, 11457-11471.
- Hu, J. H., Park, J. M., Park, S., Xiao, B., Dehoff, M. H., Kim, S., Hayashi, T., Schwarz, M. K., Huganir, R. L., Seeburg, P. H., Linden, D. J., and Worley, P. F. (2010). Homeostatic scaling requires group I mGluR activation mediated by Homer1a. Neuron 68, 1128-1142.
- Huang, L., Xi, Y., Peng, Y., Yang, Y., Huang, X., Fu, Y., Tao, Q., Xiao, J., Yuan, T., An, K., Zhao, H., Pu, M., Xu, F., Xue, T., Luo, M., So, K. F., and Ren, C. (2019). A Visual Circuit Related to Habenula Underlies the Antidepressive Effects of Light Therapy. Neuron 102, 128-142.
- Huganir, R. L., and Nicoll, R. A. (2013). AMPARs and synaptic plasticity: the last 25 years. Neuron 80, 704-717.
- Ilango, A., Shumake, J., Wetzel, W., Scheich, H., and Ohl, F. W. (2012). The role of dopamine in the context of aversive stimuli with particular reference to acoustically signaled avoidance learning. Front Neurosci 6, 132.
- Isaac, J. T., Crair, M. C., Nicoll, R. A., and Malenka, R. C. (1997). Silent synapses during development of thalamocortical inputs. Neuron 18, 269-280.
- Iwasaki-Sekino, A., Mano-Otagiri, A., Ohata, H., Yamauchi, N., and Shibasaki, T. (2009). Gender differences in corticotropin and corticosterone secretion and corticotropin-releasing factor mRNA expression in the paraventricular nucleus of the hypothalamus and the central nucleus of the amygdala in response to footshock stress or psychological stress in rats. Psychoneuroendocrinology 34, 226-237.

- Jackman, S. L., Turecek, J., Belinsky, J. E., and Regehr, W. G. (2016). The calcium sensor synaptotagmin 7 is required for synaptic facilitation. Nature 529, 88-91.
- Jahr, C. E., and Stevens, C. F. (1993). Calcium permeability of the N-methyl-D-aspartate receptor channel in hippocampal neurons in culture. Proc Natl Acad Sci U S A 90, 11573-11577.
- Jennings, J. H., Sparta, D. R., Stamatakis, A. M., Ung, R. L., Pleil, K. E., Kash, T. L., and Stuber, G. D. (2013). Distinct extended amygdala circuits for divergent motivational states. Nature 496, 224-228.
- Jhou, T. C., Fields, H. L., Baxter, M. G., Saper, C. B., and Holland, P. C. (2009a). The rostromedial tegmental nucleus (RMTg), a GABAergic afferent to midbrain dopamine neurons, encodes aversive stimuli and inhibits motor responses. Neuron 61, 786-800.
- Jhou, T. C., Geisler, S., Marinelli, M., Degarmo, B. A., and Zahm, D. S. (2009b). The mesopontine rostromedial tegmental nucleus: A structure targeted by the lateral habenula that projects to the ventral tegmental area of Tsai and substantia nigra compacta. J Comp Neurol 513, 566-596.
- Jiang, M., Polepalli, J., Chen, L. Y., Zhang, B., Südhof, T. C., and Malenka, R. C. (2017). Conditional ablation of neuroligin-1 in CA1 pyramidal neurons blocks LTP by a cell-autonomous NMDA receptor-independent mechanism. Mol Psychiatry 22, 375-383.
- Johnson, J. W., and Ascher, P. (1987). Glycine potentiates the NMDA response in cultured mouse brain neurons. Nature 325, 529-531.
- Kalin, N. H., Takahashi, L. K., and Chen, F. L. (1994). Restraint stress increases corticotropin-releasing hormone mRNA content in the amygdala and paraventricular nucleus. Brain Res 656, 182-186.
- Kamboj, S. K., Swanson, G. T., and Cull-Candy, S. G. (1995). Intracellular spermine confers rectification on rat calcium-permeable AMPA and kainate receptors. J Physiol 486, 297-303.
- Kang-Park, M., Kieffer, B. L., Roberts, A. J., Siggins, G. R., and Moore, S. D. (2015). Interaction of CRF and kappa opioid systems on GABAergic neurotransmission in the mouse central amygdala. J Pharmacol Exp Ther 355, 206-211.
- Kang, M., Pyun, K. H., Jang, C. G., Kim, H., Bae, H., and Shim, I. (2005). Nelumbinis Semen reverses a decrease in hippocampal 5-HT release induced by chronic mild stress in rats. J Pharm Pharmacol 57, 651-656.
- Kendler, K. S., Karkowski, L. M., and Prescott, C. A. (1998). Stressful life events and major depression: risk period, long-term contextual threat, and diagnostic specificity. J Nerv Ment Dis 186, 661-669.
- Kim, B. K., and Seo, J. H. (2013). Treadmill exercise alleviates post-traumatic stress disorder-induced impairment of spatial learning memory in rats. J Exerc Rehabil 9, 413-419.
- Kim, J., Lee, S., Fang, Y. Y., Shin, A., Park, S., Hashikawa, K., Bhat, S., Kim, D., Sohn, J. W., Lin, D., and Suh, G. S. B. (2019). Rapid, biphasic CRF neuronal responses encode positive and negative valence. Nat Neurosci 22, 576-585.
- Kim, J., Pignatelli, M., Xu, S., Itohara, S., and Tonegawa, S. (2016). Antagonistic negative and positive neurons of the basolateral amygdala. Nat Neurosci 19, 1636-1646.
- Kim, J., Zhang, X., Muralidhar, S., LeBlanc, S. A., and Tonegawa, S. (2017). Basolateral to Central Amygdala Neural Circuits for Appetitive Behaviors. Neuron 93, 1464-1479.e5.
- Kim, U., and Lee, T. (2012). Topography of descending projections from anterior insular and medial prefrontal regions to the lateral habenula of the epithalamus in the rat. Eur J Neurosci 35, 1253-1269.
- Kimble, G. A. (1955). Shock intensity and avoidance learning. J Comp Physiol Psychol 48, 281-284.
- Knowland, D., Lilascharoen, V., Pacia, C. P., Shin, S., Wang, E. H., and Lim, B. K. (2017). Distinct Ventral Pallidal Neural Populations Mediate Separate Symptoms of Depression. Cell 170, 284-297.e18.
- Kopp, C., Longordo, F., Nicholson, J. R., and Lüthi, A. (2006). Insufficient sleep reversibly alters bidirectional synaptic plasticity and NMDA receptor function. J Neurosci 26, 12456-12465.
- Korb, E., Wilkinson, C. L., Delgado, R. N., Lovero, K. L., and Finkbeiner, S. (2013). Arc in the nucleus regulates PML-dependent GluA1 transcription and homeostatic plasticity. Nat Neurosci 16, 874-883.

- Krishnan, V., Han, M. H., Graham, D. L., Berton, O., Renthal, W., Russo, S. J., Laplant, Q., Graham, A., Lutter, M., Lagace, D. C., Ghose, S., Reister, R., Tannous, P., Green, T. A., Neve, R. L., Chakravarty, S., Kumar, A., Eisch, A. J., Self, D. W., Lee, F. S., Tamminga, C. A., Cooper, D. C., Gershenfeld, H. K., and Nestler, E. J. (2007). Molecular adaptations underlying susceptibility and resistance to social defeat in brain reward regions. Cell 131, 391-404.
- Krypotos, A. M., Effting, M., Kindt, M., and Beckers, T. (2015). Avoidance learning: a review of theoretical models and recent developments. Front Behav Neurosci 9, 189.
- Kudryavtseva, N. N., Bakshtanovskaya, I. V., and Koryakina, L. A. (1991). Social model of depression in mice of C57BL/6J strain. Pharmacol Biochem Behav 38, 315-320.
- Kumar, S. S., and Huguenard, J. R. (2003). Pathway-specific differences in subunit composition of synaptic NMDA receptors on pyramidal neurons in neocortex. J Neurosci 23, 10074-10083.
- Kushner, M. G., Riggs, D. S., Foa, E. B., and Miller, S. M. (1993). Perceived controllability and the development of posttraumatic stress disorder (PTSD) in crime victims. Behav Res Ther 31, 105-110.
- Kwon, H. B., and Castillo, P. E. (2008). Long-term potentiation selectively expressed by NMDA receptors at hippocampal mossy fiber synapses. Neuron 57, 108-120.
- Lammel, S., Lim, B. K., Ran, C., Huang, K. W., Betley, M. J., Tye, K. M., Deisseroth, K., and Malenka, R. C. (2012). Input-specific control of reward and aversion in the ventral tegmental area. Nature 491, 212-217.
- Laryea, G., Arnett, M. G., and Muglia, L. J. (2012). Behavioral Studies and Genetic Alterations in Corticotropin-Releasing Hormone (CRH) Neurocircuitry: Insights into Human Psychiatric Disorders. Behav Sci (Basel) 2, 135-171.
- Lauterborn, J. C., Palmer, L. C., Jia, Y., Pham, D. T., Hou, B., Wang, W., Trieu, B. H., Cox, C. D., Kantorovich, S., Gall, C. M., and Lynch, G. (2016). Chronic Ampakine Treatments Stimulate Dendritic Growth and Promote Learning in Middle-Aged Rats. J Neurosci 36, 1636-1646.
- Lazaridis, I., Tzortzi, O., Weglage, M., Märtin, A., Xuan, Y., Parent, M., Johansson, Y., Fuzik, J., Fürth, D., Fenno, L. E., Ramakrishnan, C., Silberberg, G., Deisseroth, K., Carlén, M., and Meletis, K. (2019). A hypothalamus-habenula circuit controls aversion. Mol Psychiatry 24, 1351-1368.
- Lecca, S., Melis, M., Luchicchi, A., Muntoni, A. L., and Pistis, M. (2012). Inhibitory inputs from rostromedial tegmental neurons regulate spontaneous activity of midbrain dopamine cells and their responses to drugs of abuse. Mol Psychiatry 37, 1164-1176.
- Lecca, S., Meye, F. J., Trusel, M., Tchenio, A., Harris, J., Schwarz, M. K., Burdakov, D., Georges, F., and Mameli, M. (2017). Aversive stimuli drive hypothalamus-to-habenula excitation to promote escape behavior. Elife 6:e30697.
- Lecca, S., Pelosi, A., Tchenio, A., Moutkine, I., Lujan, R., Hervé, D., and Mameli, M. (2016). Rescue of GABAB and GIRK function in the lateral habenula by protein phosphatase 2A inhibition ameliorates depression-like phenotypes in mice. Nat Med 22, 254-261.
- Lecourtier, L., Neijt, H. C., and Kelly, P. H. (2004). Habenula lesions cause impaired cognitive performance in rats: implications for schizophrenia. Eur J Neurosci 19, 2551-2560.
- LeDoux, J. E., and Gorman, J. M. (2001). A call to action: overcoming anxiety through active coping. Am J Psychiatry 158, 1953-1955.
- LeDoux, J. E., Moscarello, J., Sears, R., and Campese, V. (2017). The birth, death and resurrection of avoidance: a reconceptualization of a troubled paradigm. Mol Psychiatry 22, 24-36.
- Lee, H. K., and Kirkwood, A. (2019). Mechanisms of Homeostatic Synaptic Plasticity *in vivo*. Front Cell Neurosci 13:520.
- Lee, H. K., Kameyama, K., Huganir, R. L., and Bear, M. F. (1998). NMDA induces long-term synaptic depression and dephosphorylation of the GluR1 subunit of AMPA receptors in hippocampus. Neuron 21, 1151-1162.
- Lee, H. K., Takamiya, K., He, K., Song, L., and Huganir, R. L. (2010). Specific roles of AMPA receptor subunit GluR1 (GluA1) phosphorylation sites in regulating synaptic plasticity in the CA1 region of hippocampus. J Neurophysiol 103, 479-489.
- Leem, Y. H., and Chang, H. (2017). Arc/Arg3.1 protein expression in dorsal hippocampal CA1, a candidate event as a biomarker for the effects of exercise on chronic stress-evoked behavioral abnormalities. J Exerc Nutrition Biochem 21, 45-51.

- Lenze, E. J., Dixon, D., Mantella, R. C., Dore, P. M., Andreescu, C., Reynolds, C. F., Newcomer, J. W., and Butters, M. A. (2012). Treatment-related alteration of cortisol predicts change in neuropsychological function during acute treatment of late-life anxiety disorder. Int J Geriatr Psychiatry 27, 454-462.
- Lester, R. A., Clements, J. D., Westbrook, G. L., and Jahr, C. E. (1990). Channel kinetics determine the time course of NMDA receptor-mediated synaptic currents. Nature 346, 565-567.
- Levine, S. (1966). UCS intensity and avoidance learning. J Exp Psychol 71, 163-164.
- Li, B., Ge, T., and Cui, R. (2018). Long-Term Plasticity in Amygdala Circuits: Implication of CB1-Dependent LTD in Stress. Mol Neurobiol 55, 4107-4114.
- Li, B., Piriz, J., Mirrione, M., Chung, C., Proulx, C. D., Schulz, D., Henn, F., and Malinow, R. (2011). Synaptic potentiation onto habenula neurons in the learned helplessness model of depression. Nature 470, 535-539.
- Li, H., Pullmann, D., and Jhou, T. C. (2019a). Valence-encoding in the lateral habenula arises from the entopeduncular region. Elife 8:e41223.
- Li, H., Vento, P. J., Parrilla-Carrero, J., Pullmann, D., Chao, Y. S., Eid, M., and Jhou, T. C. (2019b). Three Rostromedial Tegmental Afferents Drive Triply Dissociable Aspects of Punishment Learning and Aversive Valence Encoding. Neuron 104, 987-999.e4.
- Li, J., Kang, S., Fu, R., Wu, L., Wu, W., Liu, H., Gregor, D., Zuo, W., Bekker, A., and Ye, J. H. (2017). Inhibition of AMPA receptor and CaMKII activity in the lateral habenula reduces depressive-like behavior and alcohol intake in rats. Neuropharmacology 126, 108-120.
- Li, K., Zhou, T., Liao, L., Yang, Z., Wong, C., Henn, F., Malinow, R., Yates, J. R., and Hu, H. (2013). βCaMKII in lateral habenula mediates core symptoms of depression. Science 341, 1016-1020.
- Linden, D. J., Smeyne, M., and Connor, J. A. (1993). Induction of cerebellar long-term depression in culture requires postsynaptic action of sodium ions. Neuron 11, 1093-1100.
- Lisman, J. (1989). A mechanism for the Hebb and the anti-Hebb processes underlying learning and memory. Proc Natl Acad Sci U S A 86, 9574-9578.
- Lisman, J., Schulman, H., and Cline, H. (2002). The molecular basis of CaMKII function in synaptic and behavioural memory. Nat Rev Neurosci 3, 175-190.
- Lissin, D. V., Gomperts, S. N., Carroll, R. C., Christine, C. W., Kalman, D., Kitamura, M., Hardy, S., Nicoll, R. A., Malenka, R. C., and von Zastrow, M. (1998). Activity differentially regulates the surface expression of synaptic AMPA and NMDA glutamate receptors. Proc Natl Acad Sci U S A 95, 7097-7102.
- Liu, L., Wong, T. P., Pozza, M. F., Lingenhoehl, K., Wang, Y., Sheng, M., Auberson, Y. P., and Wang, Y. T. (2004). Role of NMDA receptor subtypes in governing the direction of hippocampal synaptic plasticity. Science 304, 1021-1024.
- Liu, S. Q., and Cull-Candy, S. G. (2000). Synaptic activity at calcium-permeable AMPA receptors induces a switch in receptor subtype. Nature 405, 454-458.
- Liu, Z. P., Song, C., Wang, M., He, Y., Xu, X. B., Pan, H. Q., Chen, W. B., Peng, W. J., and Pan, B. X. (2014). Chronic stress impairs GABAergic control of amygdala through suppressing the tonic GABAA receptor currents. Mol Brain 7, 32.
- Louvart, H., Maccari, S., Ducrocq, F., Thomas, P., and Darnaudéry, M. (2005). Long-term behavioural alterations in female rats after a single intense footshock followed by situational reminders. Psychoneuroendocrinology 30, 316-324.
- Louvart, H., Maccari, S., Lesage, J., Léonhardt, M., Dickes-Coopman, A., and Darnaudéry, M. (2006). Effects of a single footshock followed by situational reminders on HPA axis and behaviour in the aversive context in male and female rats. Psychoneuroendocrinology 31, 92-99.
- Lukkes, J. L., Meda, S., Thompson, B. S., Freund, N., and Andersen, S. L. (2017). Early life stress and later peer distress on depressive behavior in adolescent female rats: Effects of a novel intervention on GABA and D2 receptors. Behav Brain Res 330, 37-45.
- Lupien, S. J., de Leon, M., de Santi, S., Convit, A., Tarshish, C., Nair, N. P., Thakur, M., McEwen, B. S., Hauger, R. L., and Meaney, M. J. (1998). Cortisol levels during human aging predict hippocampal atrophy and memory deficits. Nat Neurosci 1, 69-73.

- Lüscher, C., and Malenka, R. C. (2012). NMDA receptor-dependent long-term potentiation and long-term depression (LTP/LTD). Cold Spring Harb Perspect Biol 4(6):a005710.
- Lüscher, C., Xia, H., Beattie, E. C., Carroll, R. C., von Zastrow, M., Malenka, R. C., and Nicoll, R. A. (1999). Role of AMPA receptor cycling in synaptic transmission and plasticity. Neuron 24, 649-658.
- Lussier, M. P., Sanz-Clemente, A., and Roche, K. W. (2015). Dynamic Regulation of N-Methyl-d-aspartate (NMDA) and α-Amino-3-hydroxy-5-methyl-4-isoxazolepropionic Acid (AMPA) Receptors by Posttranslational Modifications. J Biol Chem 290, 28596-28603.
- Lynch, G. (2004). AMPA receptor modulators as cognitive enhancers. Curr Opin Pharmacol 4, 4-11.
- MacDermott, A. B., Mayer, M. L., Westbrook, G. L., Smith, S. J., and Barker, J. L. (1986). NMDA-receptor activation increases cytoplasmic calcium concentration in cultured spinal cord neurones. Nature 321, 519-522.
- Mahar, I., Bambico, F. R., Mechawar, N., and Nobrega, J. N. (2014). Stress, serotonin, and hippocampal neurogenesis in relation to depression and antidepressant effects. Neurosci Biobehav Rev 38, 173-192.
- Maier, S. F., and Watkins, L. R. (2005). Stressor controllability and learned helplessness: the roles of the dorsal raphe nucleus, serotonin, and corticotropin-releasing factor. Neurosci Biobehav Rev 29, 829-841.
- Mammen, A. L., Kameyama, K., Roche, K. W., and Huganir, R. L. (1997). Phosphorylation of the alpha-amino-3-hydroxy-5-methylisoxazole4-propionic acid receptor GluR1 subunit by calcium/calmodulin-dependent kinase II. J Biol Chem 272, 32528-32533.
- Man, H. Y., Sekine-Aizawa, Y., and Huganir, R. L. (2007). Regulation of {alpha}-amino-3-hydroxy-5-methyl-4-isoxazolepropionic acid receptor trafficking through PKA phosphorylation of the Glu receptor 1 subunit. Proc Natl Acad Sci U S A 104, 3579-3584.
- Mantz, J., Thierry, A. M., and Glowinski, J. (1989). Effect of noxious tail pinch on the discharge rate of mesocortical and mesolimbic dopamine neurons: selective activation of the mesocortical system. Brain Res 476, 377-381.
- Marcilhac, A., and Siaud, P. (1997). Identification of projections from the central nucleus of the amygdala to the paraventricular nucleus of the hypothalamus which are immunoreactive for corticotrophin-releasing hormone in the rat. Exp Physiol 82, 273-281.
- Maren, S., Phan, K. L., and Liberzon, I. (2013). The contextual brain: implications for fear conditioning, extinction and psychopathology. Nat Rev Neurosci 14, 417-428.
- Markram, H., Lübke, J., Frotscher, M., and Sakmann, B. (1997). Regulation of synaptic efficacy by coincidence of postsynaptic APs and EPSPs. Science 275, 213-215.
- Maroteaux, M., and Mameli, M. (2012). Cocaine evokes projection-specific synaptic plasticity of lateral habenula neurons. J Neurosci 32, 12641-12646.
- Mason, J. W., Giller, E. L., Kosten, T. R., Ostroff, R. B., and Podd, L. (1986). Urinary free-cortisol levels in posttraumatic stress disorder patients. J Nerv Ment Dis 174, 145-149.
- Matsumoto, M., and Hikosaka, O. (2007). Lateral habenula as a source of negative reward signals in dopamine neurons. Nature 447, 1111-1115.
- Matsumoto, M., and Hikosaka, O. (2009). Representation of negative motivational value in the primate lateral habenula. Nat Neurosci 12, 77-84.
- Matsuzaki, M., Honkura, N., Ellis-Davies, G. C., and Kasai, H. (2004). Structural basis of long-term potentiation in single dendritic spines. Nature 429, 761-766.
- McCall, J. G., Al-Hasani, R., Siuda, E. R., Hong, D. Y., Norris, A. J., Ford, C. P., and Bruchas, M. R. (2015). CRH Engagement of the Locus Coeruleus Noradrenergic System Mediates Stress-Induced Anxiety. Neuron 87, 605-620.
- McCall, J. G., Siuda, E. R., Bhatti, D. L., Lawson, L. A., McElligott, Z. A., Stuber, G. D., and Bruchas, M. R. (2017). Locus coeruleus to basolateral amygdala noradrenergic projections promote anxiety-like behavior. Elife 6:e18247.
- Mcdonald, A. J. (1996). Glutamate and aspartate immunoreactive neurons of the rat basolateral amygdala: colocalization of excitatory amino acids and projections to the limbic circuit. J Comp Neurol 365, 367-379.
- McEwen, B. S., and Morrison, J. H. (2013). The brain on stress: vulnerability and plasticity of the prefrontal cortex over the life course. Neuron 79, 16-29.
- McEwen, B. S., Nasca, C., and Gray, J. D. (2016). Stress Effects on Neuronal Structure: Hippocampus, Amygdala, and Prefrontal Cortex. Neuropsychopharmacology 41, 3-23.

- McKernan, M. G., and Shinnick-Gallagher, P. (1997). Fear conditioning induces a lasting potentiation of synaptic currents *in vitro*. Nature 390, 607-611.
- Mendes-Gomes, J., Motta, S. C., Passoni Bindi, R., de Oliveira, A. R., Ullah, F., Baldo, M. V. C., Coimbra, N. C., Canteras, N. S., and Blanchard, D. C. (2020). Defensive behaviors and brain regional activation changes in rats confronting a snake. Behav Brain Res 381, 112469.
- Meye, F. J., Soiza-Reilly, M., Smit, T., Diana, M. A., Schwarz, M. K., and Mameli, M. (2016). Shifted pallidal co-release of GABA and glutamate in habenula drives cocaine withdrawal and relapse. Nat Neurosci 19, 1019-1024.
- Meye, F. J., Valentinova, K., Lecca, S., Marion-Poll, L., Maroteaux, M. J., Musardo, S., Moutkine, I., Gardoni, F., Huganir, R. L., Georges, F., and Mameli, M. (2015). Cocaine-evoked negative symptoms require AMPA receptor trafficking in the lateral habenula. Nat Neurosci 18, 376-378.
- Miller, E. K. (2000). The prefrontal cortex and cognitive control. Nat Rev Neurosci 1, 59-65.
- Miller, N. E. (1948). Studies of fear as an acquirable drive fear as motivation and fear-reduction as reinforcement in the learning of new responses. J Exp Psychol 38, 89-101.
- Miyazaki, T., Nakajima, W., Hatano, M., Shibata, Y., Kuroki, Y., Arisawa, T., Serizawa, A., Sano, A., Kogami, S., Yamanoue, T., Kimura, K., Hirata, Y., Takada, Y., Ishiwata, Y., Sonoda, M., Tokunaga, M., Seki, C., Nagai, Y., Minamimoto, T., Kawamura, K., Zhang, M. R., Ikegaya, N., Iwasaki, M., Kunii, N., Kimura, Y., Yamashita, F., Taguri, M., Tani, H., Nagai, N., Koizumi, T., Nakajima, S., Mimura, M., Yuzaki, M., Kato, H., Higuchi, M., Uchida, H., and Takahashi, T. (2020). Visualization of AMPA receptors in living human brain with positron emission tomography. Nat Med 26, 281-288.
- Mo, B., Feng, N., Renner, K., and Forster, G. (2008). Restraint stress increases serotonin release in the central nucleus of the amygdala via activation of corticotropin-releasing factor receptors. Brain Res Bull 76, 493-498.
- Moga, M. M., and Saper, C. B. (1994). Neuropeptide-immunoreactive neurons projecting to the paraventricular hypothalamic nucleus in the rat. J Comp Neurol 346, 137-150.
- Monyer, H., Burnashev, N., Laurie, D. J., Sakmann, B., and Seeburg, P. H. (1994). Developmental and regional expression in the rat brain and functional properties of four NMDA receptors. Neuron 12, 529-540.
- Mosko, S. S., and Jacobs, B. L. (1974). Midbrain raphe neurons: spontaneous activity and response to light. Physiol Behav 13, 589-593.
- Mowrer, O. H. (1951). Two-factor learning theory: summary and comment. Psychol Rev 58, 350-354.
- Mulkey, R. M., Endo, S., Shenolikar, S., and Malenka, R. C. (1994). Involvement of a calcineurin/inhibitor-1 phosphatase cascade in hippocampal long-term depression. Nature 369, 486-488.
- Mulkey, R. M., Herron, C. E., and Malenka, R. C. (1993). An essential role for protein phosphatases in hippocampal long-term depression. Science 261, 1051-1055.
- Müller, T., Albrecht, D., and Gebhardt, C. (2009). Both NR2A and NR2B subunits of the NMDA receptor are critical for long-term potentiation and long-term depression in the lateral amygdala of horizontal slices of adult mice. Learn Mem 16, 395-405.
- Murphy, B. L., Arnsten, A. F., Goldman-Rakic, P. S., and Roth, R. H. (1996). Increased dopamine turnover in the prefrontal cortex impairs spatial working memory performance in rats and monkeys. Proc Natl Acad Sci U S A 93, 1325-1329.
- Murray, E. A., and Rudebeck, P. H. (2018). Specializations for reward-guided decision-making in the primate ventral prefrontal cortex. Nat Rev Neurosci 19, 404-417.
- Muzerelle, A., Scotto-Lomassese, S., Bernard, J. F., Soiza-Reilly, M., and Gaspar, P. (2016). Conditional anterograde tracing reveals distinct targeting of individual serotonin cell groups (B5-B9) to the forebrain and brainstem. Brain Struct Funct 221, 535-561.
- Myers, D. A., Gibson, M., Schulkin, J., and Greenwood Van-Meerveld, B. (2005). Corticosterone implants to the amygdala and type 1 CRH receptor regulation: effects on behavior and colonic sensitivity. Behav Brain Res 161, 39-44.
- Nabavi, S., Fox, R., Proulx, C. D., Lin, J. Y., Tsien, R. Y., and Malinow, R. (2014). Engineering a memory with LTD and LTP. Nature 511, 348-352.

- Nägerl, U. V., Eberhorn, N., Cambridge, S. B., and Bonhoeffer, T. (2004). Bidirectional activity-dependent morphological plasticity in hippocampal neurons. Neuron 44, 759-767.
- Namboodiri, V. M., Rodriguez-Romaguera, J., and Stuber, G. D. (2016). The habenula. Curr Biol 26, R873-R877.
- Navratilova, E., Xie, J. Y., Okun, A., Qu, C., Eyde, N., Ci, S., Ossipov, M. H., King, T., Fields, H. L., and Porreca, F. (2012). Pain relief produces negative reinforcement through activation of mesolimbic reward-valuation circuitry. Proc Natl Acad Sci U S A 109, 20709-20713.
- Nicoll, R. A., Tomita, S., and Bredt, D. S. (2006). Auxiliary subunits assist AMPA-type glutamate receptors. Science 311, 1253-1256.
- Nieman, L. K. (2018). Diagnosis of Cushing's Syndrome in the Modern Era. Endocrinol Metab Clin North Am 47, 259-273.
- O'Brien, R. J., Kamboj, S., Ehlers, M. D., Rosen, K. R., Fischbach, G. D., and Huganir, R. L. (1998). Activity-dependent modulation of synaptic AMPA receptor accumulation. Neuron 21, 1067-1078.
- Omelchenko, N., Bell, R., and Sesack, S. R. (2009). Lateral habenula projections to dopamine and GABA neurons in the rat ventral tegmental area. Eur J Neurosci 30, 1239-1250.
- Overmier, J. B., and Seligman, M. E. (1967). Effects of inescapable shock upon subsequent escape and avoidance responding. J Comp Physiol Psychol 63, 28-33.
- Page, M. E., and Abercrombie, E. D. (1999). Discrete local application of corticotropin-releasing factor increases locus coeruleus discharge and extracellular norepinephrine in rat hippocampus. Synapse 33, 304-313.
- Pan-Vazquez, A., Wefelmeyer, W., Gonzalez Sabater, V., Neves, G., and Burrone, J. (2020). Activity-Dependent Plasticity of Axo-axonic Synapses at the Axon Initial Segment. Neuron 106, 265-276.e6.
- Paoletti, P., Bellone, C., and Zhou, Q. (2013). NMDA receptor subunit diversity: impact on receptor properties, synaptic plasticity and disease. Nat Rev Neurosci 14, 383-400.
- Pariante, C. M., and Lightman, S. L. (2008). The HPA axis in major depression: classical theories and new developments. Trends Neurosci 31, 464-468.
- Park, H., Rhee, J., Lee, S., and Chung, C. (2017). Selectively Impaired Endocannabinoid-Dependent Long-Term Depression in the Lateral Habenula in an Animal Model of Depression. Cell Rep 20, 289-296.
- Partridge, J. G., Forcelli, P. A., Luo, R., Cashdan, J. M., Schulkin, J., Valentino, R. J., and Vicini, S. (2016). Stress increases GABAergic neurotransmission in CRF neurons of the central amygdala and bed nucleus stria terminalis. Neuropharmacology 107, 239-250.
- Penn, A. C., Zhang, C. L., Georges, F., Royer, L., Breillat, C., Hosy, E., Petersen, J. D., Humeau, Y., and Choquet, D. (2017). Hippocampal LTP and contextual learning require surface diffusion of AMPA receptors. Nature 549, 384-388.
- Pignatelli, M., Tejeda, H. A., Barker, D. J., Bontempi, L., Wu, J., Lopez, A., Palma Ribeiro, S., Lucantonio, F., Parise, E. M., Torres-Berrio, A., Alvarez-Bagnarol, Y., Marino, R. A. M., Cai, Z. L., Xue, M., Morales, M., Tamminga, C. A., Nestler, E. J., and Bonci, A. (2020). Cooperative synaptic and intrinsic plasticity in a disynaptic limbic circuit drive stress-induced anhedonia and passive coping in mice. Mol Psychiatry. https://doi.org/10.1038/s41380-020-0686-8.
- Pivonello, R., Ferone, D., Lombardi, G., Colao, A., Lamberts, S. W. J., and Hofland, L. J. (2007). Novel insights in dopamine receptor physiology. Eur J Endocrinol 156 Suppl 1, S13-S21.
- Pompeiano, M., Palacios, J. M., and Mengod, G. (1994). Distribution of the serotonin 5-HT2 receptor family mRNAs: comparison between 5-HT2A and 5-HT2C receptors. Brain Res Mol Brain Res 23, 163-178.
- Poncer, J. C., Esteban, J. A., and Malinow, R. (2002). Multiple mechanisms for the potentiation of AMPA receptor-mediated transmission by alpha-Ca^{2+}/calmodulin-dependent protein kinase II. J Neurosci 22, 4406-4411.
- Purba, J. S., Hoogendijk, W. J., Hofman, M. A., and Swaab, D. F. (1996). Increased number of vasopressin- and oxytocin-expressing neurons in the paraventricular nucleus of the hypothalamus in depression. Arch Gen Psychiatry 53, 137-143.
- Pynoos, R. S., Ritzmann, R. F., Steinberg, A. M., Goenjian, A., and Prisecaru, I. (1996). A behavioral animal model of posttraumatic stress disorder featuring repeated exposure to situational reminders. Biol Psychiatry 39, 129-134.

- Quina, L. A., Tempest, L., Ng, L., Harris, J. A., Ferguson, S., Jhou, T. C., and Turner, E. E. (2015). Efferent pathways of the mouse lateral habenula. J Comp Neurol 523, 32-60.
- Radley, J. J., Gosselink, K. L., and Sawchenko, P. E. (2009). A discrete GABAergic relay mediates medial prefrontal cortical inhibition of the neuroendocrine stress response. J Neurosci 29, 7330-7340.
- Radley, J. J., Rocher, A. B., Miller, M., Janssen, W. G., Liston, C., Hof, P. R., McEwen, B. S., and Morrison, J. H. (2006). Repeated stress induces dendritic spine loss in the rat medial prefrontal cortex. Cereb Cortex 16, 313-320.
- Ragozzino, M. E. (2007). The contribution of the medial prefrontal cortex, orbitofrontal cortex, and dorsomedial striatum to behavioral flexibility. Ann N Y Acad Sci 1121, 355-375.
- Rainnie, D. G., Bergeron, R., Sajdyk, T. J., Patil, M., Gehlert, D. R., and Shekhar, A. (2004). Corticotrophin releasing factor-induced synaptic plasticity in the amygdala translates stress into emotional disorders. J Neurosci 24, 3471-3479.
- Ramirez, F., Moscarello, J. M., LeDoux, J. E., and Sears, R. M. (2015). Active avoidance requires a serial basal amygdala to nucleus accumbens shell circuit. J Neurosci 35, 3470-3477.
- Ramos, B. P., Colgan, L., Nou, E., Ovadia, S., Wilson, S. R., and Arnsten, A. F. (2005). The beta-1 adrenergic antagonist, betaxolol, improves working memory performance in rats and monkeys. Biol Psychiatry 58, 894-900.
- Ramot, A., Jiang, Z., Tian, J. B., Nahum, T., Kuperman, Y., Justice, N., and Chen, A. (2017). Hypothalamic CRFR1 is essential for HPA axis regulation following chronic stress. Nat Neurosci 20, 385-388.
- Rauner, C., and Köhr, G. (2011). Triheteromeric NR1/NR2A/NR2B receptors constitute the major N-methyl-D-aspartate receptor population in adult hippocampal synapses. J Biol Chem 286, 7558-7566.
- Rebola, N., Carta, M., Lanore, F., Blanchet, C., and Mulle, C. (2011). NMDA receptor-dependent metaplasticity at hippocampal mossy fiber synapses. Nat Neurosci 14, 691-693.
- Rebola, N., Lujan, R., Cunha, R. A., and Mulle, C. (2008). Adenosine A2A receptors are essential for long-term potentiation of NMDA-EPSCs at hippocampal mossy fiber synapses. Neuron 57, 121-134.
- Regev, L., Tsoory, M., Gil, S., and Chen, A. (2012). Site-specific genetic manipulation of amygdala corticotropin-releasing factor reveals its imperative role in mediating behavioral response to challenge. Biol Psychiatry 71, 317-326.
- Ren, J., Friedmann, D., Xiong, J., Liu, C. D., Ferguson, B. R., Weerakkody, T., DeLoach, K. E., Ran, C., Pun, A., Sun, Y., Weissbourd, B., Neve, R. L., Huguenard, J., Horowitz, M. A., and Luo, L. (2018). Anatomically Defined and Functionally Distinct Dorsal Raphe Serotonin Sub-systems. Cell 175, 472-487.e20.
- Ridley, A. J., Schwartz, M. A., Burridge, K., Firtel, R. A., Ginsberg, M. H., Borisy, G., Parsons, J. T., and Horwitz, A. R. (2003). Cell migration: integrating signals from front to back. Science 302, 1704-1709.
- Root, D. H., Hoffman, A. F., Good, C. H., Zhang, S., Gigante, E., Lupica, C. R., and Morales, M. (2015). Norepinephrine activates dopamine D4 receptors in the rat lateral habenula. J Neurosci 35, 3460-3469.
- Root, D. H., Mejias-Aponte, C. A., Qi, J., and Morales, M. (2014a). Role of glutamatergic projections from ventral tegmental area to lateral habenula in aversive conditioning. J Neurosci 34, 13906-13910.
- Root, D. H., Mejias-Aponte, C. A., Zhang, S., Wang, H. L., Hoffman, A. F., Lupica, C. R., and Morales, M. (2014b). Single rodent mesohabenular axons release glutamate and GABA. Nat Neurosci 17, 1543-1551.
- Roth, B. L. (2016). DREADDs for Neuroscientists. Neuron 89, 683-694.
- Rumpel, S., LeDoux, J., Zador, A., and Malinow, R. (2005). Postsynaptic receptor trafficking underlying a form of associative learning. Science 308, 83-88.
- Sabatini, B. L., Oertner, T. G., and Svoboda, K. (2002). The life cycle of $Ca^{(2+)}$ ions in dendritic spines. Neuron 33, 439-452.
- Saha, S., and Datta, S. (2005). Two-way active avoidance training-specific increases in phosphorylated cAMP response element-binding protein in the dorsal hippocampus, amygdala, and hypothalamus. Eur J Neurosci 21, 3403-3414.
- Sakimura, K., Kutsuwada, T., Ito, I., Manabe, T., Takayama, C., Kushiya, E., Yagi, T., Aizawa, S., Inoue, Y., and Sugiyama, H. (1995). Reduced hippocampal LTP and spatial learning in mice lacking NMDA receptor epsilon 1 subunit. Nature 373, 151-155.
- Salas, R., Baldwin, P., de Biasi, M., and Montague, P. R. (2010). BOLD Responses to Negative Reward Prediction Errors in Human Habenula. Front Hum Neurosci 4, 36.
- Sapolsky, R. M. (2003). Stress and plasticity in the limbic system. Neurochem Res 28, 1735-1742.

- Sapolsky, R. M., Romero, L. M., and Munck, A. U. (2000). How do glucocorticoids influence stress responses? Integrating permissive, suppressive, stimulatory, and preparative actions. Endocr Rev 21, 55-89.
- Sara, S. J., and Bouret, S. (2012). Orienting and reorienting: the locus coeruleus mediates cognition through arousal. Neuron 76, 130-141.
- Sautter, F. J., Bissette, G., Wiley, J., Manguno-Mire, G., Schoenbachler, B., Myers, L., Johnson, J. E., Cerbone, A., and Malaspina, D. (2003). Corticotropin-releasing factor in posttraumatic stress disorder (PTSD) with secondary psychotic symptoms, nonpsychotic PTSD, and healthy control subjects. Biol Psychiatry 54, 1382-1388.
- Sawchenko, P. E., and Swanson, L. W. (1983). The organization of forebrain afferents to the paraventricular and supraoptic nuclei of the rat. J Comp Neurol 218, 121-144.
- Schöne, C., Cao, Z. F., Apergis-Schoute, J., Adamantidis, A., Sakurai, T., and Burdakov, D. (2012). Optogenetic probing of fast glutamatergic transmission from hypocretin/orexin to histamine neurons in situ. J Neurosci 32, 12437-12443.
- Schultz, W., Apicella, P., and Ljungberg, T. (1993). Responses of monkey dopamine neurons to reward and conditioned stimuli during successive steps of learning a delayed response task. J Neurosci 13, 900-913.
- Schweimer, J. V., and Ungless, M. A. (2010). Phasic responses in dorsal raphe serotonin neurons to noxious stimuli. Neuroscience 171, 1209-1215.
- Schwenk, J., Harmel, N., Zolles, G., Bildl, W., Kulik, A., Heimrich, B., Chisaka, O., Jonas, P., Schulte, U., Fakler, B., and Klöcker, N. (2009). Functional proteomics identify cornichon proteins as auxiliary subunits of AMPA receptors. Science 323, 1313-1319.
- Scudder, S. L., Goo, M. S., Cartier, A. E., Molteni, A., Schwarz, L. A., Wright, R., and Patrick, G. N. (2014). Synaptic strength is bidirectionally controlled by opposing activity-dependent regulation of Nedd4-1 and USP8. J Neurosci 34, 16637-16649.
- Sego, C., Gonçalves, L., Lima, L., Furigo, I. C., Donato, J., and Metzger, M. (2014). Lateral habenula and the rostromedial tegmental nucleus innervate neurochemically distinct subdivisions of the dorsal raphe nucleus in the rat. J Comp Neurol 522, 1454-1484.
- Seo, J. S., Zhong, P., Liu, A., Yan, Z., and Greengard, P. (2018). Elevation of p11 in lateral habenula mediates depression-like behavior. Mol Psychiatry 23, 1113-1119.
- Shabel, S. J., Proulx, C. D., Piriz, J., and Malinow, R. (2014). Mood regulation. GABA/glutamate co-release controls habenula output and is modified by antidepressant treatment. Science 345, 1494-1498.
- Shabel, S. J., Proulx, C. D., Trias, A., Murphy, R. T., and Malinow, R. (2012). Input to the lateral habenula from the basal ganglia is excitatory, aversive, and suppressed by serotonin. Neuron 74, 475-481.
- Shabel, S. J., Wang, C., Monk, B., Aronson, S., and Malinow, R. (2019). Stress transforms lateral habenula reward responses into punishment signals. Proc Natl Acad Sci U S A 116, 12488-12493.
- Sharp, B. M. (2017). Basolateral amygdala and stress-induced hyperexcitability affect motivated behaviors and addiction. Transl Psychiatry 7, e1194.
- Sheikh, N., Ahmad, A., Siripurapu, K. B., Kuchibhotla, V. K., Singh, S., and Palit, G. (2007). Effect of Bacopa monniera on stress induced changes in plasma corticosterone and brain monoamines in rats. J Ethnopharmacol 111, 671-676.
- Shekhar, A., Truitt, W., Rainnie, D., and Sajdyk, T. (2005). Role of stress, corticotrophin releasing factor (CRF) and amygdala plasticity in chronic anxiety. Stress 8, 209-219.
- Sheng, M., Cummings, J., Roldan, L. A., Jan, Y. N., and Jan, L. Y. (1994). Changing subunit composition of heteromeric NMDA receptors during development of rat cortex. Nature 368, 144-147.
- Shepherd, J. D., and Huganir, R. L. (2007). The cell biology of synaptic plasticity: AMPA receptor trafficking. Annu Rev Cell Dev Biol 23, 613-643.
- Shi, S. H., Hayashi, Y., Petralia, R. S., Zaman, S. H., Wenthold, R. J., Svoboda, K., and Malinow, R. (1999). Rapid spine delivery and redistribution of AMPA receptors after synaptic NMDA receptor activation. Science 284, 1811-1816.
- Shi, S., Hayashi, Y., Esteban, J. A., and Malinow, R. (2001). Subunit-specific rules governing AMPA receptor trafficking to synapses in hippocampal pyramidal neurons. Cell 105, 331-343.

- Siegler Retchless, B., Gao, W., and Johnson, J. W. (2012). A single GluN2 subunit residue controls NMDA receptor channel properties via intersubunit interaction. Nat Neurosci 15, 406-13, S1.
- Siegmund, A., and Wotjak, C. T. (2007). A mouse model of posttraumatic stress disorder that distinguishes between conditioned and sensitised fear. J Psychiatr Res 41, 848-860.
- Siuda, E. R., McCall, J. G., Al-Hasani, R., Shin, G., Il Park, S., Schmidt, M. J., Anderson, S. L., Planer, W. J., Rogers, J. A., and Bruchas, M. R. (2015). Optodynamic simulation of β-adrenergic receptor signalling. Nat Commun 6, 8480.
- Smagin, G. N., Swiergiel, A. H., and Dunn, A. J. (1995). Corticotropin-releasing factor administered into the locus coeruleus, but not the parabrachial nucleus, stimulates norepinephrine release in the prefrontal cortex. Brain Res Bull 36, 71-76.
- Smith, K. S., Bucci, D. J., Luikart, B. W., and Mahler, S. V. (2016). DREADDS: Use and application in behavioral neuroscience. Behav Neurosci 130, 137-155.
- Smith, M. A., Davidson, J., Ritchie, J. C., Kudler, H., Lipper, S., Chappell, P., and Nemeroff, C. B. (1989). The corticotropin-releasing hormone test in patients with posttraumatic stress disorder. Biol Psychiatry 26, 349-355.
- Snyder, K., Wang, W. W., Han, R., McFadden, K., and Valentino, R. J. (2012). Corticotropin-releasing factor in the norepinephrine nucleus, locus coeruleus, facilitates behavioral flexibility. Neuropsychopharmacology 37, 520-530.
- Soares, J. M., Sampaio, A., Ferreira, L. M., Santos, N. C., Marques, F., Palha, J. A., Cerqueira, J. J., and Sousa, N. (2012). Stress-induced changes in human decision-making are reversible. Transl Psychiatry 2, e131.
- Sorg, B. A., and Kalivas, P. W. (1993). Effects of cocaine and footshock stress on extracellular dopamine levels in the medial prefrontal cortex. Neuroscience 53, 695-703.
- Spencer, S. J., Buller, K. M., and Day, T. A. (2005). Medial prefrontal cortex control of the paraventricular hypothalamic nucleus response to psychological stress: possible role of the bed nucleus of the stria terminalis. J Comp Neurol 481, 363-376.
- Sprengel, R., Suchanek, B., Amico, C., Brusa, R., Burnashev, N., Rozov, A., Hvalby, O., Jensen, V., Paulsen, O., Andersen, P., Kim, J. J., Thompson, R. F., Sun, W., Webster, L. C., Grant, S. G., Eilers, J., Konnerth, A., Li, J., McNamara, J. O., and Seeburg, P. H. (1998). Importance of the intracellular domain of NR2 subunits for NMDA receptor function *in vivo.* Cell 92, 279-289.
- Stamatakis, A. M., and Stuber, G. D. (2012). Activation of lateral habenula inputs to the ventral midbrain promotes behavioral avoidance. Nat Neurosci 15, 1105-1107.
- Stamatakis, A. M., Jennings, J. H., Ung, R. L., Blair, G. A., Weinberg, R. J., Neve, R. L., Boyce, F., Mattis, J., Ramakrishnan, C., Deisseroth, K., and Stuber, G. D. (2013). A unique population of ventral tegmental area neurons inhibits the lateral habenula to promote reward. Neuron 80, 1039-1053.
- Stamatakis, A. M., Van Swieten, M., Basiri, M. L., Blair, G. A., Kantak, P., and Stuber, G. D. (2016). Lateral Hypothalamic Area Glutamatergic Neurons and Their Projections to the Lateral Habenula Regulate Feeding and Reward. J Neurosci 36, 302-311.
- Starkman, M. N., Gebarski, S. S., Berent, S., and Schteingart, D. E. (1992). Hippocampal formation volume, memory dysfunction, and cortisol levels in patients with Cushing's syndrome. Biol Psychiatry 32, 756-765.
- Staubli, U., Rogers, G., and Lynch, G. (1994). Facilitation of glutamate receptors enhances memory. Proc Natl Acad Sci U S A 91, 777-781.
- Stelly, C. E., Pomrenze, M. B., Cook, J. B., and Morikawa, H. (2016). Repeated social defeat stress enhances glutamatergic synaptic plasticity in the VTA and cocaine place conditioning. Elife 5:e15448.
- Stephenson-Jones, M., Yu, K., Ahrens, S., Tucciarone, J. M., van Huijstee, A. N., Mejia, L. A., Penzo, M. A., Tai, L. H., Wilbrecht, L., and Li, B. (2016). A basal ganglia circuit for evaluating action outcomes. Nature 539, 289-293.
- Sterley, T. L., Baimoukhametova, D., Füzesi, T., Zurek, A. A., Daviu, N., Rasiah, N. P., Rosenegger, D., and Bains, J. S. (2018). Social transmission and buffering of synaptic changes after stress. Nat Neurosci 21, 393-403.
- Stern, W. C., Johnson, A., Bronzino, J. D., and Morgane, P. J. (1979). Effects of electrical stimulation of the lateral habenula on single-unit activity of raphe neurons. Exp Neurol 65, 326-342.
- Stopper, C. M., and Floresco, S. B. (2014). What's better for me? Fundamental role for lateral habenula in promoting subjective decision biases. Nat Neurosci 17, 33-35.

- Straub, C., and Tomita, S. (2012). The regulation of glutamate receptor trafficking and function by TARPs and other transmembrane auxiliary subunits. Curr Opin Neurobiol 22, 488-495.
- Ströhle, A., Scheel, M., Modell, S., and Holsboer, F. (2008). Blunted ACTH response to dexamethasone suppression-CRH stimulation in posttraumatic stress disorder. J Psychiatr Res 42, 1185-1188.
- Stuber, G. D., Klanker, M., de Ridder, B., Bowers, M. S., Joosten, R. N., Feenstra, M. G., and Bonci, A. (2008). Reward-predictive cues enhance excitatory synaptic strength onto midbrain dopamine neurons. Science 321, 1690-1692.
- Südhof, T. C. (2008). Neuroligins and neurexins link synaptic function to cognitive disease. Nature 455, 903-911.
- Swaab, D. F., Bao, A. M., and Lucassen, P. J. (2005). The stress system in the human brain in depression and neurodegeneration. Ageing Res Rev 4, 141-194.
- Swanson, G. T., Kamboj, S. K., and Cull-Candy, S. G. (1997). Single-channel properties of recombinant AMPA receptors depend on RNA editing, splice variation, and subunit composition. J Neurosci 17, 58-69.
- Syrovatkina, V., Alegre, K. O., Dey, R., and Huang, X. Y. (2016). Regulation, Signaling, and Physiological Functions of G-Proteins. J Mol Biol 428, 3850-3868.
- Szőnyi, A., Zichó, K., Barth, A. M., Gönczi, R. T., Schlingloff, D., Török, B., Sipos, E., Major, A., Bardóczi, Z., Sos, K. E., Gulyás, A. I., Varga, V., Zelena, D., Freund, T. F., and Nyiri, G. (2019). Median raphe controls acquisition of negative experience in the mouse. Science 366(6469):eaay8746.
- Takahashi, Y. K., Batchelor, H. M., Liu, B., Khanna, A., Morales, M., and Schoenbaum, G. (2017). Dopamine Neurons Respond to Errors in the Prediction of Sensory Features of Expected Rewards. Neuron 95, 1395-1405.e3.
- Takase, L. F., Nogueira, M. I., Baratta, M., Bland, S. T., Watkins, L. R., Maier, S. F., Fornal, C. A., and Jacobs, B. L. (2004). Inescapable shock activates serotonergic neurons in all raphe nuclei of rat. Behav Brain Res 153, 233-239.
- Takeuchi, T., Duszkiewicz, A. J., and Morris, R. G. (2014). The synaptic plasticity and memory hypothesis: encoding, storage and persistence. Philos Trans R Soc Lond B Biol Sci 369, 20130288.
- Tang, Y. P., Shimizu, E., Dube, G. R., Rampon, C., Kerchner, G. A., Zhuo, M., Liu, G., and Tsien, J. Z. (1999). Genetic enhancement of learning and memory in mice. Nature 401, 63-69.
- Taylor, J. R., Birnbaum, S., Ubriani, R., and Arnsten, A. F. (1999). Activation of cAMP-dependent protein kinase A in prefrontal cortex impairs working memory performance. J Neurosci 19, RC23.
- Tchenio, A., Lecca, S., Valentinova, K., and Mameli, M. (2017). Limiting habenular hyperactivity ameliorates maternal separation-driven depressive-like symptoms. Nat Commun 8, 1135.
- Thornton, E. W., and Davies, C. (1991). A water-maze discrimination learning deficit in the rat following lesion of the habenula. Physiol Behav 49, 819-822.
- Tian, J., and Uchida, N. (2015). Habenula Lesions Reveal that Multiple Mechanisms Underlie Dopamine Prediction Errors. Neuron 87, 1304-1316.
- Toda, A. M., and Huganir, R. L. (2015). Regulation of AMPA receptor phosphorylation by the neuropeptide PACAP38. Proc Natl Acad Sci U S A 112, 6712-6717.
- Tomita, S., Chen, L., Kawasaki, Y., Petralia, R. S., Wenthold, R. J., Nicoll, R. A., and Bredt, D. S. (2003). Functional studies and distribution define a family of transmembrane AMPA receptor regulatory proteins. J Cell Biol 161, 805-816.
- Toni, N., Buchs, P. A., Nikonenko, I., Povilaitite, P., Parisi, L., and Muller, D. (2001). Remodeling of synaptic membranes after induction of long-term potentiation. J Neurosci 21, 6245-6251.
- Tooley, J., Marconi, L., Alipio, J. B., Matikainen-Ankney, B., Georgiou, P., Kravitz, A. V., and Creed, M. C. (2018). Glutamatergic Ventral Pallidal Neurons Modulate Activity of the Habenula-Tegmental Circuitry and Constrain Reward Seeking. Biol Psychiatry 83, 1012-1023.
- Torrado Pacheco, A., Bottorff, J., Gao, Y., and Turrigiano, G. G. (2020). Sleep Promotes Downward Firing Rate Homeostasis. Neuron 109, 1–15.
- Traynelis, S. F., Wollmuth, L. P., McBain, C. J., Menniti, F. S., Vance, K. M., Ogden, K. K., Hansen, K. B., Yuan, H., Myers, S. J., and Dingledine, R. (2010). Glutamate receptor ion channels: structure, regulation, and function. Pharmacol Rev 62, 405-496.

- Tronche, F., Kellendonk, C., Kretz, O., Gass, P., Anlag, K., Orban, P. C., Bock, R., Klein, R., and Schütz, G. (1999). Disruption of the glucocorticoid receptor gene in the nervous system results in reduced anxiety. Nat Genet 23, 99-103.
- Trusel, M., Nuno-Perez, A., Lecca, S., Harada, H., Lalive, A. L., Congiu, M., Takemoto, K., Takahashi, T., Ferraguti, F., and Mameli, M. (2019). Punishment-Predictive Cues Guide Avoidance through Potentiation of Hypothalamus-to-Habenula Synapses. Neuron 102, 120-127.e4.
- Turrigiano, G. G. (2008). The self-tuning neuron: synaptic scaling of excitatory synapses. Cell 135, 422-435.
- Turrigiano, G. G., Leslie, K. R., Desai, N. S., Rutherford, L. C., and Nelson, S. B. (1998). Activity-dependent scaling of quantal amplitude in neocortical neurons. Nature 391, 892-896.
- Tye, K. M., Mirzabekov, J. J., Warden, M. R., Ferenczi, E. A., Tsai, H. C., Finkelstein, J., Kim, S. Y., Adhikari, A., Thompson, K. R., Andalman, A. S., Gunaydin, L. A., Witten, I. B., and Deisseroth, K. (2013). Dopamine neurons modulate neural encoding and expression of depression-related behaviour. Nature 493, 537-541.
- Ulrich-Lai, Y. M., and Herman, J. P. (2009). Neural regulation of endocrine and autonomic stress responses. Nat Rev Neurosci 10, 397-409.
- Valdez, G. R., Inoue, K., Koob, G. F., Rivier, J., Vale, W., and Zorrilla, E. P. (2002). Human urocortin II: mild locomotor suppressive and delayed anxiolytic-like effects of a novel corticotropin-releasing factor related peptide. Brain Res 943, 142-150.
- Vale, W., Spiess, J., Rivier, C., and Rivier, J. (1981). Characterization of a 41-residue ovine hypothalamic peptide that stimulates secretion of corticotropin and beta-endorphin. Science 213, 1394-1397.
- Valentino, R. J., and Van Bockstaele, E. (2008). Convergent regulation of locus coeruleus activity as an adaptive response to stress. Eur J Pharmacol 583, 194-203.
- Van Bockstaele, E. J., Biswas, A., and Pickel, V. M. (1993). Topography of serotonin neurons in the dorsal raphe nucleus that send axon collaterals to the rat prefrontal cortex and nucleus accumbens. Brain Res 624, 188-198.
- Van den Berg, C. L., Lamberts, R. R., Wolterink, G., Wiegant, V. M., and Van Ree, J. M. (1998). Emotional and footshock stimuli induce differential long-lasting behavioural effects in rats; involvement of opioids. Brain Res 799, 6-15.
- Vandenberghe, W., Robberecht, W., and Brorson, J. R. (2000). AMPA receptor calcium permeability, GluR2 expression, and selective motoneuron vulnerability. J Neurosci 20, 123-132.
- Vander Weele, C. M., Siciliano, C. A., Matthews, G. A., Namburi, P., Izadmehr, E. M., Espinel, I. C., Nieh, E. H., Schut, E. H. S., Padilla-Coreano, N., Burgos-Robles, A., Chang, C. J., Kimchi, E. Y., Beyeler, A., Wichmann, R., Wildes, C. P., and Tye, K. M. (2018). Dopamine enhances signal-to-noise ratio in cortical-brainstem encoding of aversive stimuli. Nature 563, 397-401.
- Vergnano, A. M., Rebola, N., Savtchenko, L. P., Pinheiro, P. S., Casado, M., Kieffer, B. L., Rusakov, D. A., Mulle, C., and Paoletti, P. (2014). Zinc dynamics and action at excitatory synapses. Neuron 82, 1101-1114.
- Vicini, S., Wang, J. F., Li, J. H., Zhu, W. J., Wang, Y. H., Luo, J. H., Wolfe, B. B., and Grayson, D. R. (1998). Functional and pharmacological differences between recombinant N-methyl-D-aspartate receptors. J Neurophysiol 79, 555-566.
- Vijayraghavan, S., Wang, M., Birnbaum, S. G., Williams, G. V., and Arnsten, A. F. (2007). Inverted-U dopamine D1 receptor actions on prefrontal neurons engaged in working memory. Nat Neurosci 10, 376-384.
- Vollmayr, B., and Gass, P. (2013). Learned helplessness: unique features and translational value of a cognitive depression model. Cell Tissue Res 354, 171-178.
- Vollmayr, B., Bachteler, D., Vengeliene, V., Gass, P., Spanagel, R., and Henn, F. (2004). Rats with congenital learned helplessness respond less to sucrose but show no deficits in activity or learning. Behav Brain Res 150, 217-221.
- Vom Berg-Maurer, C. M., Trivedi, C. A., Bollmann, J. H., De Marco, R. J., and Ryu, S. (2016). The Severity of Acute Stress Is Represented by Increased Synchronous Activity and Recruitment of Hypothalamic CRH Neurons. J Neurosci 36, 3350-3362.
- Wahl-Schott, C., and Biel, M. (2009). HCN channels: structure, cellular regulation and physiological function. Cell Mol Life Sci 66, 470-494.

- Walker, D. L., and Davis, M. (1997). Double dissociation between the involvement of the bed nucleus of the stria terminalis and the central nucleus of the amygdala in startle increases produced by conditioned versus unconditioned fear. J Neurosci 17, 9375-9383.
- Wallace, M. L., Huang, K. W., Hochbaum, D., Hyun, M., Radeljic, G., and Sabatini, B. L. (2020). Anatomical and single-cell transcriptional profiling of the murine habenular complex. Elife 9:e51271.
- Walletschek, H., and Raab, A. (1982). Spontaneous activity of dorsal raphe neurons during defensive and offensive encounters in the tree-shrew. Physiol Behav 28, 697-705.
- Wang, D., Li, Y., Feng, Q., Guo, Q., Zhou, J., and Luo, M. (2017a). Learning shapes the aversion and reward responses of lateral habenula neurons. Elife 6:e23045.
- Wang, M., Ramos, B. P., Paspalas, C. D., Shu, Y., Simen, A., Duque, A., Vijayraghavan, S., Brennan, A., Dudley, A., Nou, E., Mazer, J. A., McCormick, D. A., and Arnsten, A. F. (2007). Alpha2A-adrenoceptors strengthen working memory networks by inhibiting cAMP-HCN channel signaling in prefrontal cortex. Cell 129, 397-410.
- Wang, M., Yang, Y., Wang, C. J., Gamo, N. J., Jin, L. E., Mazer, J. A., Morrison, J. H., Wang, X. J., and Arnsten, A. F. (2013). NMDA receptors subserve persistent neuronal firing during working memory in dorsolateral prefrontal cortex. Neuron 77, 736-749.
- Wang, Q., Chiu, S. L., Koropouli, E., Hong, I., Mitchell, S., Easwaran, T. P., Hamilton, N. R., Gustina, A. S., Zhu, Q., Ginty, D. D., Huganir, R. L., and Kolodkin, A. L. (2017b). Neuropilin-2/PlexinA3 Receptors Associate with GluA1 and Mediate Sema3F-Dependent Homeostatic Scaling in Cortical Neurons. Neuron 96, 1084-1098.e7.
- Wang, R. Y., and Aghajanian, G. K. (1977). Physiological evidence for habenula as major link between forebrain and midbrain raphe. Science 197, 89-91.
- Wang, S. J., and Gean, P. W. (1999). Long-term depression of excitatory synaptic transmission in the rat amygdala. J Neurosci 19, 10656-10663.
- Warden, M. R., Selimbeyoglu, A., Mirzabekov, J. J., Lo, M., Thompson, K. R., Kim, S. Y., Adhikari, A., Tye, K. M., Frank, L. M., and Deisseroth, K. (2012). A prefrontal cortex-brainstem neuronal projection that controls response to behavioural challenge. Nature 492, 428-432.
- Watt, A. J., van Rossum, M. C., MacLeod, K. M., Nelson, S. B., and Turrigiano, G. G. (2000). Activity coregulates quantal AMPA and NMDA currents at neocortical synapses. Neuron 26, 659-670.
- Webster, J. F., Vroman, R., Balueva, K., Wulff, P., Sakata, S., and Wozny, C. (2020). Disentangling neuronal inhibition and inhibitory pathways in the lateral habenula. Sci Rep 10, 8490.
- Weera, M. M., Shackett, R. S., Kramer, H. M., Middleton, J. W., and Gilpin, N. W. (2020). Central amygdala projections to lateral hypothalamus mediate avoidance behavior in rats. J Neurosci. JN-RM-0236-20.
- Wei, Q., Lu, X. Y., Liu, L., Schafer, G., Shieh, K. R., Burke, S., Robinson, T. E., Watson, S. J., Seasholtz, A. F., and Akil, H. (2004). Glucocorticoid receptor overexpression in forebrain: a mouse model of increased emotional lability. Proc Natl Acad Sci U S A 101, 11851-11856.
- Weinstock, M., Poltyrev, T., Schorer-Apelbaum, D., Men, D., and McCarty, R. (1998). Effect of prenatal stress on plasma corticosterone and catecholamines in response to footshock in rats. Physiol Behav 64, 439-444.
- Weiss, T., and Veh, R. W. (2011). Morphological and electrophysiological characteristics of neurons within identified subnuclei of the lateral habenula in rat brain slices. Neuroscience 172, 74-93.
- Wenzel, J. M., and Cheer, J. F. (2018). Endocannabinoid Regulation of Reward and Reinforcement through Interaction with Dopamine and Endogenous Opioid Signaling. Neuropsychopharmacology 43, 103-115.
- Wenzel, J. M., Oleson, E. B., Gove, W. N., Cole, A. B., Gyawali, U., Dantrassy, H. M., Bluett, R. J., Dryanovski, D. I., Stuber, G. D., Deisseroth, K., Mathur, B. N., Patel, S., Lupica, C. R., and Cheer, J. F. (2018). Phasic Dopamine Signals in the Nucleus Accumbens that Cause Active Avoidance Require Endocannabinoid Mobilization in the Midbrain. Curr Biol 28, 1392-1404.e5.
- White, N. M., Packard, M. G., and McDonald, R. J. (2013). Dissociation of memory systems: The story unfolds. Behav Neurosci 127, 813-834.
- Whitlock, J. R., Heynen, A. J., Shuler, M. G., and Bear, M. F. (2006). Learning induces long-term potentiation in the hippocampus. Science 313, 1093-1097.

- Widagdo, J., Chai, Y. J., Ridder, M. C., Chau, Y. Q., Johnson, R. C., Sah, P., Huganir, R. L., and Anggono, V. (2015). Activity-Dependent Ubiquitination of GluA1 and GluA2 Regulates AMPA Receptor Intracellular Sorting and Degradation. Cell Rep 10, 783-795.
- Wiens, K. M., Lin, H., and Liao, D. (2005). Rac1 induces the clustering of AMPA receptors during spinogenesis. J Neurosci 25, 10627-10636.
- Wilkinson, L. O., and Jacobs, B. L. (1988). Lack of response of serotonergic neurons in the dorsal raphe nucleus of freely moving cats to stressful stimuli. Exp Neurol 101, 445-457.
- Willner, P., Towell, A., Sampson, D., Sophokleous, S., and Muscat, R. (1987). Reduction of sucrose preference by chronic unpredictable mild stress, and its restoration by a tricyclic antidepressant. Psychopharmacology (Berl) 93, 358-364.
- Wirtshafter, D., Asin, K. E., and Pitzer, M. R. (1994). Dopamine agonists and stress produce different patterns of Fos-like immunoreactivity in the lateral habenula. Brain Res 633, 21-26.
- Wolf, O. T., Schommer, N. C., Hellhammer, D. H., McEwen, B. S., and Kirschbaum, C. (2001). The relationship between stress induced cortisol levels and memory differs between men and women. Psychoneuroendocrinology 26, 711-720.
- Won, J., and Silva, A. J. (2008). Molecular and cellular mechanisms of memory allocation in neuronetworks. Neurobiol Learn Mem 89, 285-292.
- Wu, X., Morishita, W. K., Riley, A. M., Hale, W. D., Südhof, T. C., and Malenka, R. C. (2019). Neuroligin-1 Signaling Controls LTP and NMDA Receptors by Distinct Molecular Pathways. Neuron 102, 621-635.e3.
- Yang, H., Yang, J., Xi, W., Hao, S., Luo, B., He, X., Zhu, L., Lou, H., Yu, Y. Q., Xu, F., Duan, S., and Wang, H. (2016). Laterodorsal tegmentum interneuron subtypes oppositely regulate olfactory cue-induced innate fear. Nat Neurosci 19, 283-289.
- Yang, Y., Cui, Y., Sang, K., Dong, Y., Ni, Z., Ma, S., and Hu, H. (2018). Ketamine blocks bursting in the lateral habenula to rapidly relieve depression. Nature 554, 317-322.
- Yashiro, K., and Philpot, B. D. (2008). Regulation of NMDA receptor subunit expression and its implications for LTD, LTP, and metaplasticity. Neuropharmacology 55, 1081-1094.
- Yehuda, R., Boisoneau, D., Lowy, M. T., and Giller, E. L. (1995). Dose-response changes in plasma cortisol and lymphocyte glucocorticoid receptors following dexamethasone administration in combat veterans with and without posttraumatic stress disorder. Arch Gen Psychiatry 52, 583-593.
- Yehuda, R., Golier, J. A., Halligan, S. L., Meaney, M., and Bierer, L. M. (2004). The ACTH response to dexamethasone in PTSD. Am J Psychiatry 161, 1397-1403.
- Yehuda, R., Lowy, M. T., Southwick, S. M., Shaffer, D., and Giller, E. L. (1991). Lymphocyte glucocorticoid receptor number in posttraumatic stress disorder. Am J Psychiatry 148, 499-504.
- Yerkes, R. M., and Dodson, J. D. (1908). The relation of strength of stimulus to rapidity of habit formation. J Comp Neurol Psychol 18, 459–482.
- Yi, E. S., Oh, S., Lee, J. K., and Leem, Y. H. (2017). Chronic stress-induced dendritic reorganization and abundance of synaptosomal PKA-dependent CP-AMPA receptor in the basolateral amygdala in a mouse model of depression. Biochem Biophys Res Commun 486, 671-678.
- Yoo, J. H., Zell, V., Gutierrez-Reed, N., Wu, J., Ressler, R., Shenasa, M. A., Johnson, A. B., Fife, K. H., Faget, L., and Hnasko, T. S. (2016). Ventral tegmental area glutamate neurons co-release GABA and promote positive reinforcement. Nat Commun 7, 13697.
- Yu, X. M., and Salter, M. W. (1998). Gain control of NMDA-receptor currents by intracellular sodium. Nature 396, 469-474.
- Yuan, Y., Wu, W., Chen, M., Cai, F., Fan, C., Shen, W., Sun, W., and Hu, J. (2019). Reward Inhibits Paraventricular CRH Neurons to Relieve Stress. Curr Biol 29, 1243-1251.e4.
- Yuen, E. Y., Liu, W., Karatsoreos, I. N., Feng, J., McEwen, B. S., and Yan, Z. (2009). Acute stress enhances glutamatergic transmission in prefrontal cortex and facilitates working memory. Proc Natl Acad Sci U S A 106, 14075-14079.

- Yuen, E. Y., Liu, W., Karatsoreos, I. N., Ren, Y., Feng, J., McEwen, B. S., and Yan, Z. (2011). Mechanisms for acute stress-induced enhancement of glutamatergic transmission and working memory. Mol Psychiatry 16, 156-170.
- Yuen, E. Y., Wei, J., Liu, W., Zhong, P., Li, X., and Yan, Z. (2012). Repeated stress causes cognitive impairment by suppressing glutamate receptor expression and function in prefrontal cortex. Neuron 73, 962-977.
- Zahm, D. S., and Root, D. H. (2017). Review of the cytology and connections of the lateral habenula, an avatar of adaptive behaving. Pharmacol Biochem Behav 162, 3-21.
- Zhang, G. W., Shen, L., Zhong, W., Xiong, Y., Zhang, L. I., and Tao, H. W. (2018a). Transforming Sensory Cues into Aversive Emotion via Septal-Habenular Pathway. Neuron 99, 1016-1028.e5.
- Zhang, H., Li, K., Chen, H. S., Gao, S. Q., Xia, Z. X., Zhang, J. T., Wang, F., and Chen, J. G. (2018b). Dorsal raphe projection inhibits the excitatory inputs on lateral habenula and alleviates depressive behaviors in rats. Brain Struct Funct 223, 2243-2258.
- Zhang, L., Hernández, V. S., Swinny, J. D., Verma, A. K., Giesecke, T., Emery, A. C., Mutig, K., Garcia-Segura, L. M., and Eiden, L. E. (2018c). A GABAergic cell type in the lateral habenula links hypothalamic homeostatic and midbrain motivation circuits with sex steroid signaling. Transl Psychiatry 8, 50.
- Zhang, L., Hernández, V. S., Vázquez-Juárez, E., Chay, F. K., and Barrio, R. A. (2016). Thirst Is Associated with Suppression of Habenula Output and Active Stress Coping: Is there a Role for a Non-canonical Vasopressin-Glutamate Pathway. Front Neural Circuits 10, 13.
- Zhang, R., Asai, M., Mahoney, C. E., Joachim, M., Shen, Y., Gunner, G., and Majzoub, J. A. (2017). Loss of hypothalamic corticotropin-releasing hormone markedly reduces anxiety behaviors in mice. Mol Psychiatry 22, 733-744.
- Zhou, L., Liu, M. Z., Li, Q., Deng, J., Mu, D., and Sun, Y. G. (2017). Organization of Functional Long-Range Circuits Controlling the Activity of Serotonergic Neurons in the Dorsal Raphe Nucleus. Cell Rep 18, 3018-3032.
- Zhou, Q., Homma, K. J., and Poo, M. M. (2004). Shrinkage of dendritic spines associated with long-term depression of hippocampal synapses. Neuron 44, 749-757.
- Zhou, W., Jin, Y., Meng, Q., Zhu, X., Bai, T., Tian, Y., Mao, Y., Wang, L., Xie, W., Zhong, H., Zhang, N., Luo, M. H., Tao, W., Wang, H., Li, J., Li, J., Qiu, B. S., Zhou, J. N., Li, X., Xu, H., Wang, K., Zhang, X., Liu, Y., Richter-Levin, G., Xu, L., and Zhang, Z. (2019). A neural circuit for comorbid depressive symptoms in chronic pain. Nat Neurosci 22, 1649-1658.
- Zingg, B., Chou, X. L., Zhang, Z. G., Mesik, L., Liang, F., Tao, H. W., and Zhang, L. I. (2017). AAV-Mediated Anterograde Transsynaptic Tagging: Mapping Corticocollicular Input-Defined Neural Pathways for Defense Behaviors. Neuron 93, 33-47.
- Zobel, A. W., Nickel, T., Sonntag, A., Uhr, M., Holsboer, F., and Ising, M. (2001). Cortisol response in the combined dexamethasone/CRH test as predictor of relapse in patients with remitted depression. a prospective study. J Psychiatr Res 35, 83-94.